THE INVESTIGATION OF ELF5 DURING SKIN DEVELOPMENT AND HOMEOSTASIS

Anhua Hu

A thesis submitted in partial fulfilment of the

requirements of Nottingham Trent University for the

degree of Doctor of Philosophy.

January 2024

Acknowledgements

I am profoundly grateful for the opportunity to express my sincerest thanks to those who have contributed to my journey through the challenging yet rewarding path of my Ph.D.

Firstly, I extend my deepest gratitude to my supervisory team, Dr. Mark Turner, Dr. Mohammed Ahmed, and Dr. Alan Hargreaves. Their guidance, support, and encouragement have been the bedrock of my research journey. Their expertise and insightful feedback have been invaluable in shaping both my thesis and my growth as a scholar.

I am also deeply thankful to Dr. Cleveland Barnett, Prof. Mary O'Neil, and Mary Pearson for their unwavering support and invaluable contributions to my PhD completion.

Special thanks are due to Dr. Graham Hickman for his expertise in microscopy, Dr. Stephen Reed for his assistance with FACS, and Dr. Andrew Marr and his team for their dedication to the animal work. Dr. Biola Egbowon's lab support in IBRC has also been crucial in facilitating my research.

The PGR community in IBRC, ERD, ISTeC, CELS, and JvG, especially Dr. SatinderDeep Kaur, and my friends outside the university, who have made this Ph.D. experience truly enjoyable and memorable. Their companionship and support have been a source of joy and relief during challenging times.

My heartfelt thanks go to my parents, Prof Yunlan Li and Prof Qingyu Hu, whose unconditional love, support, guidance, and encouragement have been my guiding light. Their influence has shaped me into the honest, sincere, generous, and authentic person I am today. My mother, in particular, has been an exemplary figure, teaching me the joy and value of lifelong curiosity and learning.

I am especially grateful to Dr. Vincent Chassaing, Maître Herve Chassaing, and Claudine Chassaing for their support and encouragement from France. Their support has been a source of strength and inspiration. A special acknowledgment is reserved for Dr. Bertrand Chassaing, whose support, encouragement, generosity, and spiritual guidance, particularly towards the end of his life, have left an indelible mark on my heart and my work.

Each of these individuals has played a significant role in my academic and personal development, and for this, I am eternally grateful. Their collective wisdom, support, and kindness have been pillars of strength throughout my Ph.D. journey.

In loving memory and dedication, this thesis is devoted to my late little sister Bin Hu, whose life was a poignant narrative of courage and resilience. She valiantly battled congenital diseases and faced multiple medical challenges throughout her journey. Her profound strength and unwavering spirit in the face of adversity have been a constant source of inspiration to me.

Her ultimate sacrifice, giving her life for the sake of motherhood, speaks volumes of her selfless love and bravery. Now, in paradise, she and her baby are free from the shackles of sickness and suffering, resting in eternal peace and serenity.

This work in the field of skin research is not just an academic pursuit but a heartfelt endeavor inspired by her. It is my hope and aspiration that my research can make a meaningful contribution to the lives of those who, like my sister, suffer from skin conditions. This thesis is a tribute to her memory, a pursuit to extend the beauty she embodied to those who struggle to feel beautiful due to their medical conditions.

Her spirit and story have been the guiding lights in my research, constantly reminding me of the real-life implications and potential impact of my work. In her memory, I strive to make a difference, however small, in the world of skin health and treatment.

Every page of this thesis carries a piece of her legacy, and it is my honor to dedicate my Ph.D. research to her memory. Her life, though fraught with challenges, was a testament to the human spirit's resilience and capacity for love. May her story continue to inspire and bring hope to many.

Copyright statement and Published articles

Work from this thesis contributed towards the following poster presentation in International Societies For Investigative Dermatology (ISID) 2023 Tokyo: “

"Elf5, a novel regulator of skin stem/progenitor cells fate during skin development?", awarded by International Societies For Investigative Dermatology (ISID), 2023 in Tokyo.

and Manuscript “A Previously Uncharacterised Stem/Progenitor Marker, Elf5, Is Required for Normal Skin Development” (Hu, A., Pickup, M.E., & Ahmed ,M.I. 2024).

Partially contributed to the following publication:

Pickup, M. E., Hu, A., Patel, H. J., & Ahmed, M. I. (2023). MicroRNA-148a Controls Epidermal and Hair Follicle Stem/Progenitor Cells by Modulating the Activities of ROCK1 and ELF5. *The Journal of investigative dermatology*, 143(3), 480–491.e5. https://doi.org/10.1016/j.jid.2022.06.028

Abstract

In mammals, skin as a complex organ necessitates exact control over the growth and differentiation in both spatial and temporal aspects, essential for the organism's critical functions. Skin development and homeostasis are complex dynamic processes that include the formation and maintaining of the homeostasis of the epidermis, a stratified self-renewing epithelium and its appendices, such as hair follicles. Elf5 is a member of the epithelium-specific Ets subfamily of transcription factors and is essential for epithelial development, homeostasis and prevention of tumorigenesis. However, the role of Elf5 in regulating skin and hair follicle (HF) development/homeostasis and regeneration remains largely unknown. This study brings new insights into novel expression patterns of Elf5 correlating with functionally important regulation of cellular processes involving proliferation and differentiation in stem/progenitor cell populations in skin and HFs. Utilising colony forming assay with FACS-sorted mouse basal and HF-bulge stems cells (SCs), I observed reduced ability of these SCs to form colonies after gain and/or loss of Elf5 functions. Target identification of Elf5-associated pathways was conducted using RNA and ChIP sequencing analysis in both primary keratinocytes and SCs of skin and HFs. This identified that cell proliferation and differentiation are potential functions regulated by Elf5. I hypothesise that Elf5 plays a crucial role in controlling skin-SCs self-renewal, proliferation and differentiation and/or their balance during skin and hair development/homeostasis and regeneration. This study offers novel insight into the biological importance of Elf5 during skin and hair development, homeostasis and the possible use of Elf5 and its targets for potential stem cell-based therapies for skin and hair disorders in the near future.

Contents

Table of Contents

Figure List

Table List

Abbreviations

3’UTR 3’-untranslated region

AML Acute myeloid leukemia

AP Alkaline phosphatase

AP-2: Family of transcription factors **(**Ensembl Family ENSF00000001105**)**

APM Arrector pili muscle

αSMA alpha-smooth muscle actin

BM Basement membrane

BMP Bone morphogenic protein

BMPR1a BMP receptor 1 a

BSA Bovine serum albumin

cAMP Cyclic Adenosine Monophosphate

Ccn2 Connective tissue growth factor (also referred to as Ctgf)

Ccnb2 Cyclin B2

Ccnd1 Cyclin D1

Ccnd2 Cyclin D2

Ccne1 Cyclin E1

Cdk Cyclin dependent kinase

cDNA Complimentary DNA

C/EBP CCAAT/Enhancer-Binding Protein

CKIs Cyclin-dependent kinase inhibitors

ChIP Chromatin immunoprecipitation

Cks1b Cyclin dependent kinase regulatory subunit 1 /Cdc28 Protein Kinase Regulatory

Subunit 1B

COL-I Type I collagen

Col1a1 Collagen Type I Alpha 1 Chain

COL-III Type III collagen

Col3a Collagen Type III Alpha 1 Chain

Col6a1 Collagen Type VI Alpha 1 Chain

Col6a2 Collagen Type VI Alpha 2 Chain

Creb3 Cyclic AMP-responsive element-binding protein 3

Creb3l1 Cyclic AMP-Responsive Element-Binding Protein 3-Like 1

CTS Connective tissue sheath

DAVID Database for Annotation, Visualization, and Integrated Discovery

Dgcr8 DiGeorge critical region 8

DIG Digoxigenin

Dkk4 Dickkopf 4

Dlx3 Distal-less homeobox 3

DP Dermal papilla

DS Dermal sheath

Dusp6 Dual Specificity Phosphatase 6

E Embryonic day

ECM Extracellular matrix

EGF Epidermal growth factor

EGFR Epidermal growth factor receptor

ELF5 E74 Like Transcription Factor 5

EMT Epithelial-mesenchymal transition

EpiSC Epidermal stem cell

ER Oestrogen receptor

Ets E26 transformation specific

Exp5 Exportin-5

FACS Fluorescent activated cell sorting

FFPE Formalin fixed and paraffin-embedded

FGF Fibroblast growth factor

FLG Filaggrin

FOXA1 Forkhead box protein A1

Frz8 Frizzled 8

GFP Green fluorescent protein

GO Gene ontology

HBSS Hanks balanced salt solution

HF Hair follicle

HFSCs Hair follicle SCs

HG Hair germ

Hh Hedgehog

HS Hair shaft

IGF The insulin-like growth factor

IGFBPs The insulin-like growth factor binding proteins

IGF1R Insulin-like Growth Factor 1 Receptor

INV Involucrin

IPA Ingenuity Pathway Analysis

IRS Inner root sheath

K Keratin

KEGG Kyoto Encyclopedia of Genes and Genomes

Krt keratinocyte

Lhx2 LIM homeobox 2

LOR Loricrin

LRP6 Low-Density Lipoprotein Receptor-Related Protein 6

M Matrix

MACS Model-based Analysis of ChIP-Seq

MAPK Mitogen-activated protein kinase

MiR/miRNA MicroRNA

Mx Matrix

NF-Kβ Nuclear factor kappa B

NGS Next-generation sequencing

ΔNp63 Delta Np63

Orc5 Origin recognition complex subunit 5

ORS Outer root sheath

P Post-natal day

PDG-A Platelet-derived growth factor A

PI3K/AKT phosphatidylinositol 3-kinase (PI3K)/protein kinase B (Akt)

PKC Protein kinase C

PMEKs Primary mouse keratinocytes

PR Progesterone receptor

RNAi RNA interference

Rock Rho-Associated Kinase

SC Stem cell

SCC Squamous cell carcinoma

Sca-1 Stem cell antigen-1

SDS Sodium dodecyl sulphate

SEF Sclerosing Epithelioid Fibrosarcoma

Sfi1 SFI1 centrin binding protein

SG Sebaceous gland

SHG Secondary hair germ

Shh Sonic hedgehog

SiRNA Short interfering RNAs

SPRR Small proline-rich protein

Sprr1a Small proline-rich protein (SPRR) 1A

T3 3,3',5-Triiodo-L-thyronine sodium salt

TAp63α N-terminal Transactivating domain p63 alpha

TG Transglutaminase

TGF Transforming growth factor

TGFβ Transforming Growth Factor Beta

TNBCs Triple-negative breast cancers

TNF Tumor necrosis factor

Tuba1b Tubulin alpha 1b

Wnt Wingless and Int-1SCSC

Wnt3A Wingless-Type MMTV Integration Site Family, Member 3A.

Chapter 1

Introduction

1.1 Skin

The integumentary system is a composite of the skin and its appendages, including hair follicles (HFs). As the largest organ, skin covers the body with about 1.8 m² surface area and weighs about 16% of total body weight. Full-thickness skin has three layers: the epidermis, the dermis and the subcutis (Figure.1.1). The outmost layer of the skin, epidermis constructs the barrier to physical, chemical, and mechanical harm and to microorganism invasion; It also prevents body liquid loss, and photodamage from UV radiation and acts as a thermoregulator, and sensory organ (Blanpain & Fuchs, 2009; Gawkrodger & Ardern-Jones, 2017; Kolarsick, 2011).

Structure of the skin

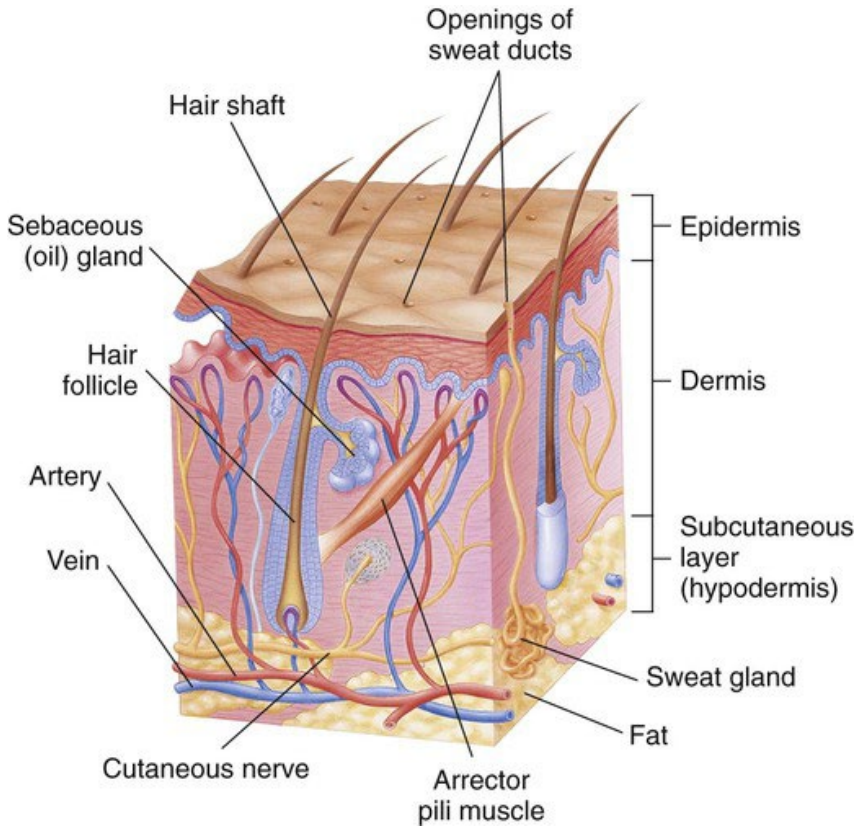

Figure 1.1 Structure of the skin. The main structure of skin includes the epidermis, made of the keratinized, stratified squamous epithelium. The dermis is comprised of connective tissues and includes blood and lymph vessels, HFs, sweat glands, nerves and other structures. The hypodermis is comprised of connective and adipose tissue. (Gawkrodger & Ardern-Jones, 2017; McLafferty et al.,2012).

The epidermis is comprised of a multilayered epithelium, the interfollicular epidermis, with associated appendages such as HFs, sebaceous glands, and eccrine sweat glands.

The BM separates the epidermis and dermis, which offers structural reinforcement and supports the nutrients to the skin (Barbieri et al.,2014). The dermis comprises the extracellular matrix (ECM). It houses various cell types such as fibroblasts, macrophages, and mast cells. Additionally, the dermis contains vascular, lymphatic, and nervous structures (Honari & Maibach, 2014). It displays an important role in epidermal development and hair growth in adults through epidermal–dermal interactions (Alonso & Fuchs, 2006; Blanpain & Fuchs, 2009; Kretzschmar et al.,2015).

The hypodermis is mainly made up of adipose tissue, acting as an insulator and an energy reserve for the body. It not only provides a protective cushion for the skin but also supports the nerves, vessels, and lymphatics found within its septa, nourishing the area above (Koster & Roop, 2007; Honari & Maibach, 2014).

As in other epithelial tissues in adults, the homeostasis of healthy skin relies on the self-renew and continual proliferation capacity of epidermal stem cells (EpiSCs) as well as reparation of tissue damage (Giangreco et al.,2008; Blanpain & Fuchs, 2009; Kretzschmar & Watt, 2014).

1.1.1 Epidermis and Hair Follicle Development

Although there are specific SC populations in the adult epidermis, evidence show that they all originate from a single SC layer in embryonic skin (Watt & Jensen, 2009). During murine embryonic skin development, from embryonic day 9.5 (E9.5) to E12.5 the single layer

ectodermal progenitors progress differently through different signaling pathways to make epidermis and appendages (Fuchs, 2007; Blanpain & Fuchs,2009) (Figure.1.2).

Early signaling steps in the specification of embryonic skin

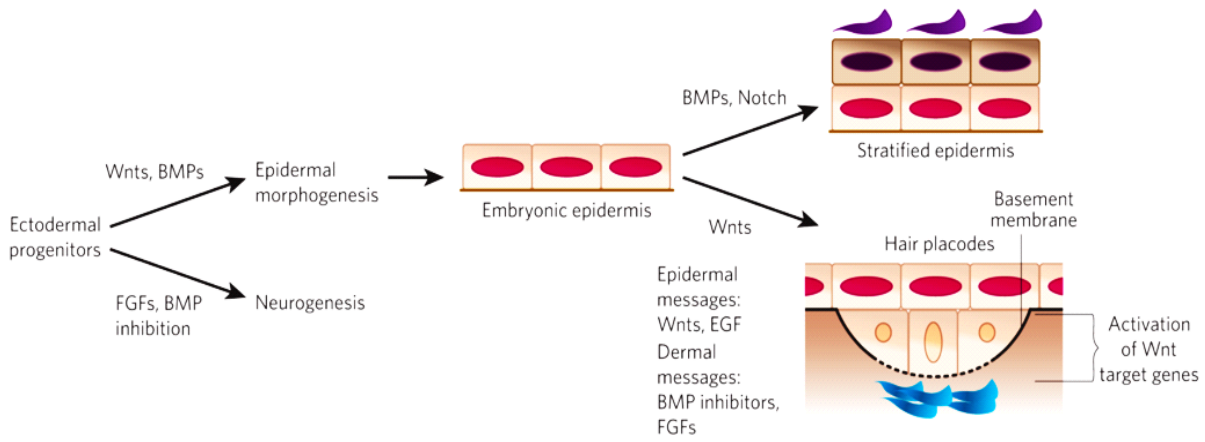

Figure 1.2 Early signaling steps in the specification of embryonic skin. The skin epithelium is derived from the surface of ectoderm during embryonic development. Wingless and Int-1 (Wnt) signaling blocks the Fibroblast growth factor (FGF) signaling and Bone morphogenic protein (BMPs) are expressed to give rise to epidermis development. Based on the responses to different signals, embryonic epidermis cells process to different fates: epidermal cells or appendage (Fuchs, 2007).

The inactivation of Wnt signaling to FGFs response results in ectodermal progenitor cell positive response to BMP signaling in the early stage to progress towards epidermal morphogenesis. The mesenchymal cells populated in the skin give signals to induce the stratification of the epidermis and direct the position towards down growths, which marks the initial departure of HF morphogenesis (Fuchs, 2007; Fuchs, 2008; Blanpain & Fuchs, 2009; Carlson, 2014). Some of the embryonic epidermal cells are instructed to become epidermal cells through BMP, EGF and Notch signaling and then undergo differentiation into different layers. Some of the embryonic epidermis cells are fated to make hair placodes through Wnt

signaling accompanied by the influence of epidermal and dermal induction (Figure. 1.2) (Fuchs, 2007; Fuchs, 2008; Blanpain & Fuchs, 2009; Carlson, 2014).

1.1.1.1 Epidermal Development

As detailed earlier, at around E 9.5, the single layer of progenitor cells commits to an epidermal lineage and shift to expressing the specific keratin (K) pair, K5-K14 (Zhang, 2018). The stratification stages initiate embryonic day 12.5-15.5 (E12.5–E15.5) once surface ectoderm cells decide to adopt an epidermal fate through a meticulously orchestrated stratification process (Koster & Roop, 2007). Throughout time, a transient protective layer called periderm is formed on the surface of the epidermis and will shed from the epidermis once the epidermis has completely achieved stratification and differentiation around E17.5 (M'Boneko & Merker, 1988; Benitah & Frye,2012). Although variation exists regionally, stratification completes largely by E17.5, by which point the epidermis composites of an inner layer of basal cells with proliferative potential and layers of terminally differentiating, but soon differentiated suprabasal cells. During this phase, K5/K14 are replaced by K1 and K10.

The suprabasal keratinocytes (Krts) undergo terminal differentiation and persistently move upward to form the granular layer. These granular Krts express late-stage differentiation markers, including Filaggrin (FLG), Loricrin (LOR), and Involucrin (INV). The fully stratified epidermis consists of various layers, each representing a distinct stage of krt differentiation: Stratum basale, Stratum spinosum, Stratum granulosum, and Stratum corneum. Each stage is characterized by its unique molecular markers (Fuchs, 2007; Fuchs, 2008; Blanpain & Fuchs, 2009; Carlson, 2014; Zhang, 2018). By E18.5, the epidermis reaches full maturity. The terminally differentiated Krts transform into enucleated corneocytes, creating the outermost cornified layer with a fully functional barrier (Zhang, 2018).

Epidermis development

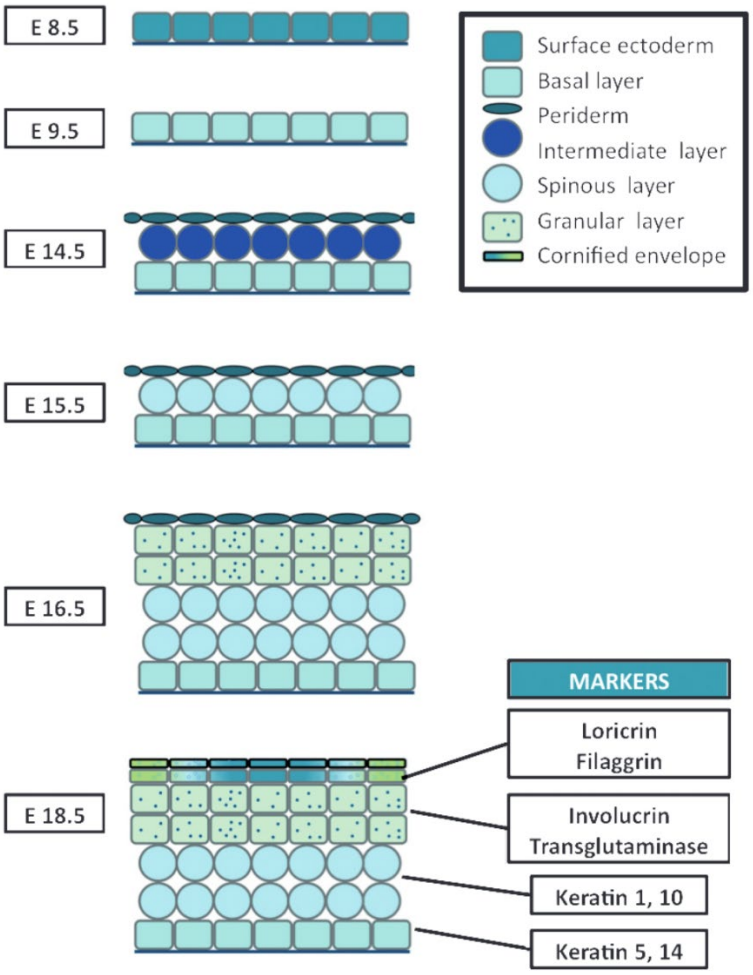

Figure 1.3 Epidermis development. The single outmost layer of the early embryo, known as ectodermal cells, adheres to an underlying BM of ECM. With development, the epidermis acquires progressive stratification, form different layers of different stages of krt differentiation from Stratum basale, Stratum spinosum, Stratum granulosur and Stratum corneux, and each stage develops its specific molecular markers and establishes a functional barrier (Forni et al.,2012).

By birth, postnatal day (P0), the epidermis is formed completely as stratified squamous epithelium with a single basal layer and differentiated suprabasal layers (Mack et al.,2005; Flora and Ezhkova, 2020).

1.1.1.2 Hair Follicle Development

The formation of HFs fundamentally involves a sequence of three phases: induction, organogenesis, and cytodifferentiation (Fig 1.3) (Lin et al.,2022; Carbonnel et al.,2020). HF development is a result of serial interactions between the epithelial epidermis and mesenchymal dermis induction by mediations of BMP, FGF and Sonic hedgehog (Shh). The process of HF morphogenesis commences from induction, with the development of the placode, which involves the thickening of the epidermal cells. These events are orchestrated by the alignment of overlying epidermal krts above specific dermal condensates, a process tightly regulated by signaling interactions between the underlying dermis and epidermis. Embryonic placode induces the mesenchymal cell aggregation to form the dermal condensate (dermal papillae), they are organized and processed temporally and spatially to form the epidermal down growth (hair germ), which overgrows in the following weeks the dermal papilla to form an early HF (Schmidt-Ullrich & Paus, 2005; Saxena et al.,2019). After the establishment of the placode, it starts the organogenesis, the process of HF downgrowth is triggered, leading to the development of the hair germ (HG) as epidermal cells invaginate into the dermis. In mice, this stage commences at approximately E15 (Saxena et al.,2019). As organogenesis progresses, specifically during the formation of the hair peg, the invaginating HF extends deeper into the dermis and starts to encircle the dermal condensate, which will ultimately evolve into the dermal papilla (DP) (Schmidt-Ullrich & Paus, 2005).

The process of cytodifferentiation can also be categorized as the maturation phase within the context of HF morphogenesis. After the hair peg has been established, the formation of IRS commences. At this stage, two bulges along the follicle in the deep dermis form the sebaceous glands. (Blanpain & Fuchs 2006; Schneider et al.,2009; Carbonnel et al.,2020). As the

maturation of the HF progresses, the IRS undergoes elongation, and the HF extends further into the dermis (Saxena et al.,2019).

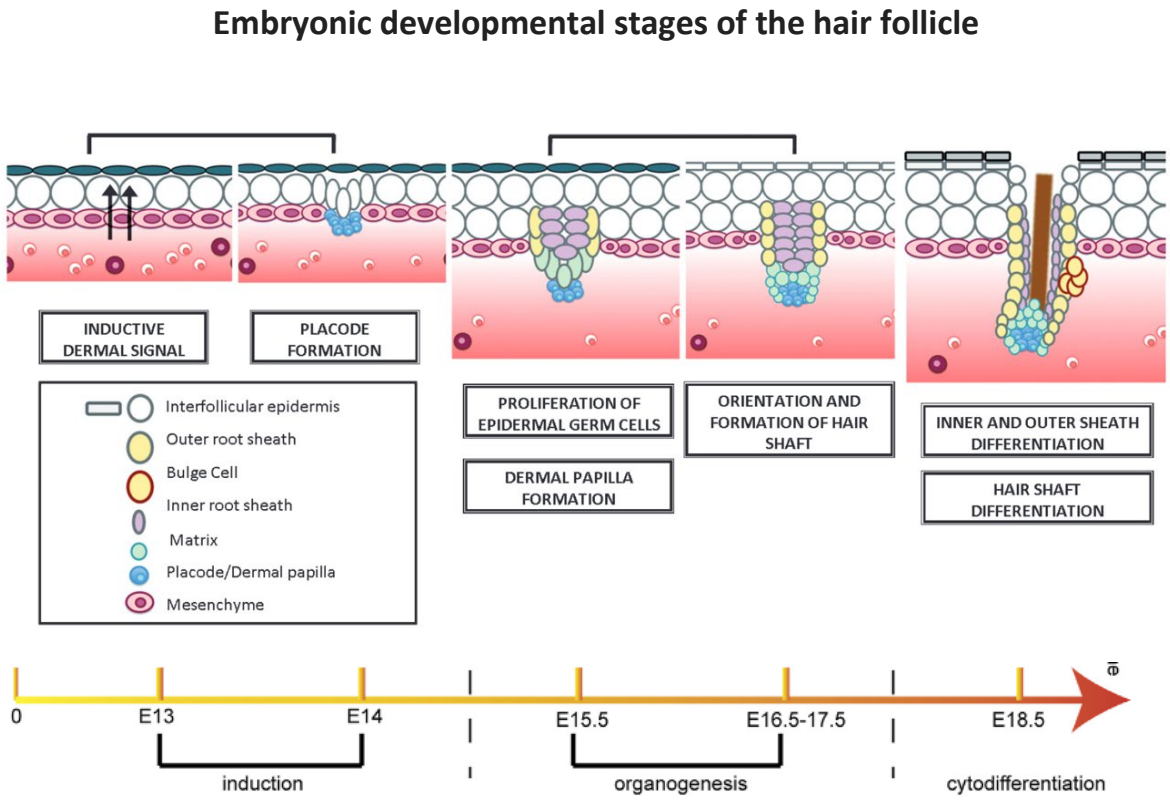

Figure 1.4 Embryonic developmental stages of the hair follicle. Morphogenesis and timing of HF during mouse embryonic development. The most important developmental stages of mouse pelage HFs are divided into induction, organogenesis and cytodifferentiation (Based on Forni et al.,2012; Lin et al.,2022)

Throughout this embryonic developmental stage, some of the basal cells have the fate to develop into future HF because of underlying dermis stimulation signal. Subsequently, the epidermis gives instruction to the dermis to form the DP. Finally, the DP gives signal to the developing follicle, which allows its growth and differentiate into the different lineages of the HFs and its hair shaft (HS). The basal layer of the follicle becomes the outer root sheath (ORS). At the bottom of the mature follicle is matrix (Mx), which locates the highly proliferative cells.

The matrix cells differentiate to form the concentric layers: the hair shaft, its channel (IRS), and the companion layer (Fig 1.4; Fig 1.5; Fig 1.6).

The structure of the hair bulb in human scalp and mouse pelage

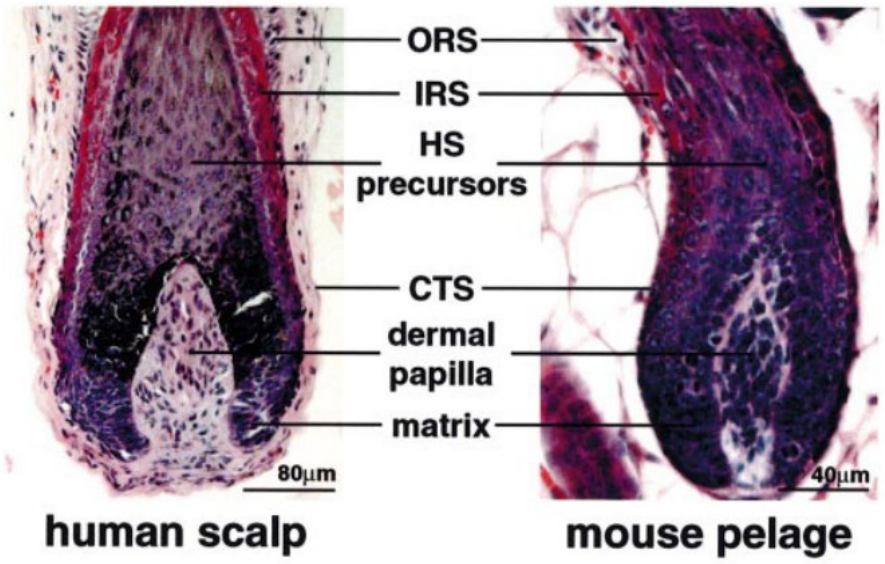

Figure 1.5 The structure of the hair bulb in human scalp and mouse pelage. Paraffin sections were stained with hematoxylin and eosin and photographed at magnifications of 310 (human) and 320 (mouse). IRS, inner root sheath; ORS, outer root sheath; CTS, connective tissue sheath; HS, hair shaft (From Millar, 2002).

During mature hair development, a small bulge resides underneath the sebaceous glands and becomes EpiSCs. Once HF morphogenesis is achieved, the lower two-thirds of the HF starts degenerative process through apoptosis named catagen, and the higher portion, also called the permanent portion, initiates a resting phase, named telogen, till a novel hair growth starts (Blanpain & Fuchs 2006). The culmination of HF morphogenesis is marked by the formation of a fully matured HF, characterized by a fully developed HS, IRS, ORS, and a mature sebaceous gland, along with the establishment of the bulge region (Saxena et al.,2019).

The mature HF is formed by postnatal day 7 (P7) At the end of the hair growth phase (anagen), around P14, the HF undergoes regression (catagen) before entering a resting phase (telogen) at P21 (Schneider et al.,2009). After morphogenesis, HFs are regenerated cyclically during the whole adult life (Magerl et al.,2001; Schmidt-Ullrich & Paus, 2005). The fully developed (anagen) HF can be separated into a 'permanent' upper section that does not exhibit visible cycling and a lower portion that undergoes continuous remodeling during each hair cycle. Hair growth originates from actively dividing cells situated at the base of the follicle; a region known as the bulb. When these bulb cells undergo apoptosis, hair growth halts, and the lower part of the follicle contracts to its shortest length during the resting (telogen) phase. Subsequently, the entire lower follicle regenerates, giving rise to a new hair (Schneider et al.,2009).

Mature HFs comprise the ORS, which consists of the basal cells layer underneath the BM and expresses K14 and K5; The HF progenitors, named matrix cells from the base, which are highly proliferative during HF maturation, go through differentiation process and form the IRS, the external layer of hair shaft in the future. By postnatal day 8 in mice, follicle maturation is accomplished, and in next 7 days, matrix cells continue proliferating and differentiating to form the six concentric layers of the IRS and HS (Blanpain & Fuchs, 2006).

The Hair follicle cycle and Hair follicle lineage

A

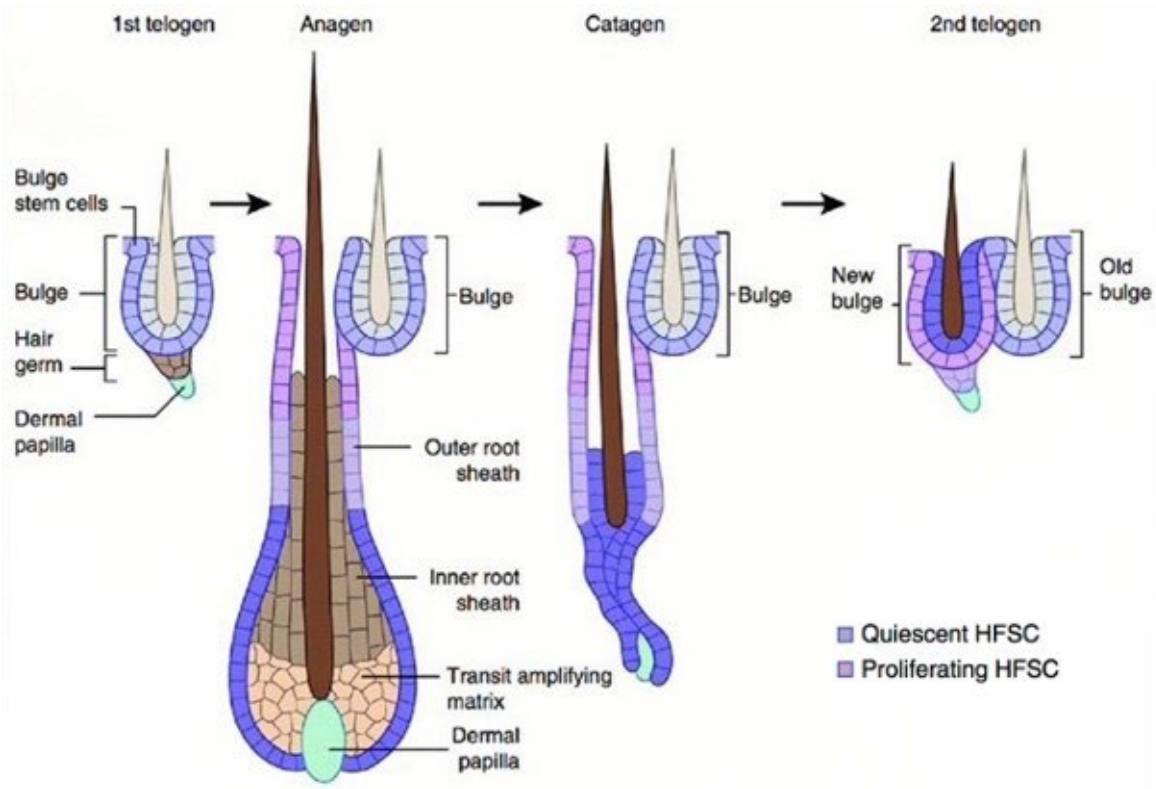

B

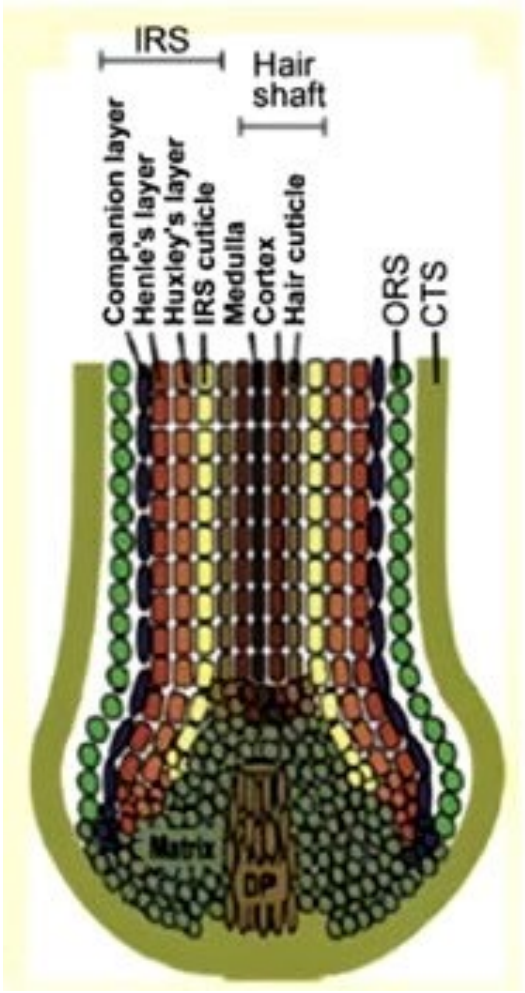

Figure 1.6 The Hair follicle cycle and Hair follicle lineage. (A): The HF SCs, situated within the bulge, the HF transit amplifying progenitors known as matrix cells are found at the base. These highly proliferative matrix cells continuous dividing and differentiating to construct the six concentric layers of the IRS and the hair shaft, eventually forming the inner root sheath (IRS), which becomes the outermost layer of the hair shaft. (Meilana et al.,2015). (B): Schematic drawing illustrating the concentric layers of the ORS, IRS, and shaft in the bulb. Current Biology 19, R132-R142 2009 ©2009 Elsevier

The mature HF undergoes cycles of growth (anagen), regression (catagen), resting (Telogen) and shedding (Exogen) (Saxena et al.,2018; Carlson, 2014). Sebaceous glands are also formed and one part of HF, which guarantee the water impermeable function of hair and provide the lubrication to the hair channel and skin surface (Blanpain & Fuchs, 2006). See Appendix A for **Glossary of hair follicle anatomy** (Schneider et al.,2009).

The timeline of Hair Growth Cycle

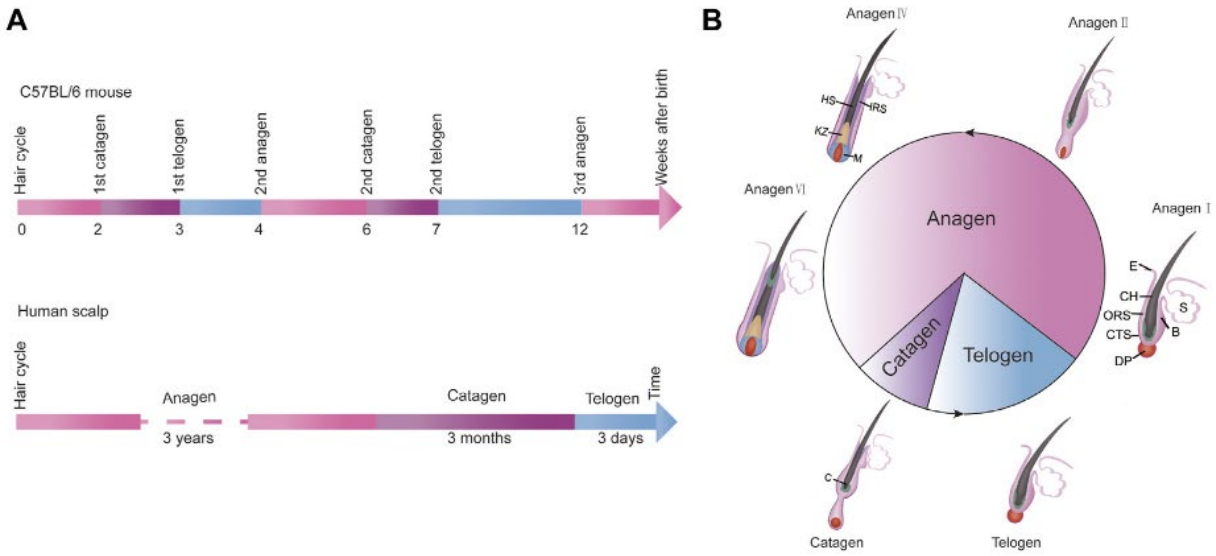

Figure 1.7 The timeline of Hair Growth Cycle: (A) The timeline for the hair growth cycle in female C57BL/6 mice spans the initial 14 weeks post-birth (depicted in the top section). For humans, the hair growth cycle timeline is shown in the bottom section. (B) HFs undergo various morphological changes during different phases of the hair growth cycle. These phases include: Anagen: The active growth phase; Catagen: The transitional phase where growth regresses; Telogen: The dormant or resting phase.

Under normal circumstances, the duration of each cycle is consistent and specific. For instance, C57BL/6 mice have a well-defined timeline for the anagen, catagen, and telogen phases of HF. Newborn mice transition into the catagen phase during the second week after birth, move into the telogen phase in the third week, and then enter the anagen phase by the fourth week (Fig 1.7) (Chen et al.,2019). On an adult's scalp, the anagen phase persists for roughly 3 years. This is succeeded by the catagen phase, which spans around 3 weeks, and then the telogen phase, which lasts for about 3 months (Fig 1.7) (Grymowicz et al.,,2020; Oh et al.,2016).

1.2 Epidermis Homeostasis During Adult Life

By the time that skin morphogenesis is complete, the epidermal progenitors and appendages keep their contact with the BM and express unique krt progenitor markers. During the adult life, progenitors develop into considerable diversities with more specific molecular characters. (Hsu et al.,2014a, 2014b; Yang et al.,2017). The adult skin is built with molecular blocks, which include the pilosebaceous unit (HF and sebaceous gland) and IFE, which surrounds the pilosebaceous unit. (Blanpain & Fuchs,2008). Every segment of the skin epithelium comprises a HF along with its adjacent epidermis (Blanpain et al.,2004). Krts are the largest population in epidermis. Other cell types, such as Merkel cells, melanocytes, and Langerhans cells, are also in mammalian epidermis. (Kretzschmar & Watt, 2014). The BM separates the epidermis and the underneath collagen-rich dermis (Watt & Fujiwara 2011).

Epidermal homeostasis is regulated by SCs with different proliferation dynamics through distinct turnover rates from different specific niches (Cotsarelis et al.,1990). These SCs provide new cells to replace the lost krts either through normal differentiation and tissue turnover, or through apoptosis due to damages occurred after injury (Blanpain & Fuchs, 2009; Ojeh et al.,2015).

1.2.1 Epidermal Stem Cells (EpiSCs)

Adult SCs play a crucial role in maintaining physiological tissue homeostasis and in tissue regeneration following injury (Li & Clevers, 2010). They have the characteristics to be able to self-renew and go through differentiation to give rise to multiple cell types within a tissue (Schultz & Sinclair,2016). SCs can replicate in two ways: symmetrically, where a SC divides to create two identical daughter cells, or asymmetrically, where a SC yields one identical daughter cell and another that is more differentiated (Zouboulis et al.,2008). The EpiSCs have the same stemness characteristics. (Blanpain & Fuchs, 2009; Ojeh et al.,2015). They are characterized *in vivo* by their slow turnover rate, label retention, location in the epidermis, and enrichment of SCs markers, and in vitro by colony forming capacity, the capacity to multiple serial passages

and to adhere rapidly to ECM (Kolodka et al.,1998; Chu et al.,2018). The reduction of skin SCs amounts, and deficiency of their functions are related to unbalanced skin homeostasis such as premature ageing and skin cancers. (Panich et al.,2016).

Epithelial stem cell proliferation and differentiation in the skin

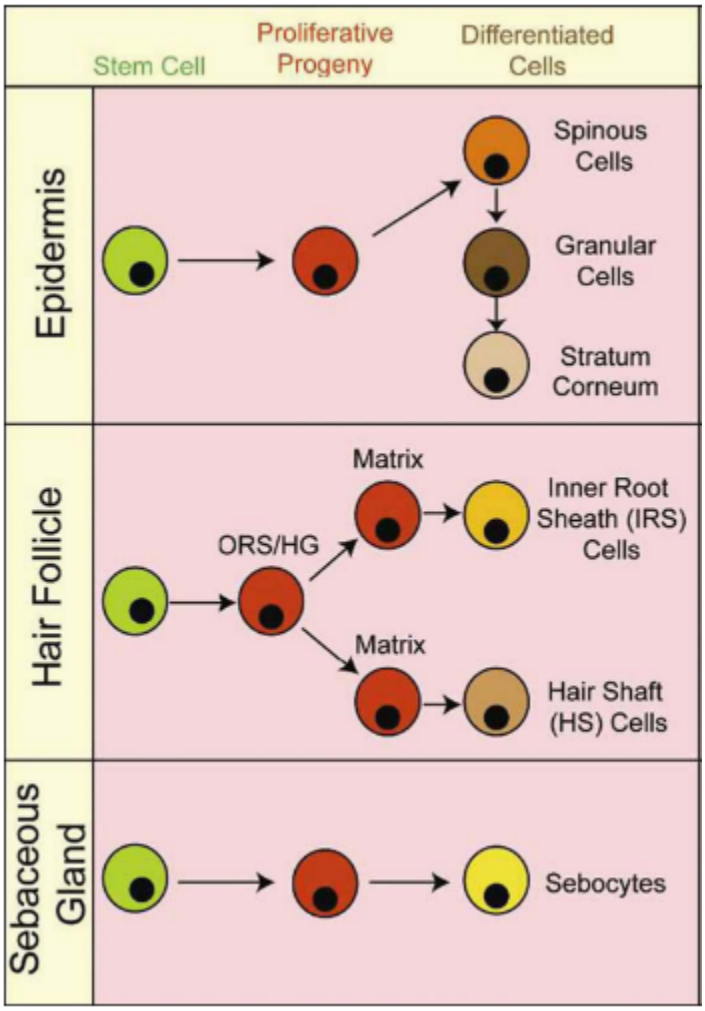

Figure 1.8 Epithelial stem cell proliferation and differentiation in the skin. Epidermal proliferating SCs produce three differentiated cell types: the spinous cells, the granular cells, and the stratum corneum. The HF SCs in the bulge region produce multiple progenitor cells in the ORS/HG and the matrix, which ultimately produce two differentiated lineages: the hair shaft cells and the inner root sheath cells. The unipotent sebaceous gland SCs produce sebocytes. (Zouboulis et al.,2008).

There are different SCs compartments in skin epidermis, where resident different SCs with transit-amplifying progenitor cells (Blanpain & Fuchs, 2009) (Fig 1.8). At least three major SC populations in the epidermis: the basal layer of interfollicular epithelium, the HF bulge, and the sebaceous gland. The epidermis maintains homeostasis independently by proliferation of a single inner (basal) layer cells. The bulge SCs fuel normal follicle homeostasis by undergoing HF cycle and when they exit the SC niche, they become active and proliferate to provide cells that initiate HF regeneration (Soboul's et al.,2008). Subject to conditions such as trauma, wounding, and some inflammatory stimuli, the HF SCs can also participate and/or completely regenerate a lost epidermis, e.g., after burns (Díaz-García et al.,2021). The sebaceous glands' development is highly associated to HFs and epidermis' differentiation (Zouboulis, 2004). Here we focus on SCs of interfollicular epidermis and of HF.

1.2.1.1 Stem Cells of the Interfollicular Epidermis (IFE)

In adult human skin, it should take 4 weeks for a basal layer cell to arise from BM, proliferate new cells that will undergo terminal differentiation into krts towards the surface of the skin, slough from the skin. For adult mouse back skin, this normal physiological process has been estimated shorter, generally a week (Potten et al.,1987; Blanpain & Fuchs, 2009; Sada et al.,2016). This forms different layers: Stratum basale, Stratum spinosum, Stratum granulosur and Stratum corneux, which can be identified by distinguish morphological changes and expression markers: K5 and/or K14 are highly specific basal proliferative KC, and K1 and/or K10 have been robustly used to mark KC in the early differentiation stage. While FLG, LOR, and INV mark the late-stage differentiation (Blanpain & Fuchs, 2009; Fuchs, 2008; Carlson, 2014; Zhang, 2018) (Fig 1.2; Fig 1.7). Human skin has a thicker composition with more layers in the epidermis compared to mouse skin. Additionally, human skin firmly attaches to the tissues beneath it. Features unique to human skin include rete ridges, eccrine sweat glands, and neutrophil defensins, which are not found in the skin of mice (Fig 1.9) (Zomer & Trentin, 2018).

Structure of mouse and human interfollicular epidermis

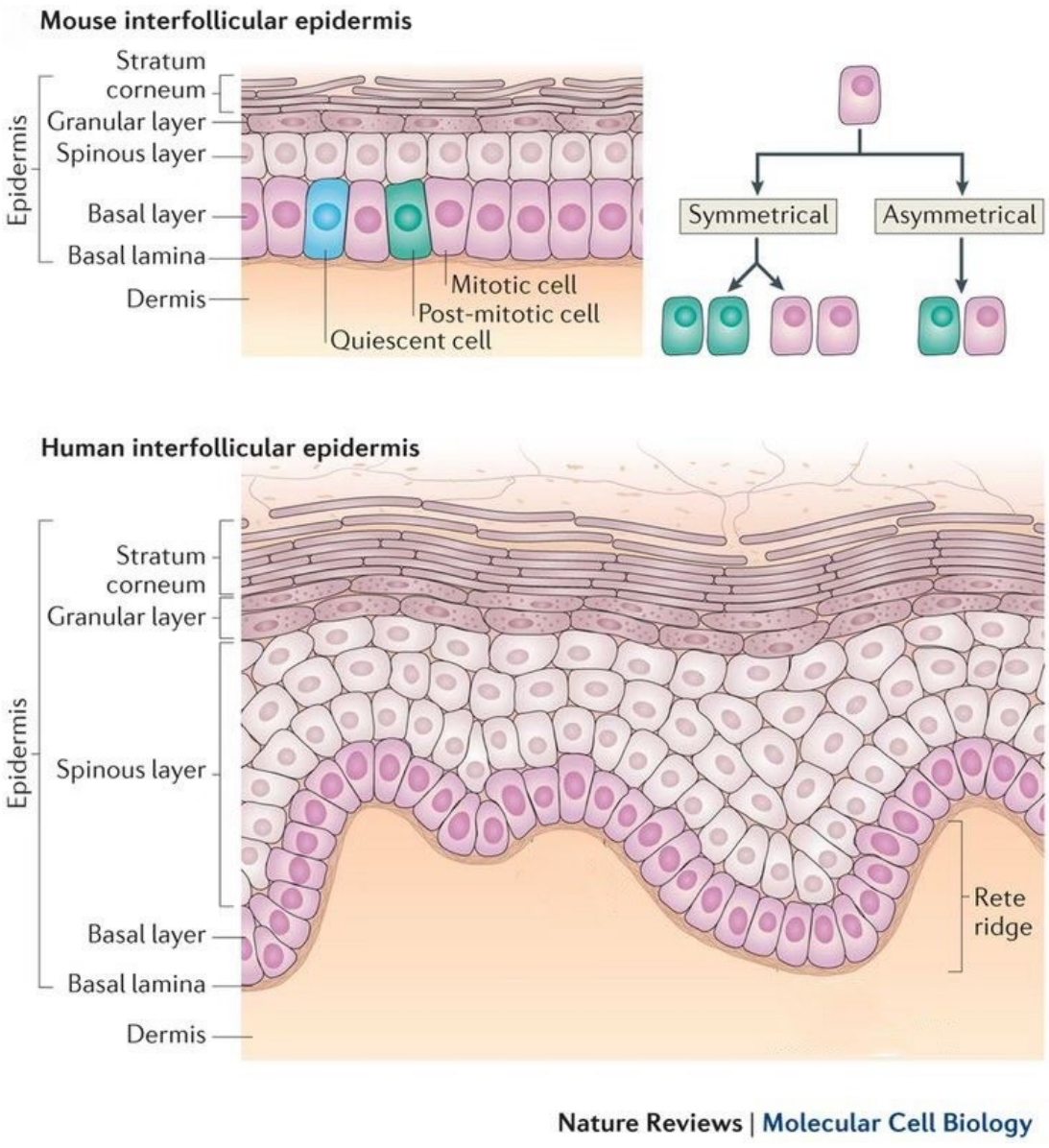

Figure 1.9 Structure of mouse and human interfollicular epidermis. The epidermis contains different layers of different stages of keratinocyte differentiation, the basal SCs attach to the BM and become mitotically active, give rise to cells of the outer epidermal layers via symmetrically or a symmetrically division and further differentiation: Stratum basale, Stratum spinosum, Stratum granulosur and Stratum corneux. Human skin is thicker with additional epidermal layers compared to mouse skin and firmly attaches to the tissues beneath and has rete ridges that are not found in mouse skin.

To maintain the tissue homeostasis, the engaged SCs go through proliferation with a constant cell number, the fate of each cell depends on the division rate and the proportion of cells that differentiate thereafter, and there should be an exquisite balance between the number of cells lost by desquamation and cells that proliferate at a given time point. (Sotiropoulou & Blanpain, 2012). EpiSCs in the basal layer are clonogenic cells and progress through the cell cycle very slowly under normal conditions. Hyperplasiogenic conditions, such as wounding, can activate SCs; DNA damage caused by carcinogenic agents may affect cell proliferation (Blanpain & Fuchs, 2009; Fuchs, 2008; Carlson, 2014).

1.2.1.2 Hair Follicle Bulge Stem Cells

During mature hair development, a small bulge resides underneath the sebaceous glands and becomes EpiSCs. (Saxena et al.,2018; Carlson, 2014). Mature HF undergoes cycles of growth (anagen), regression (catagen), resting (Telogen) and shedding (Exogen). (Carlson, 2014).

The bulge resides the undifferentiated, quiescent multipotent SCs. The first functional characteristic of bulge SCs was their relative quiescence (Cotsarelis et al.,1990). The activation of these infrequently cycling SCs in different systemic cues or stimuli leads to generate new HF and repair epidermis wound. (Cotsarelis, 2006; Fuchs, 2007; Schneider et al.,2009).

Hair follicle cycle and diagram of the follicle stem cell niche

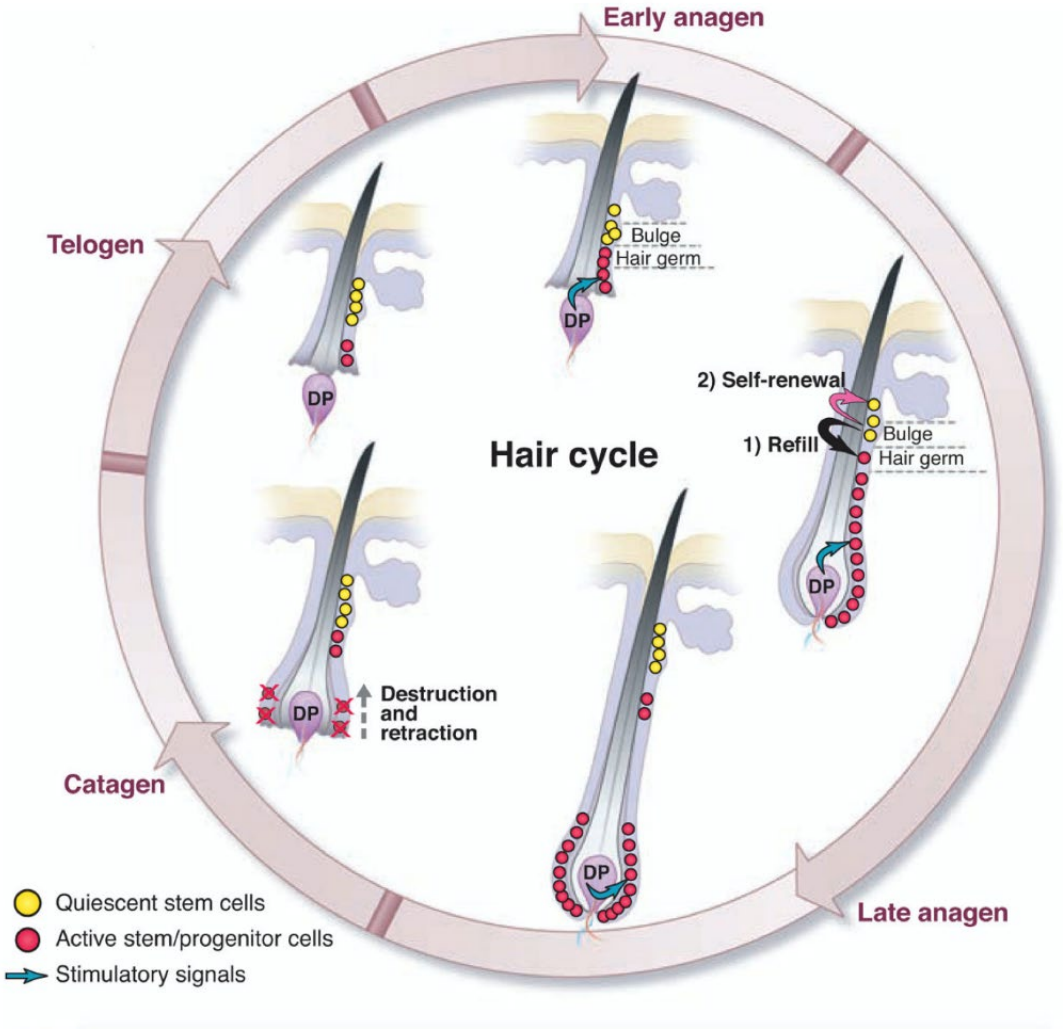

Figure 1.10 Hair follicle cycle and diagram of the follicle stem cell niche. The proliferating matrix-cell progenitors initiate the first anagen phase and its regression results in catagen phase, then the HF undergoes the continuous cycles: cycles of growth (anagen), regression (catagen), resting (Telogen). The matrix cells differentiate into distinct cell layers of HF. The SCs in bulge remain in quiescence as a reservoir. The transient amplifying cells derived from the bulge migrate towards to matrix region during anagen to give rise new HF or migrate in response to epidermal injury for tissue repair purpose. (Cotsarelis, 2006; Fuchs, 2007).

The lower part of the HF extends into the dermis and gives rise to specialized cell types that enable hair growth (Lee & Tumbar, 2012; Sennett & Rendl, 2012). The proliferating matrix-cell progenitors initiate the first anagen phase. The progenitor cells of the leading front end of HF (matrix) differentiation when they grow downward in contact with DP during anagen phase to generate new HS and IRS. The regressive decline of matrix cells and slowdown of its differentiation initiate the anagen to apoptosis mediated catagen transition.

Ultimately, hair growth ceases and enters a degenerative phase (catagen). During this phase, the lower part of the HF deteriorates and shrinks, leaving behind a lasting area known as the bulge; The DP approaches the bulge and maintains this proximity to the bulge through telogen. After catagen, the follicles stay dormant in telogen phase till the new round of hair growth when the bulge SCs are stimulated to initiate the growth of a new HF (Cotsarelis, 2006; Fuchs, 2007; Tadeu & Horsley, 2014).

1.3 Signaling Pathways and Gene Networks in Epidermis Development and Homeostasis

During development, the interactions between epithelial and mesenchymal cells orchestrate the determination and fate of skin's epithelial SCs from a single SC layer. These interactions lead to the formation of the epidermis, HF, and sebaceous glands as described previously. In adulthood, during normal homeostasis, each of these three epithelial paths has its own set of SCs that ensure self-renewal and maintain tissue balance (Fuchs & Horsley, 2008; Watt & Jensen, 2009). Furthermore, within each SC compartment, distinct subpopulations of SCs exist, each with different proliferative capabilities, and these subpopulations can be distinguished by different markers (Watt & Jensen, 2009).

Different signaling pathways are involved in the regulation of EpiSCs activities, including Wnt signaling and EGF receptor signaling (Watt & Jensen, 2009). These mechanisms are detailed below.

1.3.1 Epidermal Stratification, Renewal, and Differentiation

The multilayered or stratified epidermis of the IFE is adhered to the BM through integrin-mediated adhesion (Blanpain & Fuchs, 2006). The cells in the stratum corneum are continuously being shed. Therefore, the proliferating basal cells continuously replenish these specific cells of the IFE (Tadeu & Horsley, 2014). A precise equilibrium between EpiSC self-renewal and differentiation is essential for preserving epidermal homeostasis and ensuring the barrier function (Blanpain & Fuchs, 2009; Nassar & Blanpain, 2012; Flora & Ezhkova, 2020).

While the exact processes overseeing the mechanisms controlling epidermal stratification, homeostasis, and regeneration are still being explored, several cue molecules for these activities have been discovered. The first transcription factor distinctly expressed in the epidermis is p63, which is a part of the tumor-suppressor p53 family (Sotiropoulou & Blanpain, 2012). The existing evidence firmly suggests that p63 acts as a central controller of krt proliferation and differentiation (Truong & Khavari, 2007). Mice with a p63 mutation or lack of p63 show significant defects in skin development and display pronounced abnormalities in all layered epithelia, including the epidermis. They die shortly after birth due to the lack of a skin barrier (Mills et al.,1999; Yang et al.,1999; Koster & Roop 2007; Suzuki & Senoo, 2013). P63 expresses in the skin SCs, and it plays crucial role for initiating epithelial stratification in development and preserving the proliferative capacity of SCs (Senoo et al.,2007; Zhu et al.,2014). Moreover, p63 is associated with numerous genes known to play a pivotal role in enhancing differentiation (Truong & Khavari, 2007). p63 and p53 have contrasting effects on a group of target genes related to cell proliferation. Specifically, p63 suppresses genes that induce cell cycle arrest, while p53 activates them (El-Deiry et al.,1993; Westfall et al.,2003; Truong & Khavari, 2007; Chen, 2016).

A crosstalk exists between Notch and p63, which is involved in the balance between krt self-renewal and differentiation (Nguyen et al.,2006). The canonical Notch pathway plays a pivotal role in regulating IFE differentiation. Notch receptors 'expression can be found in the suprabasal cells in the IFE, while their ligand, Jagged2, is expressed in the basal layer (Watt et al.,2008). The Notch pathway is primarily active in suprabasal cells (Blanpain et al.,2006; Vooijs et al.,2007; Moriyama et al.,2008). Inactivation of Notch pathway results in an absence of spinous differentiation and a failure in skin barrier formation (Pan et al.,2004; Blanpain et al.,2006; Moriyama et al.,2008). On the other hand, an overexpression of the Notch in the epidermis results in the expansion of the spinous layer (Uyttendaele et al.,2004; Blanpain et al.,2006).

Many studies demonstrate that the Notch pathway governs the initial phases of IFE commitment and differentiation. Notch also collaborates with the AP2 protein family to control the expression of C/EBP transcription factors, which subsequently impact terminal differentiation and the formation of the skin barrier (Wang et al.,2008). The active Notch signaling reduces p63 expression, whereas continuous p63 activity hinders Notch's capability to encourage cell cycle arrest and epidermal differentiation (Nguyen et al.,2006).

The mitogen-activated protein kinase (MAPK) pathway plays a pivotal role in maintaining the equilibrium between epidermal growth and differentiation (Tarutani et al.,2003; Scholl et al.,2004; Shaul & Seger, 2007; Scholl et al.,2007; Dumesic et al.,2009; Meng et al.,2018). During normal homeostasis, the MAPK pathway is activated by tyrosine kinase receptors like the epidermal growth factor receptor (EGFR) and basal integrins. Meanwhile, adhesion molecules serve to negatively control this activation (Sotiropoulou &Blanpain, 2012). Consequently, diminished EGF signaling results in decreased IFE proliferation. In contrast, continuous activation of EGFR causes excessive proliferation and the formation of epidermal tumors (Janes & Watt, 2006). Conversely, continuous activation of the Ras-MAPK pathway results in hyperproliferative epidermis (Vasioukhin et al.,2001; Perez-Moreno et al.,2006).

Besides these signaling pathways, there are other genes that regulate the subsequent stages of IFE differentiation such as Irf6, Klf4, Sprr2a, Grhl3 (Segre et al.,1999; Jaubert et al.,2003; Ting et al.,2005; Auden et al.,2006; Ingraham et al.,2006; Richardson et al.,2006; Boglev et al.,2011). It is suggested that various signaling pathways and transcription factors work together to maintain the equilibrium between the renewal and differentiation of the skin epidermis (Sotiropoulou & Blanpain 2012).

1.3.2 Hair Follicle Morphogenesis and Cycling

HF development has intrinsic connection to the stratification of the embryonic epidermis (Abe & Tanaka, 2017). It's development and cycling are complex processes that are regulated by a series of intertwined molecular pathways. These pathways ensure the proper formation, growth, and regeneration of HFs throughout the life of an organism. Different signal pathways and factors combine to form a complex molecular regulatory network, the activity of which results in the proper morphogenesis and regeneration of HFs such as canonical WNT and BMP signaling pathways (Lin et al.,2022).

Various families of signaling molecules that are secreted during the formation of embryonic epidermis, such as BMP, FGF, Hedgehog (Hh), and Wnt. Notably, among these, The WNT signaling pathway plays as the dominant pathway in controlling HF formation and growth cycles (Lim & Nusse, 2013; Choi, 2020; Zhao et al.,2022). Wnt seems to be the initial signal recognized for fostering epidermal development (Reddy et al.,2001; Suzuki et al.,2009; Andl et al.,2002).

The signaling of Wnt from the epidermis to the dermis triggers mesenchymal reactions by initiating a BMP-FGF signaling sequence (Zhu et al.,2014). The choice of developmental fate is profoundly affected by Wnt signaling, which inhibited the ectoderm's response to fibroblast growth factors (FGFs). In the absence of FGF signaling, ectodermal cells can produce bone morphogenetic proteins (BMPs). These BMPs hinder neural induction and guide the cells to transform into keratin-producing cells (keratinocytes), which then constitute the epidermis (Wilson & Hemmati-Bri-vanlou, 1995; Wilson et al.,2001).

The Wnt/β-catenin signaling pathway is the initial mechanism responsible for HF specification (Sotiropoulou & Blanpain, 2012). Upon receiving the initial dermal signal, the Wnt/β-catenin signaling pathway is stimulated to become active in the epidermis, which favors placode development by E14.5, both Wnt ligands and receptors are present in the mouse epidermis (Andl et al.,2002; Andl et al.,2004; Reddy et al.,2001) and the Wnt/β-catenin pathway is essential for placode development (van Genderen et al.,1994; Kratochwil et al.,1996). In postnatal skin, the onset of a new growth phase, along with the associated proliferation, differentiation, and gradual elongation of the follicle, appears to involve significant bidirectional interactions between dermal and epidermal cells.

Many molecular studies indicate that the signaling pathways active during HF morphogenesis are also employed in the cycles of postnatal hair. Specifically, the Wnt/β-catenin signaling pathway is recognized as crucial in various stages of the hair cycle, from the initial transition from rest to growth, to its role in determining cell lineage during follicle differentiation (Oliver & Jahoda,1988; Schmidt-Ullrich & Paus,2005; Lim & Nusse, 2013).

Minimal, if any, Wnt/β-catenin signaling occurs during the majority of the telogen phase. The upregulation of the Wnt/β-catenin signaling is to happen only towards the end of telogen, facilitating the transition into the anagen phase. The choice to transition from the telogen phase to the anagen phase seems to be influenced by the opposing interactions among BMP, TGF-β, and Wnt/β-catenin signaling within the follicular SCs. While Wnt/β-catenin signaling and TGF-β encourage the commencement of the anagen phase, BMP signaling acts as a deterrent (Kobielak et al.,2003, 2007; Andl et al.,2004; Oshimori & Fuchs, 2012). When the follicle transitions into the growth (anagen) phase, BMP signaling is suppressed while Wnt/β-catenin signaling intensifies. Concurrently, bulge cells start proliferation, leading to the expansion of the follicle and the migration of bulge/HG cells along the expanding ORS (Greco et al.,2009; Hsu et al.,2011).

Wnt/β-catenin signaling implies and remains active throughout anagen's duration. Moreover, as the follicular krts undergo differentiation to create the hair shaft, some of genes, which

activate several keratin genes, are believed to be targets of Wnt signaling (Reddy et al.,2001; Reddy et al.,2004; Millar et al.,1999; Zhou et al.,1995; Merrill et al.,2001; Fuchs, 2007). Additional Wnt-responsive genes, including Sonic Hedgehog and the Notch ligand Jagged1 are activated within the anagen matrix. They play roles in facilitating the proliferation and differentiation of krts (Gate et al.,1998; LoCelso et al.,2004; Silva-Vargas et al.,2005; Estrach et al.,2006).

There is evidence suggesting that β-catenin is essential for the regular decline of the HF and for activating genes associated with the catagen stage (Huelsken et al.,2001). The Wnt/β-catenin signaling pathway is viewed as a primary controller of EpiSC renewal and the lineage determination of HFSCs (Wang et al.,2022). An idea level of Wnt/β-catenin signaling is essential for maintaining skin homeostasis. Deviations in this signaling, whether through over-activation or reduction, can result in tumor development (Lim & Nusse, 2013).

BMP and Wnt/β-catenin signaling mutually influence one another, managing the equilibrium between HFSCs and the regeneration of the epidermis (Silva-Vargas et al.,2005). The healthy development and upkeep of HFs depend on the balance between BMP ligands, such as BMP2 and BMP4, and BMP antagonists like Noggin (Botchkarev et al.,2001; Jamora et al.,2003). Bmpr1a is essential for the regulation of the terminal differentiation and growth in hair follicles after birth (Andl et al.,2004). In adult mice, BMP signaling controls the quiescence of bulge SC SCs (Plikus et al.,2008). As the resting stage progresses, there's a decline in dermal BMP expression. This results in the transition from quiescence to activation of bulge SCs, leading to the commencement of HF renewal (Plikus et al.,2008).

Hh signaling is downstream of the traditional Wnt signaling sequence. The Shh signaling pathway is essential for the functionality of β-catenin. As skin develops, the activation of β-catenin triggers the expression of Shh in the epidermis (Gat et al.,1998). Shh is manifested in the embryonic epidermis of HF extensions shortly following placode development (Huelsken et al.,2001; Andl et al.,2002). Shh plays pivotal function of in HFSC progenitor growth and differentiation (St-Jacques et al.,1998). Shh remains active in regulating follicle cycles in adults,

facilitating the shift of HFs from the telogen phase to the anagen phase (Gao et al.,2019; Zhang et al.,2021).

In adults, Shh is manifested in the HG, subsequently in the prospective IRS cells periodically throughout the hair cycle (Panteleyev et al.,2001). Furthermore, Shh is also found in the mesenchymal component of the hair and Shh signaling might influence the epithelial-mesenchymal interactions that govern the hair cycle. (Dlugosz, 1999; Sato et al.,1999; Paladini et al.,2005; Oro & Higgins, 2003; Woo et al.,2012). Recently, Hh signaling has been recognized as an important pathway that stimulates the proliferative activation of HFSCs (Wang et al.,2022).

Multiple signaling pathways and factors converge to establish an intricate molecular control system, the activity of which results in the proper morphogenesis and regeneration of HF (Lin et al.,2022), such as the PI3K/AKT signaling pathway, which impacts downstream signaling entities, guided by an array of upstream or alternative signaling molecules, and serves as a link between external cues and internal reactions (Wang et al.,2022). The transcription factor Runx1 in mouse skin adjusts Wnt signaling intensities, which in turn governs the timely specification of HFs, ensures the appropriate maturation of HFSCs during embryogenesis, and facilitates prompt SC activation during adult homeostasis (Scheitz & Tumbar, 2013). Additionally, miRNAs can also contribute to the regulation of morphogenesis and regeneration of HF. (Lin et al.,2022; Pickup et al.,2023).

Signaling pathways linked with the morphogenesis, development, and differentiation of HFSCs offer specific targets that play crucial roles in enhancing HFSCs involved in tissue healing and preventing abnormal proliferation (Wang et al.,2022).

1.4 Stem Cells in Skin Ageing and Carcinogenesis

1.4.1 Skin Ageing

Ageing is a complicated process at the physiological and molecular level, manifested by a progressive decline or loss of homeostasis and the capacity of regeneration in tissues and organs. (Liu & Rando, 2011; Ahmed et al.,2019). An increasing ageing population has become a major social issue in many countries however, with huge expense associated with age related social and healthcare costs. (McMaughan et a.,2020; WHO, 2023).

SCs contribute to maintaining the homeostatic and regenerative activity in almost all tissues, (Liu & Rando, 2011; Oh et al.,2014; Ermolaeva et al.,2018), and decrease of SC amount or its stemness is a feature of ageing in most tissues. (Giangreco et al.,2010). Our ageing process is influenced by internal factors like DNA damage, and external factors such as alterations in the supportive niches (Sharpless & DePinho.,2007). Together, this can lead to age linked genomic, epigenomic and proteomic alterations. This results in loss of lineage specificity, self-renewal capacity as well as causing cell senescence, and malignant transformation.

Dysfunctions in SCs can result in irregular cell differentiation within tissues In addition, these malignancies are increased with age, especially in epithelia due to their high turnover rates such as skin (Liu & Rando, 2010). The reduction of skin SCs amount, and deficiency of their functions are related to unbalanced skin homeostasis and can result in premature ageing and skin cancers. (Panich et al.,2016).

Skin aging is the outcome of both intrinsic factors, which include chronological aging, and extrinsic factors, such as photoaging. Human ageing skin is characterized by wrinkles and loss of dermal elasticity, decrease of epidermal barrier maintenance, deficiency of regeneration in response to injury, hair loss and increase of cancer risk, associated with tissue structure and molecular changes. (Giangreco et al.,2008; Naylor et al.,2011). EpiSCs persist throughout an individual's lifespan, even in the presence of notable age-related alterations in dermal thickness, epidermal proliferation, and the abundance of peripheral immune cells (Giangreco et al.,2008).

1.4.2 Skin Carcinogenesis

Maintaining body homeostasis requires rigorous regulation of SCs self-renewal and differentiation. Both internal and external factors tightly regulate SCs, and any deviation from this regulation is believed to be a pivotal phase in carcinogenesis. Growing evidence suggests that cancer begins with the accumulation of oncogenic mutations within long-lived SCs or their direct progenitors (indicating an internal control failure), which is then accompanied by changes in the nearby microenvironment (indicating an external control failure) (Gudjonsson & Magnusson, 2005).

Evidence suggests that skin tumors originate from precursors of epidermal krts, which could be either SCs, progenitor cells, or both, such as the predominant epithelial tumors in mouse skin: papilloma and squamous cell carcinoma (SCC) (Martin et al.,2016; Morris, 2000.; Wang et al.,2022). Basal cell carcinoma (BCC) is the most prevalent skin cancer in human BCCs can originate from various SC groups, such as the HF bulge and the IFE (Hahn et al.,1996; Wang et al.,2022).

While SCs from different organs may have distinct developmental potentials, they all must strike a balance between self-renewal and differentiation. Research indicates that several pathways traditionally linked with cancer also influence SC self-renewal and differentiation. Insights into the roles of Wnt, Hedgehog, Shh, and Notch signaling pathways in SC regulation provide a fresh perspective on the origins of cancer (Reya et al.,2001; Taipale & Beachy, 2001; Reguart et al.,2005).

The regulation of self-renewal in normal and transformed SCs may share similar signaling pathways (Cr owe et al.,2004), such as Squamous carcinoma, which exhibit elevated levels of proteins typically found in the basal layer of the epidermis, including p63, which is essential for cell proliferation and homeostasis (Blanpain & Fuchs., 2007; Rocco et al.,2006) and BCC is linked to disrupted Hedgehog signaling (Bale & Yu, 2001; Otsuka et al.,2015; Wang et al.,2022). Indications suggest that EpiSCs are the probable targets for carcinogens (Morris, 2000;

Gudjonsson and Magnusson, 2005; Horsley, 2020; Ingthorsson et al.,2016; Krtolica, 2005; Martin et al.,2016; Wu, 2008; Wang et al.,2022).

Stem cell ageing and the outcomes of damaged stem cells

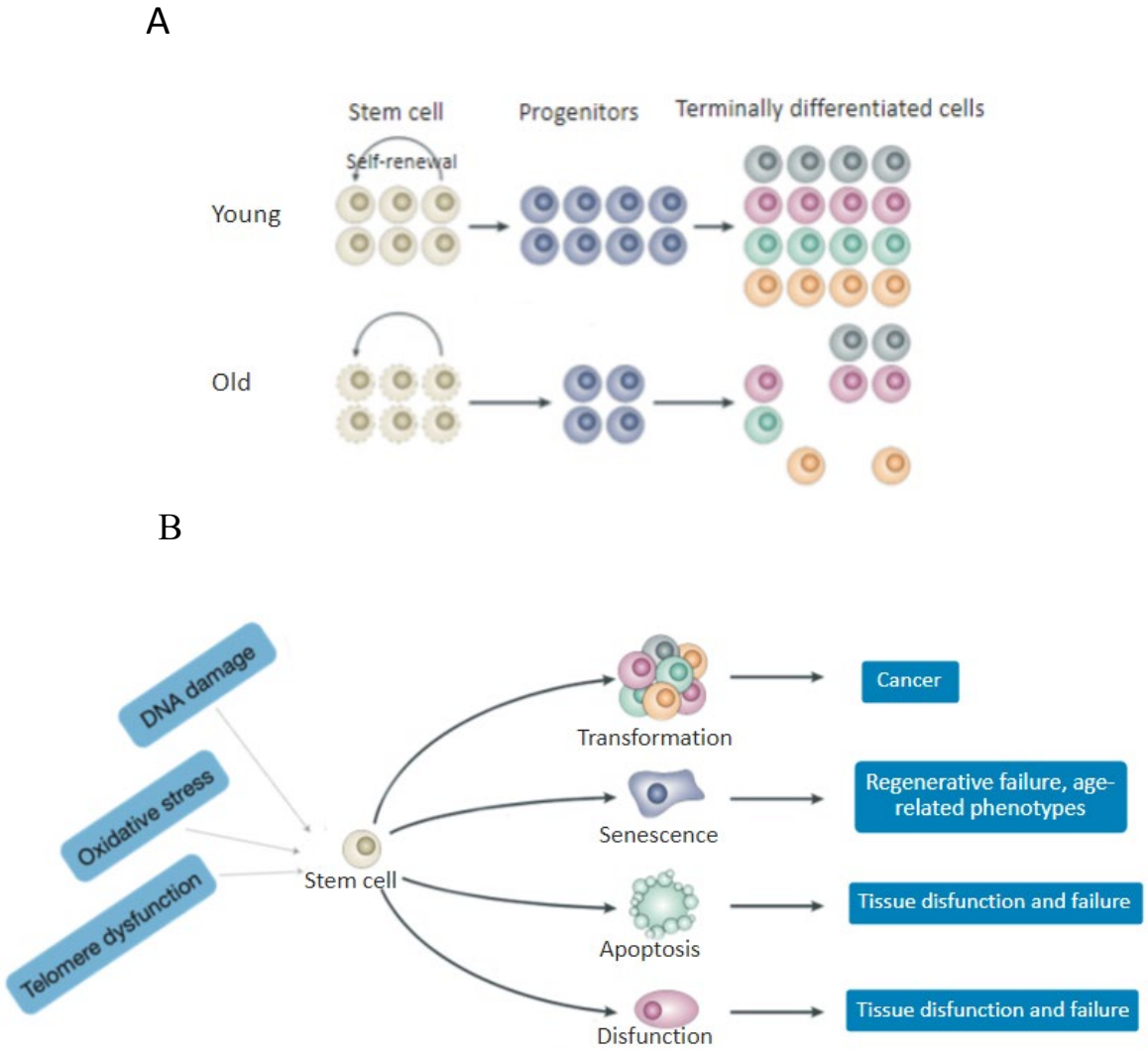

Figure 1. 11 The process of stem cell ageing and the outcomes of damaged stem cells. (A): The number of SCs and their capacity for self-renewal (illustrated by the curved arrow) may not necessarily decrease with age. However, the functional ability to generate progenitor cells (in blue) and specialized effector cells (represented by various colors) does decline; (B): Accumulated damage disrupts normal SC

function, leading to several potential outcomes: transformation, senescence, apoptosis, or dysfunction. Additionally, if oncogenic DNA damage-induced lesions accumulate, self-renewing clones containing these lesions can undergo positive selection, ultimately leading to cancer. (Liu & Rando, 2011; Sharpless & DePinho, 2007).

1.5 E74 Like Transcription Factor 5 (ElF5)

The set of transcription factors (TFs) present in a specific cell plays a crucial role in determining its identity and developmental potential. Therefore, TFs are essential in controlling the ability of SCs to self-renew and differentiate (Latos et al.,2015).

Illustrative depiction of the transcription process for a single gene, influenced by a solitary transcription factor

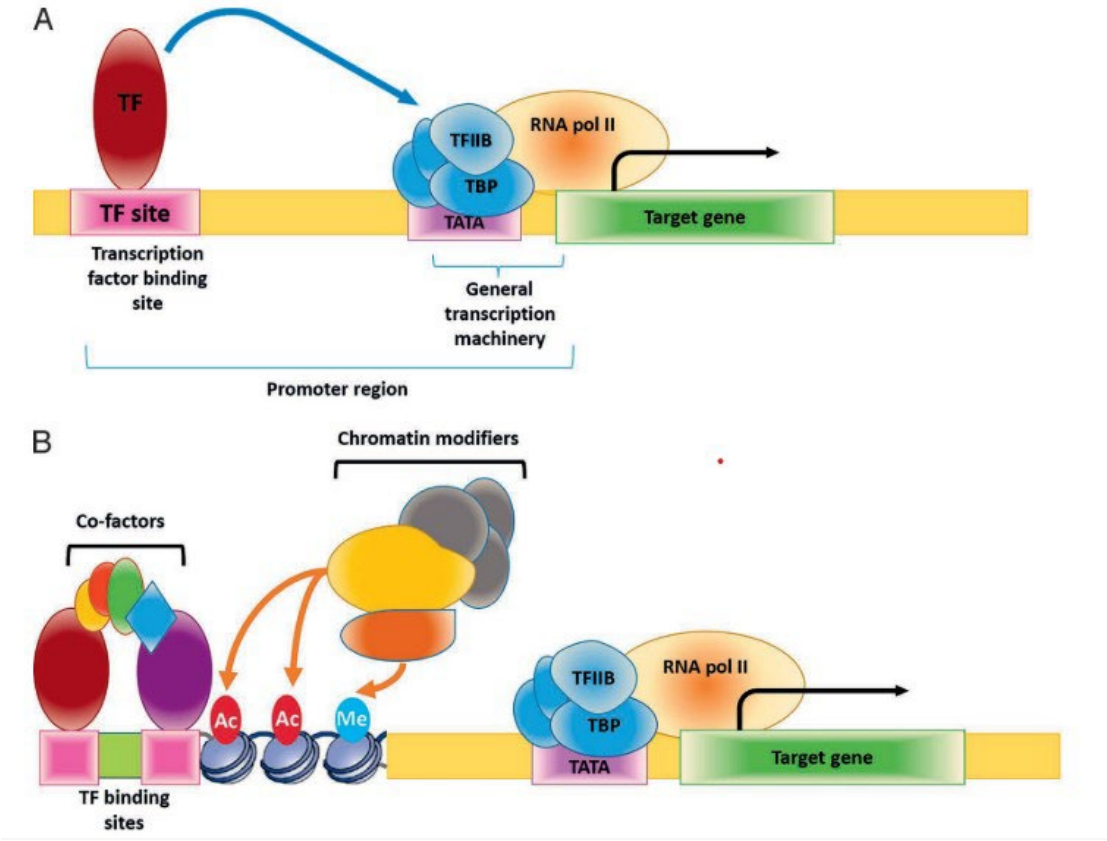

Figure 1.12 Illustrative depiction of the transcription process for a single gene, influenced by a solitary transcription factor. (A) A basic perspective on the transcription of a single gene, facilitated by a single transcription factor. (B) A comprehensive overview of the primary elements associated with the regulation of a single gene, encompassing both enhancers and inhibitors under the categories of cofactors and chromatin modifiers. Ac: acetylation; Me: methylation; TF: transcription factor; TBP: TATA-binding protein; RNA pol II: RNA polymerase II; TFIIB: transcription factor IIB (Nam & Reineke, 2017).

At its most basic level, transcription happens when a transcription factor attaches to a gene's promoter, boosting the creation of a primary transcript by enlisting the general transcription apparatus (as shown in Figure 1.12A). However, this basic viewpoint is generally considered

insufficient. A more comprehensive understanding of gene transcription encompasses the interactions among one or more transcription factors and a set of proteins with enzymatic functions. These enzymes modify the chromatin around the gene's promoter, a necessary precondition for the general transcription machinery to bind and initiate mRNA synthesis (as shown in Figure 1.12B) (Latos et al., 2015).

The epithelium-specific ETS (ESE) transcription factors are defined by their epithelial-specific expression profile (Luk et al.,2018). All ETS factors possess a common 85 amino acid (aa) ETS DNA binding domain. They control gene expression by attaching to the primary GGAA/T regulatory sequence and they are specific to epithelial cells that hold a distinct role in determining epithelial growth, differentiation, and carcinogenesis (Sharrocks,2001; Feldman et al.,2003).

Based on the homology of their DNA binding domain, these are divided into 2 groups: ELF3, ELF5 and EHF, SPDEF (Luk et al.,2018). Like all the transcription factors, ETS transcription factors integrate into multiple signaling pathways and affect gene expression. In this way, they regulate essential cellular processes such as proliferation, differentiation, and apoptosis, thus display an important role in various tissues development and specific epithelial tissues' homeostasis. (Piggin et al.,2016; Luk et al.,2018).

Elf5 expression was found in some organs such as prostate, kidney, lung, skin krts and exocrine glands during embryo organogenesis. (Gallego-Ortega et al.,2013). The studies of Zhou et al.,2005 and Donnison et al.,2005 showed deletion of Elf5 leads to embryonic death in knockout mice (Donnison et al.,2005; Zhou et al.,2005).

It has been shown that Elf5 is necessary for early embryogenesis in mice (Zhou et al.,2005) and it displays a decisive role in the trophoblast SC (TSC) fate processes of the very life stage (Ng et al., 2008; Hemberger et al., 2010; Gallego-Ortega et al.,2013). Analyses of genome-wide binding sites for Elf5 in TSCs show that it often binds to the same target locations, including its own

genes. This creates a self-sustaining transcriptional network specific to TSCs (Kidder & Palmer, 2010; Adachi et al.,2013; Chuong et al.,2013; Latos et al.,2015).

Elf5 expression is typically limited to organs and tissues with an abundance of glandular or secretory epithelial cells, like the kidney and mammary gland, as well as the mature krts of the skin (Choi et al.,2008). In the mammary gland, ELF5 is very richly expressed in the luminal cells and increased significantly during pregnancy and lactation. It is necessitated for the proliferation and differentiation of mammary epithelial cells during pregnancy and lactation (Luk et al.,2018).

Elf5 also determines secretory alveolar epithelial cell fate from luminal progenitor cell population. Overexpression of Elf5 induces the differentiation of virgin mammary epithelium and the deletion of Elf5 leads to the failure of alveolar cells differentiation. (Oakes et al.,2010; Chakrabarti et al.,2012). The increased SC/progenitor cells population and activity are also found in Elf5-null virgin animals. (Chakrabarti et al.,2012).

Review of publicly accessible genomic data shows that mutations in ELF5 are rare in human cancers. However, in cancer, the ELF5 expression is significantly changed compared to normal tissues. In breast cancer, ELF5 has been observed to play both oncogenic and tumor-suppressive roles. In most of the studies conducted so far, ELF5 has been shown to act as a tumor suppressor in prostate, bladder, ovarian, and renal cancers. ELF5 expression in cell line models of these cancers hinders cell proliferation and survival (Lapinskas et al.,2011; Chakrabarti et al.,2012; Kalyuga et al.,2012; Gallego-Ortega et al.,2015; Wu et al.,2015; Yao et al.,2015; Piggin et al.,2016; Li et al.,2017; Yan et al.,2017; Omata et al.,2018).

Amplification of Elf5 is observed in 2–6% of cases in cancers of the upper gastrointestinal tract (including esophageal and gastric cancers), as well as in ovarian, head and neck, and breast cancers. In contrast, occasional deletions of Elf5 have been identified in prostate, sarcoma, bladder, and lung cancers, as well as in acute myeloid leukemia (AML) and gliomas.

Elf5 has been reported to exhibit both tumor-promoting and tumor-suppressive roles in breast cancer, with these functions potentially linked to the molecular subtype of the disease (Luk et al.,2018). Analysis using Oncomine (www.oncomine.org) revealed that Elf5 expression is low in tumors expressing oestrogen receptor (ER), progesterone receptor (PR), or ERBB2, and elevated in the "triple-negative" subtype lacking these markers. Furthermore, Elf5 expression is associated with high tumor grade and adverse clinical outcomes, including early recurrence, metastasis, and mortality.

Elf5 expression is significantly correlated with the overall survival of triple-negative breast cancer (TNBC) patients (Kalyuga et al.,2012; Omata et al.,2018). These effects contribute to the specification of an oestrogen-insensitive cell fate, mediated through the modulation of ER, Forkhead box protein A1 (FOXA1), and other transcriptional regulators in luminal cells, alongside the induction of basal-like characteristics in basal cells.

It has been demonstrated that Elf5's transcriptional activity suppresses oestrogen signaling in luminal breast cancer, enhances the expression of basal phenotypic traits, and defines gene expression patterns that distinguish molecular subtypes. Additionally, Elf5 exerts a proliferative influence that can contribute to the development of resistance to antioestrogen therapy in luminal breast cancer (Kalyuga et al.,2012).

In prostate cancer, the loss of Elf5 protein expression is correlated with a reduction in the expression of the epithelial marker E-Cadherin and an increase in the expression of the mesenchymal marker N-Cadherin. Knockdown of Elf5 in prostate cancer cell lines has been shown to induce epithelial-mesenchymal transition (EMT), particularly in the presence of Transforming Growth Factor Beta (TGFβ). Moreover, Elf5 has been demonstrated to inhibit EMT by blocking TGFβ signaling, achieved through binding to and suppressing SMAD3 (Yao et al.,2015).

In ovarian cancer, some studies revealed a decrease in Elf5 mRNA expression in epithelial ovarian cancer tissues. This reduction in expression is implicated in the onset and progression

of the disease. Elf5 may inhibit the invasion and metastasis of ovarian cancer cells through the regulation of matrix metalloproteinase-2 (MMP-2) and MMP-9. Furthermore, it appears to accelerate the cell cycle and promote apoptosis by upregulating the expression of P21 and caspase-3 in human ovarian cancer tissues (Yan et al.,2017).

In the skin, Elf5 expression is restricted in the differentiated cells of the inner root sheath of the hair follicle and increases during krts differentiation *in vitro.* (Luk et al.,2018). Yet, ELF5's role in skin development, homeostasis, cancer and ageing is unknown.

1.6 Aim of Thesis

In adult, SCs inhabit specific microenvironments within each tissue. These cells replace tissue cells lost during standard homeostasis and mend injured tissues. The capacity of a SC for self-renewal hinges on the nature of the dynamic interactions between SC proteins with external cues from the surrounding niche. The understanding and regulation of these interactions is not just crucial for typical SC biology but is also pivotal for understanding ageing and cancer processes.

While the skin is used as a primary example to discuss major aspects of this phenomenon, insights from various adult SC systems are integrated to pinpoint common principles and outline unique mechanisms across different adult SCs. EpiSCs possess multipotent capabilities and they can be easily sourced without the ethical and political concerns associated with embryonic SCs.

Given the characters of EpiSCs, including their abundance, accessibility, and ability to form and differentiate the epidermis, leveraging these cells presents a promising approach to tissue restoration (Yang et al.,2019). Moreover, the HF, which is often referred to as a unique dynamic regenerating mini organ throughout adult life, is intricately regulated for the purpose of

generating, sustaining, and continually cycling HF. Additionally, it contributes to the production of the keratinized hair shaft and plays a role in the re-epithelialization of damaged skin. This multifaceted regulation covers systems biology, SC biology, regenerative medicine, chrono-biology, and translational medicine studies from alopecia to carcinogenesis and regenerative medicine. Key regulatory concepts that have been identified in mice (i.e. HFSC activation, quiescence and overall cellular dynamics during HF cycling and morphogenesis), also apply to human HFs. This translates the marker expression profile of murine HFSCs to human system with the well-known knowledge of the similarity and difference (Ji et al.,2021; Li & Tumbar.,2021; Ohyama, 2007; Owczarczyk-Saczonek et al.,2018; Schneider et al.,2009).

There are limited options to isolate and grow skin EpiSCs and control their activation and proliferation, differentiation *in vitro*, which could be used to develop potential cell or gene therapy in skin ageing and cancers. Therefore, there is important to review the EpiSCs isolation and growing method and then investigate potential targets to control the SCs' activation, proliferation, and differentiation through molecular manipulation such as Elf5 and its target genes.

The aim of this body of work was to investigate the role of Elf5 in regulation of EpiSCs and associated progenitor activation, proliferation, and differentiation from skin morphogenesis to homeostasis. The first part of this thesis is to investigate the expression patterns of Elf5 during mouse skin and HF embryogenesis and homeostasis. Then the functions of Elf5 in krts were assessed with loss/gain function *in vitro.* The second part focuses on the functional role of Elf5 in epidermal basal SCs and HF bulge SCs through colony forming assays. At the end, target identification of Elf5-associated pathways was performed using RNA and ChIP sequencing analysis in both primary krts and SCs of skin and HFs. Taken together, this body of work aims to identify potential therapeutic targets for SC-based interventions in conditions related to skin homeostasis, ageing and disorders, including cancers. This involves the cultivation and regulation of EpiSCs and their progenitors, with the goal of influencing and controlling their cellular activities.

Chapter 2

Materials and Methodology

2.1 Reagents and solutions

2.1.1 Reagents and materials

Reagent	Catalogue number	Company
0.25% Trypsin-EDTA	25200-072	ThermoFisher
0.45µm nitrocellulose membrane	1620115	BIO-RAD
2-Mercaptoethanol	125470010	ThermoFisher
3,3',5-Triiodo-L-thyronine sodium salt (T3)	TT5516	Merck
30% Acrylamide/Bis solution (37.5:1)	1610158	BIO-RAD
5X Saline-sodium citrate (SSC)	15557-044	ThermoFisher
Acetic acid	10171460	ThermoFisher
Acetic anhydride	320102	Merck
Adenine	A8626	Merck
Agarose	11496950	ThermoFisher
Ammonium persulfate (APS)	161-0700	BIO-RAD
Ampicillin Sodium Salt	BP1760	Fisher Scientific
Baphthol AS-BI phosphate	N2125	Merck
Blocking reagent	11096176001	Roche
BM Purple AP substrate	11442074001	Roche
Bovine serum albumin (BSA)	BP9702	Fisher Scientific
BT chelex 100 resins	143-2832	BIO-RAD
Calcium chloride ($CaCl_2$) 0.5M	C/1400/60	Fisher Scientific
Cholera Toxin	C8052	Merck
Chondroitin sulfate sodium salt from shark cartilage (CSC)	C4384	Merck
cOmplete ULTRA Protease inhibitor cocktail tablets, Mini EDTA-free	04906837001	Merck
DAPI	D9542	Merck
Deionised (DI) formamide	F9037	Merck
Diethyl pyro carbonate (DEPC)	D5758	Merck
DMEM media (+4.5g/L D-glucose, -L-glut, -pyruvate)	11960-044	ThermoFisher

DMEM/F-12 Ham (3:1) High Glucose (+L-glutamine, CaCl2, -Sodium bicarbonate)	AT189	HIMEDIA
DPX mounting medium	06522	Merck
EDTA UltrPure 0.5M, pH8.0	15575-020	ThermoFisher
Epidermal growth factor from murine submaxillary gland	E4127	Merck
Ethanol	BP8202	Fisher Scientific
Formamide	F9037	Merck
Glycerol	G/0650/17	Fisher Scientific
Hanks' Balanced Salt Solution (HBSS) without Ca^{2+}, Mg^{2+}	88284	ThermoFisher
Hydrochloric acid	7647-01-0	Merck
Heat-inactivated Fetal bovine serum	11550356	Fisher Scientific
Hematoxylin	BP2424	Fisher Scientific
Heparin	BP2524	Fisher Scientific
HEPES	BP310-100	Fisher Scientific
Hydrocortisone	H0888	Merck
Insulin from bovine pancreas	16634	Merck
Isopropanol	BP2618	Fisher Scientific
Kanamycin Sulfate	BP906-5	Fisher Scientific
LB Broth	L3022	Sigma-Aldrich
Levamisole hydrochloride	187870100	ThermoFisher
L-Glutamine (200mM)	25030-081	ThermoFisher
Lipofectamine 3000	L3000001	ThermoFisher
Magnesium Chloride ($MgCl_2$)	223210010	ThermoFisher
Milk powder		Marvel
(EMEM) Minimum Essential Medium -Eagle with Earle's BSS (with non-essential amino acids, L-glutamine, without calcium)	BE06-174G	Lonza
Mitomycin C (MMC)	BP2531	ThermoFisher
N, N, -Dimethylformamide (DMF)	D4551	Merck
New Fuchsin	2121410000	ThermoFisher
MEM Non-essential amino acid solution 100X	M7145	Merck

Normal Donkey Serum	S30	Merck
Normal Goat Serum	191356	MP Biomedicals
Nuclear fast red solution	N3020-100	Merck
OCT medium	KMA-0100-00A	ThermoFisher
Paraformaldehyde	P/0840/53	Fisher Scientific
Penicillin/Streptomycin (10,000U/ml)	15140122	ThermoFisher
Polybrene	TR-1003-G	Merck
Ponceau S	10454915	ThermoFisher
Propidium Iodide	P1304MP	ThermoFisher
PsiCHECK-2	C8021	Promocell
PureCol Collagen Type I (Bovine)	5005	Advanced Biometrix
qPCRBIO SyGreen High ROX	PB089618-041-6	PCR Biosystems
Reduced serum OptiMEM	31985070	ThermoFisher
Rhodamine B	132311000	ThermoFisher
RiboRuler High Range RNA ladder	SM1821	ThermoFisher
RNase A	10109169001	Roche
Sheep Serum	16070096	ThermoFisher
SOC outgrowth medium	B9020S	New England Biolabs
Sodium Chloride (NaCl)	10316943	Fisher Scientific
Sodium Deoxycholate	D6750	Merck
Sodium dodecyl sulphate (SDS)	BP1311-1	Fisher Scientific
Sodium nitrite	G7398	Merck
Subcloning Efficiency DH5α Competent Cells	18265017	ThermoFisher
SybrSafe	533102	ThermoFisher
TEMED	161-0800	BIO-RAD
Triethanolamine (TEA)	421630010	ThermoFisher
Tris Base	BP152	Fisher Scientific
Tris-HCl	BP1758	Fisher Scientific
Tri-sodium citrate (dihydrate)	6132-04-3	Merck
Triton X-100	BP151-500	Fisher Scientific
TRIzol	R050-1-50	Zymo-Research
Tween-20	BP337-500	Fisher Scientific
Vectashield antifade mounting medium with DAPI	H-1200	Vector Labs
Versene	15040-033	ThermoFisher

Filter paper, 5-13µm pore size	11445248	ThermoFisher
Xylene	534056	Fisher Scientific
Yeast RNA	AM7118	ThermoFisher
PCRBIO DNA ladder IV	PB40.14-01	PCR Biosystems
Pageruler plus pre-stained protein ladder	26619	ThermoFisher

2.1.2 Solutions and Buffers

SOLUTIONS	COMPOSITION
PBS (Phosphate buffered saline) 10X	137mM NaCl, 2.7mM KCl. 10mM Na_2HPO_4, 2mM KH_2PO_4, pH7.4
RIPA Buffer	150mM NaCl, 0.5% Deoxycholate, 0.1% SDS, 50mM Tris Base, 1% Triton 100, 1 X protease inhibitor tablet, pH 7-8.
4 X Sample Buffer	0.25M Tris-HCl, 0.28M SDS, 40% glycerol, pH 6.8
Lower Buffer	1.5M Tris HCl, 0.4% SDS, pH 8.8
Upper Buffer	1.5M Tris HCl, 0.4% SDS, pH 6.8
Running Buffer	25mM tris-base, 0.192M glycine, 3.5mM SDS, pH7.4
Transfer Buffer	25 mM Tris, 192 mM Glycine, 20% (v/v) Methanol
TBS (Tris Buffered Saline)	50mM Tris-Cl, 150mM NaCl, pH7.6
TBST	TBS + 0.1% TWEEN20
ponceau	5% acetic acid, 0.1% ponceau

2.1.3 Kits:

Kit	Catalogue number	Company
Direct-zol RNA MiniPrep Kit	R2050	Zymo-Research
Micro BCA Protein Assay Kit	23235	ThermoFisher
qPCRBIO cDNA Synthesis Kit	PB30.11-02	PCR Biosystems
Quick-DNA Miniprep Plus Kit	D4068S	Zymo-Research
SuperSignal West Pico PLUS Chemiluminescent Substate	34577	ThermoFisher
EZ-PCR Mycoplasma Detection Kit	20-700-20	Biological Industries Israel Beit Haemek Ltd

2.1.4 Plasticware

Item	Catalogue number	Company
1.5ml microcentrifuge tubes	72.690.001	Sarstedt
12-well plate	CC7682-7512	StarLab
15ml sterile tubes	62.554.503	Sarstedt
2.0ml microcentrifuge tubes	72.695.500	Sarstedt
24-well plate	CC7682-7524	StarLab
40µm cell strainer	22-363-547	ThermoFisher
50ml sterile tubes	62.547.254	Sarstedt
60mm dish	CC7682-3359	ThermoFisher
6-well plate	CC7682-7506	StarLab
70µm cell strainer	1-800-766-7000	ThermoFisher
96 well semi-skirted plates	E1403-6200	StarLab
96-well plate	83.3924	Sarstedt
96-well plate white bioluminescence plate	165306	ThermoFisher
Glass coverslips	12323148	ThermoFisher
Haemocytometer	145-0011	BIO-RAD
Petri-dishes	12654785	ThermoFisher
Polyolefin sealing film for qPCR, Self-adhesive	E2796-9895	StarLab
Serological pipettes, 10ml	86.1254.001	Sarstedt
Slide mailers	HEA15986	HeathrowScientific
SuperFrost plus microscope slides	631-0108	VWR
T75 flasks	83.3910.002	Sarstedt
Cell Scraper	08100241	ThermoFisher

2.1.5 Antibodies:

Name	Catalogue number	Company
Allophycocyanin (APC) Streptividin	405207	BioLegend
Anti-Digoxygenin-Rhodamine, Fab fragments	11207750910	Roche
Anti-Guinea Pig IgG Alexa Fluor 555	A21435	ThermoFisher
Anti-Mouse IgG, HRP linked	7076S	Cell Signaling
Anti-Rabbit IgG Alexa Fluor Plus 488	A32731	ThermoFisher
Anti-Rabbit IgG Alexa Fluor Plus 647	A32733	ThermoFisher
Anti-Rabbit IgG, HRP linked	7074S	Cell Signaling
Anti-Rat IgG Cyanine5	A10525	ThermoFisher
CD34	ab8158	Abcam
CD34 (RAM34)	13-0341-82	ThermoFisher
CD49f (integrin α6)	555736	BD Biosceinces
Cytokeratin 1 (Krt1)	ab93652	Abcam
Cytokeratin 15 (Krt15)	BP5077	OriGene
Elf5	A718	2B Scientific
GAPDH	ab8245	Abcam
Histone 3 (H3) XP	4499	Cell Signaling
Ki67	Ab16667	Abcam
Ly-6A/E (Sca-1)	11-5981-82	ThermoFisher
Rock1	MBS9610378	MyBioSource

2.1.6 Transfection/Transduction Kits and Reagents

Reagent	Catalogue number	Company
pControl EGFP	MG203230	OriGene
Elf5 (NM_010125) Mouse Tagged ORF Clone (pCMV6-AC-GFP)	MG203230	OriGene
ON-TARGETplus Mouse Elf5 (13711) siRNA -SMARTpool	SO-2917858G	Dharmacon
mirVana miRNA Mimic Negative Control #1	4464058	ThermoFisher
Scrambled shRNA control in pGFP-C-shLenti shRNA Vector Original plasmid	TR30021	OriGene
Elf5 Mouse shRNA Plasmid (pGFP-C-shLenti TR30023) A, B, C, D	TL510161	OriGene
Elf5 (NM_010125) Mouse Tagged ORF Clone mGPF (pLenti-C-mGFP-P2A-Puro PS100093)	MR203230L4	OriGene
Lenti-vpak Packaging Kit	TR30036/7	OriGene
qPCR Lentivirus Complete Titration Kit	LV900	Abm

2.2. Cell culture

2.2.1 Cell line

Cell line	**Characteristic**
HEK293T cells (Human embryonic kidney 293T cells, ATCC CRL-11268)	The HEK293 cell line was established through transformation of human embryonic kidney cells exposed with adenovirus type 5 DNA fragments (Graham et al., 1977). HEK293-T is a derivative of the HEK293, which expresses SV40 T-antigen mutant. This T-antigen expression enables plasmids constructed with the SV40 origin of replication to replicate into the cell during transfection (DuBridge et al., 1987). Because of their easy and highly efficient transfection to produce vectors, they are commonly used as intermediate human-based packing cell lines to produce lentiviral vectors. (Merten et al.,2016).
Swiss 3T3 cells (Swiss mouse embryonic 3T3 dermal fibroblasts, ATCC CCL-92)	3T3 cell line was immortalized from Murine embryonic dermal fibroblasts with characters as its name: “3T3”, an abbreviation of the protocol 3-day transfer period with 3×105 cells plated at each passage. (Hynds et al., 2018). The growth-arrested 3T3 cells as feeder cells by g-irradiation (GI) and mitomycin-C (MC) treatments have been used for decades to grow target cells especially at low or clonal density. (Llames et al.,2015)

2.2.2 Cell Media Preparation and Cell Culture

The HEK293T cells were cultured in DMEM high glucose medium, L-Glutamine, Pyruvate (Gibco, 41966-029) supplemented with 10% (v/v) Heated inactivated FBS (ThermoFisher, UK), 1% (v/v) non-essential amino acids (ThermoFisher, UK) without antibiotics. Cells were seeded in T75 tissue treated flaks and incubated at 37°C in a 95% air/5% CO2 atmosphere. Cells were passaged at about 70% confluency. Swiss 3T3 cells were cultured in DM supplemented with 10% (v/v) heat-inactivated fetal bovine serum, 2% (v/v) penicillin/streptomycin and 2mM L-glutamine. Cells were seeded in T25 tissue treated flaks and incubated at 37°C in a 95% air/5% CO2 atmosphere. Cells were passaged every 3 days at about 80-90% confluency.

2.2.3 Cryo-conservation and Recovery of Frozen Cells

Cells in T75 flasks were cultured until they reached approximately 80-85% confluency. Afterward, the growth media was aspirated, and the cells were treated with 3 ml of 0.25% Trypsin-EDTA for around 2-5 minutes at 37°C to facilitate cell detachment. These cells were then gathered into 6 ml of complete growth media and centrifuged at 300 x g for 5 minutes at ambient temperature. The resulting cell pellets were reconstituted in 5 ml of Freezing Medium Cryo-SFM (Sigma-Aldrich, C-29912) and aliquoted into five cryovials, with each vial containing 1 ml. These vials were then stored in a -80°C freezer using a specialized freezing container, ensuring a cooling rate close to -1°C/min. After 24 hours to 2 months, the cells were shifted to liquid nitrogen for extended storage. For revival, cells retrieved from long-term storage underwent rapid thawing, after which they were resuspended and gently seeded into the appropriate growth media and suitable cell culture containers for subsequent incubation and treatment.

2.2.4 Cell Passage and Cell Counting

When cells achieved expected confluency, the growth media was aspirated and 3ml 0.25% Trypsin-EDTA for T75 Flask or 1 ml for T25 Flask was added. After 2-5 mins incubation at 37°C until at least 90% cell detachment. Then an equal volume of complete growth media was used to neutralize Trypsin-EDTA. The detached cells were collected and centrifuged at 300 x g for 5 mins at room temperature. Cell pellets were resuspended in appropriate volume of complete growth media before cell counting and seeding at specific densities in new tissue culture treated vehicles based on experiments designs. Take out an appropriate volume of aliquot from the cell suspension, and the vital cells were counted with 0.4% of trypan blue automatically using cell counting slides (Bio-RAD, #1450015, Cell Counting Slides for TC10™/TC20™ Cell Counter, Dual-Chamber) and automatic cell counter (BIO-RAD, TC20TM Automatic Cell Counter).

Sample of one automatic counting result:

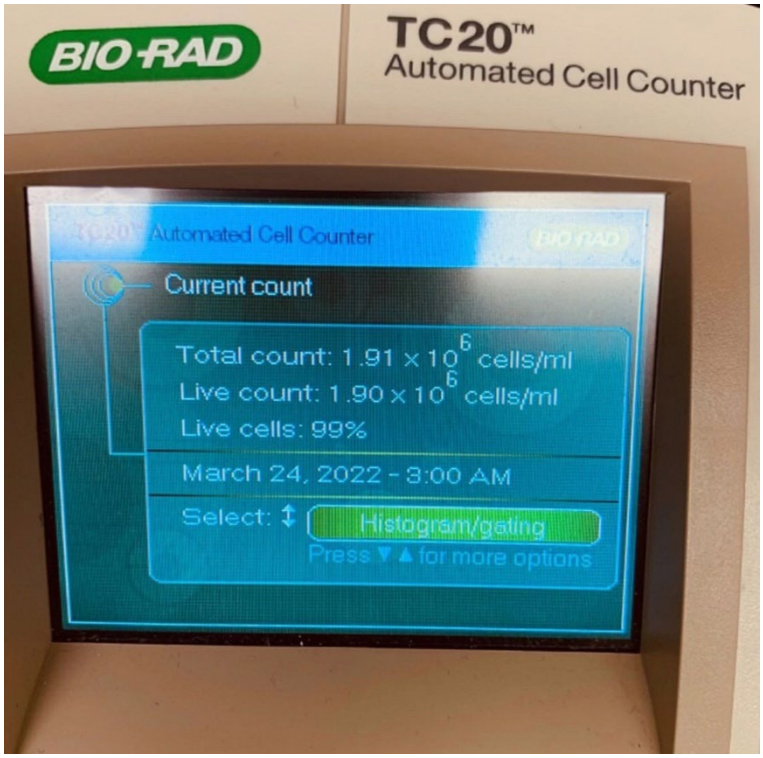

Figure 2.1 Sample of one automatic counting result with TC20TM Automatic Cell Counter

2.2.5 Mycoplasma Screening

All cell lines were regularly tested for Mycoplasma infection using EZ-PCR Mycoplasma Detection Kit (Biological Industries, Israel, Cat. No.: 20-700-20) following kit instruction. The primer sets targeted a highly conserved segment within the mycoplasma's 16s rRNA gene region. When subjected to a PCR reaction and subsequently run on an agarose gel, they yield a 270bp band. With this kit, a mycoplasma-positive sample presents bands at both 270bp and 357bp. In contrast, a mycoplasma-negative sample reveals only a 357bp band. If PCR inhibition occurs, no bands will be visible, while the negative control consistently shows a 357bp band. Mycoplasma PCR reactions were performed with supernatant of cultured cells that were collected from growing cell cultures over a minimum of 24 hours. All used cell lines for the following experiments were tested Mycoplasma negative.

1ml of cell culture supernatant was collected and centrifuged at briefly at 250xg to settle any cellular debris. Then, move the clear supernatant to a fresh sterile tube and centrifuge at 15,000-20,000xg for 10 minutes to collect mycoplasma. Even if not always visible, a pellet may form. Gently pour off the supernatant, retaining the pellet. Reconstitute the pellet in 50µl of the provided Buffer Solution, ensuring thorough mixing using a micropipette. Finally, heat the mixture to 95°C for 3 minutes. Prepare the following reaction mixtures in PCR tubes: Sample(s), Negative control, and Positive control, combine them using the reagents indicated below:

1. Test samples: Prepare the reaction mixture in a PCR tube by combining the reagents shown below:

Reagents	Volume
H_2O (for PCR)	33µl
Reaction Mix	10µl
Internal control DNA	1µl
Internal control primers mix	5µl
Positive control DNA	1µl
Total	50µl

2. Negative control: in a separate PCR tube, use 5µl of distilled H2O as test sample in the reaction mixture above.

3. Control DNA templates: prepare the reaction mixture in a separate PCR tube by combining the reagents shown below:

Reagents	Volume
H_2O (for PCR)	29µl
Reaction Mix	10µl
Test sample	5µl
Internal control DNA template	1µl
Internal control primers mix	5µl
Total	50µl

Table 2.1 EZ-PCR Mycoplasma Detection Kit PCR amplification preparation

Number and Cycles	Temperature (°C)	Time
1	94	30 seconds
35	94	30 seconds
	60	120 seconds
	72	60 seconds
1	94	30 seconds
1	60	120 seconds
1	72	5 minutes
	4	∞

Table 2.2 EZ-PCR Mycoplasma Detection Kit PCR amplification setting

The PCR-amplified samples were run on a 2% agarose gel to confirm the presence and size of the amplified product.

An example of our negative sample is shown in Figure 2.2.

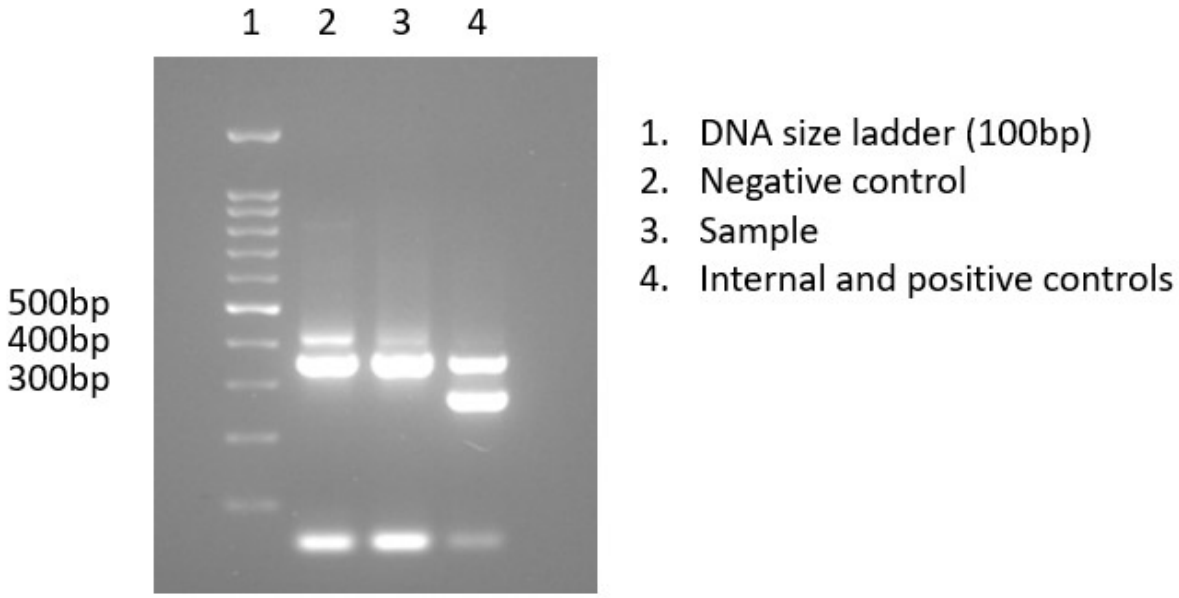

Figure 2.2 Mycoplasma Screening. Negative mycoplasma detection example- Absence of band at 270bp but shows only a 357bp band with Internal DNA template as control.

2.3 Mice and primary cell culture

2.3.1 Mice Strain

The mice used were C57BL/6 wild type mice (Charles River Laboratories, UK). They were maintained in a 12-hour light/12- hour dark cycle and fed standardly. All animal procedures were conducted following guidance of UK Home office Animals (Scientific procedures) Act 1986 and approved by Nottingham Trent University (Nottingham, UK) Ethics Committee.

2.3.2 Isolation and culture of Primary Mouse Keratinocytes (PMEKs) from new-born mice

2.3.2.1 Isolation of Primary Mouse Keratinocytes (PMEKs) from new-born mice

The complete Primary Mouse Epidermal Keratinocyte (PMEK) media was prepared prior to mouse dissection with EMEM calcium-free medium (Lonza, Switzerland) supplemented with 0.05mM calcium (ThermoFisher, UK), 4% (v/v) chelated heat-inactivated fetal bovine serum (ThermoFisher, UK) see Appendix B 1 for chelating heat-inactivated fetal bovine serum), 0.4µg/ml hydrocortisone (Merck, UK), 5µg/ml insulin (Merck, UK), 10ng/ml epidermal growth factor (Merck, UK), 10-10M cholera toxin (Merck, UK), 2-9M 3,3',5-Triiodo-L-thyronine sodium salt (T3; Merck, UK), 100U/ml penicillin (ThermoFisher, UK), 100 µg/ml streptomycin (ThermoFisher, UK), and 2mM L-glutamine (ThermoFisher, UK).

Tissue culture (TC) plates were pre-coated with collagen coating solution (5ml of hanks balanced salt solution (HBSS, ThermoFisher, UK), 500µl 1M HEPES (ThermoFisher, UK), 100µl 5% BSA (Fisher Scientific, UK), 50µl of 3mg/ml PureCol collagen type I (Advanced BIOMATRIX, UK), excess was aspirated and the plates were left without cover to air dry the coating in a laminar-flow hood before seeding PMEKs in the complete PMEK media.

New-born mice post-natal day 2 or day 3 were sacrificed following National and Institutional regulations. Killed mice were immersed in 50 ml tubes with 70% ethanol for 1 min, three times

and then rinsed with PBS for 1 min, three times and then place tubes on ice; In a laminar-flow hood, remove the skin using sterile dissection tool in the inside side of the 100-mm sterile culture dish. Refer to Appendix B 3 for the procedure images (Based on Lichti et al., 2008).

The collected epidermises were minced with scissors until the suspension can be pipetted up and down easily with a 5-ml pipette. After pipetting about 50 times up and down with a 5ml pipette, filter the minced suspension through a 70µm cell strainer into a new 50-ml conical tube. Centrifuge the cell suspension at 250 x g for 5 min at 4°C. The supernatant was discard carefully and the pellet was resuspend in PMEK complete media. Cells were counted and plated in dedicated collagen type I coated plates for the downstream designed experiments. Cells were incubated at 33°C in a 92% air/8% CO2 atmosphere.

2.3.2.2 The complete Low calcium and High Calcium Primary Mouse Epidermal Keratinocyte (PMEK) media preparation

To investigate the effects of cell proliferation and differentiation in vitro, the isolated neonatal PMEK cells were incubated for 24 hours, 48 hours and 72 hours in Low calcium and High calcium complete media. The previously mentioned complete Primary Mouse Epidermal Keratinocyte (PMEK) media was used as complete low Calcium Primary Mouse Epidermal Keratinocyte (PMEK) media with 0.05mM CaCl2, the complete high Calcium Primary Mouse Epidermal Keratinocyte (PMEK) media is based on the complete low Calcium Primary Mouse Epidermal Keratinocyte (PMEK) media but upgraded to higher calcium concentration, with final concentration CaCl2 of 2mM.

2.3.3 Isolation and culture of epidermal stem cells isolation and cell culture from adult female mice

2.3.3.1 Complete mouse epidermal stem cells media

The Complete mouse epidermal stem cells media was prepared but without adding Calcium with DMEM/F-12 (3:1, HimediaLabs, Bulgaria)) supplemented with 10% (v/v) chelated fetal bovine serum (See Appendix B 1 for the Preparation of chelated Fetal Bovine Serum), 10ng/ml epidermal growth factor, 0.5µg/ml hydrocortisone, 10^{-10}M cholera toxin, 5µg/ml insulin, 1.8^{-4}M Adenine (Merck, UK), 100U/ml penicillin, 100µg/ml streptomycin, 0.3mM Calcium.

2.3.3.2 Epidermal stem cells isolation

The 7-9 weeks old female C57BL/6 mice were sacrificed following National and Institutional regulations. The dorsal and ventral skins were collected and shaved closely to skin. After rinsing with 70% ethanol an iced PBS as for new-born mice described previously. The hypodermis was scraped off with scalpel. The epidermis and dermis were cut into about 2cm square pieces and were immerged in 0.25% trypsin-EDTA (ThermoFisher, UK) with dermis downside overnight at 4°C as for new-born mice described previously. The next day, the skin pieces were put in one 10-mm culture dish containing ice cold 0.25% trypsin-EDTA, the epidermis with HFs were scrapped from dermis using scalpel. Complete mouse epidermal stem cells media but without Calcium was added to neutralize trypsin-EDTA. After 30 mins of stirring at 37°C, the mixture was minced and homogenized as for new-born mice described previously, then filtered using a 70µm and 40µm cell strainer. The cell suspension was centrifuged at 300 x g for 10 minutes and the pellet was suspended in 1ml of EMEM calcium-free medium, ready for the downstream FACS step.

Refer to Appendix B 4 for the procedure of Stem cell isolation from adult mouse skin for live cell sorting:

2.4 Loss or gain of Elf5 activities in PMEK by transfection

2.4.1 Amplification of Plasmids by E. coli

Amplifying a plasmid using Escherichia coli (E. coli) involves transforming the plasmid into the bacterial cells and allowing the bacteria to replicate the plasmid.

Plasmid DNA containing the target sequence and their checked map for antibiotic resistance were verified and the 1ng/ µL of stock with sterile molecular biology-grade water was prepared. DH5α competent E. coli cells (ThermoFisher, 18265017) were thawed on ice until fully liquid (approximately 20 minutes on ice). Subsequently, 50 µL of the thawed DH5α competent E. coli cells were added to a pre-chilled 1.5 mL Eppendorf tube. To 50 µL of the thawed DH5α competent E. coli cells on ice, 5 µL of plasmid (1 ng/µL stock) was added, and the mixture was gently mixed with a tip. The competent cell/DNA mixture was incubated on ice for 20 minutes. Each transformation tube was subjected to heat shock by being placed into a 42°C heating block or water bath for 45 seconds. Subsequently, the tubes were returned to ice for 2 minutes. 500 µL of S.O.C. Medium (ThermoFisher, KMA-0100-00A) was added at room temperature (RT).

The Eppendorf tubes were incubated at 37°C for 1 hour in an orbital shaker at 80 RPM for gentle agitation. Subsequently, 50 µL of the above mixture was added to one LB agar plate, which was typically prepared with a specific antibiotic at a concentration of 50 µg/mL and streaked using a bacterial streaker. The LB agar/competent cells mixture was placed upside down and incubated overnight (between 16-18 hours) at 37°C in a hybridization oven.

On the following day, single colonies were selectively picked using a p20 tip (yellow) and were placed into 15 mL of freshly prepared and autoclaved LB Broth bacterial growth medium (Sigma-Aldrich, # L3022), which contains 50 µg/mL of specific antibiotics. Prior to adding the colony, the mixture was thoroughly mixed. The bacterial cultures were incubated in 15 mL tubes overnight (for a duration between 16-18 hours) at 37°C using an orbital shaker at 80 RPM with the tube lids slightly loose. The bacteria/LB mixture was centrifuged at full speed at room temperature. The supernatant was carefully removed using a p1000 tip and the pellet was frozen at -20°C until DNA extraction was planned.

The DNA extraction was carried out using the Quick-DNA Miniprep Plus Kit (Zymo-Research, R2050) following kit instruction. The concentration and quality of the DNA were assessed using Nanodrop.

2.4.2 Transfection

Seeded PMEKs were transfected at about 60% confluency by incubation with appropriate quantity of Plasmids or 200nM Elf5 siRNA and their controls. The growing media was replaced by appropriate volume of transfection mixtures including Lipofectamine 3000 in reduced serum for 4 hours at 33°C in a 92% air/8% CO2 atmosphere. Then the transfection mixture was replaced by complete normal (Low Calcium) or high Calcium PMEK media and continued cell culture for subsequent 24, 48 and 72 hours before downstream step.

2.5 In house lentiviral particles production

The Elf5 lenti-shRNA/ORF (knock-down, KD or overexpression) plasmids, including Scrambled shRNA control in pGFP-C-shLenti shRNA Vector Original plasmid , Elf5 Mouse shRNA Plasmid (pGFP-C-shLenti TR30023) and Elf5 (NM_010125) Mouse Tagged ORF Clone mGPF (pLenti-C-mGFP-P2A-Puro PS100093), which were designed for gene silencing and/or expression of the ORF gene with GFP fluorescent marker, were sourced from Origen. Transcriptional activation of these lenti-shRNA/ORF plasmids leads to the binding of the DNA sequences containing the consensus nucleotide core sequence GGA[AT], resulting in TK promoter activation, which drives expression of downstream gene clone insert (~762 bp). Lentiviral Packaging Kit contents the Package Plasmids. Upon co-transfection of the plasmids in HEK293 cells, all required sequences are available to produce and package a viral particle containing the transgene of interest. Only the region between the viral LTRs of the transfer vector is packaged within the viral capsid.

2.5.1 Elf5 Lentiviral construct plasmids and packaging plasmid Co-Transfection in HEK293T cells for lentiviral particles production

Frozen HEK293T cells were Seeded in 2 X T75 flasks (1:8 T75 per vial), 48 hours later, cells achieved about 90% confluence, gave living cells counting 36 X 10^6 cells in total. Cells were split into 10-cm plates, 2 plates per group, thus 6 X 10-cm plates, at a density of 2.5 X 10^6 cells per plate in 10 ml of complete HEK293T media. Next day, the culture medium was changed with fresh media, cells were at 30-40% confluency, left cells for about 1-2h and prepared the co-transfection mix in each labelled Eppendorf tubes following Lentiviral Packaging Kit guideline.

Vessel	Cells	Lenti Plasmids	Packaging Plasmids	Transfection Reagent	Opti-MEM	Reactions per Kit
10-cm dish	$2.5x10^6$	5 µg	6 µg	33 µL	1.5 mL	10
6-well plate	$5x10^5$	1 µg	1.2 µg	6.6 µL	250 µL	50
12-well plate	$2.5x10^5$	0.5 µg	0.6 µg	3.3 µL	100 µL	100

Table 2.3: Lentiviral Packaging Kit guideline for transfection mixture preparation

1.5ml of Opti-MEM, 5ug of lenti-plasmid with 6ug packaging plasmid were pipetted and mixed gently, then 33µL of TurboFectin transfection reagent was added to the diluted DNA (not the reversed order), then pipetted gently to mix completely and incubate at RT for 15 minutes before adding 1.5ml of the transfection solution dropwise directly to each well containing complete growing media. Swirled the cells to evenly distribute the transfection mixture and cells were incubated at 37C, a 95% air/5% CO2 atmosphere. After 12-18 hours, the transfection mixture was replaced with complete growing media. 24 hours later after the changing media timepoint, the first batch of viral supernatant was harvested from the culture dish and stored at +4C. 10ml of fresh complete growing media was added. The second batch of viral supernatant was collected again 24 hours later (48h later after the first changing media timepoint) from the culture dishes and added to the first. Store at +4C for the downstream precipitation step.

2.5.2 Precipitation of Lentiviral particles

To concentrate lentivirus, Protamine sulphate (PS, Fisher UK) and Chondroitin sulphate C (CSC, SIGMA) were used. The collected viral supernatant from both baches was filtered through a 0.45 µm filter to remove cellular debris and then precipitated with 80 ug/ml of PS and 80 ug/ml of CSC. The mixtures were incubated for 16–20 h on a shaker at 4°C, and then were centrifuged for 30 min at 10,000 X g at 4°C. The lentivirus pellets acquired using the above methods were resuspended at 1/100 of the original volume using complete media and aliquots of 20ul were made to avoid frozen-thaw cycle in the future use and stored at –80°C Freezer.

2.5.3 Titration of lentiviral particles

ABM qPCR lentivirus titre kit (ABM, LV900) was used to quantify amount of virus particles present (concentration). Titration of viral particles by RT-qPCR method was performed using standards as part of kit for standard curve. qPCR performed directly from collected viral supernatant with primers from kit.

1ul of ROX reference dye provided by the kit was added to the BlasTaq 2x qPCR titre master mix for the machine QS5 (Thermofisher, Serial number: 272521899) use. Series Dilution of 'Test Viral Particles' was prepared as below with autoclaved PBS: Neat(undiluted),1:10,1:100,1:1000 and 1:10,000. Standard control dilutions were Performed, five, 10-fold serial dilutions of the standard control DNA by diluting 5ul DNA into 45ul nuclease-free H2O in each step. The dilutions range from 1/100 – 1/100,000 will be used for generating the standard curve. Set-up the reaction mixture and performed the reaction mix under the following cycling conditions based on Kit protocol:

Step	Temperature	Duration	Cycles
Enzyme activation	95C	3 mins	1
Denaturation	95C	15 seconds	35
Annealing/Extension	60C	1 min	

Table 2.4: qPCR set-up for Titration of lentiviral particles

2.5.4 Lentivirus concentration calculation

Plot Ct value (Y-axis, linear scale) vs. Virus titer (X-axis, logarithmic scale). Generate a logarithmic regression using the four Standard Control DNA dilutions to determine the unknown virus sample titer using y = mln(x) + b from the trendline equation.

2.6 Epidermal stem cells Fluorescence Activated Cell Sorting (FACS) from adult female mice skin

To separate the different epidermal stem cell subpopulations, the FACS was used with different mouse epidermal stem cell markers Ly-6A/E (Sca-1), CD34 (RAM34) and CD49f (α6).

Epidermal stem cells subpopulation	Markers
Hair follicle bulge stem cells	CD34+/CD49fHigh/Sca-1-
Basal keratinocytes	CD34-neg/ a6PE+High/Sca1+
Suprabasal keratinocytes	CD34-/CD49fLow/Sca-1-)

Table 2.5 Cell populations with different stem cells markers combinations

The freshly isolated epidermal cells from adult female mice of 7–9-week-old as described previously were filtered with a 40µm cell strainer before aliquoting into different dedicated tubes, which present different stem cell subpopulations.

The cells were incubated with different combinations of antibodies based on designed subpopulations as in the Table 2.5 in 2% (v/v) bovine serum albumin/PBS staining buffer, rotating in the darkroom for 1 hour at 4°C. Then cells were washed with 1ml of high energy

FACS wash buffer (phenol-free, Ca2+-free, Mg2+-free HBSS containing 1% penicillin-streptomycin, 20mM D-glucose, and 2% chelated heat inactivated fetal bovine serum), followed by centrifuge at 16000 X g at 4°C. Cell pellets were resuspended and stained again with secondary antibody APC streptavidin if indeed in the darkroom for 1 hour at 4°C, followed by washing and centrifuge as for primary antibodies. Then cells were resuspended in final volume (as in the Table 2.6) with iced staining buffer, and ready to go FACS. Each of the fluorochromes control was read first for the Fluorescence compensation use, then the different cell populations: HF bulge stem cells, Basal krts and Suprabasal krts were sorted by MoFlo XDP cell sorter using 'gentle FACS' to limit sorting shearing force and to achieve maximum living cells viability as described in Pruszak et al., 2007. Data was analysed through Summit software (Beckman Coulter, UK). Cells were seeded immediately for downstream colony forming assay or RT-qPCR analysis. See Table 2.6 below for FACS sample preparation and gating data sample (Appendix B 2).

Tube	Sample and Volume	Sample Type	Volume for Ab staining with Staining Buffer (µl)	Primary Abs (µl)	Secondary Abs (µl)	Resuspension Buffer (µl)	Notes	Cell population	Laser (Ex / Em)
1	Unstained (50 µl)	Control	300	-	-	1000		Negative control	
2	36 - PE (R-phycoerythrin) (50 µl)	Control	300	1:50	-	1000	BD Biosciences Cat N : 555736	Epi - SCs	480,565 / 578
3	Sca1-FITC (50 µl)	Control	300	1:50	-	1000	Fisher UK: 15248319	Epidermal progenitor	Green Laser: 495/519
4	CD34 - bio (50 µl)	Control	300	1:50	(1 : 300) 1µl into 300µl of staining buffer Streptavidin - APC	1000	Fisher UK: 15279529	HF - SCS	Green Laser: 633 nm
5	DAPI (0.5µg / ml stock) (50 µl)	Control	300	5µg / ml		100	Live / Dead stain Regular powder version.	Should be used just before running of cell	Blue Laser: 350/470
6	Analysis (750 µl)	Analyte	800	16µl of each Abs	Streptavidin - APC (1 : 300) 1µl into 300µl of staining buffer	800	Final tube with all samples (All Abs)	Experimental tube DAPI - as above tube 5	

Table 2.6: living adult mice stem cells FACS samples preparation

2.7 Colony Forming Assay (CFA)

2.7.1 Feeder Cells preparation

Swiss 3T3 cells were seeded in tissue treated 24 well plates from growing proliferating actively cells, which were pre-seeded in T25 tissue treated flaks 3 days earlier as previously described. When achieved 70-80% confluence, changed fresh complete media at least one hour before the treatment. Then added 8µg/ml mitomycin C (MMC) in each well and swirled gently. After 2 hours incubation at 37°C in a 95% air/5% CO2 atmosphere, cells were washed with autoclaved PBS and added fresh complete grow media, incubated in growing condition before stem cells seeding.

2.7.2 FACS sorted epidermal stem cells seeding and Lentivirus transduction

2.7.2.1 FACS sorted stem cells seeding

Once FACS finished, the feeder cells complete media was replaced by prepared complete mouse epidermal stem cells media as described previously. Appropriate sorted cells were seeded on the feeder cells layer bason on experiment design and cultured at 32°C in a 95% air/5% CO2 atmosphere.

2.7.2.2 Lentivirus Transduction and Imaging

2.7.2.2.1 Lentivirus MOI Calculation

Multiplicity of infection (MOI) is a ratio of infection units/infection targets.

$$MOI = \frac{\text{Virus Titre x Virus Volume}}{\text{Total Cell Number}}$$

Estimation of MOI can be optimized experimentally, higher may cause cytotoxicity. Here MOI=20 was used.

2.7.2.2.2 Lentivirus Transduction and Imaging

After 48 hours post-seeding, FACS sorted SCs were transduced with titrated Elf5 lenti-shRNA/ORF and Scrambled shRNA control lentiviruses. The appropriate volume of each lentivirus group for MOI of 20, which was calculated based on cell numbers and lentivirus titration, was added, mixed gently in fresh complete SC media, 8µg/ml polybrene was also added (ThermoFisher, UK) in the mixture before replacing the growing media to increase transduction efficiency. After 4 hours of incubation at 32°C in a 95% air/5% CO2 atmosphere, fresh growing media was replaced and then changed every 48-hours and cultured for 7-14 days based on experiment design. GFP and phase imaging of whole well was performed every day using IncuCyte S3 live cell analysis instrument (Sartorius, Germany).

2.7.3 Clonogenic assay

To investigate the colony forming capacity of the isolated SCs, the final post transduction colonies were also visualized using Rhodamine stain as described in Gillespie and Owens, 2019 in addition to IncuCyte S3 live cell analysis instrument imaging. After 7-14 days post seeding, the SCs growing media was aspirated off and 500ul of Versene was added in each well. After 1–2 min incubation at room temperature, the feeder layer was detached by gentle pipetting repeatedly (krts will not detach). Then after 2 times gentle washing with autoclaved PBS (Be careful not to detach colonies), cells were fixed with 4% PFA for 1 hour at room temperature. Gentle washing twice again with autoclaved PBS, then cells were covered with 1% rhodamine B diluted in ddH2O and stained at room temperature overnight. Next day, Rhodamine B solution was taken out and cells were washed gently with autoclaved PBS several times and the plates were put upside down to dry the wells. Afterwards, plates were imaged using Leica THUNDER imager (Leica, Germany). Colonies were counted and diameter determined using the ImageJ macro, Cell Colony Edge as done previously (Choudhry 2016, Pickup, Hu et al. 2023).

2.7.4 Colony Forming Assay (CFA) Analysis

2.7.4.1 IncuCyte S3 live cell analysis instrument images analysis

The images obtained from IncuCyte S3 live cell analysis instrument was analyzed with ImageJ software. They were analyzed as described in Guzman et al, 2014 using ColonyArea, an ImageJ Plugin to automatically quantify the colony growth area, thus the output parameter "colony area percentage" as well as the "colony intensity percentage". The border of each well was cleared out with "Clear Outside", thus cropped. Each well image was converted into an 8-bit greyscale image. The image was made in a series of stack images. The ''Colony_thresholder'' of the plugin was set up for each image, and the software reads the difference in intensity and outputs the intensity value, which distinguishes between the background (high intensity values) and GFP positive cell colonies (low intensity values). In this way, this value was set up as the background threshold. The software recreated a new series of rescaled images after removing the high intensity background by applying the initial intensity to the initial 8-bit greyscale image of each well. In this new series, images with higher intensity values reflect the higher density of stained cells. ''Colony_measurer" function was used subsequently to quantify the colony growth. The "colony area percentage" and "colony intensity percentage "were generated for each well. The former reflects more cell survival and growth, while the latter in addition also gives a sight on how the cells can grow in dense colony, which can be also used to analysis the difference between wells that have a similar colony area coverage while the numbers of cells in these colonies are different.

2.7.4.2 Rhodamine stain images analysis

Rhodamine stain images were taken using Leica THUNDER imager (Leica, Germany). Colonies were counted and diameter determined using the ImageJ macro, Cell Colony Edge as done previously (Choudhry 2016, Pickup, Hu et al. 2023) and manually. The ImageJ macro–Cell Colony Edge was downloaded from the following link: https://sourceforge.net/projects/cell-colony-edge/files/.

2.8 Flow Cytometry

Transfected PMEKs with Plasmids or 200nM Elf5 siRNA and their controls as described previously were detached with 0.25% Trypsin-EDTA. After neutralized with added complete media, cells were centrifuged at 3000 RPM for 5 mins at 4°C. The pellet was washed with precooled autoclaved PBS, centrifuged again and then resuspended the pellet by adding drop by drop Iced 70% ethanol/PBS when vortexed. The cells were fixed at -20°C for 30 minutes. Then, centrifuged the cells at 3000 RPM for 5 minutes, resuspended and washed the pellet in ice cold PBS. Centrifuged again before freezing and storing the pellet in -20°C or added 100ul of 100mg/ml RNase A to the pellet to get rid of RNA and incubated at RT for 10 minutes. PBS was added to give a final volume of 1ml. Cells suspension was filtered through a 50um filter and put cells into a new Eppendorf. 50ul from each sample was taken to a new tube to be used as background control (unstained background check). The cells were subsequently incubated with propidium iodide (20mg/ml) at 4°C for 30 minutes in the dark. After-which, cells are ready for FACs analysis, store at +4C until ready. Single cell suspension, in which double stranded DNA binding to PI, was run through Beckman Coulter Gallios, with excitation at wavelength of 535nm and an emission of 615nm. For each sample, unstained sample a control reading performed at first as fluorescence compensation and then the stained sample was run. For each sample, more than 50% gated single cells and minimum of 10,000 events were acquired and then used for cell cycle analysis with Beckman Coulter Kaluza Analysis Software (Beckman Coulter, UK). One Example for gating strategy is shown in Figure 2.4

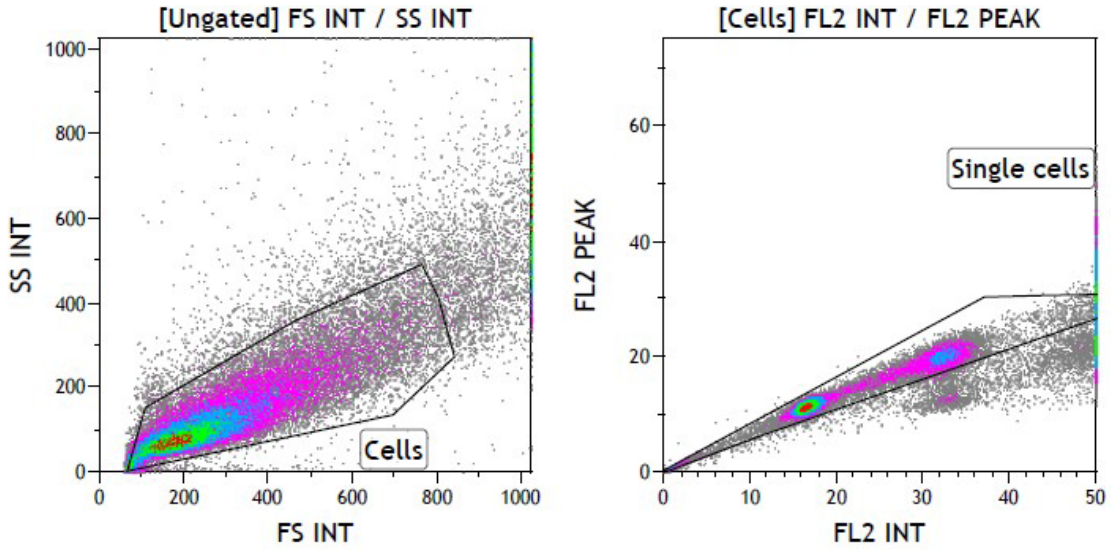

Figure 2.4 Flow Cytometry gating strategy

2.9. Gene and Protein Expression Analysis

2.9.1. RNA Analysis

2.9.1.1. RNA Extraction

Total RNA was extracted from cells grown in designed conditions using Direct-Zol RNA MiniPrep kit. Media was aspirated out and washed with autoclaved PBS. The TRIzol reagent was added to lyse cells before collecting each sample in ice cooled Eppendorf tube. RNA extraction was performed with Direct-Zol RNA MiniPrep kit following Kit instruction. An equal volume of 100% ethanol was added to the cell lysis followed by vigorous vortex. The mixture was transferred to a Zymo-spin IIC column from the kit and centrifuged at 16,000 x g at room temperature (RT) for 30 seconds. Flow through was discarded and 400µl of RNA wash buffer was added to the column and centrifuged again as precious step. The flow through was discarded. 5µl of DNase I to 75µl of DNA digestion buffer was added carefully to the silica-based column matrix at the bottom of the column, to which the Nucleic acids are bind, and incubated at RT for 15 minutes. Then 400µl of RNA PreWash was added followed by centrifugation as previous step. Flow

through was discarded and repeated this step. 700µl of RNA Wash buffer was added to the column followed by centrifugation at 16,000 x g at RT for 1 minute. Finally, 30µl of DNase/RNase free water was added carefully the column matrix, and the column was transferred to a new Eppendorf tube. After centrifugation at 16,000 x g at RT for 1 minute, the samples were stored at -80°C before subsequent step.

2.9.1.2. RNA Quantification

Extracted total RNA was quantified and at the same time the quality was checked using NanoDrop TM 8000 spectrophotometer (Thermofisher, UK). The absorbance of RNA samples was measured after blanking with DNase/RNase free water at 260nm. Nucleic acids absorb UV light at 260nm whilst proteins and ethanol absorb at 280nm. The 260/280 ratio of 2.0 is the indicator for pure RNA without protein or ethanol contaminants. The integrity of total RNA was evaluated using agarose electrophoresis stained with ethidium bromide. 800ng of total RNA aliquot was used for electrophoresis with 1% agarose in 1X TAE buffer gel and run in 1 X TAE buffer with 5µl of ethidium bromide. After approximately 30 minutes at 100 volts, the electrophoresis was finished, the gel was imaged with iBright FL1000. Two strong bands of the 18s (2kb) and 28s (5kb) indicate the intact RNA. An example of intact RNA image is shown in Figure 2.5.

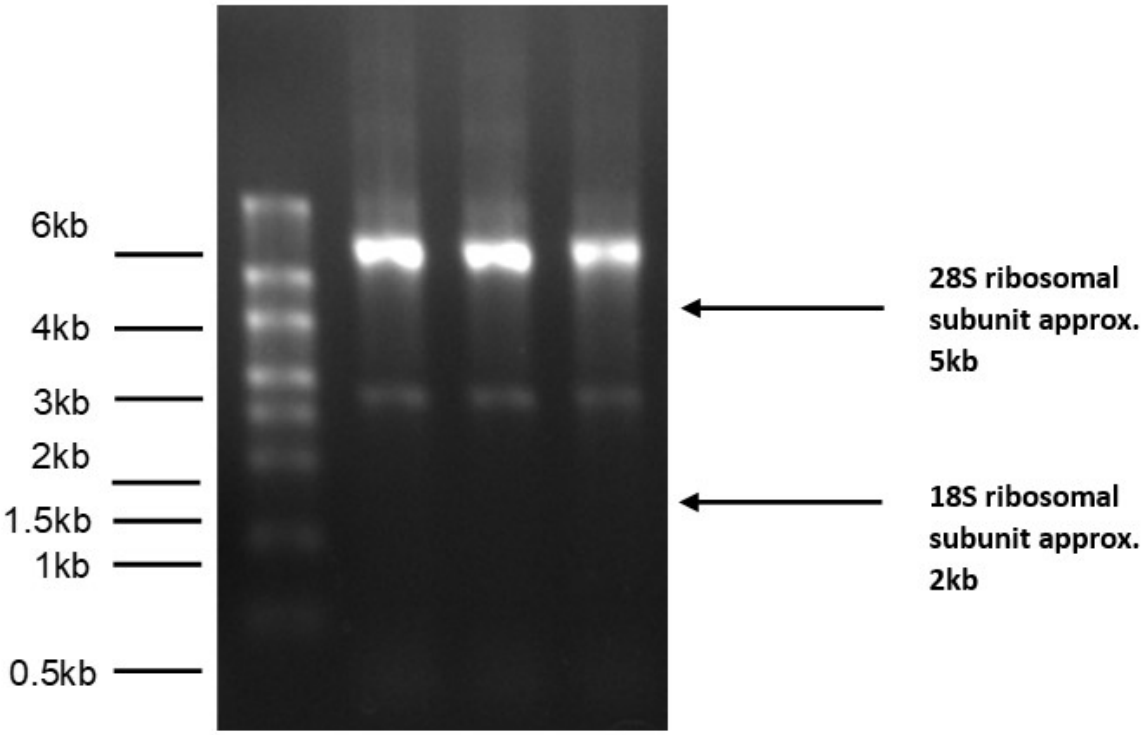

Figure 2.5 Example of an RNA Integrity Analysis by Gel Electrophoresis

2.9.1.3 cDNA Synthesis via Reverse Transcription

Complimentary DNA (cDNA) synthesis from extracted and quantified total RNA was performed using qPCRBIO cDNA synthesis kit.

The reaction was set up following kit instruction in PCR reaction tubes:

Reagent	**Volume (µl)**
5X cDNA synthesis mix	2.0
20X RTase	0.5
Total RNA (100ng)	X
deionised water	Final volume up to 10µl

Table 2.7 Reverse transcription reaction for cDNA synthesis

100ng of RNA was reverse transcribed in the total 10 µl reaction mixture of 2µl of 5x cDNA synthesis mix, 0.5µl of Reverse Transcriptase, 100ng total RNA and deionized water. The mixture was flick mixed and spun down, then incubated in a thermocycler set up for 42OC for 30 minutes, followed by 85oC for 10 minutes. Each sample was diluted to 50µl total volume with deionized water and then flick mixed and stored at -20oC until subsequent step.

2.9.1.4. Real-time quantitative PCR (RT-qPCR)

Real time qPCR measures the amplified PCR product per amplification cycle through either direct or indirect fluorescent dye binding to a specific target sequence hybridizing probe. The emitted dye signal accumulation during amplification allows the quantification of amplified target molecules. SYBR Green binds to double stranded DNA. With amplification of the target gene, the accumulating fluorescence dye increase of each cycle is recorded. This quantifiable fluorescent signal is proportional to amplified DNA quantity, therefore the relative amounts of a target sequence can be compared between samples. The threshold cycle (Ct) value is the cycle level at which fluorescence can be detected and reaches the fluorescent intensity of the threshold or background; That also from this point, the reaction curve starts the exponential phase. The lower the Ct value, the lower cycle number can be detected and higher specific DNA, thus RNA expression, therefore higher expression of specific target gene in the sample and vice versa.

2.9.1.5. Primer Design

Primers were designed using prediction tools: Primer3 (https://primer3.ut.ee/), UCSC genome browser (https://genome.ucsc.edu/) and NCBI (https://www.ncbi.nlm.nih.gov/tools/primer-blast/). NCBI primer blast was used to evaluate the specificity and quality of designed primers. Specific qPCR primers, ranging from 18-25 base pairs in length and featuring a GC content of 50-60%, were synthesized to achieve a melting temperature of 59-65°C. The specificity of these primers was validated through an NCBI primer blast search, which confirmed that the primers

were span an intron and the resulting amplicons would be between 90-200 base pairs in length, facilitating high levels of fluorescence without sacrificing efficiency. Details of these primers can be found in Appendix B 2.

2.9.1.6. Primer Denaturing and annealing temperature optimisation

PCR is composed of cycles of heating and cooling. Each temperature cycle is crucial to guarantee the quality of each defined stage. The RT-qPCR reaction mix was prepared as follow:

Reagent	Volume per 96 well plate (µl)
SYBR GreenBlue Mix + ROX	5
Forward primer (10µM)	0.4
Reverse primer (10µM)	0.4
Deionised water	3.2
cDNA	1

Table 2.8 The RT-qPCR reaction mix preparation for primers optimisation

50nm of Rox dye was added in the SYBR GreenBlue Mix to normalize the report dye. RT-qPCR reaction mixture was put into the thermocycler and different denaturing and annealing temperatures were set up and the melt curves were analyzed. The temperature at which a single, tall, distinct peak is formed was chosen as optimized temperature setting in future experiments.

Example of primer optimization analysis:

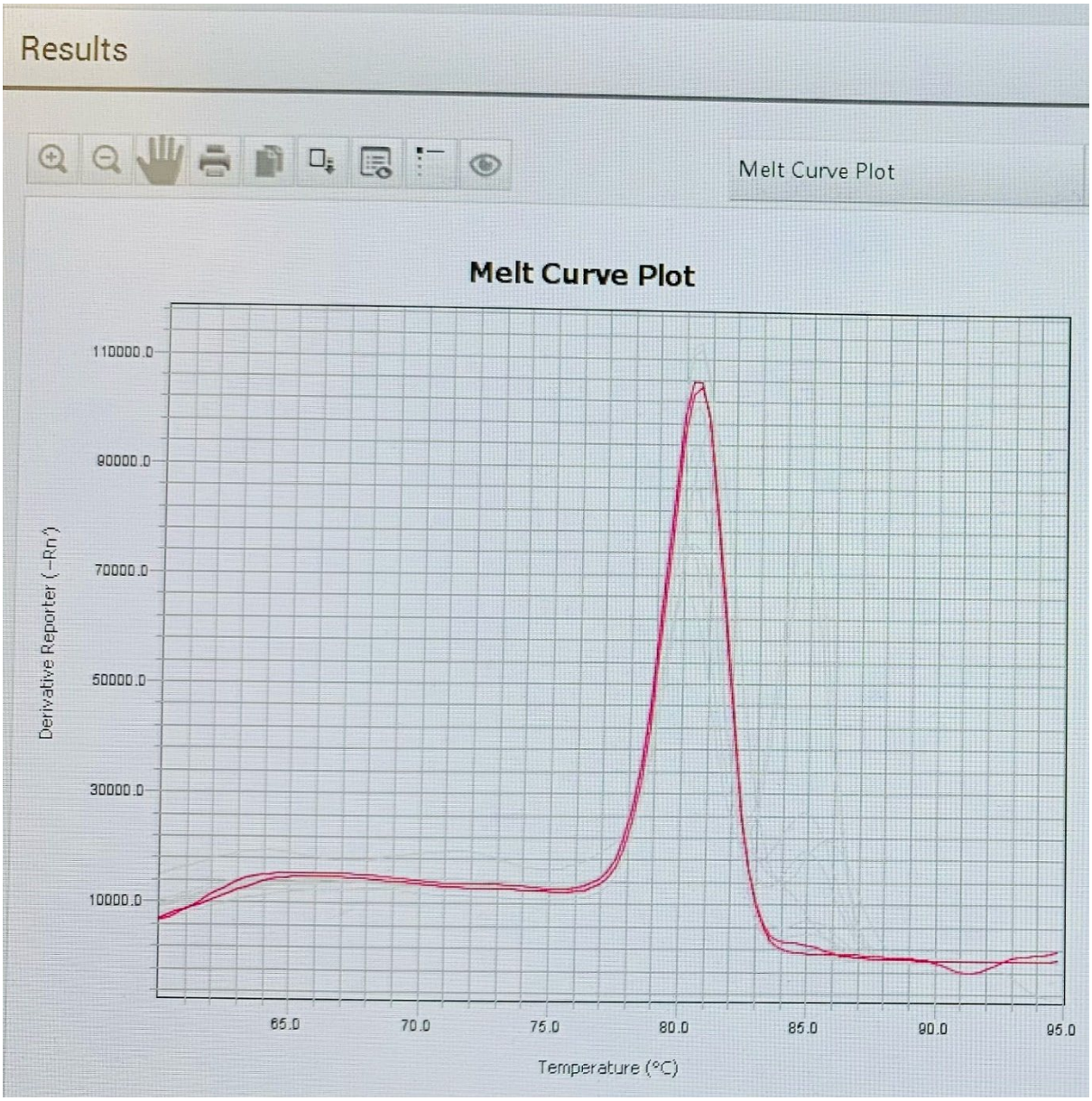

Figure 2.4 Primer optimisation melt curves analysis example with single, tall, distinct peak for each pair and its technique repeat at one of the qPCRs setting temperatures.

2.9.1.7. RT-qPCR Reaction Set up

RT-qPCR reaction was performed using SYBR Green. Designed and optimized froward and reverse paired primers for target genes, synthesized cDNA were added in the SYBR GreenBlue Mix + ROX and made up to 10µl with deionized water as described previously. Samples were run with biological triplicates and technical duplicates in QuantStudio 5 Real Time PCR system at the following conditions:

Number and Cycles	Temperature (^{O}C)	Time
1	95	2 mins
40-45	95	5 seconds
	Optimised Annealing temperature (52-66 ^{O}C)	30 seconds
	72	30 seconds
1	72	3 minutes
∞	4	∞

Table 2.9 RT-qPCR reaction set up

At least one negative control per group, in which the synthesized cDNA without Reverse transcriptase, was used to verify the amplifications of possible genomic DNA (gDNA) contamination.

2.9.1.8. RT-qPCR Data Analysis

Data was analyzed with delta-delta Ct (ΔΔCt) method, known to be used for relative quantification to calculate the relative fold change of target gene expression between different samples. Housekeeping gene Actin (Actb), which doesn't change expression between samples, was used throughout as a reference target to normalize the variations between samples. The threshold cycle (Ct) value generated from qPCR for each sample was used to calculated relative fold change in gene expression after normalization between compared samples using equation 2^ΔΔCt.

2.9.1.9. RNA Sequencing

2.9.1.9.1. RNA sequencing

The integrity of extracted and quantified total RNA samples was checked as described previously with NanoDrop TM 8000 spectrophotometer and electrophoresis on gel. Samples were sent to Novogene, UK for sequencing. However, these methods cannot check RNA degradation instead of the purity and concentration. The 28s and 18s ratio can be calculated Agilent Bbioanalyser (Santa Clara, CA). The detected percentage of degraded RNA and ratio of 2:1 of 28s and 18s is set as benchmark of intact RNA, then the RNA Integrity number (RIN) value 0-10 was calculated using software bult-in algorithm before performing sequencing using the illumine PE150 platform. A RIN value between 8-10 is considered as adequate for downstream sequencing using the Illumina PE150 platform. The data was uploaded to Galaxy web platform (https://usegalaxy.org/) for analysis.

2.9.1.9.2. Data analysis

The alignment of the data against the Mus musculus genome (mm9) was performed, and genes that exhibited statistical insignificance ($p>0.05$) were subsequently excluded from our analysis, which involved the generation of heat maps and the evaluation of gene ontology in Galaxy web platform. The FACS sorted HF bulge stem cells and basal krts after Elf5 gain and loss function through lentivirus RNA sequencing data was analyzed with Kallisto and Sleuth in R as described in Bray et al., 2016. Principal component analysis (PCA) plots and distribution of samples and sample types, were plotted in to visualize patterns and potential outliers with a high degree of sample clustering among treatments, indicating the presence of dramatic and reproducible effects on cells after treatment compared to control samples. An example of PCA plot is shown in Figure 2.5.

Figure 2.5 PCA plot of RNA sequencing samples. Each colour presents one treat group (Red: Control; Green: Elf5 inhibition; Blue: Elf5 overexpression). N=3

To identify biologically relevant pathways associated with Elf5 target genes identified through RNA-seq and ChIP-Seq, we employed the Functional Annotation tool available in Database for Annotation, Visualization, and Integrated Discovery (DAVID) v6.7. We input the relevant Entrez Gene IDs or gene symbols for this analysis (for reference, please visit david.abcc.ncifcrf.gov). Furthermore, we entered the Entrez Gene IDs into the Ingenuity Pathways Analysis (IPA) platform (http://www.ingenuity.com). This network-creation algorithm identifies key genes integrated within larger molecular pathways and networks.

2.9.2. Protein Analysis

2.9.2.1. Protein Extraction

Cells were cultured and treated based on experiments designed till ready for protein collection. The growing media was discarded, after three times washing with autoclaved PBS, the freshly made RIPA buffer was added to lyse cells but keep protein integrity of proteins. The samples were then scratched and collected, stored at -80 °C until downstream step.

2.9.2.2. Protein Quantification- Bicinchoninic acid (BCA) Assay

Micro BCA Protein assay kit was used to quantify protein by bicinchoninic acid (BCA) assay. Cu2+ ions in the reaction mix from the kit are chelated by protein and reduced to Cu1+, which reacted with BCA and produced purple colored complex with peptides of amino acids in an alkaline environment. This molecular complex can be measured with absorbance at 562nm. Serial dilution of Bovine serum albumin (BSA) from 5mg/ml to 0.08mg/ml in RIPA buffer and equal volume of RIPA as Blank were created to establish the standard calibration curve: regression line with equation. 20 µl Protein samples were diluted in RIPA buffer with 1:2, 1:3 and 1:4 dilution factors and then pipetted into a 96-well flat bottom plate as well as BSA serial dilutions and BSA Blank. 100µl of regent 'MA', 96 µl reagent 'MB' and 4 µl of regent 'MC' from kit were mixed and added into each test well. After incubation at 37°C for 2 hours in the darkness, absorbance at 562nm was read using CALRIOStar plate reader. The Regression line was plotted with equation and R square value based on known BSA concentration and obtained absorbance value minus blank absorbance. The unknown protein samples' concentration was deduced with equation. An example of one BCA Calibration Plot for Determining Protein Concentration is shown in Figure 2.6.

Example of a BCA Calibration Plot for Determining Protein Concentration

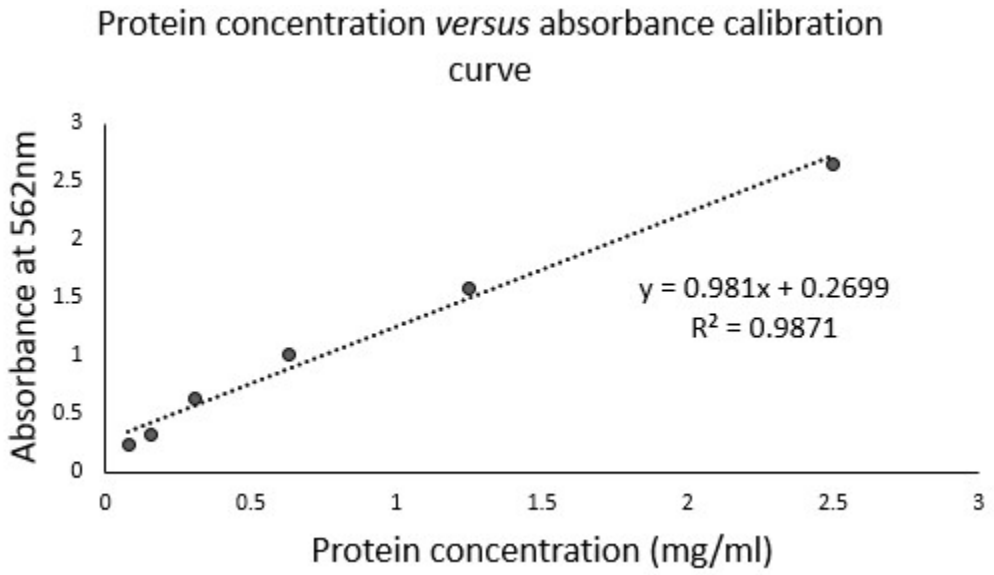

Figure 2.6 Example of a BCA Calibration Plot for Determining Protein Concentration

2.9.2.3. Western Blotting

2.9.2.3.1. SDS Gel Preparation

Sodium dodecyl sulphate-polyacrylamide gel electrophoresis (SDS-PAGE) was used to separate denatured linear proteins with a negative charge by migration towards the positive electrode based on their different molecular weight. Two polyacrylamide gels were made in BIO-RAD mini-protein tetra cell system casts: the lower resolving gel for protein separation, and the upper stacking gel, for protein loading. Gels were prepared as follow:

Ingredients for two gels	12% Resolving Gel	4% Stacking Gel
Water (ml)	4.1	3.075
4 X Upper Buffer (ml)		1.25
4X Lower Buffer (ml)	3	
30% Acrylamide (ml)	4.8	0.65
10% APS (µl)	75	25
TEMED (µl)	25	5

Table 2.10 Western blot resolving and Stacking Gel preparation

After adding TEMED at the end, mixed gently, the resolving gel mixture was pipetted into a gel chamber, 1ml of isopropanol was pipette on the top and allowed the gel to polymerize for approximately 45 minutes at room temperature, then the isopropanol was removed and left for evaporation. The stacking gel mixture was pipetted on the top and put the comb. After about 30 minutes, once gel was polymerized, the comb was removed, and the gel was transferred into an electrophoretic gel tank with appropriate volume of 1X running buffer (25mM tris-base, 0.192M glycine, 3.5mM SDS, pH7.4).

2.9.2.3.2. sample preparation, loading, separation, and transfer

5µl of 4X sample buffer (0.25M Tris-HCl, 0.28M SDS, 40% glycerol), 0.5µl of 2-Mercaptoethanol were added in 10µg of each quantified protein sample and made total volume of 20µl with RIPA buffer. The mixture was vortexed, briefly centrifuged and then heated at 98°C for 10 minutes. Samples were loaded in experiment designed order alongside an adequate molecular size ladder. 20µl of sample dye was added to any empty wells. The gel was run at 60V for stacking gel (15 minutes) and 140V for resolving gel (1 hour). The run stopped once the blue dye front had just run off the end of the gel.

Subsequently, the gel was transferred to one nitrocellulose membrane using a wet transfer method. A transfer sandwich was made from positive to negative electrode in the order of

soaked 2xs 2.5mm thick filter papers in transfer buffer, soaked 0.45µm nitrocellulose membrane, the protein gel, soaked 2xs 2.5mm thick filter papers. Then rolled with a roller to remove air bubbles. The sandwich was transferred in a transfer tank and submerged with ice cold transfer buffer (0.192M glycine, 25mM tris-base, 20% v/v methanol) in cold room at 4°C or put into one ice box. After running at 90V for 90 minutes, the membrane was taken out and stained with ponceau (5% acetic acid, 0.1% ponceau), which binds reversibly to positively charged amino acids on proteins and allows to visualize transferred proteins on the membrane. The excess ponceau was washed off with ddH2O and then 1 X TBST before downstream step or stored in 1 X TBST buffer at 4°C before next step. An example of one ponceau stained protein transferred nitrocellulose membrane is shown in Figure 2.7.

Example of a Ponceau Stained Protein Transferred Nitrocellulose Membrane

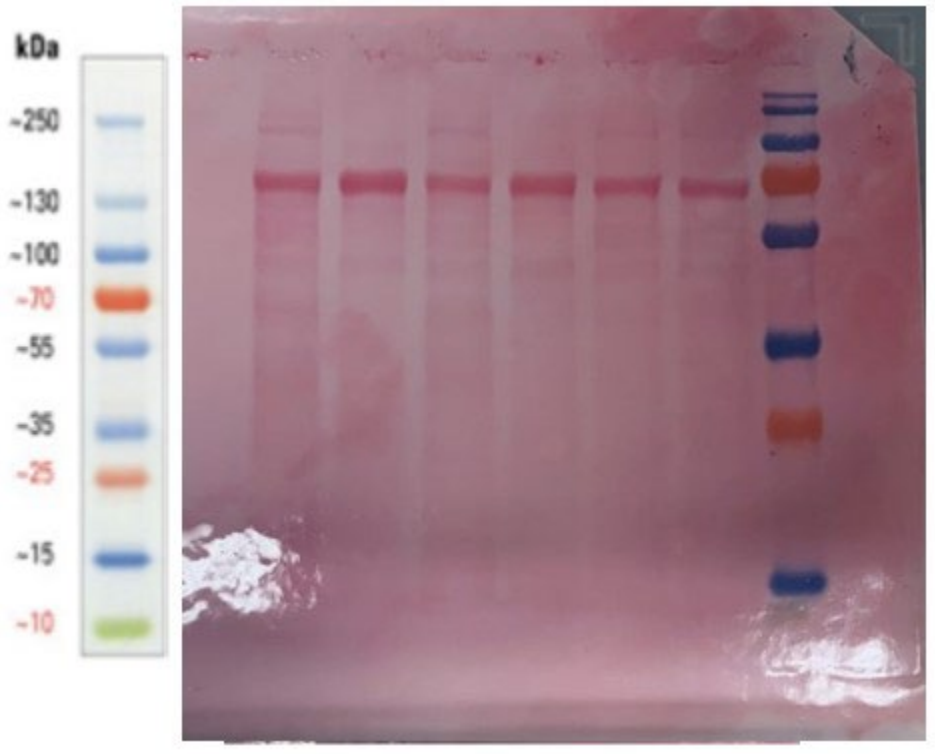

Figure 2.7 Example of a Ponceau Stained Protein Transferred Nitrocellulose Membrane

2.9.2.3.3. Immunoblotting

Membrane was blocking in 5% (w/v) milk in 1 X TBST for 1 hour at room temperature before incubated with appropriate primary antibody, diluted in 1% milk (w/v) with adequate dilution factor overnight at 4°C in dark cold room. The next day, after 3 times washes in 1 X TBST for 10 minutes, rolling at room temperature, the membrane was incubated with appropriate horseradish peroxidase conjugated secondary antibody diluted in 1% milk (w/v) with adequate dilution factor on a shaker for 1 hour at room temperature. After washes as previous step, the membrane was incubated for 5 minutes in the mixture, which contained 500µl of SuperSignal West Pico PLUS Luminol/Enhancer Solution and 500µl SuperSignal West Pico PLUS Stable Peroxide Solution from enhanced chemiluminescence system SuperSignal West Pico kit, protected from light.

The membrane was imaged with iBright FL1000 GelDoc Imager. Protein band was analyzed with densitometry using ImageJ with "Gel Analyzer" tool (Plugins > Gel > Gel Analyzer).

2.9.3. Chromatin immunoprecipitation (ChIP) and ChIP-seq

Chromatin immunoprecipitation, or ChIP, allows probing protein-DNA interactions within the natural chromatin. It was used to isolate selected enrich DNA-binding proteins along with the DNA targets. All reagents were prepared freshly prior to procedure and all used tubes (Low DNA binding tubes, sonication tubes, 15 and 30ml conical tubes) were precoated with 2% BSA in autoclaved PBS-block tubes for approx. 30 mins, rolling with blocking solution at room temperature and discard before using. The ChIP assay summary is shown in figure 2.7 below.

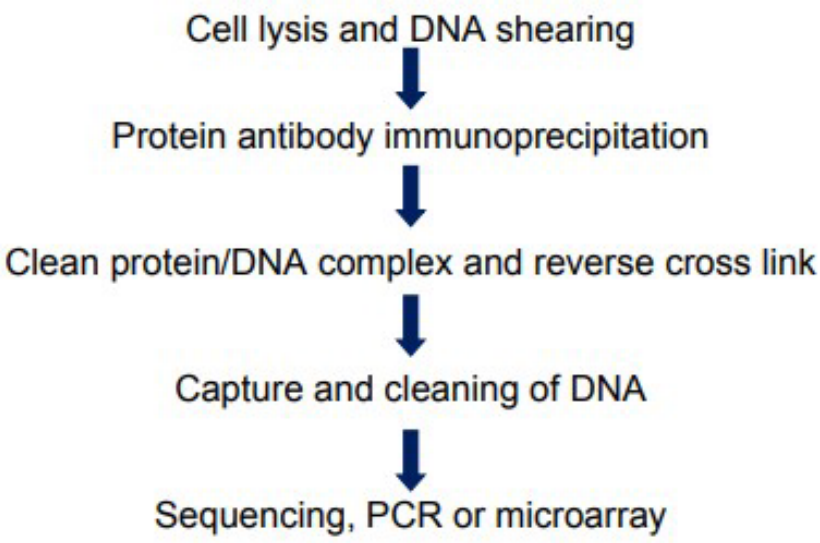

Figure 2.7 ChIP Assay summary

2.9.3.1. Crosslinking of proteins to DNA

Crosslinking reagents allow proteins "fix" to the DNA that they are binding naturally. Cells were grown at designed state till 80-90% confluence. For the target proteins that are low abundance transcription factors, the input amount should be 5 to 6 x 105 cells, our cell counting was about 4 X 106 cells per T75 Flask. The media was discarded, and cells were trypsinized and collected into a 15 ml conical tube, Cell counting was performed as previously described. Cells were centrifuged at 1000 rpm for 5 minutes at room temperature and then fixed with final 1% (m/v) freshly made 37% (m/v) methanol-free formaldehyde in fresh complete media (270 µl of 37% formaldehyde into 10ml of media) as the formaldehyde solution containing methanol can affect crosslinking. After 10 minutes at room temperature on a rocker (50-100rpm), 125nM freshly made Glycine in deionized water was added to deactivate the formaldehyde (1ml of 1.25 M Glycine for every 9ml of cross-link solution). Avoid under or over crosslinking. The mixture was centrifuged at 1000rpm for 5 minutes, then washed the pellet once with ice-cold PBS, followed by centrifugation at 1000rpm for 5 minutes. The supernatant was discarded, and the pellet was kept on ice till the downstream step. Avoid freezing samples at this stage.

2.9.3.2. Cell lysis and DNA shearing

The chromatin fragments were achieved through sonication after cell lysis.

2.9.3.2.1. Cell lysis

The cells were lysed in freshly made working lysis buffer, 6 µL of Protease Inhibitor Cocktail was added to every 10 mL of Lysis Buffer required immediately prior to use. See Lysis Buffer recipe in Appendix B 4. 200µL of lysis buffered per 1x106 cells was used to resuspend the pellet and incubated on ice for 10 minutes. After vigorous vortex for 10 seconds, the lysis suspension was centrifuged at 3000 rpm for 5 minutes. The supernatant was removed carefully and then 100ul per 1x106 cells of freshly made ChIP buffer was added to resuspend the chromatin pellet. See ChIP Buffer recipe in Appendix B 5.

The chromatin lysate was separated into two halves and transferred to two 2.0 ml low DNA binding tubes. Incubated on ice for 10 minutes and vortexed occasionally.

2.9.3.2.2. Chromatin Shearing by sonication

100ul of chromatin lysate per diagenode sonication tube was used for sonication optimization at 30s ON/30s OFF Max intensity using Diagenode Bioruptor Pico machine (Diagenode, B01060010). Following the Instrument guideline, to have the best shearing optimization, 200ul CHIP buffer were added to have final 300ul volume in the 1.5ml sonication tube. Samples were gently vortexed before and after performing each sonication round (5 cycles per round). After 30 minutes sonication, interrupt sonication after every 10 minutes and centrifuged tubes briefly or pipette gently up and down and tried to avoid bubbles and foaming. The sonicated chromatin from each chosen optimized cycle was centrifuged at 12,000 rpm at 4°C for 10 minutes and transferred the supernatant to a new vial. The chromatin solution can be used immediately or stored at -80°C after aliquoting appropriately until further use. Avoid multiple freeze/thaw cycles.

2.9.3.2.3. Sonicated chromatin fragmentation

The size of DNA fragment size should be verified before starting the immunoprecipitation step. Sonicated chromatin size check was carried out with 1.5% (m/v) agarose gel. 25 µl of each chromatin sample was piped into a 0.2 mL PCR tube followed by adding 25 µl of DNA Release Buffer and 2 µl of Proteinase K from purchased Abcam High sensitivity ChIP Kit (Abcam UK, ab185913). Then the samples were incubated at 60°C for 30 minutes followed by incubating at 95°C for 10 minutes. Then the solution was spin down to the bottom. The supernatant was transferred to a new 0.2 mL PCR vial. 30-40 µl was used for DNA fragment size analysis along with a DNA marker on a 1.5% agarose gel in 1 X TAE buffer, stained with SybrSafe for DNA visualization under ultraviolet light. The gel was run in 1 X TAE buffer at 95v for 90 minutes, then was imaged with iBright FL1000 GelDoc Imager. The length of sheared DNA should be between 100-700 bp with a peak size of 300 bp.

Then sonication of the remaining half sample with the good cycle was performed on the same day after size check. NanoDrop TM 8000 spectrophotometer was used to determine the concentration of chromatin samples, then stored at -80°C after aliquoting appropriately until further use. An example of one agarose gel analysis of the length of genomic DNA fragmented by sonication is shown in Figure 2.8.

Agarose gel analysis of the length of genomic DNA fragmented by sonication

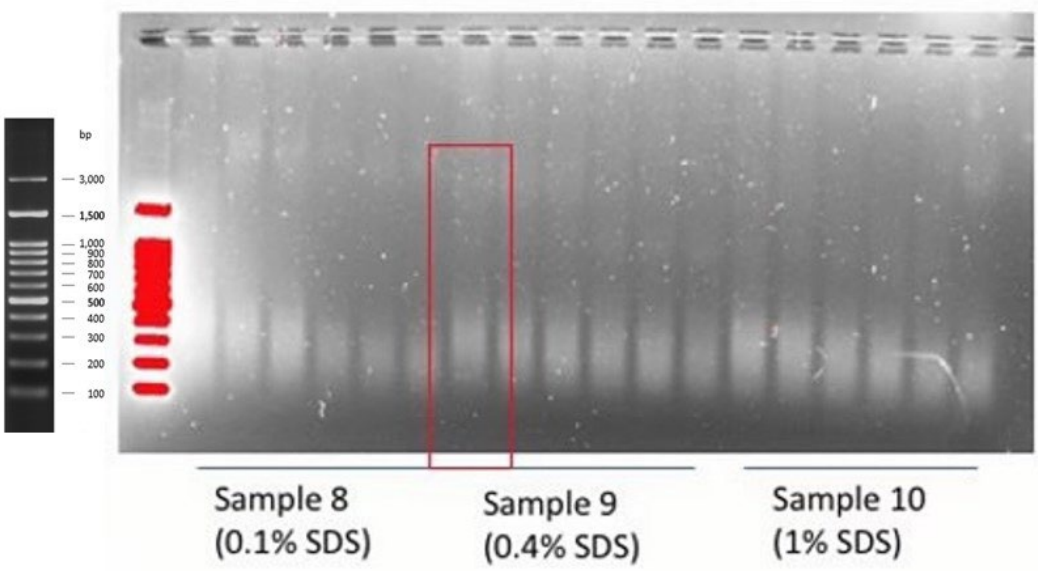

Samples order:
From Left to right:

1. Ladder
2. Sample 8 10 cycles – 30s ON/30s OFF Max intensity (25ul Chromatin solution)
3. Sample 8 15 cycles 30s ON/30s OFF Max intensity(25ul Chromatin solution)
4. Sample 8 20 cycles 30s ON/30s OFF Max intensity(25ul Chromatin solution)
5. Sample 8 25 cycles 30s ON/30s OFF Max intensity(25ul Chromatin solution)
6. Sample 8 30 cycles 30s ON/30s OFF Max intensity(25ul Chromatin solution)
7. Sample 8 35 cycles 30s ON/30s OFF Max intensity(25ul Chromatin solution)
8. Sample 9 10 cycles – 30s ON/30s OFF Max intensity (25ul Chromatin solution)
9. Sample 9 15 cycles 30s ON/30s OFF Max intensity(25ul Chromatin solution)
10. Sample 9 20 cycles 30s ON/30s OFF Max intensity(25ul Chromatin solution)
11. Sample 9 25 cycles 30s ON/30s OFF Max intensity(25ul Chromatin solution)
12. Sample 9 30 cycles 30s ON/30s OFF Max intensity(25ul Chromatin solution)
13. Sample 9 35cycles – 30s ON/30s OFF Max intensity (25ul Chromatin solution)
14. Sample 10 10 cycles 30s ON/30s OFF Max intensity(25ul Chromatin solution)
15. Sample 10 15 cycles 30s ON/30s OFF Max intensity(25ul Chromatin solution)
16. Sample 10 20 cycles 30s ON/30s OFF Max intensity(25ul Chromatin solution)
17. Sample 10 25 cycles 30s ON/30s OFF Max intensity(25ul Chromatin solution)
18. Sample 10 30 cycles 30s ON/30s OFF Max intensity(25ul Chromatin solution)
19. Sample 10 35cycles – 30s ON/30s OFF Max intensity (25ul Chromatin solution)

Figure 2.8 Agarose gel analysis of the length of genomic DNA fragmented by sonication.
Different SDS concentrations in homemade ChIP buffer and different cycles were optimised. 0.4% SDS at 10 cycles – 30s ON/30s OFF Max intensity (25ul Chromatin solution) was picked using Diagenode Bioruptor Pico machine for our samples.

2.9.3.3. Protein antibody immunoprecipitation

Freshly prepared chromatin can be directly used for the reaction. Frozen chromatin samples should be thawed quickly at RT and then placed on ice before use or kept on ice until thawed completely. Set up the Anti Elf5 ChIP grade antibody binding reactions by adding the reagents to each assay strip well from the kit according to the following table 2.11:

Reagents	Sample 1 (µl)	Sample 2 (µl)	Sample 3 (µl)	Positive control (µl)	Negative control (µl)
Antibody Buffer	50-80	50-80	50-80	50-80	50-80
Elf5 Antibody CHIP GRADE): ug/µl	0.8µg Elf5 Ab: 0.4µl	0.8ug Elf5 Ab: 0.4µl	0.8µg Elf5 Ab: 0.4µl	0.8µg Elf5 Ab: 0.4µl	0
Anti-RNA Polymerase II	0	0	0	0.8	0
Non-immune IgG	0	0	0	0	0.8

Table 2.11 Antibody binding to assay strip well reaction preparation. Note: The final amount of each component should be (a) antibodies of interest: 0.8 µg/well; (b) RNA Polymerase II: 0.8 µg/well; and (c) non-immune IgG: 0.8 µg/well.

The wells were sealed with Adhesive Covering Film Strips and incubated at room temperature for 60-90 minutes (maximum 2 hours) on an orbital shaker (100 rpm). Subsequently, the Adhesive Covering Film on the antibody binding wells was carefully peeled away to prevent contamination. The antibody reaction solution and Non-Immune IgG solution were removed from each well, followed by a single wash with 150µL of ChIP Buffer. ChIP reactions were then set up as specified in table 2.12 by adding appropriate reagents to the antibody-bound wells

(sample and positive control) or IgG-bound well (negative control), based on the measured DNA concentrations of each sample.

Reagents	Sample 1 (µl)	Sample 2 (µl)	Sample 3 (µl)	Positive control (µl)	Negative control (µl)
Antibody Buffer	50-80	50-80	50-80	50-80	50-80
Elf5 Antibody CHIP GRADE): ug/µl	0.8µg Elf5 Ab: 0.4µl	0.8ug Elf5 Ab: 0.4µl	0.8µg Elf5 Ab: 0.4µl	0.8µg Elf5 Ab: 0.4µl	0
Anti-RNA Polymerase II	0	0	0	0.8	0
Non-immune IgG	0	0	0	0	0.8

Table 2.12 Preparation of chip reaction. NOTE: The final amount of chromatin should be 2 µg/well ($2x10^5$ cells may yield 1 µg of chromatin); Sonicated chromatin can be further diluted with ChIP Buffer to desired concentration. For histone samples with sufficient chromatin (> 0.5 µg), the Enrichment Enhancer is not required and 50-80 µL of ChIP Buffer can be used. For low abundance targets, 2µL of Enrichment Enhancer and 88 µL of chromatin can be used without adding ChIP Buffer.

The wells were capped with Strip Caps and incubated at 4°C overnight on an orbital shaker (100 rpm) in cold room.

2.9.3.4. Clean protein/DNA complex and Reversal of cross-links, release, and purification of DNA

After overnight incubation, the solution was carefully removed and discarded from each well. Each well underwent a 200µL wash with Wash Buffer, allowing 2 minutes on an orbital shaker (100 rpm) for each wash at room temperature. The wash buffer was then pipetted out of the wells. Additionally, each well was subjected to a single 200µL wash with DNA Release Buffer.

To prepare the RNase A solution, 1µL of RNase A was added to 40µL (per well) of DNA Release Buffer. Subsequently, DNA Release Buffer was removed from each well, and 40µL of DNA Release Buffer + RNase A was added, followed by sealing with Strip Caps. The wells were incubated at 42°C for 30 minutes in a bacterial shaker. Following this step, 2µL of Proteinase K

(Proteinase K from Kit: 10mg/ml) was added to each well, and the wells were re-capped. Incubation continued at 60°C for 45 minutes. The resulting DNA solution from each well was promptly transferred to PCR tubes. These PCR tubes, containing the DNA solution, were then incubated at 95°C for 15 minutes in a thermocycler. Finally, the PCR tubes were placed at room temperature.

For the purification process intended for ChIP-seq, the F-spin column was positioned inside a 2 mL collection tube, designated as the F-collection tube. Subsequently, 200µL of DNA Binding Solution was added to each sample, facilitating thorough mixing by pipetting. The resulting mixture was then transferred to the labelled F-spin column, and centrifugation was conducted at 12,000 rpm for 30 seconds at room temperature (RT).

Following this initial centrifugation step, 200µL of 90% ethanol was introduced to the column, followed by centrifugation at 12,000 rpm for 30 seconds at RT. The F-spin column was subsequently removed from the collection tube, with the flow-through being discarded. A second round of 200µL of 90% ethanol was applied to each F-spin column, and another centrifugation step at 12,000 rpm for 30 seconds at RT ensued. Following this, the F-spin column was removed, and the flow-through was discarded. The column underwent an additional wash with 200µL of 90% ethanol, followed by centrifugation at 12,000 rpm for 1 minute. Subsequently, the F-spin column was placed inside a new 1.5 mL LoDNA binding tube. A volume of 20µL of DNA Elution Buffer was added directly to the filter in the F-spin column, followed by centrifugation at 12,000 rpm for 30 seconds to elute the purified DNA. The resulting purified DNA is now primed for use in PCR, ChIP-chip, and ChIP-seq applications or can be stored at –20°C.

2.9.3.5. ChIP Sequencing

Purified DNA samples were assessed using a NanoDrop™ 8000 spectrophotometer (Concentration > 2 ng/µL) and agarose gel (Main peak of 100 bp-500 bp) before being

forwarded to Novogene, UK for sequencing. The purified DNA fragments were converted into a sequencing library by adding sequencing adapters. This can be done through processes like end repair, A-tailing, and adapter ligation. The DNA library was cleaned up to remove unwanted fragments and contaminants and then amplified through PCR to increase the amount of material for sequencing. The ChIP sequencing library was loaded onto a next-generation sequencing platform Illumina. The DNA fragments were sequenced using high throughput sequencing technology, generating millions of short DNA reads. The data was uploaded to Galaxy web platform (https://usegalaxy.org/) for analysis.

The sequencing data was analyzed to identify DNA sequences associated with the protein of interest. The short reads were aligned to the reference genome. Regions enriched for the protein binding are identified through peak calling. The same analysis as performed for RNA-seq, utilizing DAVID and IPA, was carried out to identify biologically relevant pathways associated with Elf5 target genes identified through ChIP-Seq.

2.10 Immunohistochemistry

Mouse dorsal skin or human breast tissue cryosections, 10µm in thickness, were fixed using 4% paraformaldehyde for 10 minutes at room temperature and then washed with a solution of 0.2% Triton-X-100 in PBS. The cryosections were then blocked using a solution containing 0.2% Triton-X-100/PBS, 5% fetal bovine serum, 2% bovine serum albumin, and 10% regular goat or donkey serum for an hour at room temperature.

Or formalin-fixed, paraffin-embedded (FFPE) mouse dorsal skin sections, 5µm in thickness, deparaffinized and rehydrated following: Histoclear II, 3x5 minutes - 100% Ethanol, 2x 10 minutes - 95% Ethanol, 2x 10 minutes - 70% Ethanol, 2x 10 minutes - 50% Ethanol, 2x 10 minutes - Deionized Water, 2x 5 minutes at RT, then antigen retrieval was performed by boiling sections in Sodium Citrate (pH6.0), receipt see Appendix B 7. After 1 hour cooling at RT, rinsed

in TBST 3 x 5 minutes, followed by immersion in 0.1% Triton-X100 in TBS for 10 minutes, rinsed again 3 x 5 minutes with TBST. These sections were then blocked using a solution containing 0.2% Triton-X-100/PBS, 5% fetal bovine serum, 2% bovine serum albumin, and 10% regular goat or donkey serum for an hour at room temperature.

These slides were later treated with the primary antibody and left to incubate overnight at 4°C. The next day, after washing with the 0.2% Triton-X-100/PBS solution, they were exposed to the corresponding Alexa Fluor-488, Alexa Fluor-A555, or Alexa Fluor-647 secondary antibody (refer to table 6) for an hour at room temperature. Post this, the slides underwent another wash with the 0.2% Triton-X-100/PBS solution, after which they were counterstained and sealed using Vectashield anti-fade mounting medium with DAPI. Visualization and image capturing were performed with a Leica THUNDER imager.

2.11 Statistical Analysis

The student's t-test was used to calculate the p-value to determine significance between two sets of normally distributed data. This test provides a P value to quantify the statistical significance of the difference between the datasets: a P value less than 0.05 (*P<0.05) implies a 95% confidence in the difference being significant, supporting hypothesis acceptance. A P value less than 0.01 (**P<0.01) indicates a 99% confidence in the significant difference, and a P value less than 0.001 (***P<0.001) conveys a 99.9% confidence in the significance of the difference.

2.12 Ethics Approval

All animal procedures were conducted following guidance of UK Home office Animals (Scientific procedures) Act 1986 and approved by Nottingham Trent University (Nottingham, UK) Ethics Committee. Animal Licence number = I16312541.

With regards to human tissue experiments in this study, ethical approval was obtained from the Institutional Review Board of Nottingham Trent University under approval Internal Human ethical Number: 697, and external NHS REC: REC reference: 22/NE/0054 in accordance with the ethical principles set forth in the Declaration of Helsinki. Informed consent was obtained from all participants prior to the collection of tissue samples, ensuring that they were fully informed about the nature of the research, the intended use of their tissue, and the measures taken to protect the confidentiality of their data.

All tissue samples were anonymized to protect participant identity, with personal information replaced by unique codes. Only authorized personnel had access to the de-identified data, ensuring confidentiality throughout the study. The research complied with relevant national regulations, including the Human Tissue Act 2004, and adhered to the General Data Protection Regulation (GDPR) for data protection.

The use of human tissue was necessary to address the research objectives, providing the most relevant model for understanding human skin ageing in this study. Tissue samples were stored under controlled conditions in Nottingham Trent University, and ethical disposal procedures were followed after the completion of the study to ensure the responsible use of human tissue.

All procedures involving human tissue collection and handling were designed to minimize potential risks to participants. Stringent safety protocols were followed to ensure the ethical use of the tissue samples.

Chapter 3

Elf5 in Skin and Hair Follicle

3.1 Elf5 in skin and Hair Follicle

3.1.1 Introduction

The mouse embryo provides a valuable model system for the examination and characterization of epidermal developmental processes (Byrne et al., 1994). During morphogenesis, epidermis and its appendages are original from the same single layer of ectodermal cells as described in section 1.2. They build the first barrier to protect mammals from water loss and environmental damage, as well as in body temperature regulation. The complex structured and functional stratified epidermis and its appendages are established during the development. This relies on the spatiotemporal regulation and interaction of SCs and their progenitors in different niches in epidermis and dermis (liu et al.,2013).

Elf5 expression in ectoderm is restricted during early embryonic development (Donnison et al., 2005) and its regulation devoted to the embryonic and trophoblast cell lineage choices. It also plays an important role to maintain the trophoblast SC population (Ng et al., 2008). However, its role in skin morphogenesis is unknown. RT-qPCR and immunofluorescence were performed to determine Elf5 expression in skin and HF development. The conversion of the marker expression profile from murine skin to the human system builds upon the established understanding of their similarity, but It's crucial to examine the expression of Elf5 in human tissue. Elf5 expression was also assessed in young and older skin both in mouse and human through RT-qPCR and immunofluorescence.

Aim: To investigate the spatiotemporal patterns of Elf5 in skin and HF development and comparison between young and older skin.

3.1.2 Results

3.1.2.1 RT- qPCR and Immunofluorescence Analysis of Elf5 Expression in Skin and HF development

The technique of RT- qPCR enables the measurement of RNA levels to detect the changes of gene expression using target gene primers (Adams, 2020). To investigate whether Elf5 is expressed during skin and HF development, and its patterns at different time points, total skin RNA was extracted at different time points during skin and HF development, then Elf5 mRNA level measured by RT-qPCR using mouse Elf5-specific primers.

To detect protein expression of Elf5, fluorophore-conjugated antibodies were used to bind to the protein of interest in frozen tissue as described in section 2.10 . The basal marker K14, which serves as a highly specific marker for basal proliferative krts; Or K15, which is regarded as a pure SCs marker and the presence of K15-positive krts indicates a relatively undifferentiated state (Bose et al., 2013; Zhang, 2018); K15 is among the initial keratins associated with stratification that appears in all kinds of developing stratified epithelia and remains expressed in the mature epidermis (Bose et al., 2013). SC marker CD34, which is a widely recognized indicator for bulge HFSCs (Takeo et al., 2021); Elf5 and nuclear staining DAPI were then visualized by a confocal microscope.

RT-qPCR and Immunofluorescence analysis of Elf5 expression of mouse epidermal morphogenesis

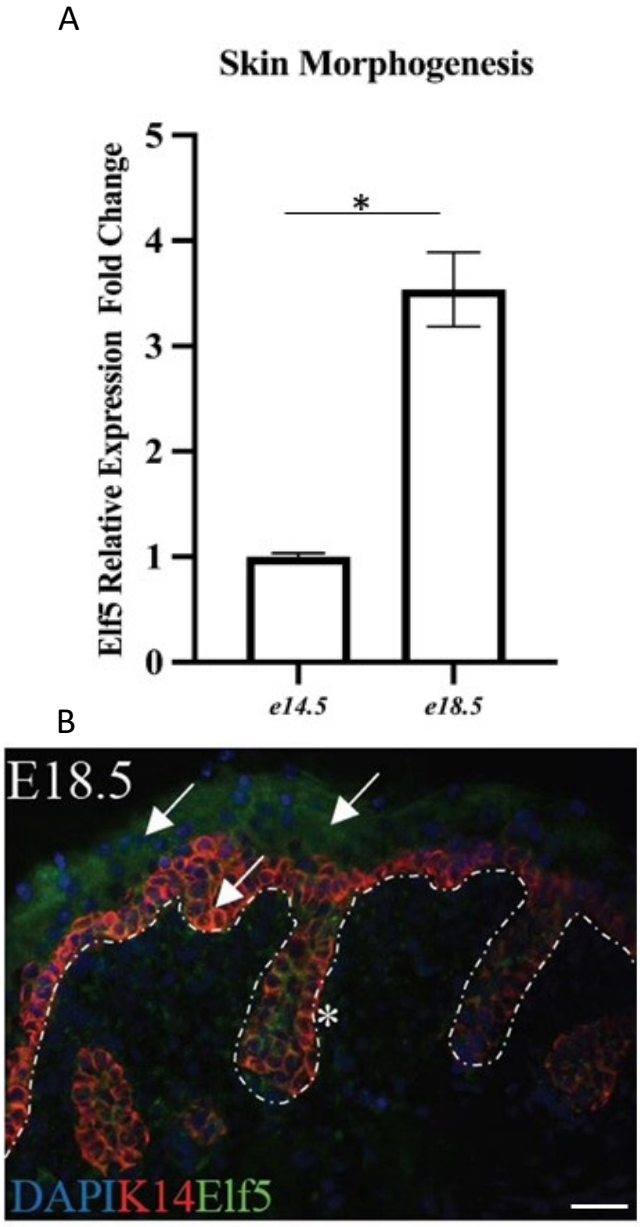

Figure 3.1 RT-qPCR and Immunofluorescence analysis of Elf5 expression of mouse epidermal morphogenesis. (A):RT-qPCR analysis of Elf5 expression of epidermal morphogenesis embryonic day 14.5 (E14.5) and embryonic day 18.5 (E18.5). Data are expressed as Mean ± SEM

from 3 independent experiments. *: P ≤ 0.05, **: P ≤ 0.01, ***: P ≤ 0.001. (B): Immunofluorescence analysis on embryonic day 18.5 (E18.5) of Elf5 (green), basal marker Keratin 14 (red) with nuclear staining (DAPI, blue). Data shown are from a single representative experiment out of three experimental repeats for each time point. Scale bar 50μm.

RT-qPCR and Immunofluorescence analysis of Elf5 expression of mouse epidermal posnatal development

A

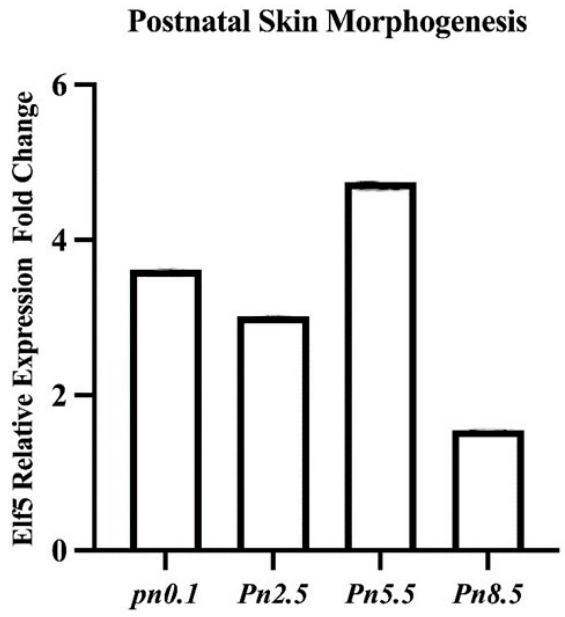

B

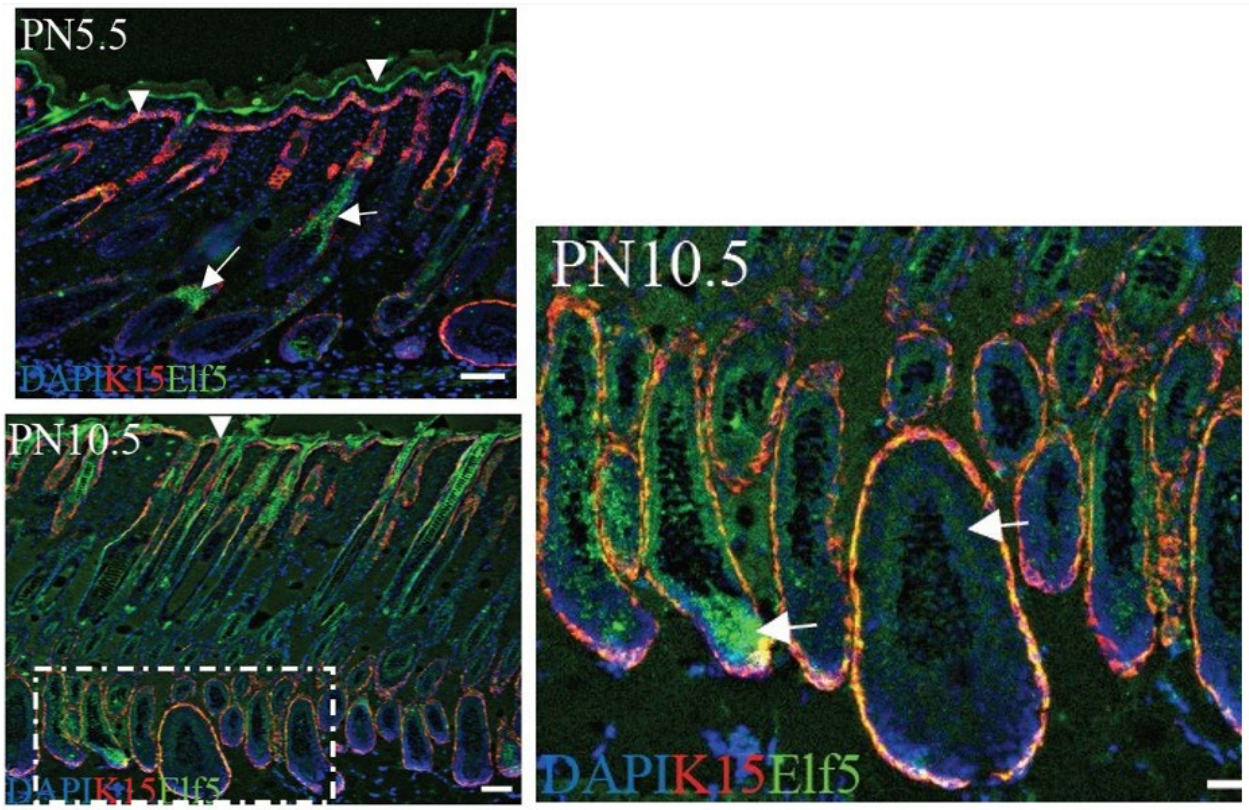

Figure 3.2 RT-qPCR and Immunofluorescence analysis of Elf5 expression of mouse epidermal posnatal development. (A):RT-qPCR analysis of Elf5 expression of epidermal morphogenesis postnatal Day 0.1 (D0.1), Day 2.5 (D2.5), Day 5.5 (D5.5) and Day 8.5 (D8.5). Data are expressed as Mean from 3 independent experiments. (B): Immunofluorescence analysis postnatal Day 5.5 (D5.5) and Day 10.5 (D10.5) of Elf5 (green), basal marker Keratin 15 (red) or SC marker CD34 (red) with nuclear staining (DAPI, blue). Data shown are from a single representative experiment out of three experimental repeats for each time point. Scale bar 50μm.

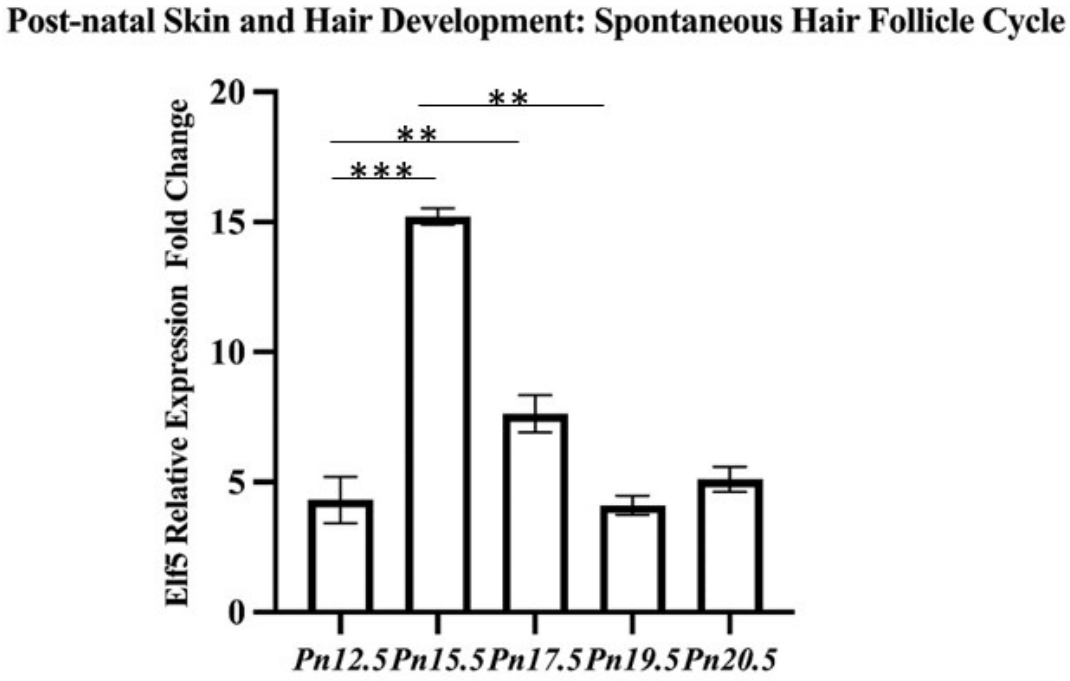

Figure 3.3 RT-qPCR analysis of Elf5 expression during spontaneous HF cycling in mouse. Elf5 levels in skin during the postnatal hair cycle: anagen-like stage (PN12-PN15.5), catagen (PN16.5–PN17.5), and telogen (PN19.5–PN20.5); Data are expressed as Mean ± SEM from 3 independent experiments. **: $P \leq 0.01$, ***: $P \leq 0.001$.

Elf5 expression analysis in mouse during depilation induced HF cycling

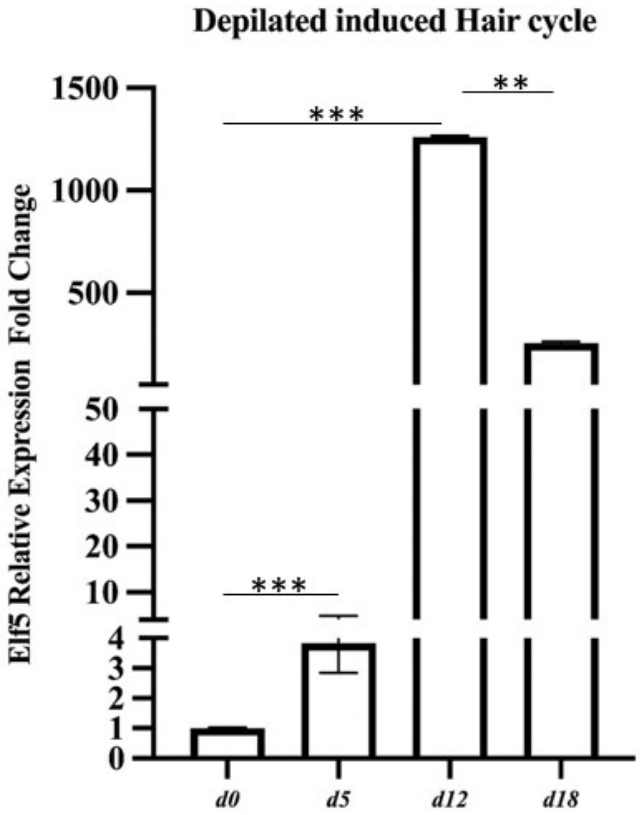

Figure 3.4 Elf5 expression analysis in mouse during depilation induced HF cycling from Day (d) 0 (telogen), through d3-12 (anagen), and d16-19 (catagen). Elf5 expression was highest during later anagen (d12) stage of induced hair cycle compared with telogen and catagen. Data are expressed as Mean ± SEM from 3 independent experiments. **: P ≤ 0.01, ***: P ≤ 0.001.

Upon RT-qPCR analysis (Fig. 3.1A), E18.5 showed higher epidermal expression of Elf5 than E14.5. Furthermore, immunofluorescence (Fig. 3.1B) showed that during skin morphogenesis Elf5 is detected in the basal and suprabasal layer of the epidermis (arrows) and developing hair bulb (asterisk). During development, from PN0.1, PN2.5, PN5.5 to PN8.5, Elf5 expression demonstrated an initial decrease, followed by an increase, and subsequently another decrease (Fig. 3.2A). However, these fluctuations were not statistically significant. In postnatal skin (PN5.5-PN10.5), Elf5 is dynamically and abundantly expressed in epidermis (Fig.3.B; basal and suprabasal, arrowheads) and proliferative and differentiating krts of the developing hair bulb

(arrows). Specifically, Elf5 expression is upregulated in anagen stages (Fig. 3.3), with dramatic reduction observed in expression in catagen and telogen stages (Fig. 3.4).

3.1.2.2 Immunofluorescence Analysis of Elf5 Expression in Skin and HF development

Immunofluorescence analysis of Elf5 with stem cells markers

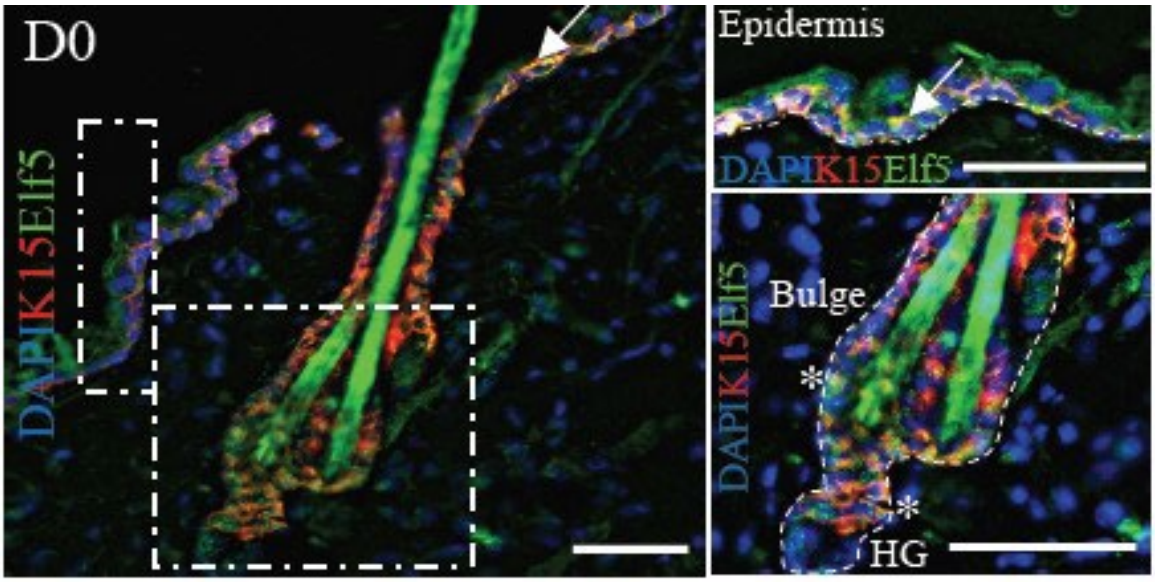

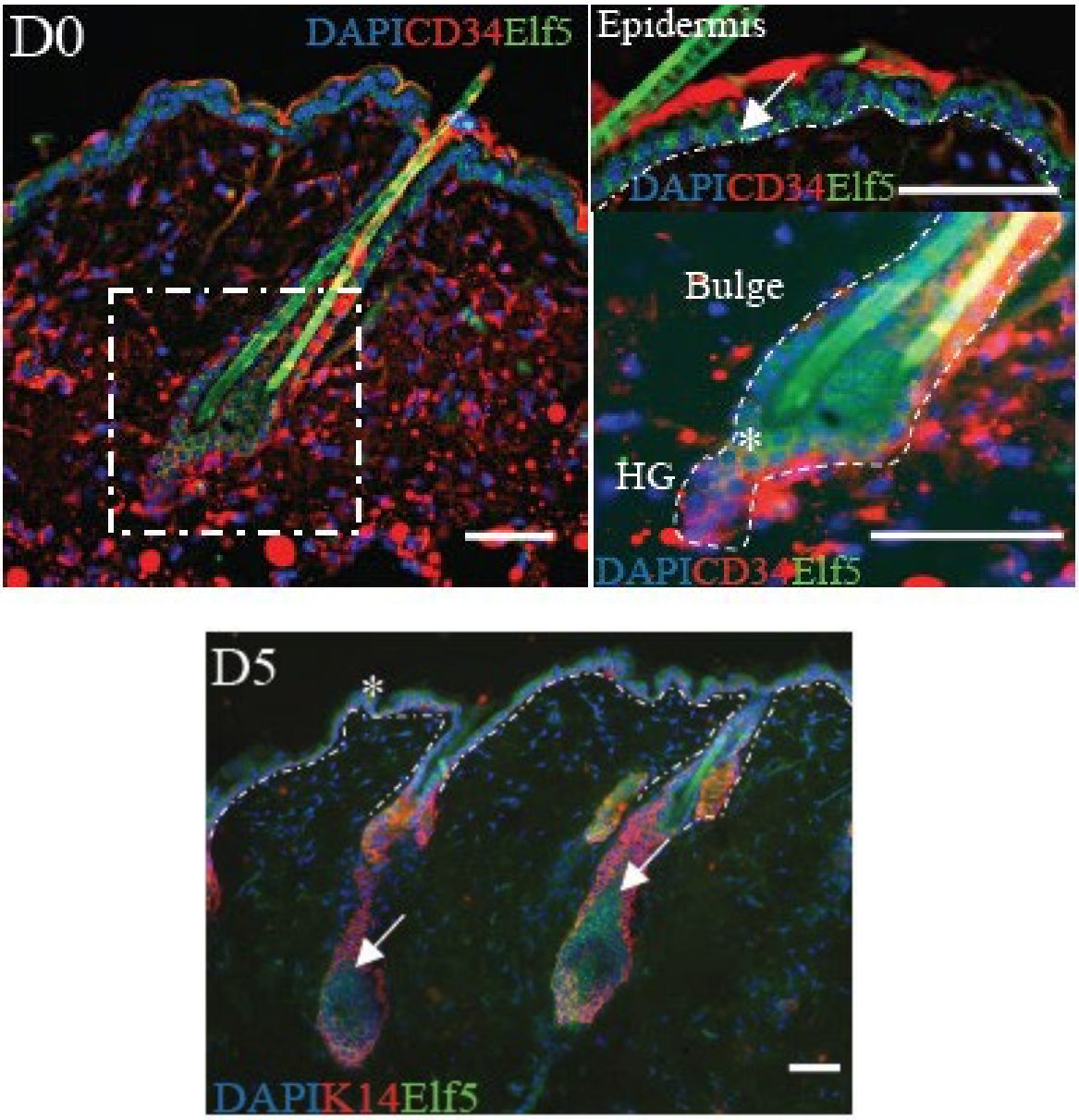
D0
DAPICD34Elf5
Epidermis
DAPICD34Elf5
Bulge
HG
DAPICD34Elf5
D5
DAPIK14Elf5

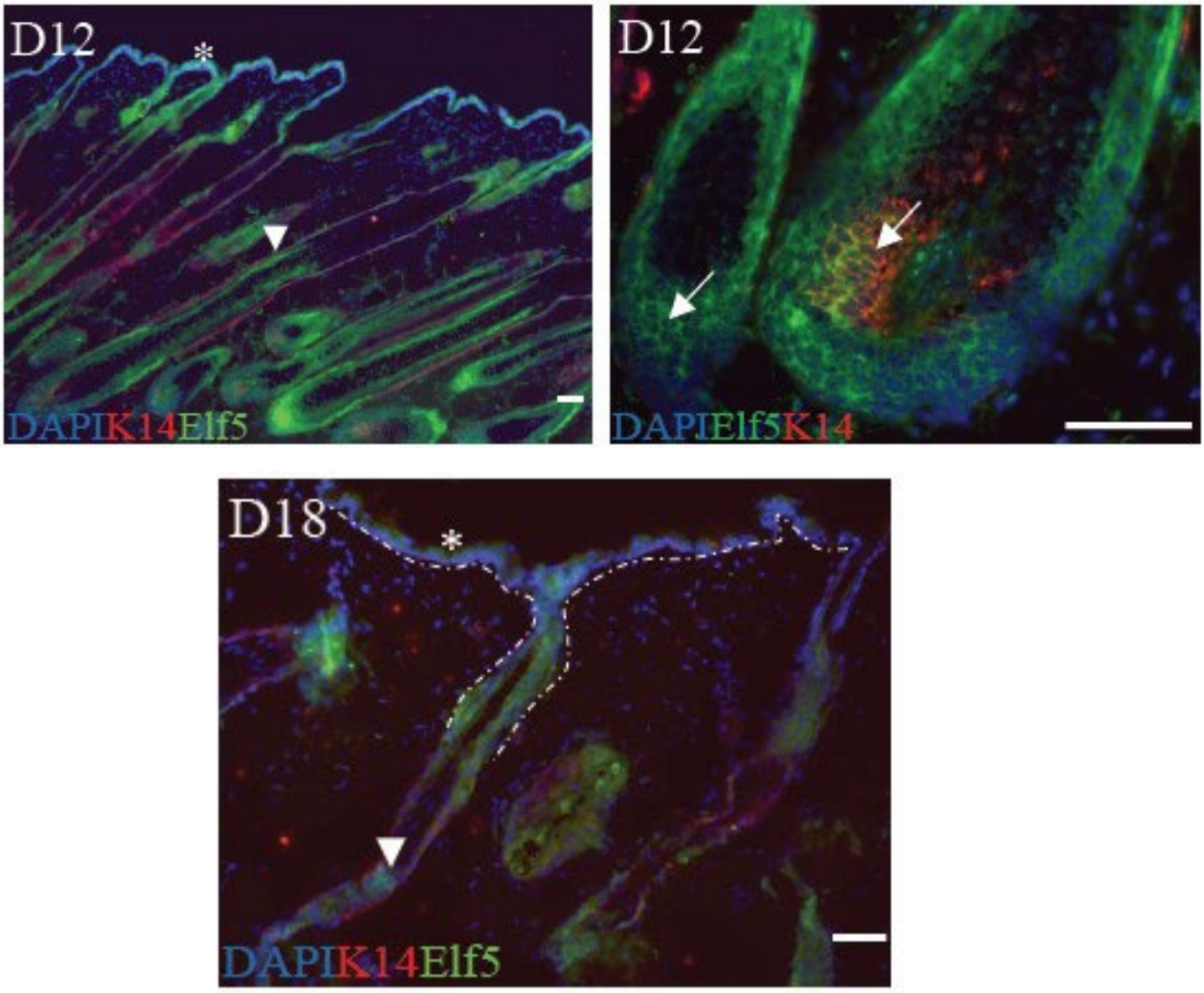

Figure 3.5 Immunofluorescence analysis of Elf5 (green), basal marker Keratin 15 or Keratin 14 (red) or SC marker CD34 (red) with nuclear staining (DAPI, blue) was performed at distinct days of mouse skin and hair cycle during depilation-induced hair cycle. Data shown are from a single representative experiment out of three experimental repeats for each time point. Scale bar 50μm.

During depilation-induced hair cycle (Fig. 3.5), in telogen skin (D0), Elf5 expression is restricted to basal layer (Elf5+/K15+/CD34-, arrows) in the epidermis and within the HF bulge and hair germ SC compartments (Elf5+/K15+/CD34+, asterisks). With progressive development of skin and HFs, Elf5 is also expressed in differentiated regions in epidermis (D5-D12, low basal and high suprabasal expression, asterisks). In HFs, Elf5 is consistently expressed in the highly

proliferative and differentiating krts in the hair bulb (D5-D12, arrows and arrowheads). While, in catagen (D18), Elf5 expressed is dramatically reduced in the epidermis (basal layer, asterisk) and restricted to the regressing HF epithelium (arrowhead).

3.1.2.3 RT-qPCR and immunofluorescence analysis Elf5 expression in adult mouse and human tissue

Elf5 expression in ageing and young mouse and human skin and HFs

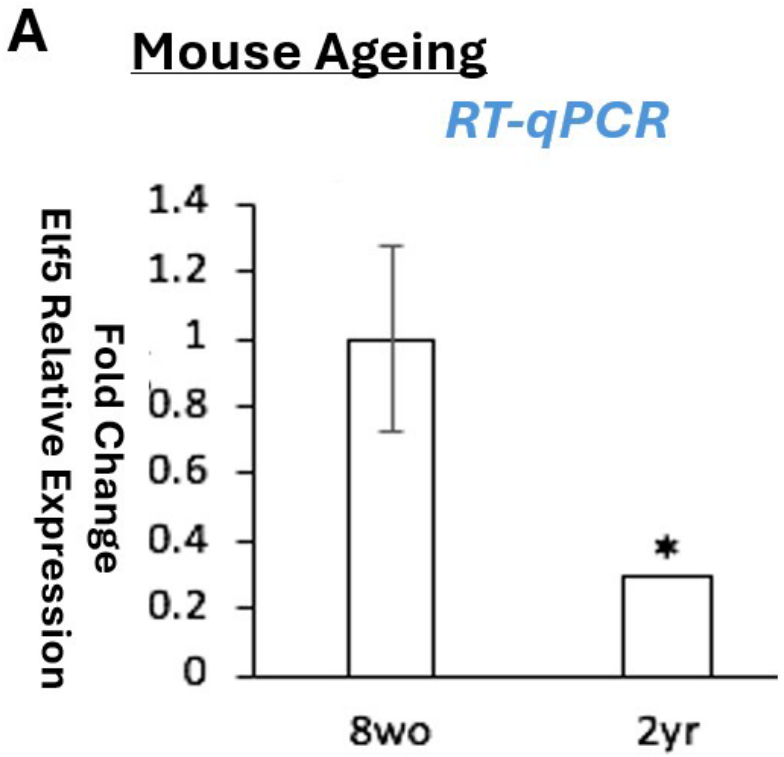

B **Mouse Ageing**

Immunofluorescence

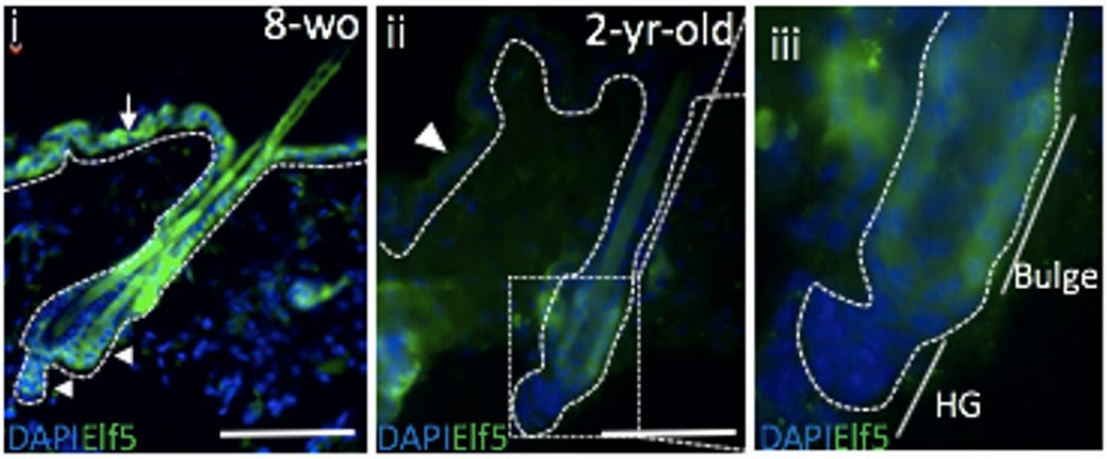

C **Human Ageing**

RT-qPCR

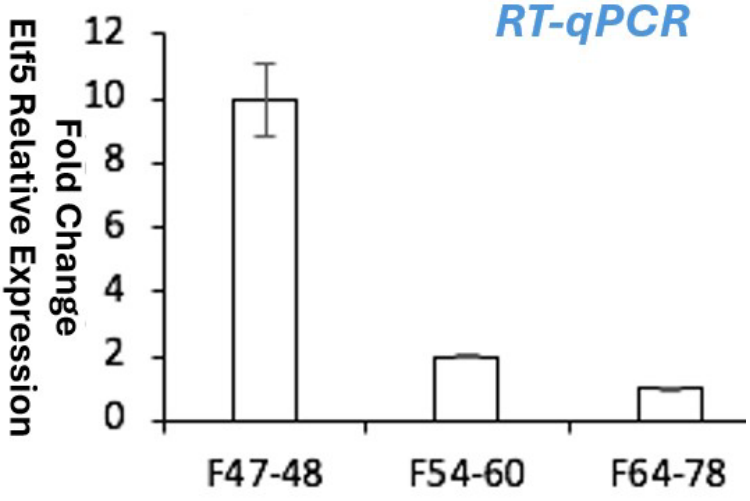

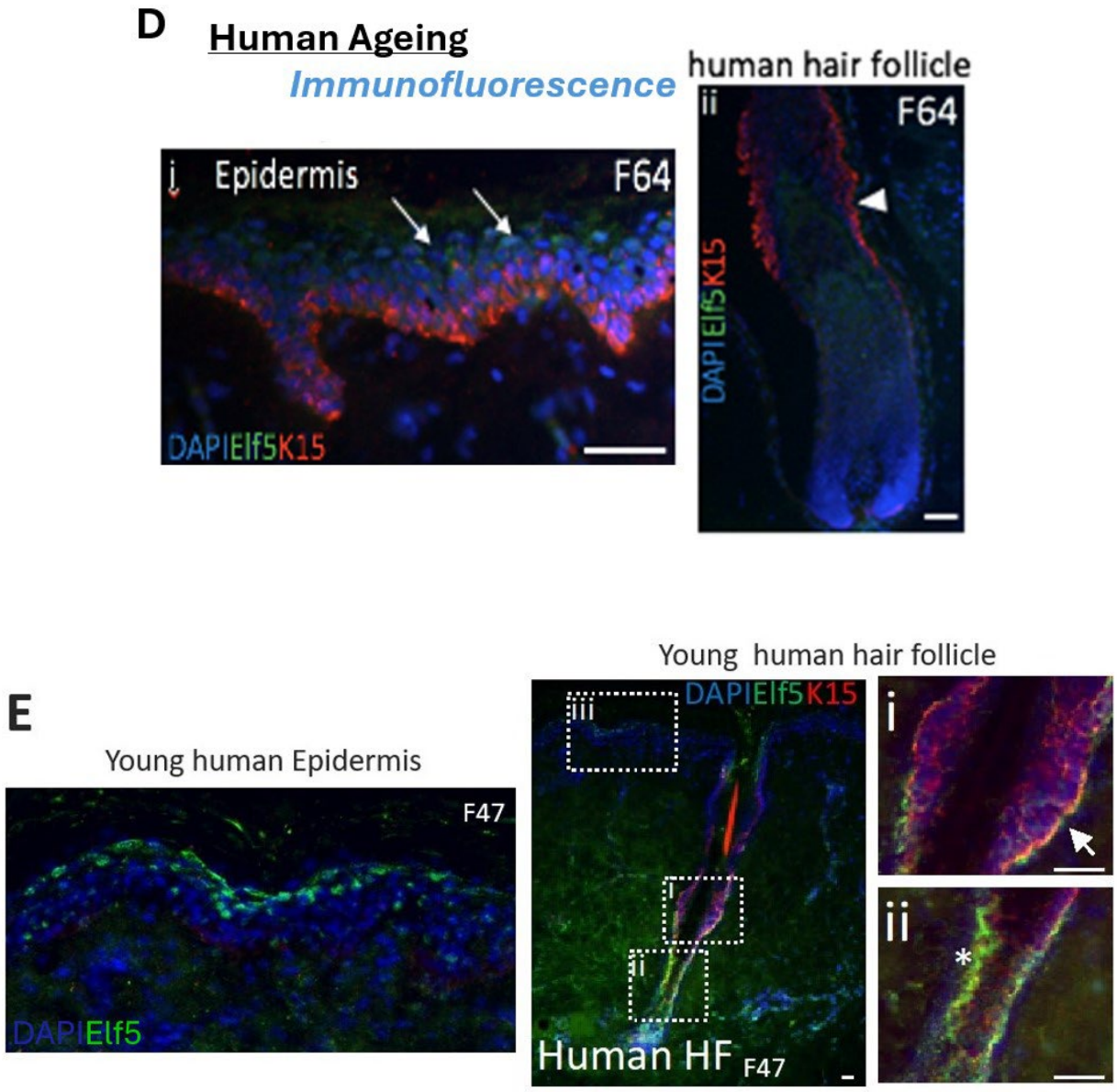

Figure 3.6 Elf5 expression in ageing and young mouse and human skin and HFs. (A, C): RT-qPCR analysis of Elf5 expression in ageing and young skin of mouse (A) and human (C). (B, D, E): Immunofluorescence assessment of Elf5 (green) and nuclear staining using DAPI (blue), was carried out on mice skin; Elf5 (green), with and without the basal marker Keratin 15 (red) and nuclear staining using DAPI (blue), was carried out on human skin; Elf5 is expressed in the ageing epidermis and HFs of both mice and humans. However, a reduced expression level is noted in ageing skin when compared to young skin in both species; (E): Elf5 is expressed in basal and suprabasal layer (iii) (arrows) in the epidermis and within the HF bulge (i) (arrowhead) and hair bulb (ii) (asterisk) SC compartments, alongside with basal

marker Keratin 15 (red). Data are expressed as Mean ± SEM from 3 independent experiments. *: P ≤ 0.05, **: P ≤ 0.01, ***: P ≤ 0.001. Data shown are from a single representative experiment out of three experimental repeats for each time point. Scale bar 50μm.

In both mice and humans, Elf5 is found in ageing skin (Fig. 3.6). However, its level of expression is notably lower compared to that in young skin.

3.1.3 Discussion

It was reported that Ets2 has ubiquitous expression in many proliferating tissues and cell lines, despite the wide variability of expression levels between different tissues and cell lines (J.Tymms & Kola, 1994). Here, the expression of Elf5 in skin and HF was investigated for the first time and showed interesting spatiotemporal patterns during embryogenesis and postnatal development (Fig 3.1-3.5). As the development procedure relies on the spatiotemporal regulation and interaction of SCs and their progenitors in different niches, and Elf5 expression was found in different EpiSCs and SC progenitors' locations (Fig 3.5), it was then hypothesized that Elf5 is involved in EpiSCs/progenitors' proliferation and/or differentiation. Elf5's expression displayed a consistent pattern and location in both aging and young skin across mice and humans (Fig 3.6). The diminishing expression of Elf5 with age, combined with its presence in various SC and progenitor compartments, supports the hypothesis that Elf5 might play a role in the balance of SC and progenitor proliferation and differentiation during both homeostasis and aging, and potentially in age-related disorders. The next step of this investigation will be to focus on Elf5's role in mouse epidermal krts' proliferation and/or differentiation.

3.2 Elf5 in Keratinocyte Proliferation and Differentiation

3.2.1 Introduction

The epidermis is composed of several layers of krts as described in 1.2.1.1, and it's integrity relies on a stable rate of production of new cells in the basal layer, as well as their migration

and differentiation (Gniadecki,1998). The healthy HF cycle also depends on the integrity of the interaction between follicular krts and mesenchymal dermal papilla cells. (Sakai & Demay ,2000) as described in section 1.2.1.2.

SCs have a much higher proliferative capacity but stay quiescent frequently in the epidermis (Alcolea & Jones, 2014; Jones et al., 1995). Thus, the balance of proliferation rate in normal healthy epidermis depends on the transit of amplifying krts, which will differentiate into terminal cells after finishing several cycles of mitosis (Gniadecki, 1998). Uncontrolled Krt proliferation can interrupt differentiation (Liu et al., 2009). The well-orchestrated balance between proliferation and differentiation of krts is crucial for maintaining epithelial homeostasis and preventing various skin disorders, such as psoriasis, abnormal wound healing, and cutaneous neoplasms (Nagarajan et al., 2008).

Available krt culture models mimic the krt proliferation and differentiation process *in vivo*, and this provides researchers the opportunity to isolate krt RNA and protein in order to study the agents that affect cell regulation and function *in vitro* (Eckert et al., 1997). Epidermal krts can be seeded in low calcium culture medium (0.05 mM), then proliferate stably and grow as a monolayer *in vivo*. They can be induced to terminal differentiation by increasing calcium (>0.07 mM) in the culture medium, and this facilitates the study of krt proliferation and differentiation experiments (Hennings et al., 1980; Yuspa et al., 1989; Nagarajan et al.,2008., Bikle et al., 2012).

Aim: To investigate the effect of Elf5 on primary mouse epidermal krt proliferation and differentiation *in vitro*.

3.2.2 Results

3.2.2.1 Elf5 expression analysis in PMEK (Primary Mouse Epidermal Keratinocytes) proliferation

The cell cycle in mammals is a meticulously coordinated and regulated process that guarantees the replication of genetic material and the division of cells. This cycle is predominantly divided

into four essential phases which facilitate cell growth and advancement: G0/G1, S, G2, and M. During the G1 phase, cells grow larger, while DNA replication occurs in the S phase. The G2 phase sees cells gearing up for division, and the division of the nucleus happens in the M phase (Behl & Ziegler, 2014; Otto & Sicinski, 2017).

Cyclin-dependent kinases (cdks), which regulate cell-cycle progression, are commonly used as a molecular tool to clarify the mechanisms controlling cell proliferation. Numerous growth factors and other substances (fat-soluble vitamins and their derivatives, ceramides, neuropeptides and neurotransmitters, steroid and peptide hormones, inflammatory mediators, interleukins, etc.) have been identified as potential factors regulating krt growth. In addition, the final signaling pathway directing towards the stimulus of growth is thought to have final upregulated cyclin D, cyclin E, and cyclin A expression during the growth progression through G1 (Gniadecki,1998).

To investigate the role of Elf5 in epidermal krt proliferation, PMEKs from new-born mice were isolated, cultured in normal (low calcium) cell media for 48 hours before downstream steps and/ or transfection. This was actioned at about 60% confluency by incubation with appropriate quantity of plasmids or 200nM Elf5 siRNA and their controls as described in section 2.3.2 and section 2.4. Total RNA and protein were extracted from cells grown in designed conditions as described in section 2.9. The collected total RNAs were extracted and quantified for subsequent first stand cDNA synthesis, qPCR and/or sequencing procedure as described in section 2.9.1. The quantified proteins were used for protein analysis as described in section 2.9.2.

RT-qPCR analysis of proliferation markers on Elf5 overexpression and knockdown

A

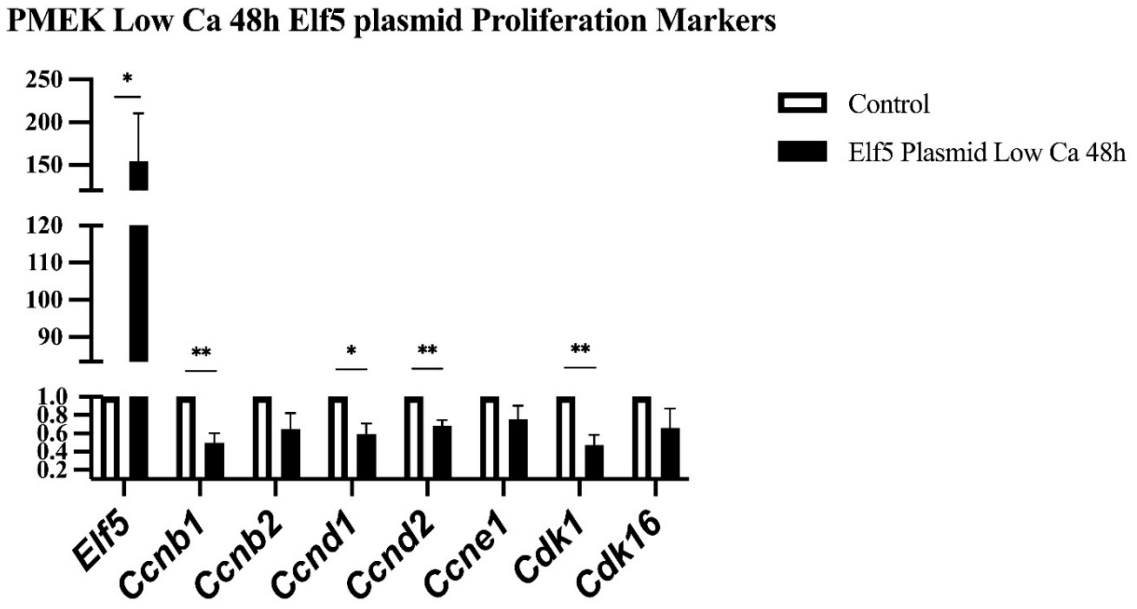

B

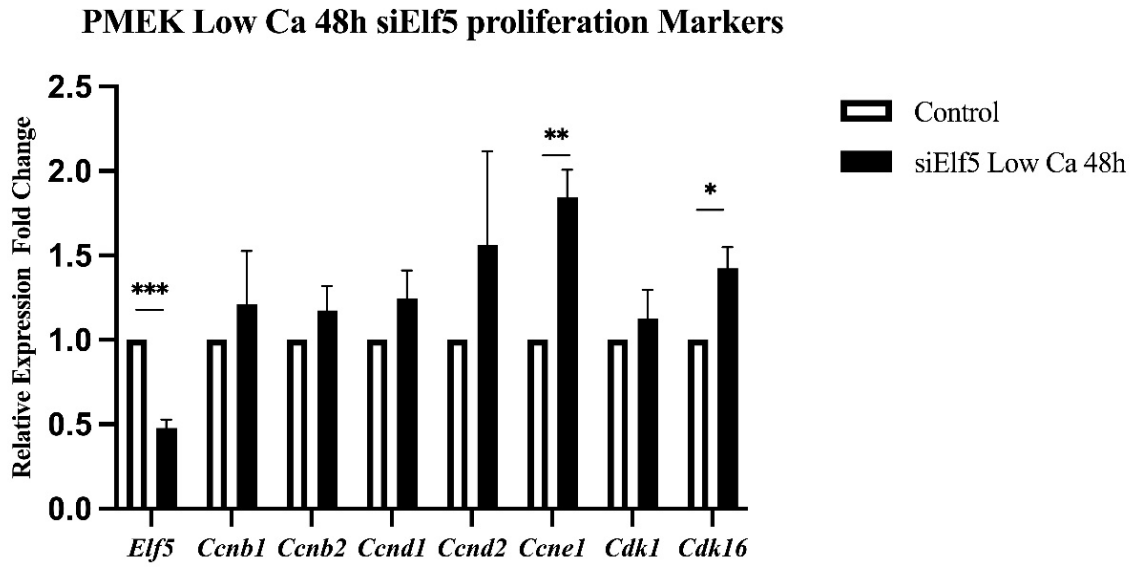

Figure 3.7 PMEK RT-qPCR analysis of proliferation markers upon Elf5 overexpression (A) and knockdown (B). Low Calcium:0.02mM. Elf5 overexpression decreases proliferation; Inhibition of Elf5

increases proliferation. Data are expressed as Mean ± SEM from 3 independent experiments. *: P ≤ 0.05, **: P ≤ 0.01, ***: P ≤ 0.001.

3.2.2.2 Elf5 Expression Cell Cycle Analysis in PMEK (Primary Mouse Epidermal Keratinocytes) by Flow Cytometry

Flow cytometry can not only measure cell size and cytoplasmic complexity, but also can differentiate cells through fluorescent parameters such as DNA dyes, (Adan et al., 2017; Watt et al., 2006). Cell cycle analysis by flow cytometry is commonly used by measuring DNA content through propidium iodide (PI) staining, which is a red-fluorescent dye that can pass through permeabilized plasma membrane and bind to double-stranded DNA. It can be excited at 488 nm wavelength and emit at 617 nm wavelength, the measurement of emission is proportional to DNA content. This allows us to see the proportion of DNA content and to uncover the cell cycle stage distribution for G1, S and G2 or cell death, which is presented by DNA fragmentation. (Shen et al., 2017; Maadi et al., 2022). In this way, the proliferation of krt can be assessed by flow cytometry (Watt et al., 2006).

PMEKs transfected with plasmids or 200nM Elf5 siRNA, and their controls, were fixed and stained as described in section 2.8. The ready single cell suspension, in which double stranded DNA is bound to PI, was run through Beckman Coulter Gallios, with excitation at wavelength of 535nm and an emission of 615nm. For each sample, unstained sample was used as a control reading performed at first as fluorescence compensation and then the stained sample was run. For each sample, more than 50% gated single cells and minimum of 10,000 events were acquired and then used for cell cycle analysis with Beckman Coulter Kaluza Analysis Software (Beckman Coulter, UK).

Flow cytometry PI staining cell cycle analysis of PMEK low Ca 48h Elf5 over expression and inhibition effects

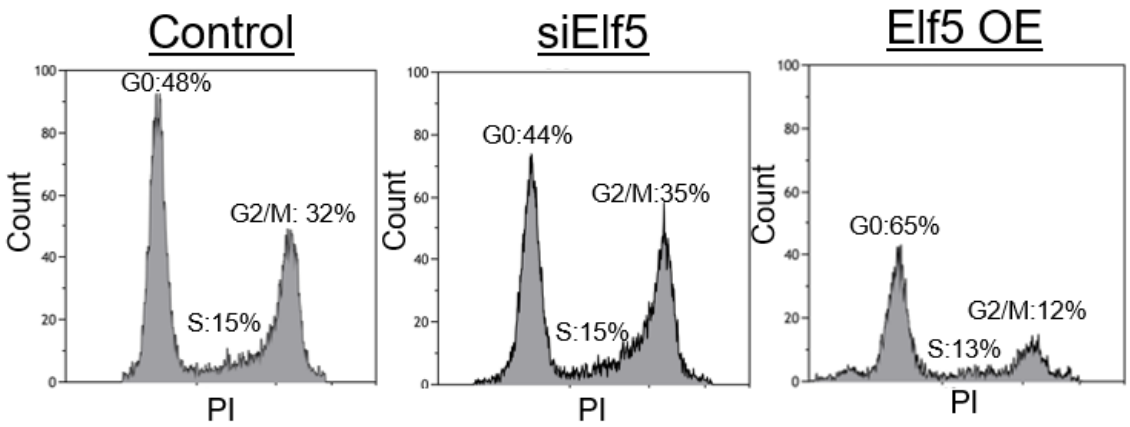

Figure 3.8 Flow cytometry PI staining cell cycle analysis of PMEK low Ca 48h Elf5 over expression and inhibition effects (low calcium: 0.02mM). Flow cytometric analysis by PI in PMEKs showed accumulation in G0-phase and, subsequently, a reduction of cells entering the S and G2/M phases of the cell cycle after Elf5 overexpression (OE). Limited effects were observed on PMEKs after siElf5 treatment compared to controls. Percentages are presented as mean values from three independent experiments. Data shown are from a single representative experiment out of three experimental repeats.

3.2.2.3 Elf5 expression analysis in PMEK (Primary Mouse Epidermal Keratinocytes) differentiation

The growing krt monolayer can be induced to differentiate in high calcium (>0.07 mM) culture medium as described previously. To investigate the role of Elf5 in epidermal krt differentiation, the PMEKs from new-born mice were isolated, cultured in normal (low calcium) media, or switched to high calcium (2mM) PMEK media and cultured for a further 24, 48 or 72 hours. The total RNA and protein were collected and quantified, then subsequently analyzed as described previously. The successful differentiation procedure can be assessed by morphology alteration under microscope observation (flattening, increased surface area) and expression of differentiation markers (e.g., K1, K10, involucrin, filaggrin, and loricrin) (Hennings et al., 1980; Yuspa et al., 1989; Nagarajan et al.,2008).

Elf5 expression analysis in PMEK differentiation

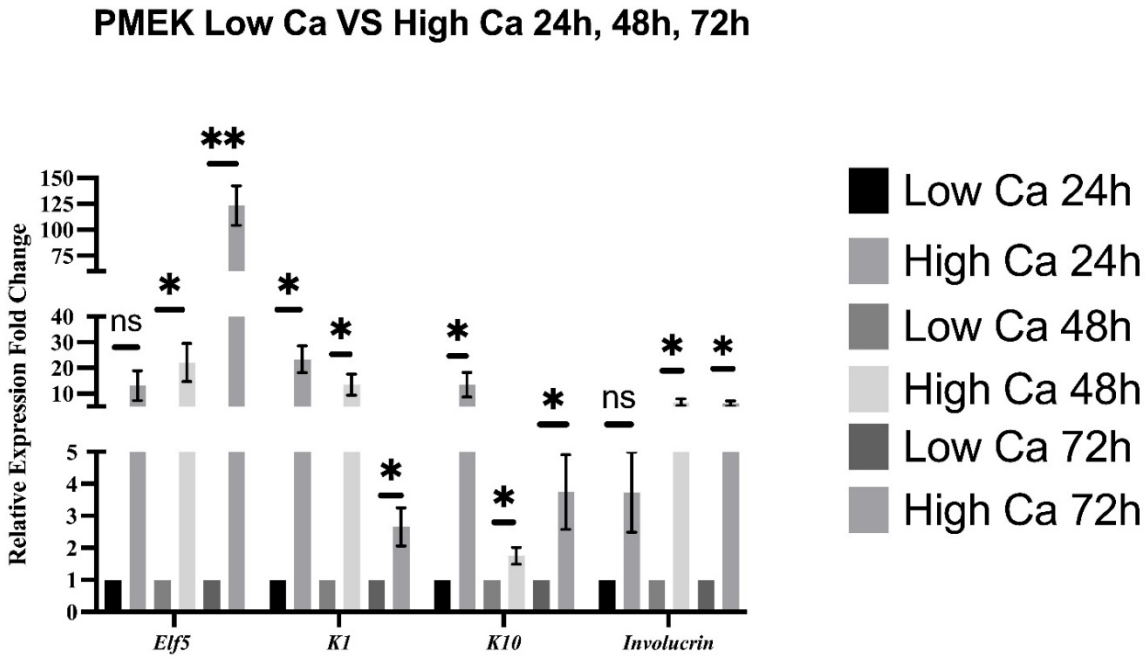

Figure 3.9 Elf5 expression analysis in PMEKs differentiation. RT-qPCR analysis of Elf5 and differentiation markers during calcium-induced krt differentiation at different time points: 24, 48 and 72 hours in PMEKs showed an increase in expression of Elf5 in high calcium treated PMEKs compared to low calcium and increase with longer differentiation time. Low Calcium:0.02mM; High Calcium: 2.0mM. Data are expressed as Mean ± SEM from 3 independent experiments. *: $P \leq 0.05$, **: $P \leq 0.01$.

Western blot analysis of Elf5 and cytokeratin 1 during calcium-induced krt differentiation in PMEKs

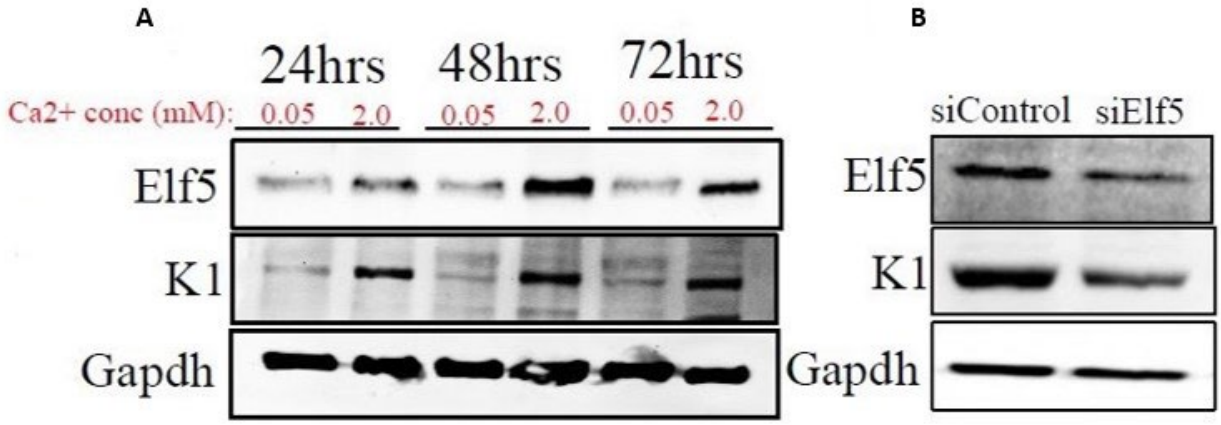

Figure 3.10 Western blot analysis of Elf5 and cytokeratin 1 (K1) during calcium-induced krt differentiation in PMEKs. (A): Consistent with RT-qPCR, Elf5 and K1 protein levels are elevated in calcium-induced PMEKs over time. Elf5 expression increases with longer differentiation timepoints. (B): Loss of Elf5 (48hrs post transfection) reduces the expression of Elf5 and K1 protein levels in differentiated PMEKs. Data shown is from a single representative experiment of three experimental repeats.

3.2.3 Discussion

As described previously, epidermis homeostasis and regeneration rely on the SCs balance of activation, proliferation, and differentiation. Here, I investigated the effect of gain and loss of function of Elf5 in PMEK proliferation and differentiation and the effect on cell cycle progression. The RT-qPCR analysis of proliferation markers with Elf5 overexpression (Fig 3.7 A) and knockout (Fig 3.7 B) show that Elf5 overexpression decreases proliferation, whereas inhibition of Elf5 increases proliferation. In cell cycle analysis (Fig 3.8), Elf5 overexpression, compared with control group, demonstrates dramatically higher proportion of cells in G0/G1 stage and lower in G2/M stage accompanied with increaseed cell death, which is presented as a "sub-G1" cell population. In the inhibition of Elf5 group the opposite effect was observed, but

with a slightly decrease level in Go/G1 and a higher level in G2/M stage, accompanied with very low level of cell death, of which no “sub-G1” cell population was present (Fig 3.8) for this group.

Cells in the G0 and G1 phases both have unreplicated genomes, resulting in them having identical DNA content. Currently, there isn't a recognized checkpoint distinguishing G0/G1, nor are there definitive markers to separate G0 from the early G1 phase (van Velthoven & Rando, 2019). Cyclins are key elements in driving the progression of the cell cycle (Sherr, 2000) and the expression of several cyclins, specifically cyclins D, E, A, and B, during the normal growth of cells happens intermittently, manifesting in distinct segments of the cell cycle (Schönthal, 2004). The regular pattern in cyclin expression acts as markers for the cell cycle, allowing for a more detailed division beyond the basic four main phases. Additionally, by comparing cyclin expression to DNA content, it is possible to differentiate cells with identical DNA content but in different stages of the cycle (Schönthal, 2004). As G0 cells, which don't express D-type cyclins or cyclin E, are distinct from G1 cells that do express cyclin D and/or cyclin E (Schönthal, 2004), and the proliferation markers ccnd1, ccnd2 and ccne1 expression increase in Elf5 inhibition group, and decrease in Elf5 overexpression group (Fig 3.7).

In addition to the krt effect, cell cycle regulation occurs largely in the G1 phase (Gniadecki,1998). One would therefore expect a higher G1 cell proportion should have been found in the Elf5 inhibition group, and lower in the Elf5 overexpression group. However, the cell cycle analysis shows the opposite effect (Fig 3.8), and it can be seen that more cells are kept in G0 by Elf5 overexpression and/or cell death. This is consistent with the decreased proliferation marker expression in the Elf5 over-expression group, whereas all of them increased upon Elf5 knockdown (Fig 3.7). In this way, the transition from G2 phase to M phase in cell cycle is regulated by the complex formed between cyclin-dependent kinase 1 and cyclin B (CDK1/CCNB), which is crucial for the onset of mitosis, and the proliferation markers cdk1, ccnb1 and ccnb2 increase in Elf5 inhibition group, and decrease in Elf5 overexpression group (Fig 3.7).

It is therefore expected that more cells should have been observed in mitosis in the Elf5 inhibition group, and opposite in Elf5 overexpression group. This is the trend observed in G2/M stage in the cell cycle analysis (Fig 2). As the cyclins D helps to maintain equilibrium between growth-promoting and growth-inhibiting factors, especially during G1 phase, and cyclins E and A become activated in differentiated krts located in the suprabasal layers (Gniadecki, 1998; Schönthal, 2004), the change of expressions of ccne1 with Elf5 inhibition and overexpression (Fig 3.7) suggest that Elf5 is related to krt differentiation. These findings correlate with the Elf5 location in histology analysis (Fig 3.5).

The relationship between Elf5 and krt differentiation was next investigated. During calcium-induced krt differentiation at different time points, it is shown that the Elf5 and differentiation marker expression increases (Fig 3.9). While Elf5's expression tends to rise with extended differentiation culture durations, the expression of certain differentiation markers diminishes over longer culture periods (Fig 3.9). The protein analysis demonstrates that Elf5 does increase with differentiation, alongside differentiation marker K1. However, as differentiation progressed, Elf5 and K1 exhibited a decrease in expression levels.

The depletion of Elf5 (observed 48 hours after transfection with Elf5 siRNA and control) from the same experiment leads to a decrease in the expression of both Elf5 and K1 protein levels in differentiated PMEKs (Fig 3.10). This likely reflects the presence of regulatory mechanisms that buffer against excessive gene expression. Given that the entire population of PMEK cells from newborn mice was used in this study, we hypothesized that Elf5 may influence not only the proliferation and differentiation processes of the whole population or specific subpopulations, but also play a role in the negative feedback regulation of advanced differentiation in these cells. This is consistent with the transcript and histology analysis (Fig 3.8 and Fig 3.9) and other studies, in which Elf5 is recognized for its expression in skin differentiated krt and the epithelial cells of HFs inner root sheath. This study also supports the hypothesis that Elf5 could be crucial in lineage specification during the hair cycle. Aligning with these findings, a previous study through a microarray screen identified Elf5 as a gene associated with the hair cycle in mouse back skin (Lin et al., 2004; Choi et al.,2008).

3.3 Summary

Overall, the exploration of Elf5 expression in skin and HFs was conducted for the first time, revealing unique spatiotemporal patterns throughout embryogenesis and subsequent postnatal development. Additionally, this expression also exhibited a consistent pattern and location in both aging and young skin, observed across both mice and humans. Elf5 demonstrates that it not only plays an important role in krt proliferation, which may keep cells in quiescence and decrease proliferation, but also in krt differentiation and possibly in cell death, which may increase differentiation and induce apoptosis. Furthermore, considering the distinct localization of Elf5 as illustrated in Figure 3.5 and its representation in various compartments of different SCs and progenitors, subsequent investigation will be dedicated to elucidating the roles played by Elf5 in the dynamic equilibrium system governing the quiescence, proliferation, differentiation, and potential apoptosis of EpiSCs. This exploration aims to contribute to our understanding of how Elf5 functions to control EpiSCs/progenitors' quiescence proliferation and differentiation.

Chapter 4

Elf5's Role in Epidermal Stem cells/Progenitor Quiescence, Proliferation, and Differentiation Processes

4.1 Introduction

As with every tissue that constantly regenerates, the population of SCs serves as a source for cells capable of differentiating into specialized forms (Lajtha, 1979; Hall & Watt, 1989). In epidermis, the lifelong regeneration of the epidermis and its associated structures relies on consistent proliferation and differentiation of EpiSCs and their progenitors as described in Section 1.2 . Adult SCs are defined by the capacity for self-renewal, and can differentiate into various cell types specific to a tissue (Schultz & Sinclair, 2016) and they stay quiescent in specialized niches. They are stimulated to undergo cell proliferation to produce proliferating "transit amplifying" daughter cells that in turn differentiate into committed offspring that either construct tissues during normal development and growth, or regular tissue homeostasis or participate in tissue regeneration after damage (Horsley et al., 2008; Evano & Tajbakhsh, 2018). Naturally, if quiescence is disrupted, this can result in abnormal proliferation, differentiation, apoptosis, or senescence, which can disturb tissue balance and hinder tissue regeneration (Evano & Tajbakhsh, 2018). Maintaining a balance between quiescence and proliferation in SC groups is crucial. Any imbalance can result in abnormal cell growth or disrupt tissue equilibrium and repair (van Velthoven & Rando, 2019). As noted previously, uncontrolled proliferation of krt can disrupt their differentiation, and it is essential to maintain a harmonious balance between the proliferation and differentiation of krt to preserve epithelial homeostasis and prevent various skin disorders.

With the introduction of culture methods for the clonal and serial expansion of epidermal krts, the study of potential SCs and other proliferative cells *in vitro* became feasible. In submerged cultures, krts display heterogeneity in terms of their cycle durations, cell cycle exit rates, and clonal growth characteristics. Holoclones display traits consistent with SCs. They exhibit a high colony-forming efficiency (CFE) and produce meroclones and paraclones, which sequentially demonstrate reduced colony-forming abilities (Rheinwald & Green, 1975; Dover & Potten,1983; ; Albers et al., 1986; Albers et al., 1987; Barrandon & Green, 1987). Holoclones, derived from the term "entire", produce large, fast-expanding colonies with less than 5% terminating

prematurely and undergoing differentiation. Morphologically, these present as substantial numbers of closely packed, large colonies. (greater than 20 mm^2; exceeding 10,000 cells) comprising smaller cells with a relatively undifferentiated appearance. On the other hand, paraclones, meaning "beyond", are predisposed for restricted growth and thus create consistently small colonies that eventually conclude their growth. Meroclones, from the term "partial", lead to the development of two distinct colonies - those that continue to grow and those that terminate; They form the colony with a covering area of less than 5 mm^2, and its boundary exhibits significant irregularities, and cell growth has completely halted, the cells within are large and have a flattened appearance. This suggests that within the meroclone, some cells transition into behaving like paraclone-forming cells. Unlike a terminal colony, which has a highly irregular shape, a growing colony possesses a defined boundary. (Barrandon & Green, 1987; Blanpain et al., 2004).

Since its inception in the mid-1950s, clonogenic assays have become a tool for many researchers to evaluate the self-renewal potential of different mammalian cell models *in vitro*. In this scenario, the term 'clonogenic' growth typically refers to a group of 50 or more cells that have arisen from a single cell (Brix et al., 2006). The clonal expansion of krt is often utilized as a measurable method to assess EpiSCs (Barrandon & Green, 1987; Hirsch et al., 2017; Jones & Watt, 1993). Across a wide spectrum of colony sizes, there was a consistent proportion between cell count and colony area. For human krt in culture, averaging 1800 cells for every square millimeter. For smaller growing colonies (under 1 mm^2), the most accurate visual correlation was around 1600 cells per square millimeter. Colonies that have undergone terminal differentiation mainly consist of larger cells, resulting in a reduced cell count per unit area (Barrandon & Green, 1987). The number and size of colonies indicate cell survival and cell growth, respectively (Guzmán et al., 2014).

Counting colonies can be conducted through traditional manual methods, which are time-consuming and subjective, or by utilizing various devices and software that offer quicker and automated counting solutions (Dahle et al., 2004; Cai et al., 2011; Geissmann, 2013; Guzmán et al., 2014; Zhang et al., 2022). Instead of counting and measuring individual colonies, it is more

straightforward to calculate the proportion of the wells surface covered by colonies (referred to as the colony coverage percentage) to assess the growth of clonogenic cells (Bettger et al., 1981; Zyzak et al., 1994; Ichinose et al., 2002; Niemela et al., 2012). The ImageJ plugin "ColonyArea" calculates both the colony area percentage, which reports on the proportion of the well area occupied by cells, and an intensity-weighted colony area percentage, known as colony intensity percentage, which evaluates the capacity of the cells to proliferate densely, based on images of colony formation assays taken from multi-well plates using a flatbed scanner (Guzmán et al., 2014).

Swiss mouse embryonic 3T3 cells in a growth-arrested state serve as feeder cells and were first reported in 1955 by Puck and Marcus. This provided a technique to grow large-scale colony production from single cells. They are Known to produce growth factors, adhesion molecules, and ECM (Li et al., 2017) and they can support *in vitro* survival and growth of some cells that would require the presence of a variety of known or unknown soluble or membrane-bound growth factors and receptors (Liams et al., 2015). They are reported as feeder cells to facilitate the growth of epidermal krts *in vitro* (Chugh et al., 2015a; Chugh et al., 20156; Chugh et al., 2016; Pinto et al., 2020). In this study, I varied seeding densities and incubation durations for Swiss 3T3 cells (CCL-92, ATCC). I also tested these cultures for the ability to stop proliferation following different concentration of mitomycin C treatments, then optimized when co-cultured with the commonly used human krt line called HaCaTs, which display characteristics of basal cells and remain responsive to various differentiation stimulants. This thus serves as an ideal model to analyse krt differentiation (Wilson, 2013). We have determined the optimal feeder and feeding cell density and the appropriate, safe concentration of mitomycin C during the suitable feeder and feeding cells co-incubation period.

Fluorescent-activated cell sorting (FACS) is a major method utilized for the isolation and characterization of SCs. Different approaches, such as encompassing the identification of cell surface markers and various cellular activities, have aided in isolating SCs from diverse tissues (del Mar Vivanco, 2015). Creating a high-quality, single cell suspension is crucial for the success of FACS (Nowak & Fuchs.,2009), so I employed one FACS method based on clinically used

successful cell sorting of human embryonic SC-derived neural cell populations (Pruszak et al., 2007.). This was optimized, leading to the developed of a “gentle FACS” method for EpiSCs sorting in this project, with optimized buffers and sheath pressure conditions (details in Methodology FACS section).

This “gentle FACS” method was used to isolate epidermal krt subpopulations based on their different expression of identified specific cell markers. Based on the expression of two specific markers, two populations were differentiated: CD34, indicative of bulge SCs, and Sca-1, representative of epidermal krts (Jensen et al., 2008). Compared to interfollicular basal cells, CD34-positive bulge cells demonstrated an enhanced clonogenic capability in terms of colony count and dimensions (Trempus et al., 2003). In mouse mature skin, SC antigen-1 marker Sca-1 surface expression presents in basal epidermal krts (Jensen et al.,2008). The expression of integrin-α6 was consistent across the basal layer of IFE and HFs (Watt, 2002). The cells, which exhibit the presence of α6 and do not exhibit CD34 but possess the SC antigen-1 (Sca-1) marker, have demonstrated the ability to undergo self-renewal and generate epidermal, follicular, and sebaceous gland lineages in living organisms (Jensen et al., 2008). Although Sca-1 is associated with integrin-α6 in both the infundibulum and IFE, it is absent in the HF bulge. On the other hand, HF bulge SCs express both CD34 and integrin-α6. This enables the distinct separation of two unique groups: HFSCs and epidermal krts (Albert et al., 2001; Jensen et al., 2008).

Krts expressing CD34 in conjunction with integrin alpha 6 (α6/CD49f) were recognized as the slow-cycling quiescent cells in the bulge region (Triel et al., 2004; Trempus et al., 2003; Holmes & Stanford, 2007; Jensen et al., 2010; Nowak & Fuchs, 2009; Pinto et al., 2020; Soteriou et al., 2016). Along with Sca-1, three distinct populations of cells were sorted through FACS: CD34+/CD49fHigh/Sca-1- represents the HFSCs; CD34-neg/CD49PE+High/Sca1+, represents epidermal basal SCs and the last subpopulation CD34-/CD49fLow/Sca-1- represents Suprabasal krts.

During the telogen phase of HF cycling, skin from the dorsal and ventral areas of C57BL/6 female mice (aged 7-9 weeks) was shaved and collected. Some were treated and were used for

histology purposes as described in the section 2.10. Image analysis was performed with ImageJ. Krts from adult mouse epidermis were isolated and fractionated into different sub-populations based on cell surface markers with “gentle FACS”. SCs from the HF bulge and basal SCs, suprabasal SCs were sorted using a MoFlo XDP cell sorter as described in section 2.6. The collected data was processed using the Summit software from Beckman Coulter, UK. Afterwards, sorted cells were subjected to either a colony-forming assay following cell culture, transduction as described in section 2.7 or RT-qPCR analysis as described in section 2.9.1.

Aim: To review and develop the EpiSCs isolation and growing protocol and to investigate the effect of Elf5 in EpiSC populations.

4.2 Results

4.2.1 Expression Analysis of Elf5 in Epidermal Stem Cell Populations in Skin and Hair Follicle

To verify the location of Elf5 in adult epidermis, immunofluorescence analysis was conducted using the SC marker CD34, Elf5, and DAPI on skin samples. After FACS sorting, comparison was made between the expression of Elf5 in HFSCs and epidermal krts using RT-qPCR.

Expression analysis of Elf5 in stem cell populations in adult mouse skin and HFs

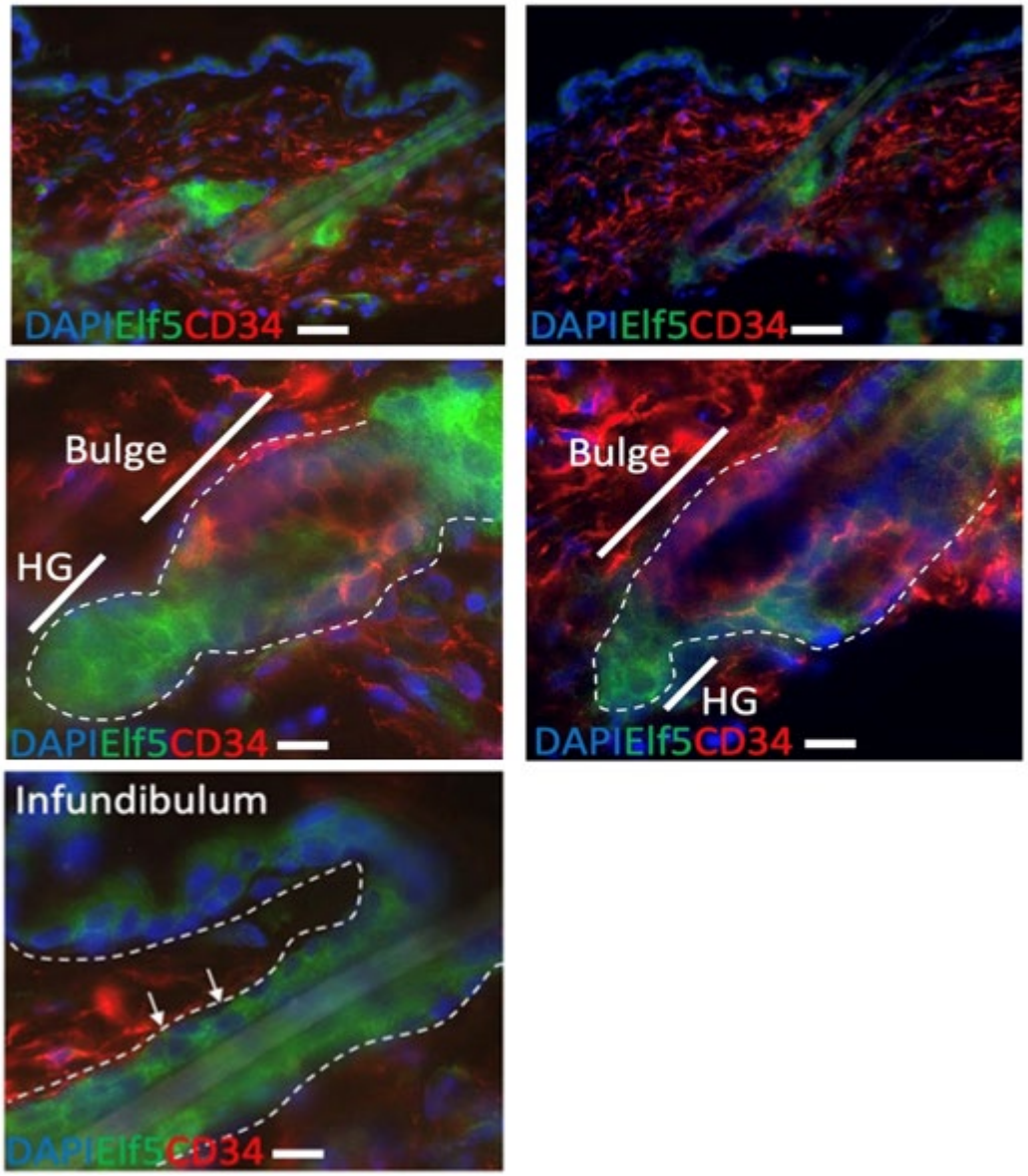

Figure 4.1 Expression analysis of Elf5 in stem cell populations in adult mouse skin and HFs. Immunofluorescence with SC marker CD34 (red) and nuclear staining (DAPI, blue) in adult uninduced Elf5CreERT2-GFP BAC transgenic mice tissue. Data provides the evidence and consistency of HF bulge as CD34+ SC compartment and the expression of Elf5 in proliferation and differentiation location (the basal and suprabasal layer) and overlapped with CD34 marked SC compartment. Scale bar: 50um. Representative images of n=3 experiments.

Elf5 expression in the epidermis can be seen in both the basal and suprabasal layers. In the HF, Elf5 is found in the SC areas, specifically in the bulge region and secondary hair germ of telogen HFs. The co-location of CD34 and Elf5 is found in the bulge. This confirms and supplements our previous discoveries.

RT-qPCR analysis of FACs sorted EpiSCs CD34 Negative *vs.* CD34+ from adult wild type mice with SC markers

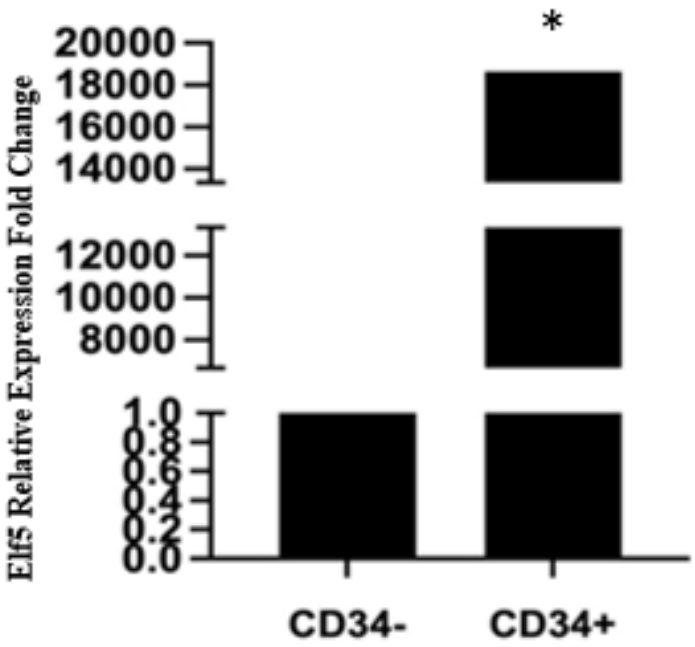

Figure 4.2 RT-qPCR analysis of FACs sorted EpiSCs CD34 Negative *vs.* CD34+ from 7–8-week-old C57/Bl6 wild type mice with SC markers CD34, α6 and Sca1. RT-qPCR analysis confirmed that expression of Elf5 was higher in CD34-positive groups compared to those in CD34-negative groups. Data are expressed as mean ± SEM from 3 independent experiments. *: $P \leq 0.05$.

This data shows that Elf5 is expressed in EpiSC compartments as well as in differentiated layers of the epidermis (Fig 4.1). However, much higher expression of Elf5 is found in CD34+ SCs (HF bulge SCs) from 7–8-week-old C57/Bl6 wild type mice through FACS sorting with SC markers CD34, α6 and Sca1 (Fig 4.2).

4.2.2 Investigation of the Function of Elf5 in FACS-Sorted Epidermal Krt populations

4.2.2.1 Optimization of Swiss 3T3 cells

Achieving growth-arrest in feeder cells is known to be cost-effectively accomplished through treatment with Mitomycin C (MC). For roughly three decades, murine Swiss 3T3 cells that were growth-arrested have been utilized to create graftable cultured epidermal sheets for treating full-thickness burns (Rheinwald & Green,1975; O'Connor et al., 1981; Green, 2008). However, the complexity of the issue is exacerbated by the significant discrepancies reported in MC concentrations, exposure durations, types of feeder cells, and exposure cell densities as highlighted in various studies (Roy et al., 2001; Ponchio et al., 2000; Gragnani et al., 2003; Nieto et al., 2007; Omoto et al., 2009; Chugh et al., 2015a; Chugh et al., 2015b). By adjusting the concentration of feeder cells and experimenting with different concentrations of harmful MC solution, we can determine the ideal concentration-dose combination that results in the optimal depletion of feeder cells, subsequently leading to the best SC growth (Chugh et al., 2017).

Optimization was carried out to induce varying degrees of feeder cell growth-arrest by adjusting volumes and subsequently determining the optimal feeder batch through target cell growth evaluation. Swiss 3T3 cell density, proven to be free from MC resistant variants, was treated with different volumes of a MC solution. The resulting feeder batches, with varied growth-arrest levels, were then assessed for both short-term and long-term viability, as well as their capability to support human epidermal krt growth. Imaging was performed every day using IncuCyte S3 live cell analysis instrument (Sartorius, Germany).

Image of Untreated Swiss 3T3 cells seeded in tissue treated 24 well plates with co cultured 100 x 10^3 HaCaTs for 5 days

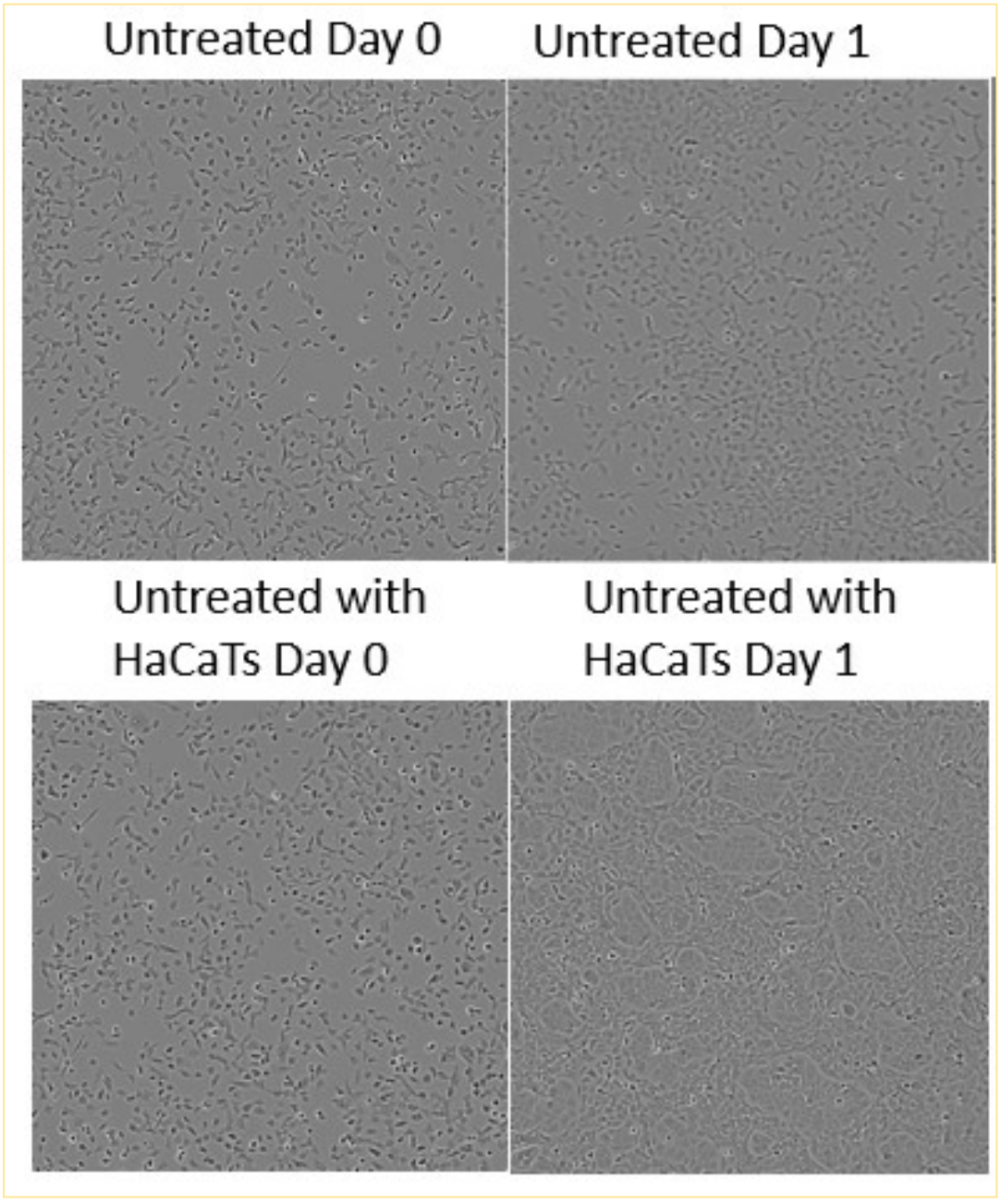

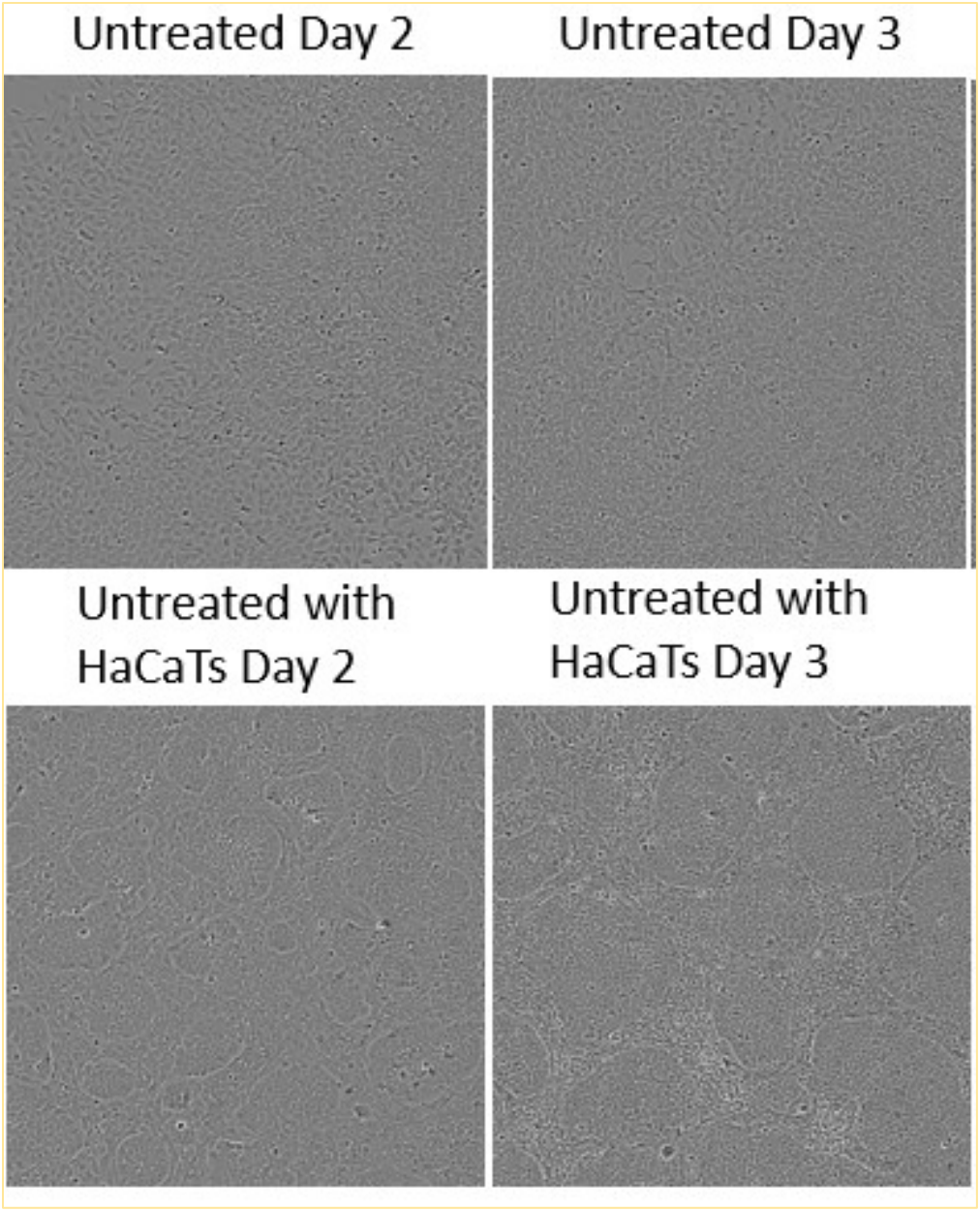
Untreated Day 2
Untreated Day 3
Untreated with HaCaTs Day 2
Untreated with HaCaTs Day 3

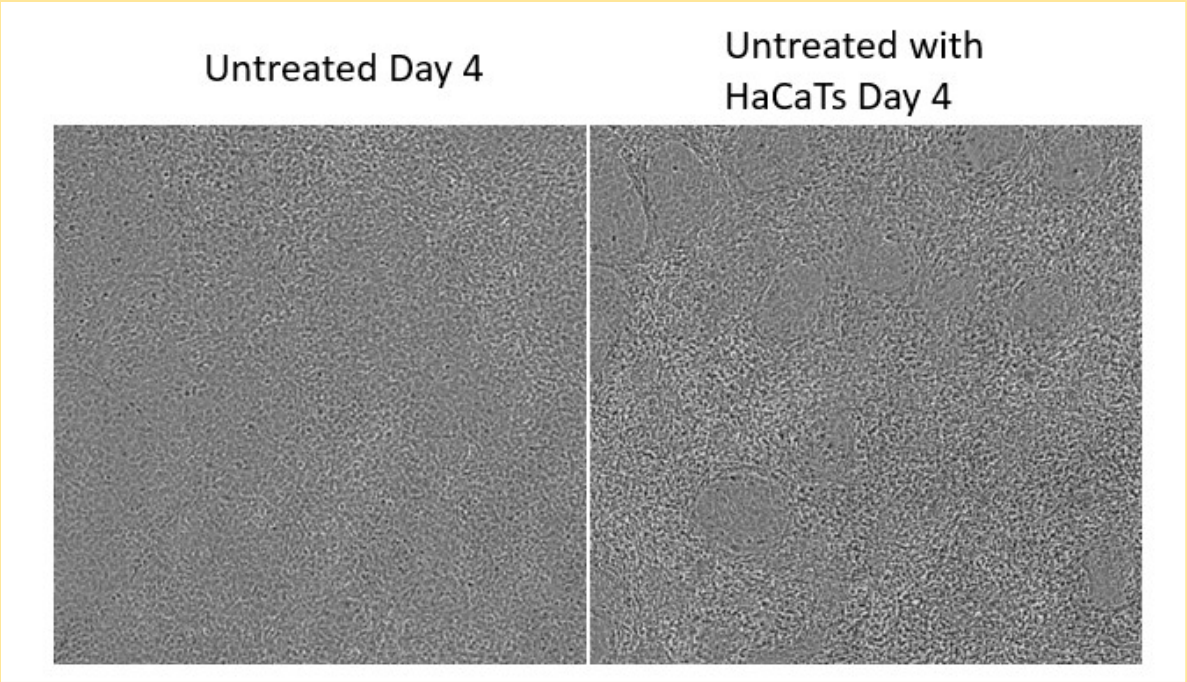

Figure 4.3 Untreated Swiss 3T3 cells were seeded in tissue treated 24 well plates with co cultured 100 x 10^3 HaCaTs for 5 days. In the co-culture, the untreated feeder cells continued to proliferate alongside the high-density feed cells, leading to the formation of cell clusters. Both the feeder and feed cells reached overconfluency rapidly, by Day 2. Images were taken with Incucyte 4X camera.

Image of treated Swiss 3T3 cells seeded in tissue treated 24 well plates with co cultured 50 x 10^3 HaCaTs for 5 days

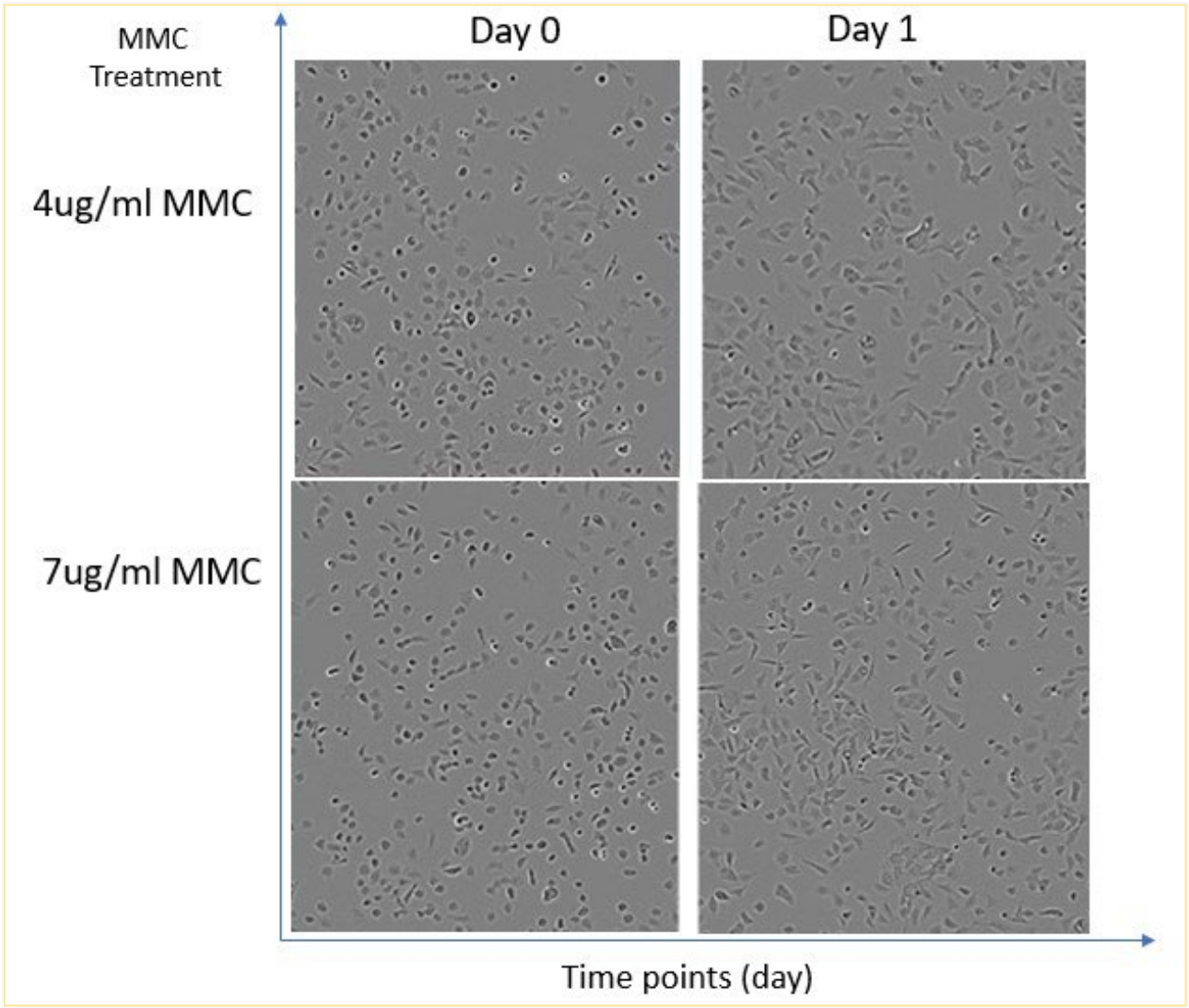

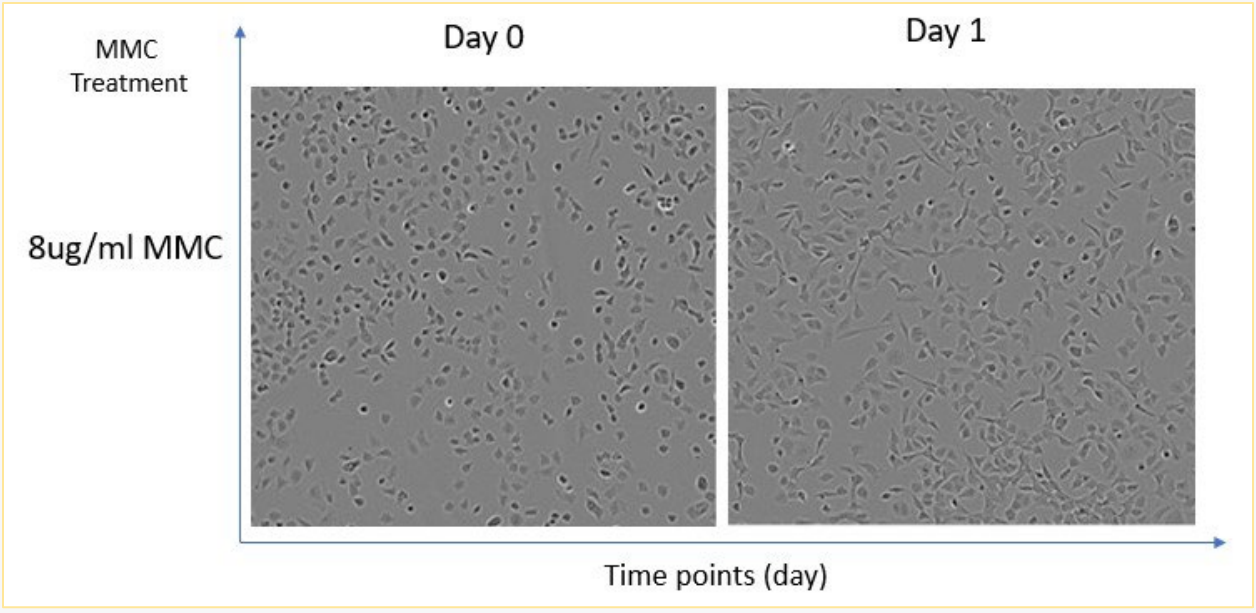
MMC
Treatment
Day 0
Day 1
8ug/ml MMC
Time points (day)

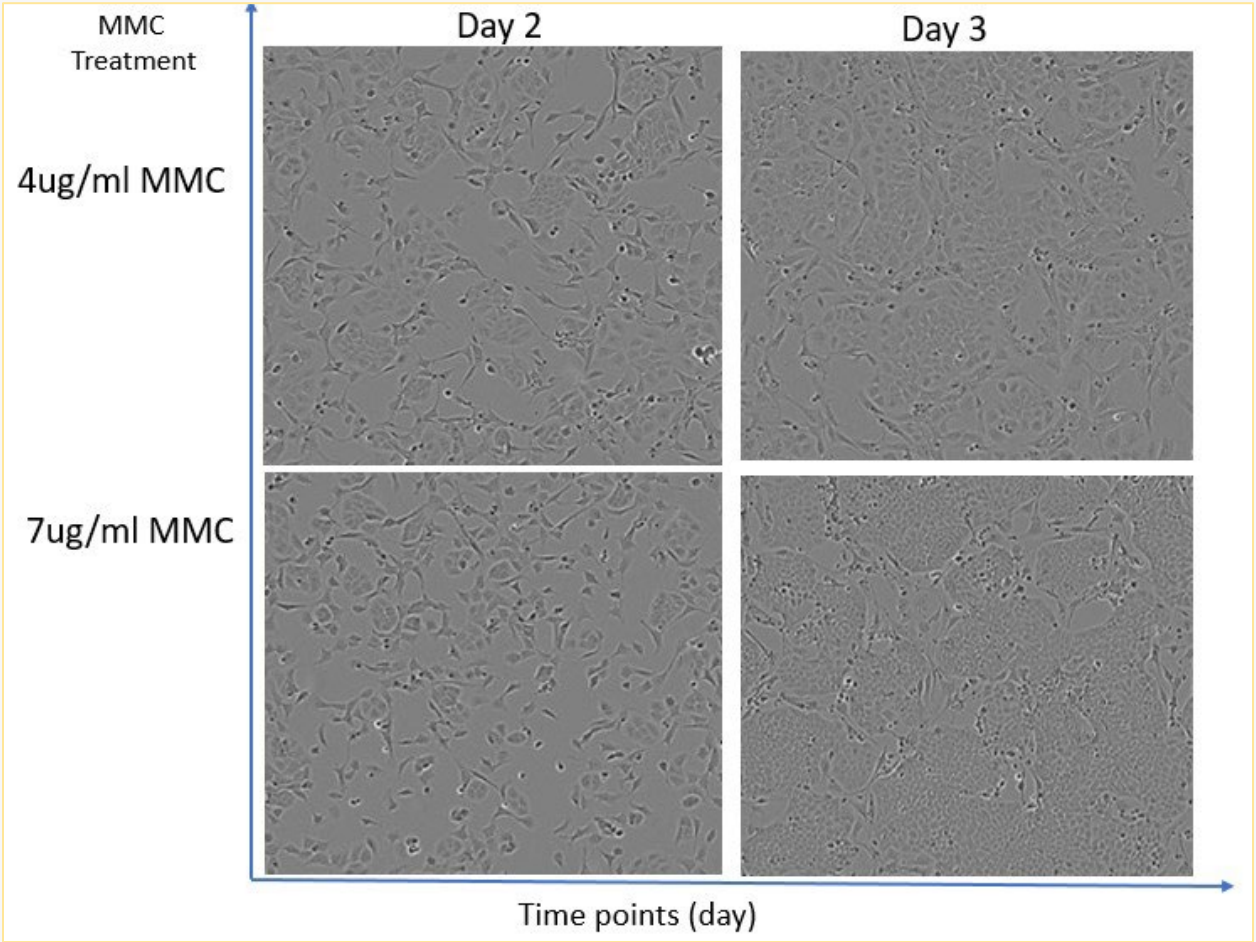
MMC
Treatment
Day 2
Day 3
4ug/ml MMC
7ug/ml MMC
Time points (day)

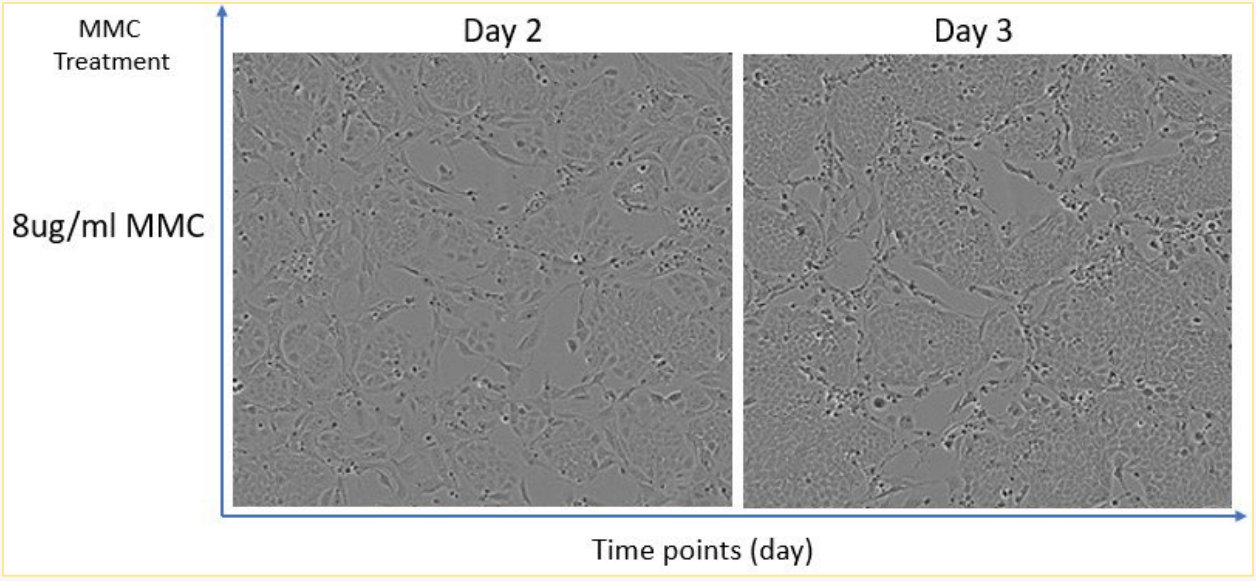
MMC
Treatment
Day 2
Day 3
8ug/ml MMC
Time points (day)

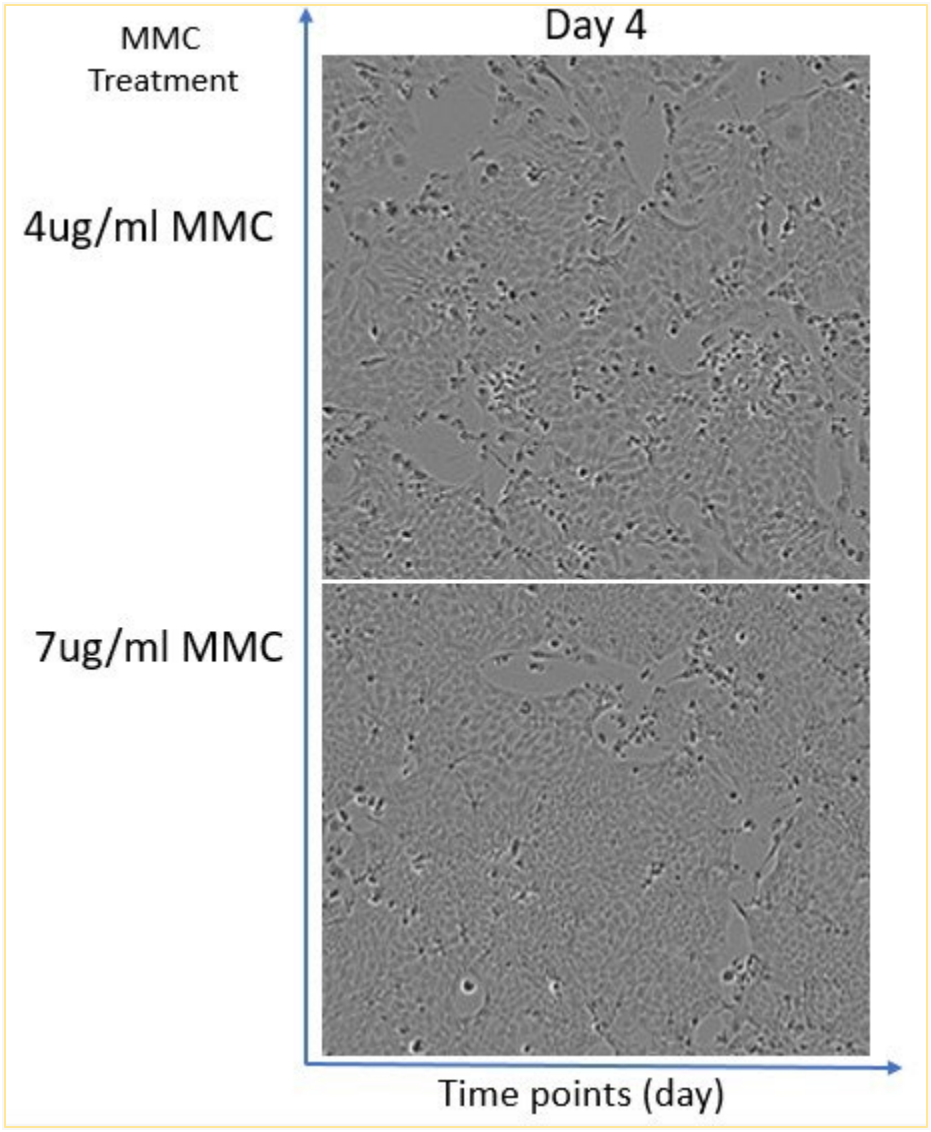
MMC
Treatment
Day 4
4ug/ml MMC
7ug/ml MMC
Time points (day)

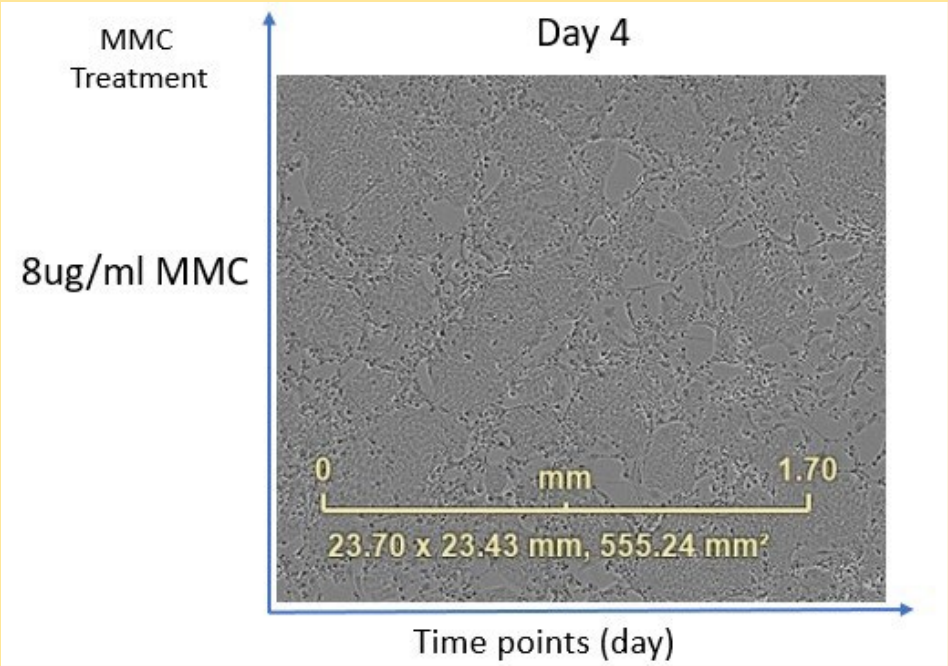

Figure 4.4 MMC treated Swiss 3T3 cells were seeded in tissue treated 24 well plates with co cultured 50 x 10^3 HaCaTs for 5 days. The spindle-shaped proliferating feeder cells continued to grow and spread in a fibrous pattern alongside the tightly packed feed cells when treated with lower concentrations of mitomycin C (4 and 7 µg/mL). In contrast, feeder cells treated with a higher concentration of MMC (8 µg/mL), which completely arrested their proliferation, provided a more favorable co-culture environment for the feed cells. Under these conditions, the polygonal HaCaT cells spread uniformly, formed confluent monolayers, and were tightly packed, characteristic of epithelial cells with well-formed junctions. Images were taken with Incucyte 4X camera. Zoom 4X.

Image of treated Swiss 3T3 cells seeded in tissue treated 24 well plates with co cultured 100 x 10^3 HaCaTs 24 hours

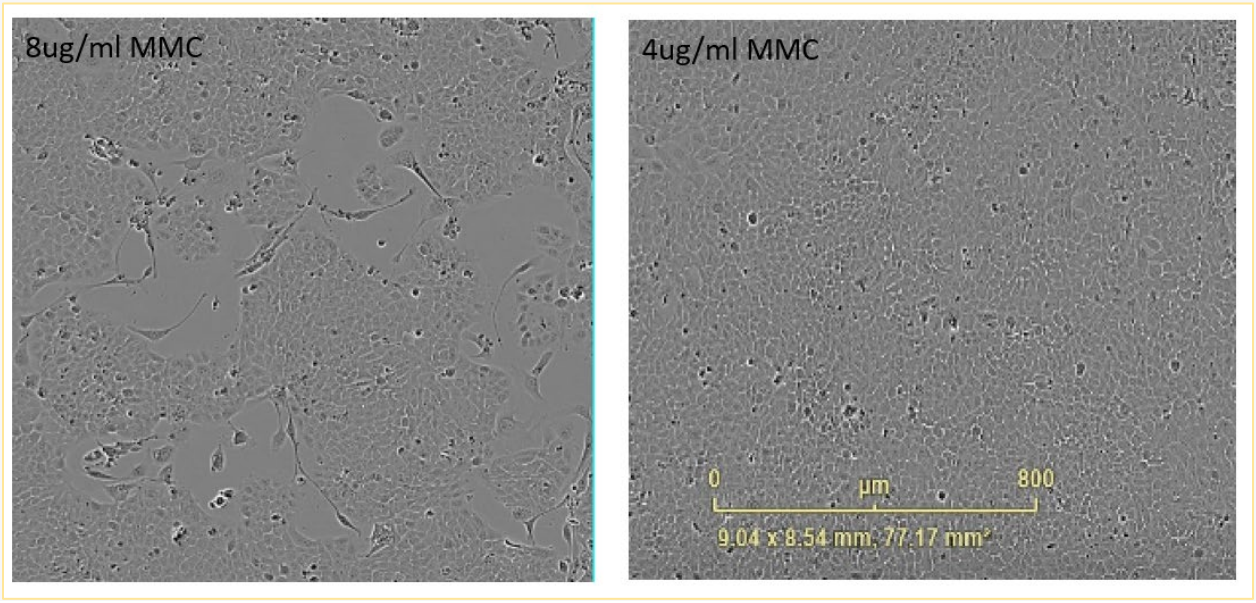

Figure 4.5 8ug MMC treated 3T3 VS 4ug MMC treated 3T3 Day 1 with HaCaTs 100 x10^3 per well (24 well plate). Feeder cells completely growth-arrested by treatment with 8 µg/mL mitomycin C (MMC) supported the growth of HaCaT cells. In contrast, feeder cells treated with a lower concentration of MMC (4 µg/mL) allowed overgrowth in co-culture with high-density HaCaT cells, resulting in the formation of cell clusters. Images were taken with Incucyte 4X camera, zoom 1.2X.

As expected, 3T3 cells have an approximate doubling time of 18 hours in a sparse culture and can achieve a saturation density of around 4 million cells per 100mm plate (Fig 4.3). These cells can be sustained at this saturation level for multiple weeks if the medium is refreshed twice a week (Nowak & Fuchs, 2009). Untreated 3T3 cells continued growing alongside with the co-cultured feed cells and formed clusters (Fig 4.3).

MMC in lower concentration 4ug/ml, 7ug/ml cannot arrest 3T3 feeder cells proliferation completely. 8ug/ml MMC treated 3T3 proved satisfying results as feeder cells after 5 days co-culture with HaCaTs (Fig 4.4). Too high density of feeder cells or continued growing feeder cells or too high density of feeding cells result in cell clusters in co-cell culture (Fig 4.3; Fig 4.5). The FACS sorted basal SCs at densities 3 x 10^3 ,10 x 10^3 and 15 x 10^3 per well (24 well plate) growing on 70-80% confluent with proliferation arrested 3T3 feeder cells within 2 weeks all gave similar and satisfying results as well as HF bulge SCs with 1.2 x 10^3 density.

4.2.2.2 FACS Sorted Epidermal Krt subpopulations growing dynamic analysis with Elf5 loss-gain function

Freshly sorted EpiSCs populations through "gentle FACS" were seeded on proliferation arrested 3T3 feeder cells in 24 well plates at appropriate density, then transduced by lentivirus as described in section 2.7. Elf5 expression was assessed via RT-qPCR after the sorting of subpopulations. The basal SCs and HF bulge SCs were transduced using lentiviral vectors carrying sequences to either inhibit or overexpress Elf5 or serve as controls (with scrambled sequences). Both the control and Elf5 inhibition/expression transduced SCs displayed high transduction efficiency, evident from the Elf5 expression in Elf5 inhibition and overexpression groups by RT-qPCR and GFP positive colonies. These GFP positive colonies were imaged and analyzed during the growth period of 10-14 days as described in section 2.7.4. Only colonies with morphology of circle 0.8-1, and diameter >0.19 pixel (50um) were analyzed.

4.2.2.2.1 Elf5 Expression Analysis in FACS-Sorted Krts Subpopulations

The different expression of Elf5 in sorted subpopulations was analyzed by RT-qPCR.

RT-qPCR analysis of distinct Elf5 expression levels in various FACS-sorted subpopulations

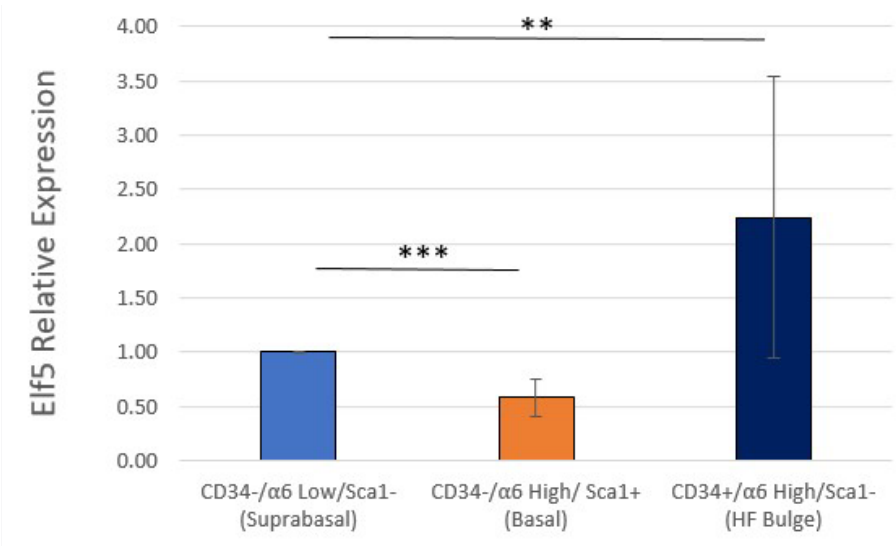

Figure 4.6 RT-qPCR analysis of distinct Elf5 expression levels in various FACS-sorted subpopulations. The CD34-/α6 High/Sca1+ group, representing basal SCs, exhibited the lowest Elf5 expression, and the associated p-value was nearly 0 when compared to the CD34-/α6 Low/Sca1- group, which represents suprabasal SCs. Conversely, the CD34+/α6 High/Sca1- group, representing HF bulge SCs, displayed the highest Elf5 expression, with a p-value of 0.008 in comparison to the suprabasal SCs group. Data are expressed as mean ± SEM from 3 independent experiments. *: $P \leq 0.05$, **: $P \leq 0.01$, ***: $P \leq 0.001$.

The results of RT-qPCR revealed varying levels of Elf5 expression in FACS-sorted subpopulations. Among these subpopulations, the group consisting of CD34-/α6 High/Sca1+ cells (representing basal SCs) exhibited the lowest Elf5 expression, with a p-value ≤ 0.001 when compared to the CD34-/α6 Low/Sca1- group (representing suprabasal SCs). On the other hand, the CD34+/α6 High/Sca1- group (comprising HF bulge SCs) displayed the highest Elf5 expression, with a p-value of 0.008 in comparison to the suprabasal SCs group.

FACS sorted basal SCs growth dynamic analysis

A

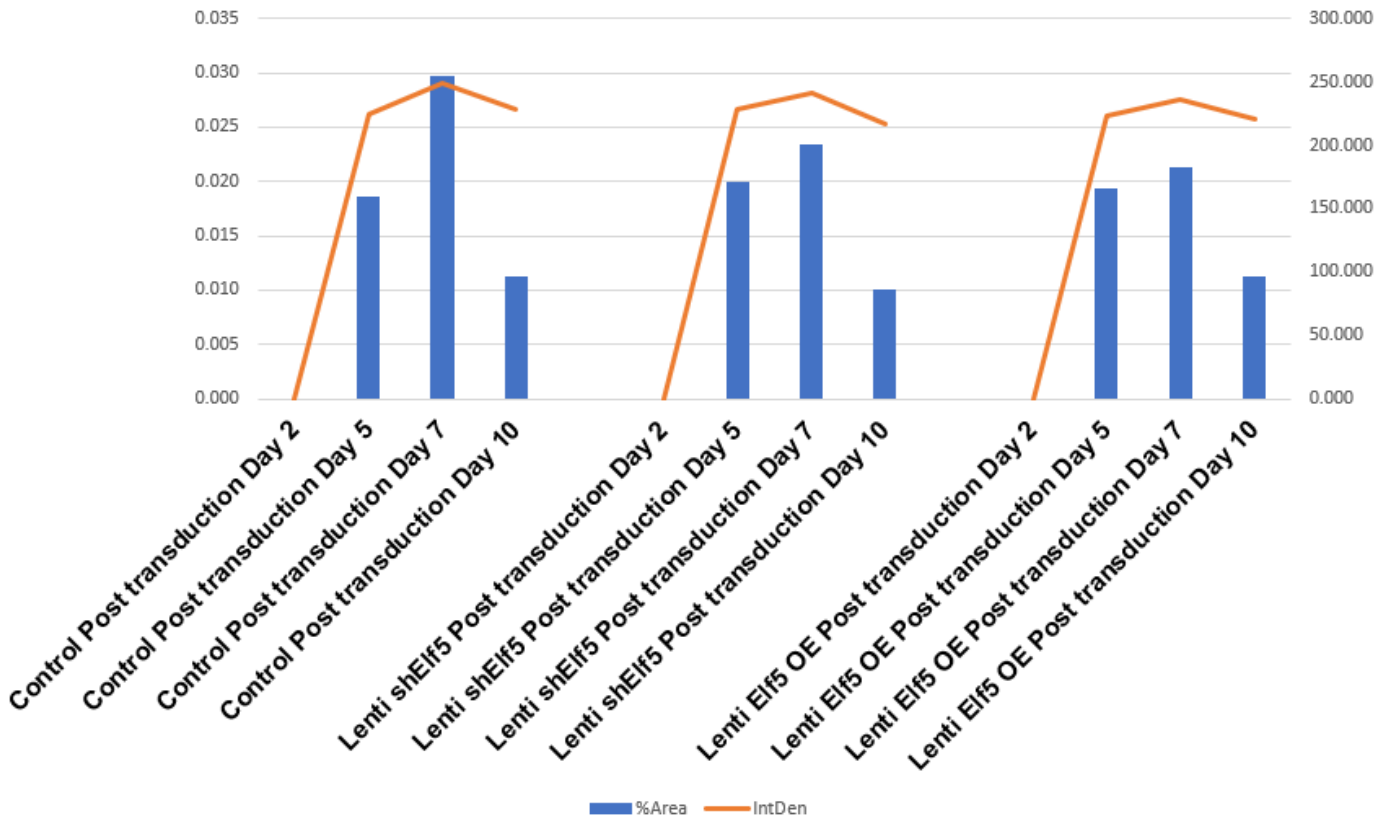

B

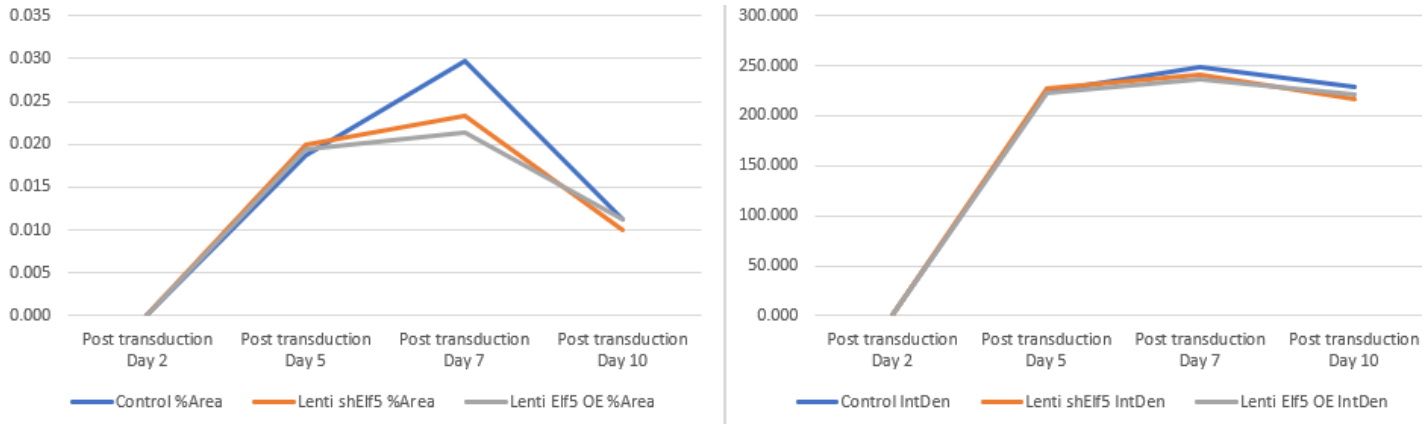

C

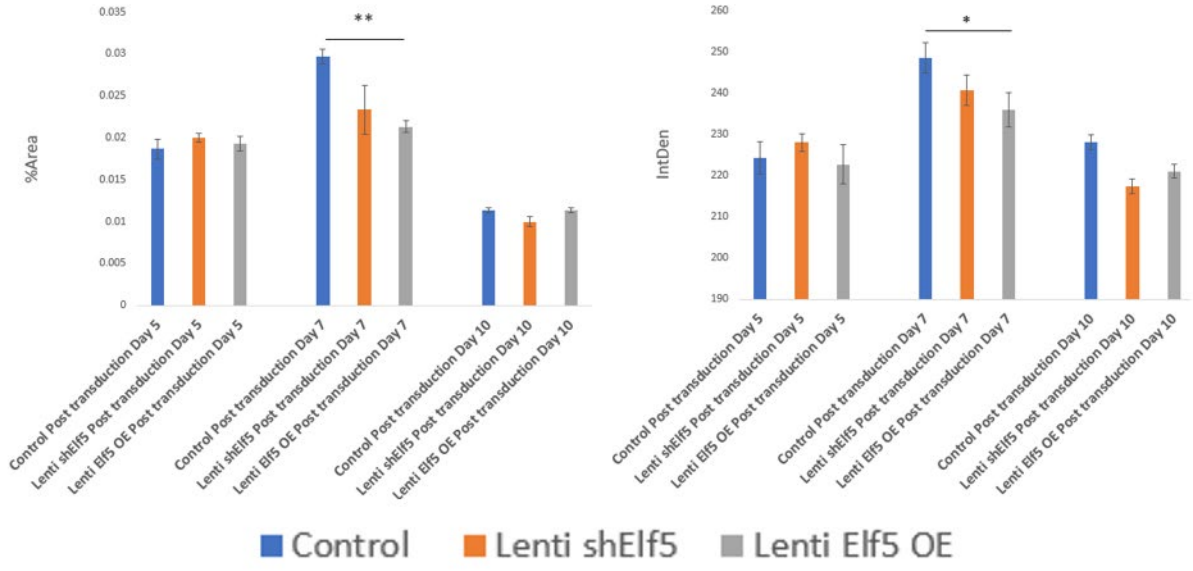

Figure 4.7 (A-C) FACS sorted basal SCs (CD34-neg/ CD49PE+High/Sca1+) seeded at 15 x 10^3 density per well (24 well plate) on 3T3 feeder cells growth dynamic analysis post transduction Day 2, 5, 7 and 10 colony area percentage (%Area) and colony intensity (IntDen). A: All groups reached their maximum clonal expansion area on day 7 post-transduction, with a significant colony growth spurt from day 2 to day 5. This was followed by a slowed growth phase between day 5 and day 7, after which there was a marked drop post day 7. The pattern of intensity was consistent with this trend; B: Between day 2 and day 5, the control group's colony expansion rate matched that of both the Elf5 loss and gain function groups. However, from day 5 to day 7, during the slowing expansion phase, the latter two groups expanded at a more measured pace than the control and occupied a reduced

colony area. Particularly, the Elf5 overexpression group displayed the slowest growth and took up the least colony space up to day 10. While colony intensities were generally alike, the control groups had a slightly elevated intensity; C: Comparing the colony area and intensity across groups at the same time point, significant differences were observed on day 7 post-transduction between the control group and the Elf5 overexpression group with p-value 0.002 for the colony area percentage, and 0.03 for colony intensity. Data are expressed as mean ± SEM from 3 independent experiments. *: P ≤ 0.05, **: P ≤ 0.01, ***: P ≤ 0.001.

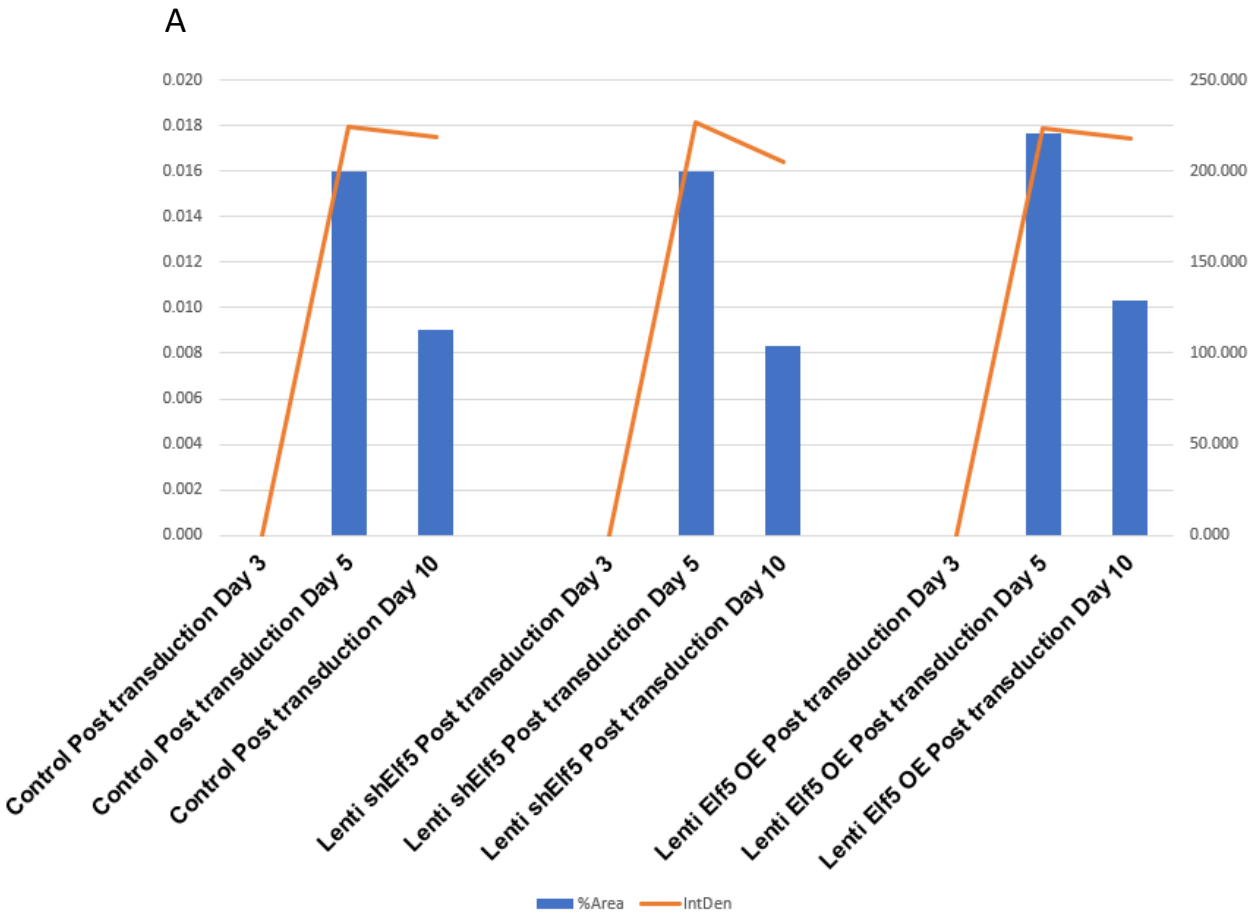

B

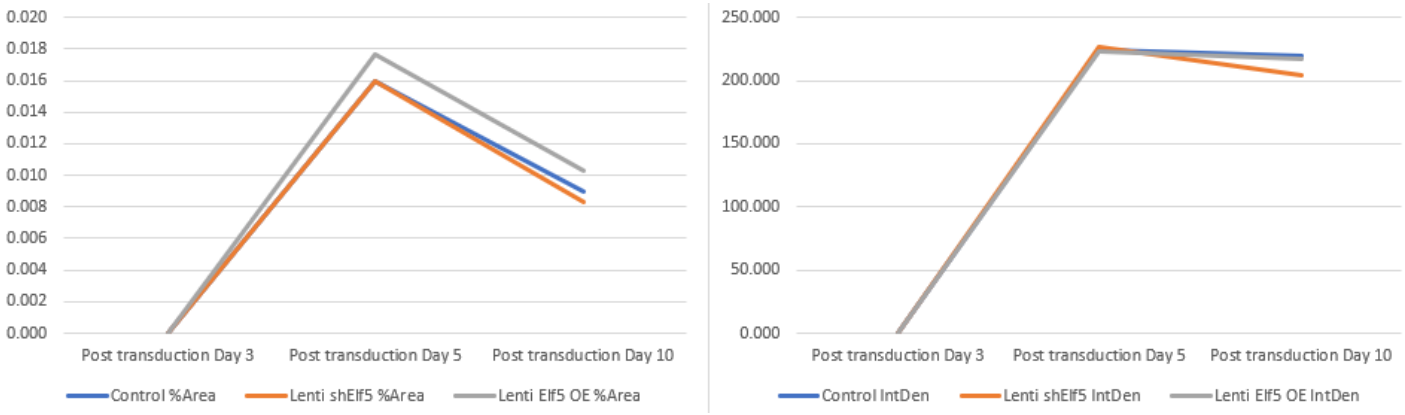

C

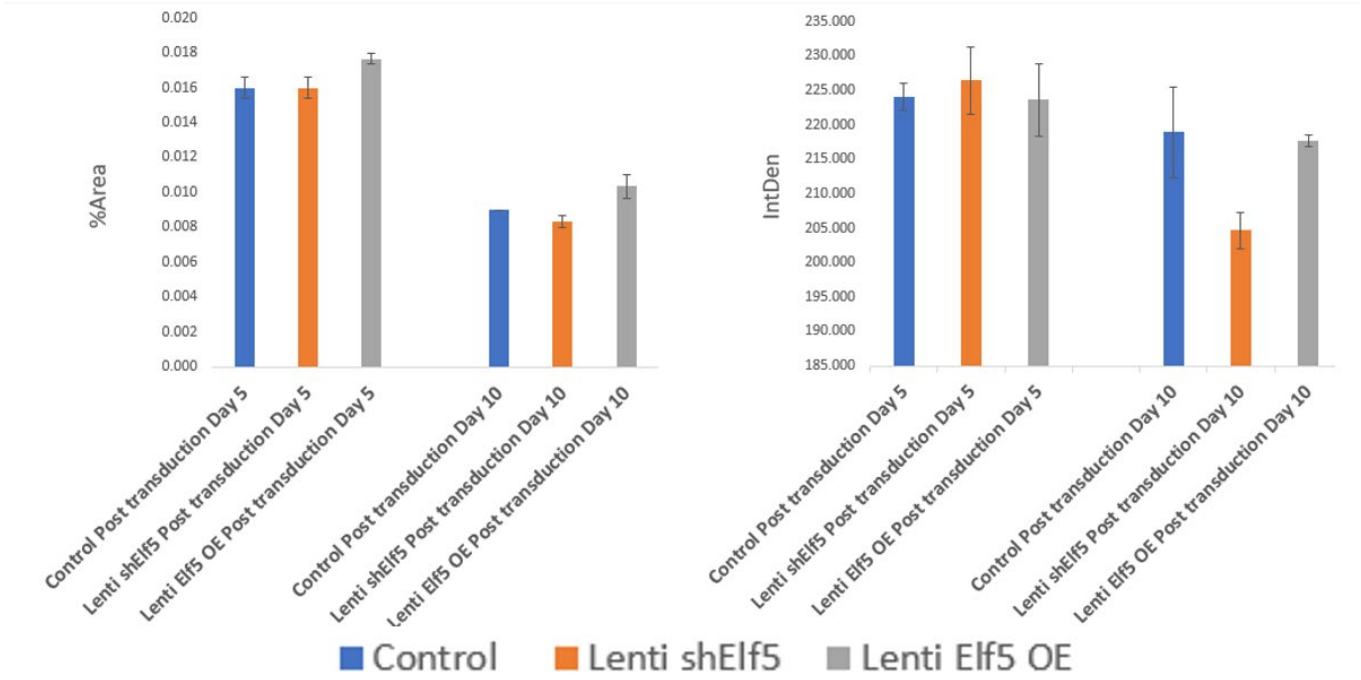

Figure 4.8 (A-C) FACS sorted HF SCs (CD34+/CD49fHigh/Sca-1-) seeded at 1.2 x 10^3 density per well (24 well plate) on 3T3 feeder cells growth dynamic analysis post transduction day 3, 5 and 10 colony area percentage (%Area) and colony intensity (IntDen). A: All the groups achieved the peak of clonal expansion arear at post transduction day 5 with one rapid colony forming period from day 3 to day 5, followed by a decline after day 5, especially in the Elf5 inhibition group, there showed a

sharp decline; The intensity shows the same pattern; B: Between day 3 and day 5, the colony expansion rate of the control group was on par with Elf5 inhibition groups, Elf5 overexpression showed faster and bigger colony expansion. However, from day 5 to day 10, Elf5 inhibition group displayed a more measured reduction rate than the control, resulting in lesser colony area occupation. All groups reached a peak in colony intensity on day 5 with comparable values. Subsequently, the intensity remained consistent for the control and Elf5 overexpression groups. In contrast, the Elf5 inhibition group exhibited the slowest growth and smallest colony occupation up to day 10, with its intensity mirroring this trend; C: When comparing colony area and intensity across groups at the same time point, no statistically significant differences were observed between the groups. Data are expressed as mean ± SEM from 3 independent experiments. *: $P \leq 0.05$, **: $P \leq 0.01$, ***: $P \leq 0.001$.

No colony expansion was observed in sorted suprabasal SCs (CD34-/CD49fLow/Sca-1-) as expected during two weeks of cells co-culture with feeder cells.

For sorted basal SCs (CD34-neg/ CD49PE+High/Sca1+) and HF bulge SCs (CD34+/CD49fHigh/Sca-1-), all the groups experienced one rapid colony forming period with increasing clonal expansion area and intensity within the first 5 days of post transduction (Fig 4.7). The sorted HF bulge SCs achieved the peak at post transduction day 5, but basal SCs continued to grow with increasing clonal expansion area and intensity at a slower rate and achieved the peak at post transduction day 7. Then, all groups showed decreased clones' area and density progressively (Fig 4.8). This is consistent with clone growth and then loss through differentiation.

For sorted basal SCs (CD34-neg/CD49PE+High/Sca1+), from day 2 to day 5, the control group exhibited a similar rapid colony expansion rate as both the Elf5 loss and gain function groups. However, from day 5 to day 7 during the slower expansion phase, both the Elf5 groups expanded at a more gradual pace compared to the control, occupying a smaller colony area. Of these, the Elf5 overexpression group had the most reduced growth rate and the smallest colony area up until day 10. In terms of colony intensity, values were comparable across groups, with the control groups showing slightly higher intensity, which presents similar proliferation density expect of the different colony expansion surface between groups. At the same time point,

when comparing colony area and intensity between groups, notable differences were evident on day 7 post-transduction between the control group and the Elf5 overexpression group. The colony area percentage had a p-value of 0.002, while the colony intensity registered a p-value of 0.03 (4.7 C).

For FACS sorted HF SCs (CD34+/CD49fHigh/Sca-1-), all groups hit their clonal expansion area apex on day 5 post-transduction, with a notable colony formation surge from day 3 to day 5. Elf5 overexpression exhibited quicker and more substantial colony growth from the beginning to the end. A decrease followed day 5, the intensity mirrored this trend (Fig 4.8). Between day 5 and day 10, the Elf5 inhibition group showed a slower decline rate compared to the control, leading to a smaller occupied colony area. While the intensity stayed stable for both the control and Elf5 overexpression groups, the Elf5 inhibition group demonstrated the most gradual growth and least colony coverage until day 10, with its intensity reflecting this pattern. Although no statistical significance was observed between the groups, a more pronounced difference was observed between the groups on day 10 post-transduction compared to day 5 for colony area and intensity, particularly between the Elf5 inhibition and control groups (Fig 4.8 C).

4.2.2.3 FACS-sorted Basal and Hair Follicle Bulge Stem Cells Clonogenicity Assay Analysis with Elf5 Loss-Gain Function

From the previous growth dynamic analysis of FACS-sorted basal SCs and HF bulge SCs, post-transduction day 7 was selected for basal SCs and day 10 for HF bulge SCs Clonogenicity assay analysis. The effectiveness of Elf5 inhibition and overexpression through transduction was assessed using RT-qPCR, complemented by the observation of GFP positive images.

Following post-transduction day 7 or day 10, apart from analyzing the GFP positive colonies, after the removal of the 3T3 cells, the krt colonies were fixed and stained with Rhodamine B, illustrative brightfield pictures of 2D colonies at day 7 for basal SCs and day 10 for HF-SCs cultures are displayed. These images provide an overview of individual wells within a 24-well

plate, captured at an approximate magnification of 4× and subsequently examined, analyzed as detailed in section 2.7.4.

4.2.2.3.1 Clonogenicity Assay of FACS-Sorted Basal Stem Cells, Evaluating the Impact of Elf5 Overexpression and Inhibition

The presence of GFP-positive colonies not only confirms successful transduction but also enables real-time monitoring of colony formation dynamics and proliferation rates. The structural organization and fluorescence intensity of GFP-positive colonies provide critical insights into cell health, population homogeneity, and differentiation status, offering a comprehensive assessment of the functional and developmental state of the stem cell population. Additionally, Rhodamine B staining analysis in skin stem cells facilitates both quantitative and qualitative assessments of colony size, number, and morphology, providing valuable insights into the characteristics of these cells.

A

Representative images of isolated basal SCs cultured and post-transduction with lentivirus for 1 week

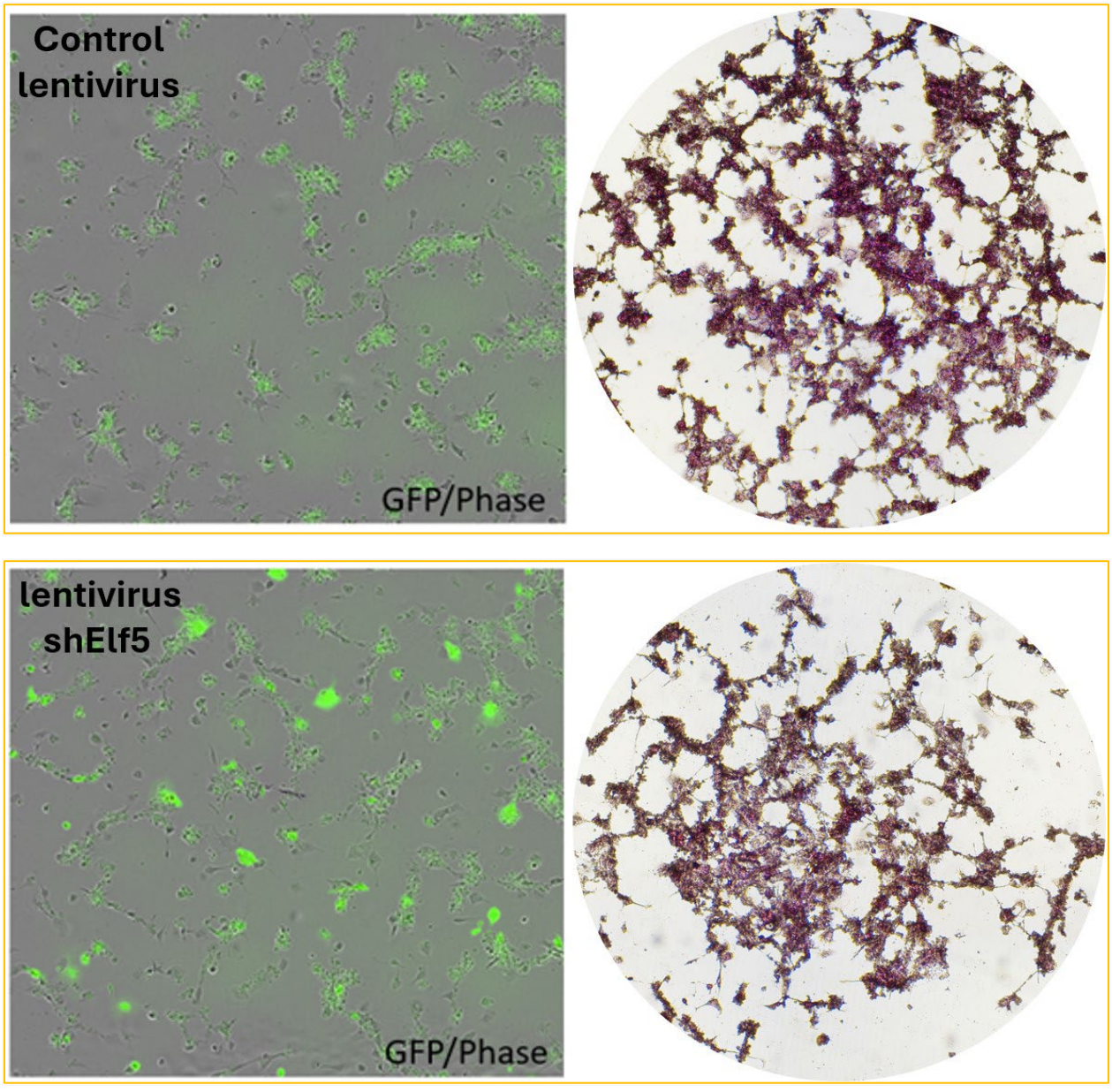

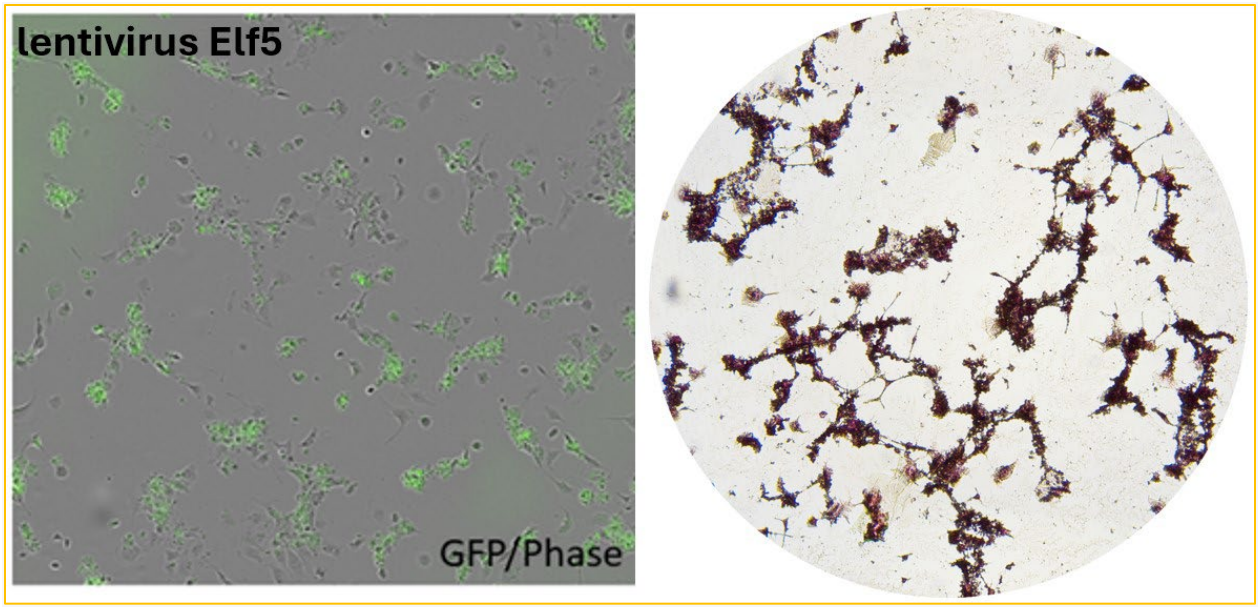

B

Quantification of size and number of colonies formed by isolated basal SCs post-lentiviral transduction day 7 after Rhodamine B staining

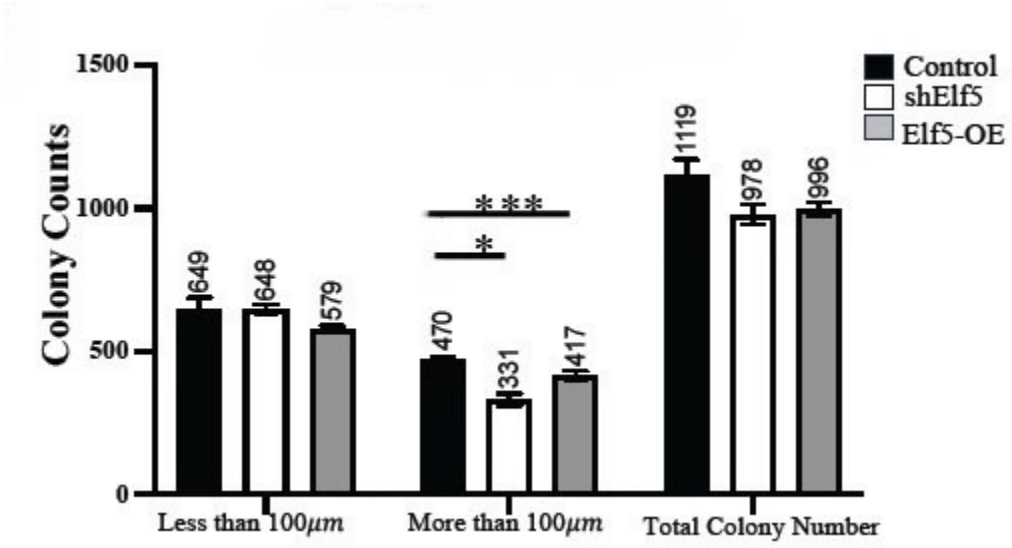

Figure 4.9 Colony formation assay of FACS sorted basal SCs (CD34-neg/ CD49PE+High/Sca1+) seeded at 15 x 10^3 density per well (24 well plate) on 3T3 feeder cells post transduction day 7. (A) Representative images of isolated basal SCs cultured and post-transduction with lentivirus for 1 week on 3T3 fibroblast feeder cells before and after Rhodamine B staining. The presence of GFP-positive

colonies not only confirms successful transduction but also reveals a reduced number of GFP-positive colonies in the treated groups, particularly in the group with Elf5 overexpression; Following Rhodamine B staining, tightly packed colonies displaying uniform red fluorescence were observed. (B) Quantification of size and number of colonies formed by isolated basal SCs post-lentiviral transduction day 7 after Rhodamine B staining. The colonies formed following the manipulation of Elf5 activity in basal SCs, it resulted in a noteworthy decrease in size (greater than 100µm) but did not affect the overall quantity of colonies when compared to the control group. Data are expressed as mean ± SEM from 3 independent experiments. *: P ≤ 0.05, ***: P ≤ 0.001.

4.2.2.3.2 Clonogenicity assay of FACS-sorted HF bulge Stem Cells, evaluating the impact of Elf5 overexpression and inhibition

A

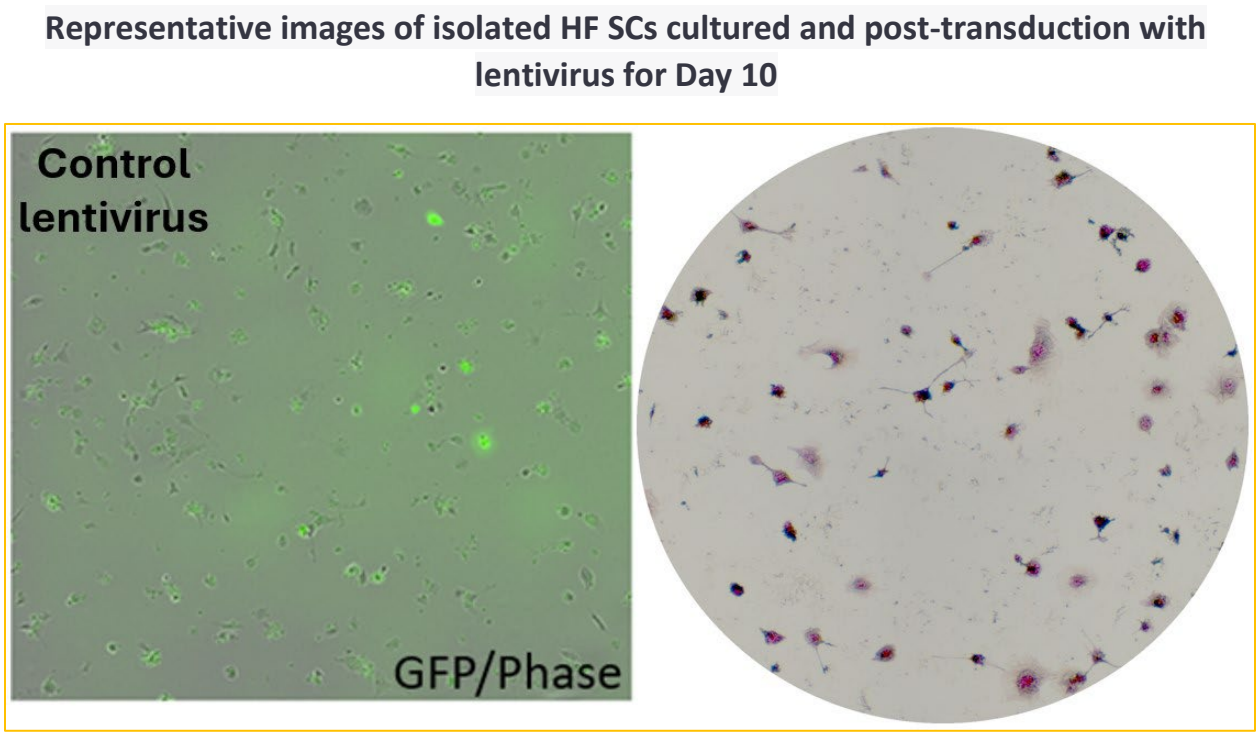

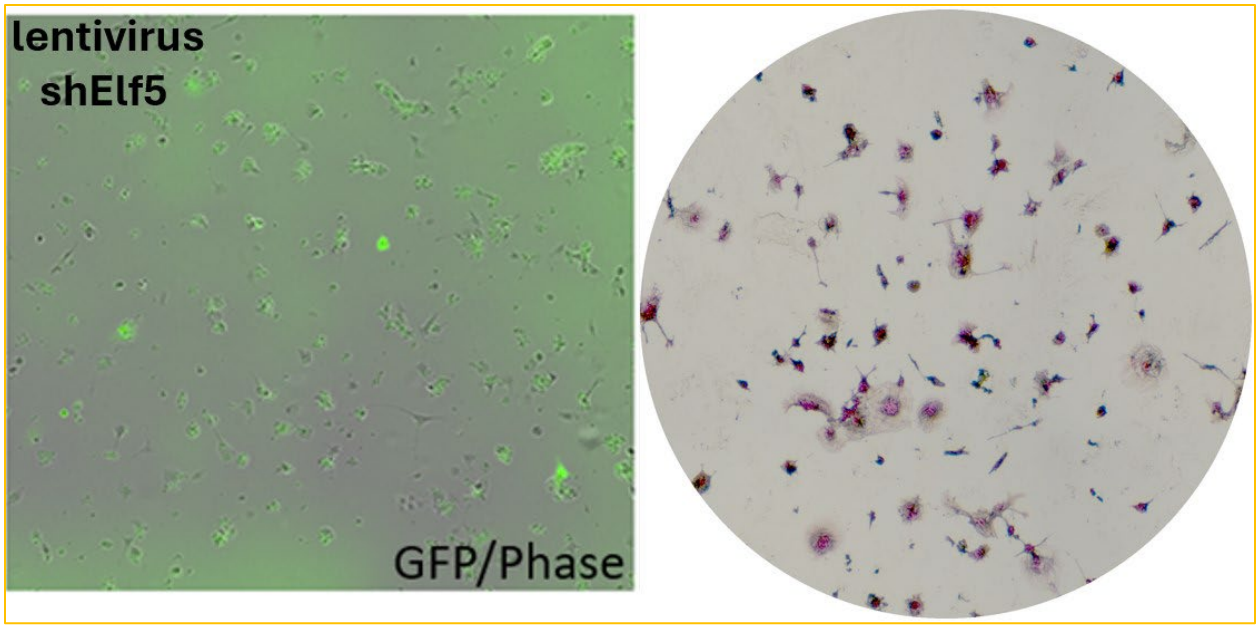

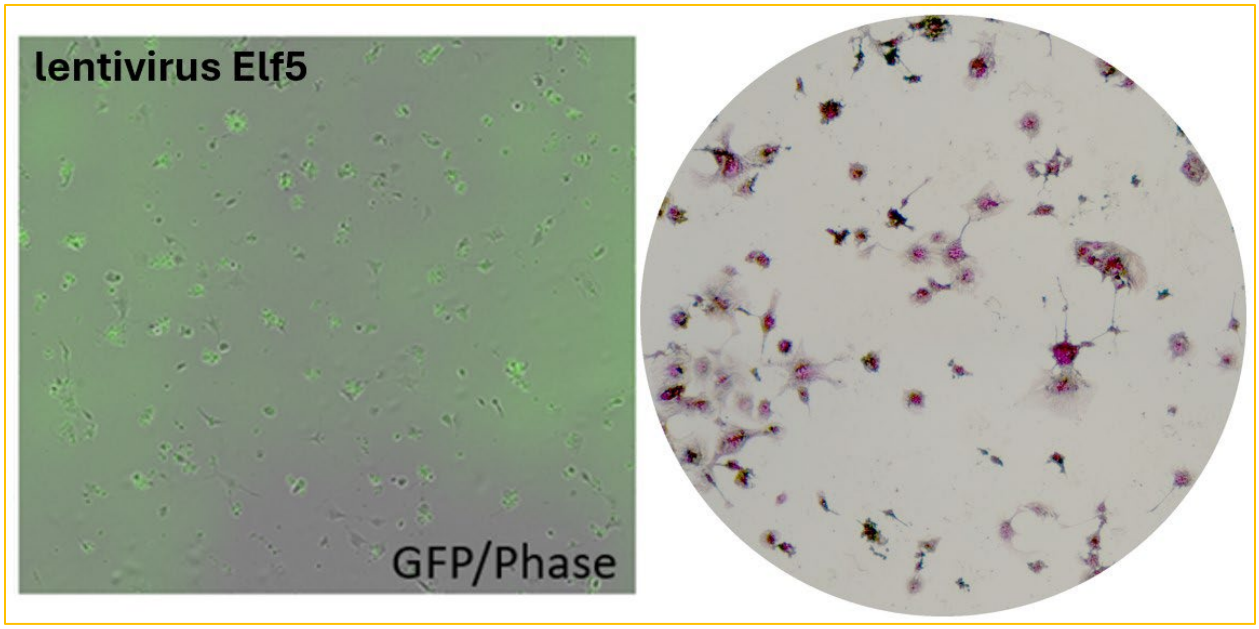

B

Quantification of size and number of colonies formed by isolated HF SCs post-lentiviral transduction Day 10 after Rhodamine B staining

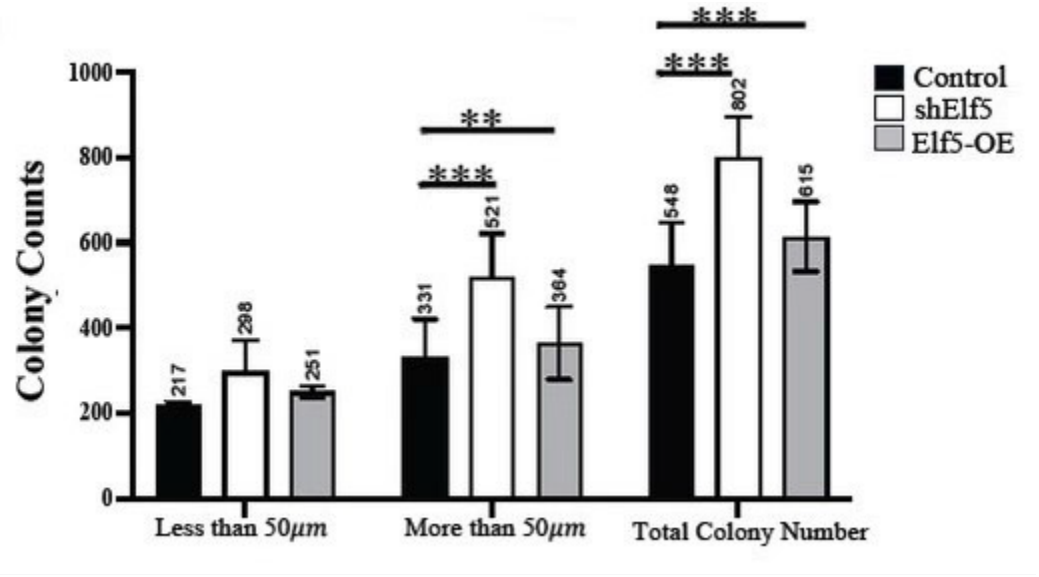

Figure 4.10 Colony formation assay of FACS sorted HF SCs (CD34+/CD49fHigh/Sca-1-) seeded at 1.2 x 10^3 density per well (24 well plate) on 3T3 feeder cells on 3T3 feeder cells post transduction day 10. (A) Representative images of isolated HF bulge cultured and post-transduction with lentivirus for 10 days on 3T3 fibroblast feeder cells before and after Rhodamine B staining. The presence of GFP-positive colonies not only confirms successful transduction but also indicates an increase in the number of GFP-positive colonies in the two treated groups; Following Rhodamine B staining, tightly packed colonies displaying uniform red fluorescence were observed. (B) Quantification of size and number of colonies formed by isolated HF bulge SCs post-lentiviral transduction day 10 after Rhodamine B staining. An increase in both the overall number and the size of HF-SC colonies (larger than 50µm) was noted following the manipulation of Elf5 activity, in contrast to the control group. Data are expressed as mean ± SEM from 3 independent experiments. *: P ≤ 0.05, **: P ≤ 0.01, ***: P ≤ 0.001.

4.3 Discussion

The FACS sorted CD34-positive cells showed much higher Elf5 expression (Fig 4.2). As CD34-positive cells from the bulge have a greater clonogenic ability than interfollicular basal cells (Trempus et al., 2003), this aligns with the notable clonogenic capacity of HF bulge SCs, and validated by the concurrent presence of CD34 and Elf5 in histological examinations (Fig 4.1). Hence, Elf5 is linked with the quiescence of HF bulge SCs. When examining Elf5 expression in distinct FACS-sorted subpopulations, it was observed that HF bulge SCs exhibited the highest

level of expression, while the sorted basal SCs displayed the lowest level. The suprabasal SCs demonstrated a higher level of expression compared to the basal group but lower than that of HF bulge SCs. This aligns with the prior findings from the Immunofluorescence analysis of Elf5 (Fig 3.5) as well as the analysis of proliferation and differentiation.

The colony growing and colony formation assay showed that, under suitable conditions, all the isolated basal SCs and HF bulge SCs successfully formed colonies. Sorted suprabasal SCs did not exhibit any colony growth. During the initial colony growth period (up to post-transduction day 5), both basal SCs and HF bulge SCs from every group exhibited a comparable rapid proliferation phase. Once the proliferation apex was attained, there was a subsequent decline. This was paired with the emergence of multicellular clones consisting solely of suprabasal cells, indicating clonal reduction due to differentiation (Clayton et al., 2007).

For the basal SCs, there is no observed variation between groups during this quick proliferation phase. This indicates that Elf5 does not influence the activation of SCs as they exhibit the same rate of proliferation. The divergence becomes apparent after this stage, where there's a deceleration in the proliferation rate. By the 7th day post-transduction, all groups attain their peak colony expansion. This is subsequently accompanied by a process of terminal differentiation and/or apoptosis, leading to a smaller colony size and lower colony intensity. It appears that overexpression and inhibition of Elf5 produce distinct effects during this subsequent proliferation phase. I hypothesize that Elf5 influences the proliferation, differentiation, and/or apoptosis of progenitor cells, rather than initiating quiescent SCs. When comparing the colony size and intensity among the groups at the same time point, notable disparities were evident on day 7 post-transduction, Elf5 overexpression group showed significant reduction effect with p-value 0.002 for the colony area percentage and 0.03 for the colony intensity. This is consistent with previous data (Fig 3.7 and Fig 3.8), which showed that Elf5 overexpression might inhibit the proliferation. However, concurrently, the Elf5 inhibition group also exhibited a reduced proliferation effect compared to the control group even though no statistical significance was observed. With deeper insight of the colonies, I observed a significant reduction in colony size (exceeding 100µm) in gain-or-loss of Elf5 groups while the

total number of colonies remained unaffected in comparison to the control groups. In the case of Elf5 overexpression, its impact is more pronounced, which could explain the greater effect on colony area occupation (Fig 4.10). This can be explained by the differentiation effect of Elf5, thus correlating with previous data (Fig 3.9 and Fig 3.10).

Compared to all the control groups, the quiescent HF bulge SCs (HF bulge SCs) displayed a faster growth rate during this time, evidenced by a steeper slope compared to the sorted basal SCs. From start to finish, the overexpression of Elf5 led to a faster and more significant colony expansion. I postulate that Elf5 may play a role in triggering the quiescent HF bulge SCs, leading to an accelerated colony growth process. This aligns with previous observations that revealed the peak expression of Elf5 in the anagen phase during the HF cycle. (Fig 3.3 and Fig 3.4). Simultaneously, suppressing Elf5 could lead to an accelerated differentiation and/or apoptosis in the progenitors. This matches the discovery that during the catagen phase, Elf5 expression is higher than in telogen but lower than in anagen (Fig 3.3 and Fig 3.4). After manipulating Elf5 activity, an increase in both the overall quantity and the size of HF-SC colonies (greater than 50μm) was observed, differing from the control group. When it comes to Elf5 inhibition, its impact becomes more pronounced (Fig 4.10). I postulate that Elf5 may modulate the hair growth by tuning the balance of activation of quiescent HF SCs and the proliferation, differentiation and/or apoptosis of HF SCs progenitors.

In summary, Elf5 exerted distinct effects on basal SCs and HF bulge SCs. It appears that Elf5 may hinder the proliferation, but stimiulate differentiation of basal SC progenitors while activating quiescent HF bulge SCs. Concurrently, Elf5 might also be involved in the proliferation and/or differentiation, as well as apoptosis, of HF "transit amplifying" cells. To gain a deeper insight of these effects, I employed RNA sequencing (RNA-seq) to detect transcriptional alterations dependent on Elf5 and utilized chromatin immunoprecipitation (ChIP) combined with deep sequencing (ChIP-seq) to pinpoint genes bound by Elf5 in PMEK, EpiSCs and their progenitors.

Chapter 5

Bioinformatic Analysis of Elf5 RNA sequencing and ChIP-Seq Data in PMEK

5.1 Transcriptome Profiling of Elf5 in PMEK

5.1.1 Introduction

Accurate assessment of gene expression levels and the detection of variations in transcript abundance between two conditions within a cell, tissue, or organism is a key method for detecting links between gene and environment. RNA-seq serves as a robust platform for conducting in-depth exploration of the transcriptome. RNA-seq analysis utilizing next-generation sequencing (NGS) data has emerged as the established method for comprehensively studying gene expression across the entire transcriptome (Ji & Sadreyev, 2018).

RNA samples collected from post-natal PMEKs subjected to Elf5 overexpression plasmid and control treatments were processed as described previously in section 2.9.1. These samples were then forwarded to Novogene, UK, where RNA sequencing was conducted using the Illumina PE150 platform. The resulting data in fasta format was subsequently uploaded to the Galaxy web platform (https://usegalaxy.org/) for in-depth analysis.

Alignment of the data was performed against the Mus musculus genome (mm9), and genes with statistical insignificance ($p>0.05$) were excluded from our analysis. Remaining genes were incorporated into the creation of heat maps and gene ontology evaluations.

Aim: To detect transcriptional alterations dependent on Elf5 in PMEK.

5.1.2 Results

A

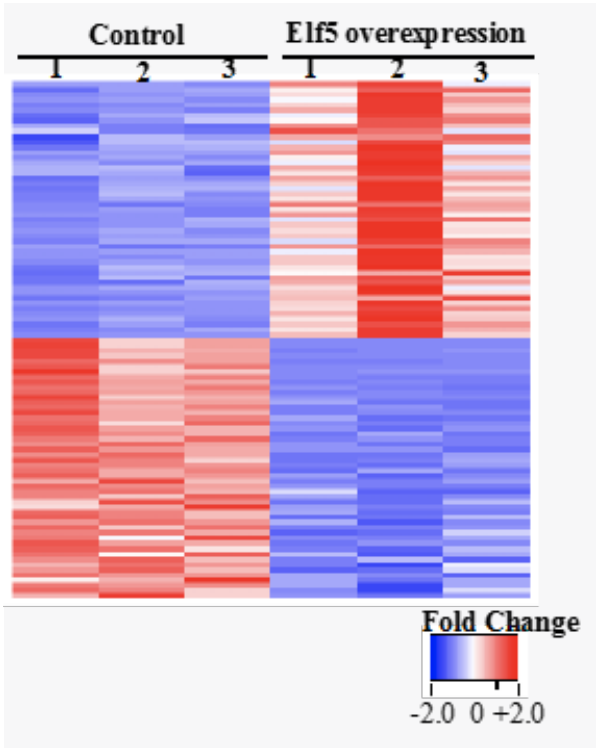

B

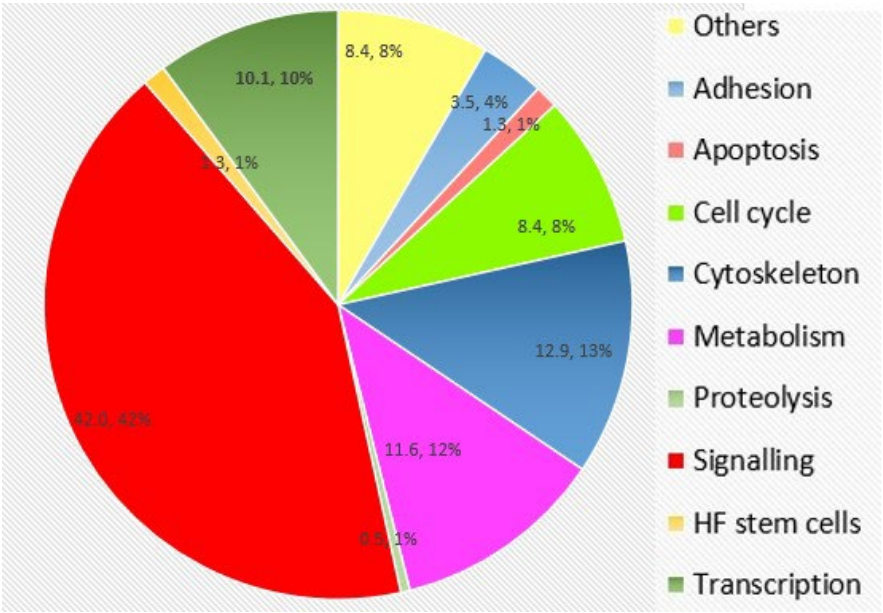

Figure 5.1 Heatmap of 50 most significantly changed genes: Elf5 Plasmid post transfection 48h vs Control in PMEKs RNA sequencing and gene ontology (GO) analysis. A: Heat map

depicting gene expression fold changes in Elf5 plasmid transfected PMEKs versus control plasmid following RNA-sequencing analysis (Red: up to 2-fold increase in expression versus blue: up to 2-fold decrease in expression). B: GO enrichment plot of total number of genes after Elf5 plasmid transfections in PMEKs versus control plasmid through the functional annotation. n= 3.

5.1.3 Discussion

After conducting total RNA sequencing analysis following Elf5 overexpression, the most significantly upregulated and downregulated genes when compared to the control group were amalysed. Gene ontology (GO) enrichment analysis revealed that approximately 42% of these genes are associated with signalling pathways, 8-8.4% with the cell cycle, 1-1.3% with apoptosis, 10% with transcription, 1-1.3% with HF SCs, 12% with metabolism, and 13% with the cytoskeleton, as well as other biological functions. This aligns with our earlier observations. However, Elf5, as all other transcription factors (TFs) interact with each other and with co-factors to establish TF complexes. The composition of these complexes can vary among distinct cell types or in response to different cellular conditions.

TF complexes play a role in regulating specific sets of target genes, thereby influencing cellular state (Mullen et al., 2011). Elf5 has the capability to either activate or inhibit transcription based on the context (Yaniw and Hu, 2005; Oakes et al., 2008; Choi et al., 2009). Considering the significant variation in the composition of the Elf5 complex and its context-sensitive activity, it is essential to examine Elf5 complexes and their target genes in a manner customized to the specific conditions, ensuring an accurate comprehension of their regulatory roles. To address this challenge, I carried out conditional Elf5 RNA sequencing and ChIP sequencing. Combining RNA sequencing and ChIP sequencing data through overlap provides us with more precise and condition-specific information.

5.2 Bioinformatic Analysis of Elf5 ChIP-Seq Data in PMEK and Identification of Elf5 Target genes

5.2.1 Introduction

Numerous biologically significant processes, including cell differentiation, cell cycle progression, gene transcription, DNA replication, chromosome stability, and epigenetic regulation, rely on vital interactions between cellular proteins and DNA. ChIP stands as a pivotal experimental technique for investigating these interactions. It has gained significant popularity as a technique for pinpointing genomic regions linked to specific proteins within the natural chromatin environment. This enables the identification of DNA-protein interactions occurring in live cells by capturing proteins at their DNA binding sites and has paved the way for groundbreaking research by providing fresh perspectives on DNA-protein interactions (Kurtenbach et al., 2019). This approach offers advantages over methods like DNase I foot-printing assays, which, being *in vitro* methods, have restricted usefulness due to their lack of a cellular context (Mundade et al., 2014).

Using formaldehyde, proteins are cross-linked to DNA, and chromatin extracted. Sonicated nuclear lysates were processed for immunoprecipitation with a mouse monoclonal anti-Elf5 antibody. After reversing the cross-links, the bound DNA fragments, typically between 200 to 1000 base pairs, can be analyzed or sequenced using various methods (DeCaprio & Kohl ,2020). See Figure 5.2 for ChIP Assay work flow.

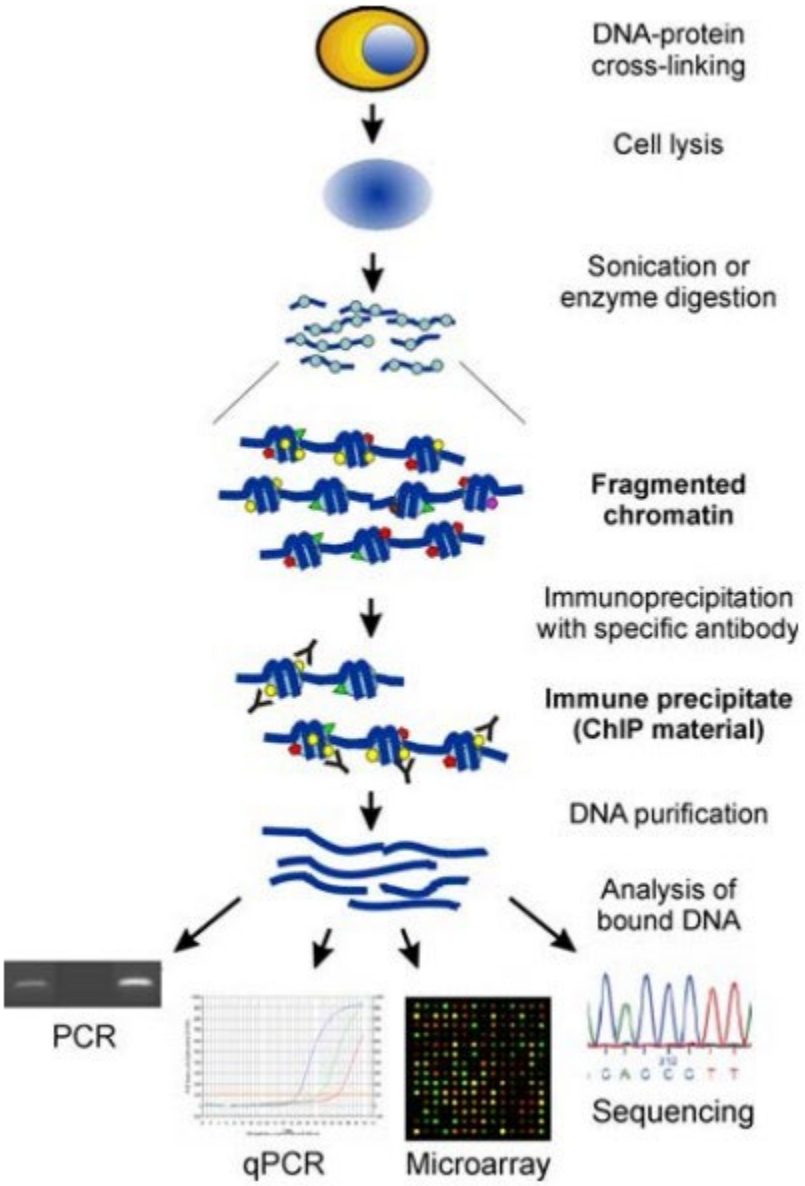

Figure 5.2 The chromatin immunoprecipitation (ChIP) assay and various methods of analysis

(Collas, 2010)

In contemporary times, next-generation sequencing (NGS) technology has undergone rapid advancements, significantly enhancing the landscape of genome research. The utilization of chromatin immunoprecipitation followed by high-throughput sequencing (ChIP-seq) is an application of next-generation sequencing (NGS) that offers an exceptionally effective approach for the comprehensive assessment of DNA-binding proteins, histone modifications, and nucleosomes at a genome-wide level (Park, 2009). This is highly effective in the identification of transcription factor (TF) binding sites.

These techniques enable the discovery of "peaks," which are specific regions of chromatin and their associated sequences enriched for TFs, employing a peak-calling algorithm to pinpoint genomic regions that show significant enrichment of ChIP-seq reads. As a result, by modifying cellular conditions, it is possible to identify condition-specific TF peaks. This, in turn, unveils the motifs recognized by DNA-binding TFs and their co-regulatory partners (Yang et al., 2017).

ChIP-seq offers higher resolution data because it directly reveals the DNA sequences of the precipitated fragments. Unlike methods, which are *In vitro* methods and fall outside the cellular context, reliant on the inconsistent and often weak binding efficiency of genomic DNA fragments to microarray-tiled oligonucleotides, ChIP assists in identifying DNA-protein interactions occurring within living cells by capturing proteins at their DNA binding sites, thereby overcoming certain limitations associated with *In vitro* methodes such as DNase I footprinting assays. Consequently, ChIP-seq delivers more precise and quantitative information (Mundade et al., 2014).

Post-natal krts from wild type mice, were isolated and cultured, induced in high calcium media to differentiate for 48 hours along with control groups as described in section 2.3. Total RNA was subsequently extracted and prepared following the procedure as described in section 2.9.1. Additionally, the same experiment was replicated, and the samples were fixed and prepared for ChIP and subsequent ChIP sequencing, as detailed in section 2.9.3.

NGS libraries were constructed, and the quality was evaluated following the methodology outlined in section 2.9.2.5. Bowtie 0.12.7 software (available at bowtie-bio.sourceforge.net) was utilized for the analysis. Following this, statistically notable peaks were pinpointed from the mapped reads using the Model-based Analysis of ChIP-Seq (MACS) software. From a technical perspective, Elf5 target genes were identified as those with ChIP-Seq peaks located within 5,000 bp either upstream or downstream of the 5' or 3' gene end, as defined by RefSeqGene (available at http://www.ncbi.nlm.nih.gov/refseq/rsg). MEME-ChIP software was used to identify the consensus motif sequences from a 150 bp segment surrounding the peak summits, extracted from the mm9 sequence track in GenomeJack.

Genes situated within 100 kb of the ChIP-enriched DNA are identified as potential Elf5 target genes. 154 potential target genes were identified (Appendix). These were overlapped with the previously identified top 50 up and down regulated target genes after Elf5 plasmid transfections in PMEKs and this identified 25 overlapped potential target genes. Subsequently, molecular pathways associated with the overlapped 25 target genes were analysed utilizing bioinformatics pathway analysis tools. qPCR was used to validate the target genes in PMEK low Ca 48 samples and ChIP-qPCR are currently ongoing to validate the chosen target genes.

To discern the pathways that are biologically pertinent to Elf5 target genes identified via RNA-seq and ChIP-Seq, the functional annotation tool from the Database for Annotation, Visualization, and Integrated Discovery (DAVID) v6.7 was utilised and associated Entrez Gene IDs or gene symbols input (refer to david.abcc.ncifcrf.gov) (Huang da et al., 2009).

DAVID pinpoints the most relevant pathway outlined by the Kyoto Encyclopedia of Genes and Genomes (KEGG). This involves determining the genes most enriched in the specified set, subsequently assessing statistical significance using a modified Fisher's exact test and making corrections via the Benjamini-Hochberg multiple comparison test. KEGG, accessible at http://www.kegg.jp, serves as an open-source database boasting manually curated reference pathways encompassing a vast array of metabolic, genetic, environmental, cellular processes,

and human diseases. Presently, it houses 271,665 pathways derived from 451 foundational pathways (Kanehisa, 2013).

In addition, Entrez Gene IDs were inputted into the Ingenuity Pathway Analysis (IPA) platform, available at http://www.ingenuity.com. IPA, a product of Ingenuity Systems, is a proprietary database housing around 3 million biological and chemical interactions, each backed by solid scientific evidence. On submitting the list of Gene IDs, IPA's network-creation algorithm pinpointed primary genes integrated within overarching molecular pathways and networks. The platform computes a score P-value, which represents the statistical significance of the link between the genes and their respective pathways or networks, using the Fisher's exact test.

Aim: To combine Elf5 ChIP sequencing with RNA sequencing to identify Elf5 direct target genes

5.2.2 Results

Through DAVID, gene ontology (GO) terms that were functionally related were identified. The most prominent GO terms encompassed cellular components, secretion of ECM constituents, cell differentiation, signaling pathways of vascular endothelial growth factor receptors, cell migration, mitotic G2 DNA damage checkpoints, MARK signaling, redox activity, cell division, cell junctions, GTP-binding, and the PI3K-Akt signaling pathway, among others.

Biological Function	Gene out of 25	Percentage
Anatomical structure development	8	34.78
Cell signalling	7	30.43
Programmed cell death	5	21.74
Cell differentiation	6	26.09
Mitotic Cell cycle	4	17.39

Table 5.1 The 25 target genes and GO analaysis of overlapped RNA seq data (Elf5 PMEKs low cal vs control) and ChIP Seq PMEKs HI Cal. Out of 25 genes which were overlapping, the majority of them belonged to cell signalling, programmed cell death, and diiferenetaion/proliferation pathways.

Through IPA pathway analysis, the listed overlapped gene pathway was identified:

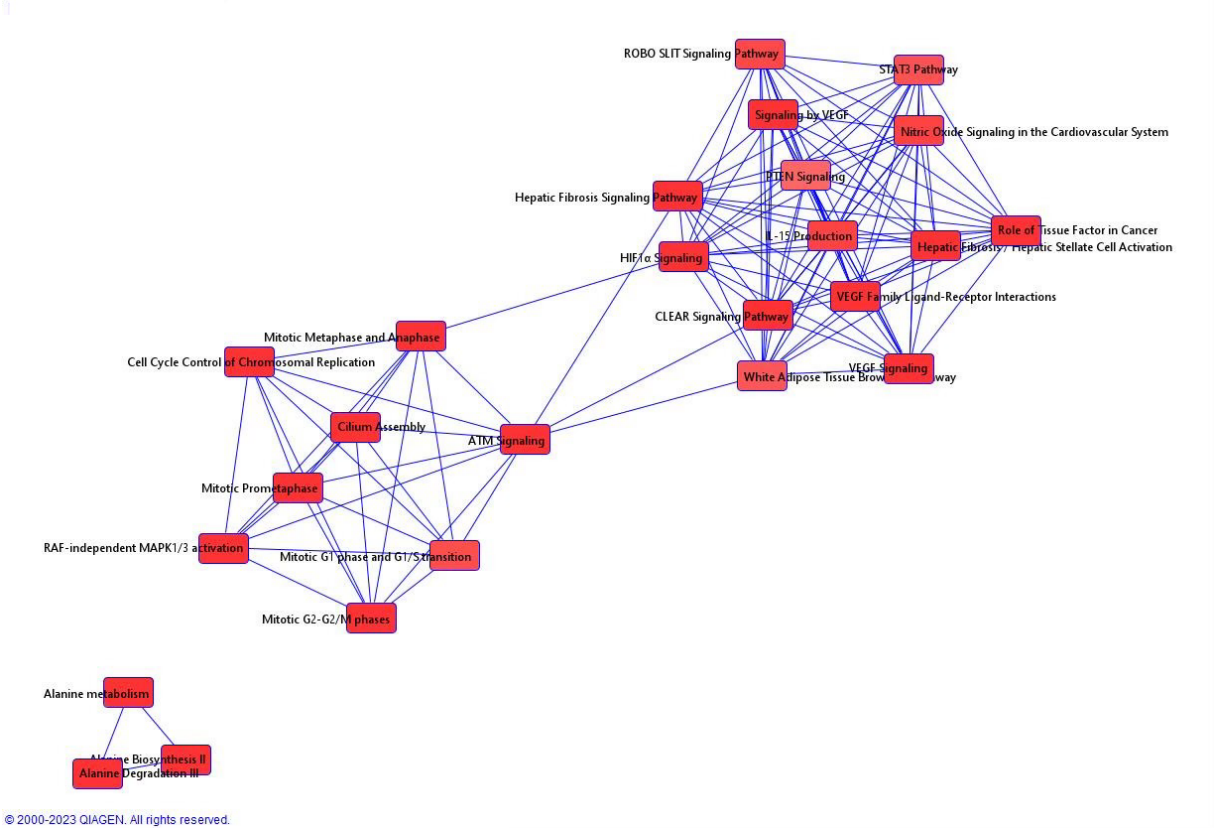

Figure 5.3 IPA overlapping canonical pathway analysis of 25 target genes from overlapped RNA seq data (Elf5 PMEKs low cal vs control) and ChIP Seq PMEKs HI Cal. These 25 target genes were involved in different overlapped canonical pathways. Some genes such as *Orc5, Sfi1, Tuba1b*, *Ccn2* are involved at the same time in important cell cycle pathways. Each ▭ represents one gene.

5.2.3 Discussion

Among the genes identified, through DAVID and IPA, various cellular processes, including cell cycle, p53 signaling pathway, cellular senescence, and gap junctions were identified. These 25 target genes played a role in various overlapping canonical pathways.

Through pathway analysis, *Orc5* (origin recognition complex subunit 5) was identified as involved in the activation of initiaion of DNA replication and mitotic G1 phase and G1/S transition and sythesis of DNA. *Sfi1* (SFI1 centrin binding protein) and *Tuba1b* (tubulin alpha 1b) from the listed genes are involved in mitotic G2-G2/M phase pathway, and also other

pathways such as protein binding, gap junction signaling, remodelling of epithelial adherence junctios, and sirtuin signaling. *Dusp6* is involved in cAMP-mediated signaling with *Creb3l1*. *Dusp6* and *Tuba1b* are involved at the same time in sirtuin signaling. *Tuba1b* is also involved in coronavirus peplication pathway. *Ccn2*, connective tissue growth factor (also referred to as Ctgf), which is instrumental in biological processes including cell adhesion, migration, proliferation, tissue wound healing, and remodeling of the ECM (Wang et al., 2021), increases with Elf5 overexpression.

This sequencing data demonstrates *Orc5* is upregulated when Elf5 is overexpressed. This suggests that one of Elf5's functions is to activate the initiation of DNA replication, the mitotic G1 phase, G1/S transition, and DNA synthesis through *Orc5* in epidermal krts. Tuba1b primarily resides within the chromosomal region and exhibits a positive correlation with processes such as DNA replication, cell cycle G2/M phase transition, chromosome segregation, and mitotic cell cycle phase transition. Interestingly, overexpression of Elf5 leads to the downregulation of *Tuba1b* and *Sfi1*, which, in turn, may have a negative regulatory effect on DNA replication and the transition of cell cycle into the G2/M phase.

Therefore, Elf5 exhibits distinct effects through different target genes in various pathways. It can positively regulate the activation of DNA replication, the mitotic G1 phase, G1/S transition, and DNA synthesis through its potential direct target gene Orc5. At the same time, Elf5 can negatively regulate the cell cycle transition to G2/M phase through *Tuba1b*, which is correlate with our previous data that a reduction of cells entering into S and G2/M phases of the cell cycle were observed after Elf5 overexpression (Fig 3.8).

5.3 Summary

After Elf5 overexpression and subsequent total RNA sequencing analysis, the most significant up and down-regulated genes compared to the control were identified. Gene Ontology (GO) analysis showed these genes are primarily involved in signaling pathways (42%), cell cycle (8-

8.4%), apoptosis (1-1.3%), transcription (10%), HF stem cells (1-1.3%), metabolism (12%), and the cytoskeleton (13%), among other functions. These results align with our earlier observations.

By overlapping RNA sequencing and ChIP sequencing data, it is possible to gain more accurate and context-specific insights. Among the 25 overlapping genes identified, most are involved in cell signaling, programmed cell death, and differentiation/proliferation pathways.

Overall, this data suggests that Elf5 is crucial for maintaining and balancing postnatal krts between proliferation and differentiation processes during skin development through different target genes, which are inolved in various pathways and requires further investigation.

Chapter 6

Transcriptome Profiling of Elf5 Loss-Gain Function RNA Sequencing in FACS-Sorted Basal and HF Bulge SCs of Adult Mice

6.1 Introduction

RNA samples collected from post-transduction day 7 FACS sorted basal SCs and cultured through Elf5 overexpression, inhibition, and control lentivirus treatments, were processed following the established protocols described in section 2.6 and 2.7. These samples were then forwarded to Novogene, UK, where RNA sequencing was conducted using the Illumina PE150 platform. The resulting data was subsequently uploaded to the Galaxy web platform (https://usegalaxy.org/) in fasta format for in-depth analysis with Kallisto and Sleuth in R.

Kallisto is an RNA-seq quantification tool that operates at a speed 100 times faster than earlier methods yet maintains comparable accuracy. Instead of aligning individual bases, Kallisto pseudo aligns reads to a reference, generating a list of transcripts matching each read. Using Kallisto, one can analyze 30 million unaligned paired-end RNA-seq reads in less than 10 minutes using a typical laptop. This significantly streamlines the RNA-seq analysis process. Sleuth is a software designed to analyze RNA-Seq experiments where transcript abundances have been quantified using Kallisto. It offers exploratory data analysis tools through Shiny by RStudio and incorporates statistical methods for differential analysis that utilize Kallisto's bootstrap estimates, (Bray et al., 2016; Harold et al., 2017).

The output of Kallisto was generated with the abundance estimates as well as the bootstrap samples using the "gencode.vM31.transcripts.fa" file obtained from the Ensembl release site. This file was utilized to construct a transcriptome index in Kallisto. Principal component analysis (PCA) plots and distribution of samples and sample types, mean-vearіance were plotted in Sleuth to visualize patterns and potential outliers and to visualize the relationship between the mean expression level and the variance of expression for genes or transcripts, and to help highlight the phenomenon of overdispersion in the before the Wald test to determine the significance of differences in expression between conditions. Pathway analysis was performed as described previously in section 2.9.1.9.2.

Aim: To detect transcriptional alterations dependent on Elf5 and utilized chromatin immunoprecipitation (ChIP) combined with deep sequencing (ChIP-seq) to pinpoint genes bound by Elf5 in EpiSCs and their progenitors.

6.2 Results

6.2.1 Elf5 Target Genes in FACS-Sorted Basal Stem Cells

The first 20 most up and down regulated genes (P value <0.05) were selected and inputted to IPA for core analysis. Canonical pathway analysis shows that these genes are involved in various cellular processes, including regulation of apoptosis, mitotic G1 phase and G1/S transition, synthesis of DNA, mitotic G2-G2/M phase, P38 MARK signiling, T53 regulates transcription of cell death genes, oestrogen receptor signaling, transcriptional regulation etc.

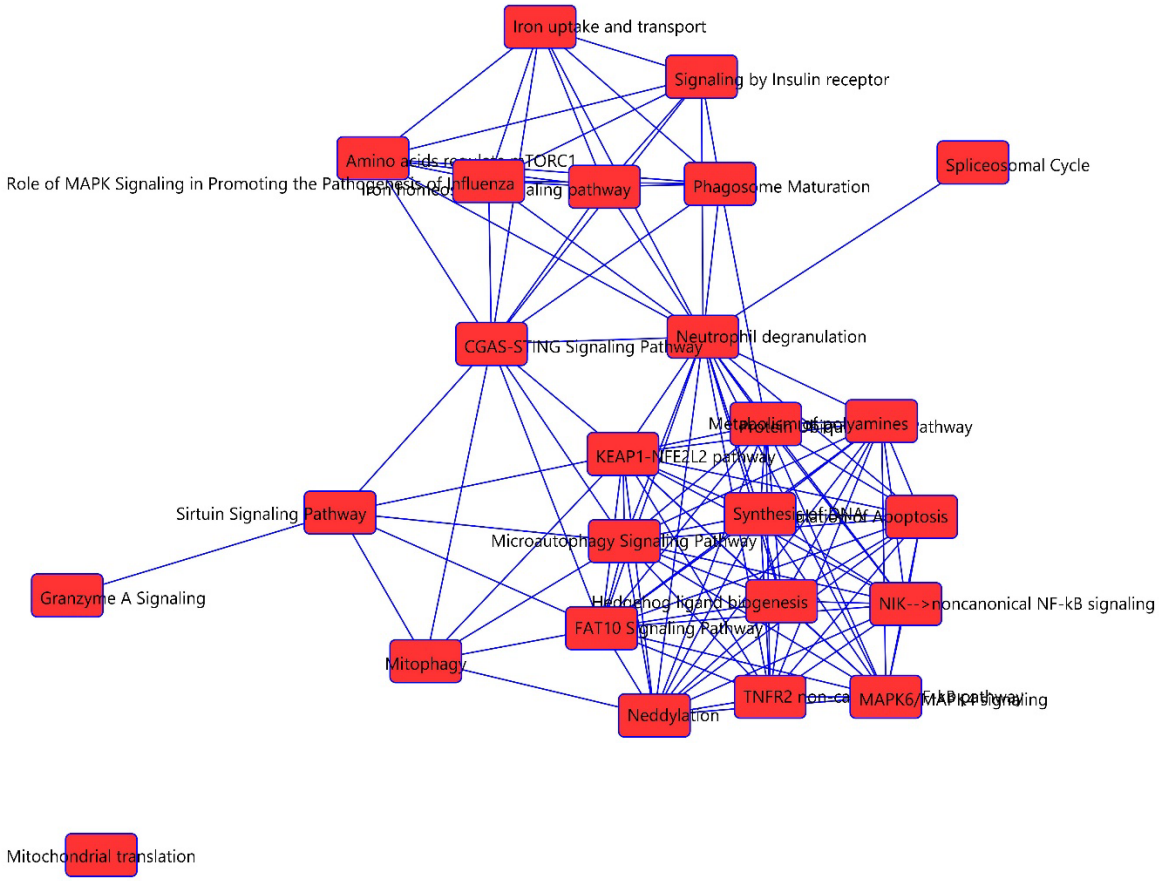

Figure 6.1 FACs-sorted basal stem cells Elf5 loss and gain function RNA sequencing the most up and down regulated genes overlapping canonical pathways. Genes intersect and participate in multiple cellular processes, such as regulation of apoptosis, mitotic G1 phase and G1/S transition, DNA synthesis, mitotic G2-G2/M phase, P38 MARK signaling, T53 transcriptional regulation of cell death genes, oestrogen receptor signaling, and other transcriptional regulatory functions. Each ▭ represents one gene.

After overlapping these 20 genes from the FACS sorted basal SCs RNA seq data with the mentioned 25 target genes through overlapping RNA seq data (Elf5 overexpression low cal vs control) and ChIP Seq PMEKs HI Cal, we narrowed the list and selected gene *Creb3l1* for further investigation as *Creb3l1* appears in both the initial set of overlapping genes and is present in a group of 262 genes from the RNA sequencing data of basal SCs.

Creb3l1, which is a transcription regulator and is involved in ATM (protein kinase ataxia-telangiectasia mutated) signaling pathway. *Creb3l1* was downregulated when Elf5 was over-expressed in PMEK RNA sequencing, basal SCs and ChIP sequencing. In case of DNA damage, ATM is activated. Once activated, ATM phosphorylates a range of downstream target proteins, initiating a signaling cascade. This pathway plays a critical role in arresting the cell cycle in response to DNA damage. It activates cell cycle checkpoints, particularly the G1/S checkpoint and the G2/M checkpoint, which temporarily halt the cell cycle to allow time for DNA repair.

The genes targeted by Creb3l1 encompass the collagen genes Col1a1 and Col1a2, as well as other genes associated with the production of matrix proteins (Chan et al., 2011). *Col1a1* and *Col3a1,* which constitute the predominant structural component of ECM, are particularly abundant in the skin (Mathew-Steiner et al., 2021; Wang et al., 2021; Gao et al., 2023). They are known as skin wound healing-related genes (Wang et al., 2021). They were downregulated in Elf5 loss fuction group while *Col3a1* showed also downregulated in Elf5 gain function group. *Col1a1* is a downstream target of *Creb3l1* and it can undergo transcriptional activation by Creb3l1, which binds to the promoter region of Col1a1 and thus plays a role in regulating collagen synthesis (Yuxiong et al., 2023).

Sprr1a (small proline rich protein 1A), which participates in the differentiation of krts and the formation of peptide cross-links and locates within the cornified envelope of stratified epithelial tissue [Source: Alliance of Genome Resources, April 2022], appears in Elf5 overexpression with upregulation. It shows that Elf5 overexpression induces differentiation.

6.2.2 Elf5 Target Genes in FACS-Sorted HF Bulge Stem Cells

The first 20 genes (p value < 0.05, fold change > 1.5) were selected and input to IPA for core analysis. The canonical pathway analysis shows that these genes are involved in various cellular processes, including ECM organization, assembly of collagen fibrils and other multimeric structures, collagen chian trimerization, collagen degradation, collagen biosynyhesis and midifying enzymes, integrin cell surface interaction, wound healing signaling pathway etc.

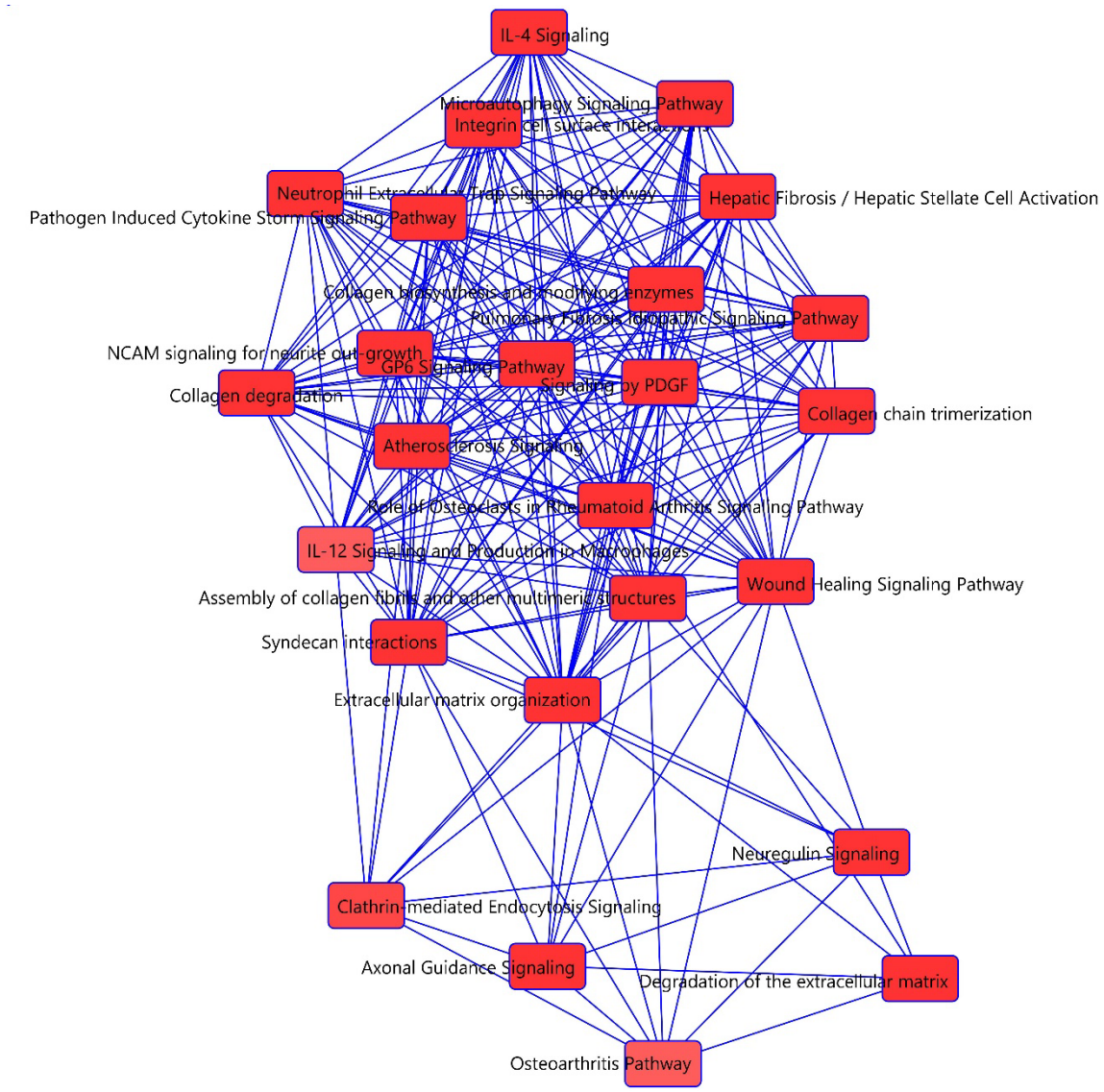

Figure 6.2 FACs-sorted HF SCs Elf5 loss and gain function RNA sequencing the most up and down regulated genes overlapping canonical pathways. These genes participate and intersect in a range of cellular processes, encompassing ECM organization, assembly of collagen fibrils and other multimeric structures, collagen chain trimerization, collagen degradation, biosynthesis and modification of collagen enzymes, integrin cell surface interactions, and the wound healing signaling pathway, among others. Each ▭ represents one gene.

Following the overlap analysis between the FACS sorted HF bulge SCs RNA seq data and the Elf5 direct taget genes from ChIP-seq data (PMEKs HI Cal), the list was refined to further explore the gene *Igfbp4* (Insulin-Like Growth Factor-Binding Protein 4), which was upregulated in the Elf5 inhibition group. IGFBPs regulate various cellular processes, including cell proliferation, survival, differentiation, migration, and invasion. More recently, they have been demonstrated to play roles in controlling senescence, autophagy, and angiogenesis (Bach, 2018). The association of IGFBPs with matrix proteins and proteoglycans has been recognised as a mechanism for enhancing the action of IGF-I (Mohan & Baylink, 2002). Based on GO annotations, *Igfbp4* negatively regulates the canonical Wnt receptor signaling pathway and Insulin-like growth factor receptor pathway. The Wnt/β-catenin pathway plays a crucial role in controlling HF growth during both embryonic and adult stages, under physiological as well as pathological conditions and it is also essential for the generation of new hair in response to wounding (Huelsken et al., 2001; Andl et al., 2002; Zhang et al.,2008; Ito et al., 2007).

IGF-1 is often the subject of extensive investigation, plays a fundamental role in controlling the hair cycle and orchestrating hair shaft differentiation during HF development. Studies have reported that IGF-1 promotes the growth of HFs *in vitro* by regulating cellular proliferation. When IGF-1 is absent, anagen HFs in organ culture setting undergo a transition into catagen. (Panchaprateep & Asawanonda, 2014). IGFBP-4 has been shown to inhibit the proliferation stimulated by IGF (Zhou et al. ,2003). Additionally, *in vivo* studies have confirmed that IGFBP-4 acts as a functional antagonist to IGF activity (Fleming et al., 2005). As Elf5 can negatively regulate Igfbp4, I postulate that Elf5 may promote HF growth, and keep HF in anagen by activating Igf-1 via Igfbp4. This correlate with some studies that IGFBP-4, found in both the dermis and epidermis, plays a role in regulating IGF-I activity within the skin, as evidenced in studies by Chen et al. (2003) and Hwa et al. (1999).

IGFBP-4 also plays a role in increasing the bioavailability of IGF to cells by decreasing the amount of IGF bound in the IGFBP/IGF complex, thereby reducing its restriction in circulation. Once released from this complex, a mechanism dependent on IGFBP-4 protease facilitates the release of IGF-I, enabling it to stimulate cells (Miyakoshi et al., 2001; Fleming et al., 2005).

Miyakoshi et al. (2001) observed that in mice, the systemic administration of native IGFBP-4, as opposed to a protease-resistant form of IGFBP-4, notably raised free IGF levels in the serum, which in turn led to an increase in bone formation. As the serum IGFBP-4 levels decrease during the ageing process (Mohan & Baylink , 1997; Wu et al., 2017), and Elf5 expression in skin decrease with age (Fig 3.6), we postulate that ELF5 can be a potential ageing biomarker in skin via IGFBP-4's reverse level in serum and also one potential molecular target in skin ageing or hair growth.

Intrestingly, *Col3a1* appears upregulated in Elf5 overexpression group, whereas *Col6a1* and *Col6a2* were downregulated in the Elf5 inhinition group group. *Col3a1*, *Col6a1*, *Col6a2* and *Itgb4* (intergin subunit beta 4) together are listed in ECM organisation and wound healing signaling pathway. *Adam8* (ADAM metellopeptidase domain 8), which upregulated with Elf5 gain hunction, at the same time upregulated too when Elf5 losses function, is involved in degradation of extrcellular matrix.

When we compare the analysis between the overlapped PMEK Elf5 overexpressin RNA sequencing and hghi calcium ChIP sequencing gene list, and the mentioned most up and down regulated genes list of last two FACs sorted basal SCs and HF SCs loss and gain function RNA sequencing data using IPA comparison analysis, the three groups genes show their involment in different pathways, but also show some hierarchical clustering through different pathways, the generated figure is partially shown below (Figure 6.3):

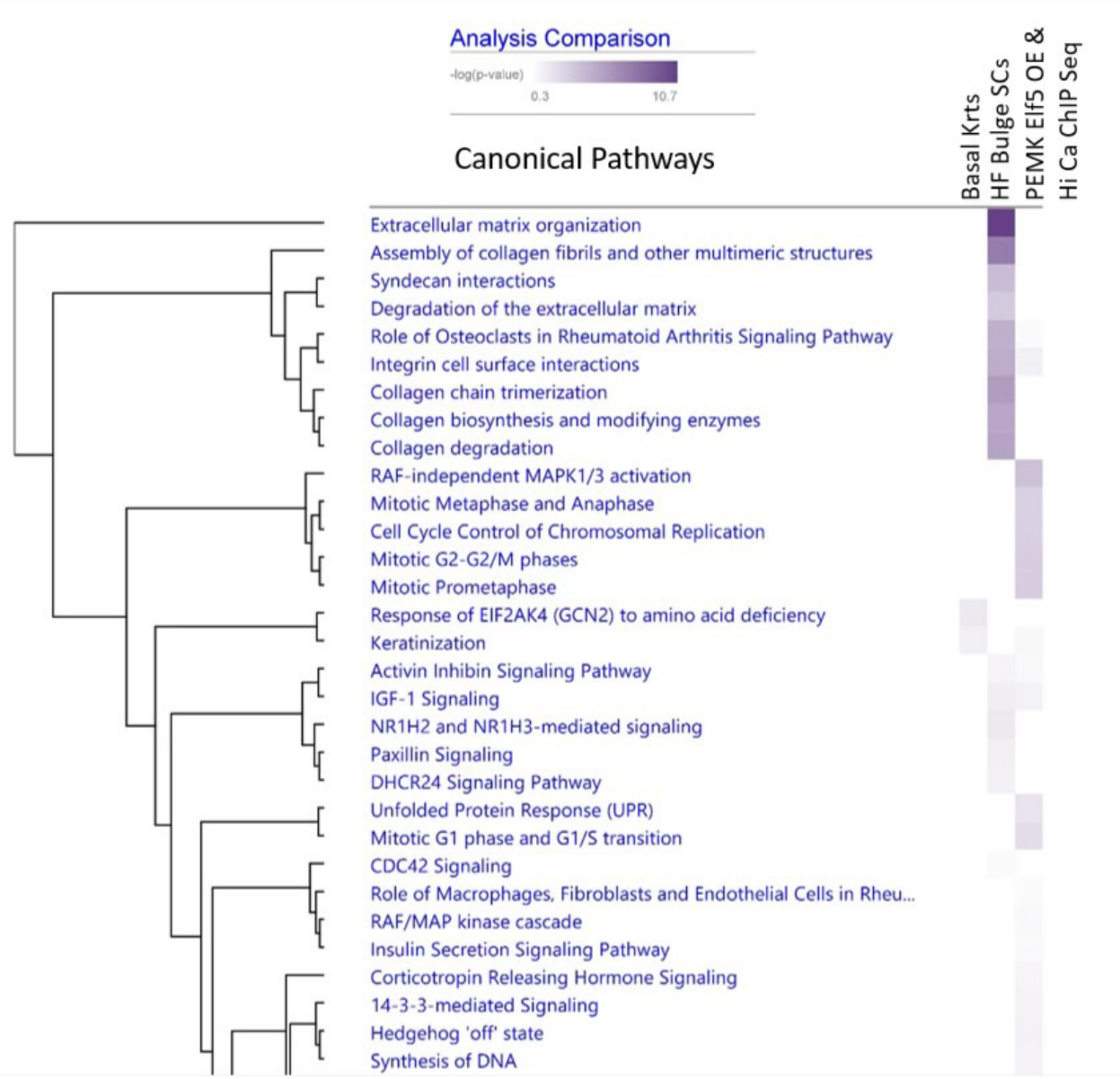

Figure 6.3 IPA comparison of canonical pathways between three groups of genes list. The comparison involves overlapping genes from PMEK Elf5 overexpression RNA sequencing and high calcium ChIP sequencing, set against the most upregulated and downregulated genes from RNA sequencing of both FACS-sorted basal stem cells and FACS-sorted hair follicle stem cells (HF SCs) with loss and gain of function.

6.3. Discussion

Analysis of RNA sequencing data from FACS-sorted basal SCs and HF bulge SCs indicates that various Elf5 target genes play distinct roles in the activities of basal SCs and HF bulge SCs through different pathways. In basal SCs, Elf5 can directly down regulate *Creb3l1. Creb3l1* has been recognized as a pivotal regulator in skin-related disorders such as hypertrophic scar (Deng et al., 2021; Zhang et al., 2022). *Creb3l1* can activate its downstream target *Col1a1,* which increases with ageing (Wu et al., 2017) and participles in skin wound healing alongside with *Col3a1* (Wang et al., 2021). Both were downregulated when loss of function of Elf5, whilst *Col3a1* showed also downregulation with gain of fuction of Elf5.

Interestingly, it has been proved that the ratio of COL-I to COL-III in mouse skin tends to increase with ageing (Wu et al., 2017) . I suggest that Elf5 can regulate ECM production through different target genes in different pathways and it is probably involved in wound healing and ageing processes. This correlates with the previous finding that ELF5 decreases with age (Fig 3.6). Elf5's role in regulating keratinicyte differentiation was confirmed with the upregulation of *Sprr1a,* which is situated within the cornified envelope of stratified epithelial tissue, when Elf5 over expressed, and this stays consistant with previous data (Fig 3.6, 3.9, 4.1).

In HF bulge SCs, Elf5 is capable of directly and negatively regulating *Igfbp4*, which is recognized as an inhibitor of both the canonical Wnt receptor signaling pathway and the Insulin-like growth factor receptor pathway. Both play crucial roles in HF homeostasis and disorders (Huelsken et al., 2001; Andl et al., 2002; Zhang et al.,2009; Ito et al., 2007; Panchaprateep & Asawanonda, 2014). Recent research indicates that the Wnt signaling pathway is intimately associated with skin wound healing and scar development (Yang et al., 2020). As IGFBP4 functions as a powerful inhibitor of IGF-I's activity, and IGF-1 promotes the growth of HFs (Panchaprateep & Asawanonda, 2014), this suggests that ELF5 can potentially activate hair growth through indirect regulation of IGF-1 via IGFBP4, which supports the previous hypothesis that Elf5 may play a role in triggering the activation of the quiescent HF bulge SCs, leading to an accelerated

colony growth process. This is also consistent with our earlier findings, which highlighted the peak expression of Elf5 during the Anagen phase of the HF (HF) cycle.

In bulge SCs, the expression levels of Col6a1 and Col6a2 are higher compared to those in differentiated krts (Chen et al., 2015). In Col6a1–/– mice, which lack collagen VI, there is a delay in hair cycling and growth under normal conditions. However, this absence promotes hair regrowth following wounding, without impacting the overall regeneration of the skin (Chen et al., 2015). As Elf5 showed higher expression in HF bulge SCs than differentiated krts (Fig 4.1, 4.2, 4.6), and can positively regulate Col6a1 and Col6a2, we suggest that Elf5 is closely related to hair growth and can promote hair cycling and growth through Col6a1 and Col6a2. GFBP-4 was also observed to hinder TGFβ -induced ECM production and exhibited inhibitory effects on ECM production in human skin *ex vivo* in organ culture (Su et al., 2019). This supports that Elf5 can regulate ECM production through different pathway via different target genes indirectly or directy. Moreover, Col3a1, Col6a1 and Col6a2 are all involved in wound healing pathway, and this correlates with the role of HF bulge SCs in skin wound healing. Elf5 may play a role in skin wound healing through ECM production and/or remodulation. This is confirmed by the most evident clusters in canonical pathways analysis (Fig 6.3).

Overall, the overlapping of the RNA sequencing data from PMEK and FACs sorted basal SCs and HF bulge SCs with ChIP seq data, enable us to find a more accrurate way to identify Elf5 terget genes. Elf5 has been demonstrated to play a role in various biological functions, including cell differentiation, production and remodeling of ECM, wound healing, and ageing, DNA repair etc. This is evident in both the epidermis and HFs (HF) through its various direct or indirect target genes and multiple important pathways.

Chapter 7

General Discussion, Conclusion

and

Future Directions

7.1 General Discussion

The skin, being the body's largest organ, primarily functions as a waterproof and mechanical barrier. Beyond these vital roles in water balance regulation and protection against microbial infection, the skin is crucial in thermoregulation and sensory perception of an animal's environment. Furthermore, skin also significantly contributes to social and reproductive behavior by conveying essential information about an individual's gender, age, and social status (Blanpain & Fuchs, 2006).

The skin epidermis, similar to various other epithelia, continually self-renews throughout an animal's life, owing to the presence of adult SC that supply new cells to replace those that are damaged or dead. Additionally, the skin possesses the ability to undergo extensive regeneration after sustaining wounds (Blanpain, 2008; Yang et al., 2020). Skin EPISCs, located in the basal layer of the epidermis and within HFs, are vital cellular sources for skin development, metabolism, and repair of injuries (Yang et al., 2020).

Groundbreaking research by H. Green and colleagues resulted in the successful cultivation of human epidermal krts, paving the way for later clinical uses of stratified epithelial SCs in regenerative medicine (Rheinwald & Green, 1975). As early as 1984, researchers first reported the use of cultured epidermal cell sheets (CES) for treating extensive burns, a method that successfully saved lives (Gregory Gallico et al., 1984). There is now a global consensus that transplanting CES into patients with extensive burns can enhance their survival rates. This is because CES is rich in EPISCs that can proliferate and differentiate after being transplanted into wounds, thereby facilitating the regeneration of epidermal tissue (Carsin et al., 2000; De Luca et al., 2006).

Regenerative medicine is currently gaining attention due to the shortage of available donor organs, with the aim of producing alternative tissues and biologically compatible structures. In this context, EpiSCs are emerging as a crucial cell source for the replacement and repair of

epithelial tissues. Therefore, they hold significant clinical value in the regenerative treatment of various epithelial tissues (Yang et al., 2020). Using skin SCs for cellular therapy in humans offers numerous theoretical benefits. Skin provides a highly accessible source of SCs, which possess an exceptional ability for cellular expansion in culture, and can be stably genetically modified (Shi et al., 2006).

Understanding the mechanisms that control EpiSC behavior is not only a fast-evolving area of scientific research but also a critical field in biomedicine for developing advanced treatments for damaged or cancerous epithelial tissues. This area of study is garnering keen interest from biologists, clinicians, and patients alike, as the intriguing characteristics of EpiSCs are progressively revealed.

The aim of this thesis was to investigate for the first time a new transcription factor Elf5 in skin, especially its role in EpiSCs/progenitors from morphogenesis to adult homeostasis. A comprehensive understanding of the regulatory mechanisms underlying the Elf5 transcription factor is of great significance in elucidating its roles in biological processes and disease mechanisms, as well as in the development of targeted therapies for tumors, wound healing, ageing and skin disorders.

The analysis of the expression of Elf5 at protein level during skin and hair morphogenesis and postnatal development showed that Elf5 was expressed predominately in differentiated skin and hair layers (the suprabasal layer and pre-cortex regions of the HFs) with some expression detected in the basal layer and HF bulge (E18.5-PN10.5, Figure 3.1 and Fig 3.2). In depilation-induced hair cycle, Elf5 expression was restricted in the basal layer of the epidermis; and in resting HFs, Elf5 expression was observed in the bulge and hair germ regions (D0, Fig 3.5). Furthermore, during progressive development of skin and HFs, Elf5 expression was found in the basal ($Elf5^{+}/K15^{+}$) and suprabasal layers of epidermis; and in HFs, Elf5 expression was found in the bulge region of anagen HFs and in the highly proliferative and differentiating cells of the hair bulb (D5-D12).

Elf5 expression was dramatically reduced in catagen skin (D18) with expression observed in the basal layer and in the regressing epithelial (Fig 3.5). Functional assessement to explore the potential role of Elf5 in skin development showed its impact on krt proliferation and differentiation. Using qRT-PCR, I determined the effects of gain-or-loss of Elf5 on proliferative genes, such as, *Cdk16*, *Cdk1*, *Ccnb2*, *Ccne1*, *Ccnd1*, *Ccnd2* and *Ccnb1* (cyclin dependent kinase 16, cyclin dependent kinase 1, cyclin B2, cyclin E1, cyclin D1, cyclin D2 and cyclin B1). I observed that loss of Elf5 had significant effects on proliferation genes (*Cdk1*, *Cdk16* and *Ccne1*, *, $p<0.05$; **, $p<0.01$).

While a significant decrease of transcripts for *Cdk1*, *Ccne1*, *Ccnb1*, *Ccnd1* and *Ccnd2* was observed after Elf5 overexpression in krts (*, $p<0.05$; **, $p<0.01$; ***, $p<0.001$, Fig 3.7). Consistent with the RT-qPCR data, cell cycle analysis by flow cytometry demonstrated that after loss of Elf5 in krts this leads to limited impact on cell cycle progression. However, overexpression of Elf5 leads to G0 arrest of the majority of cells analysed (Fig 3.8). This data suggests that overexpression of Elf5 in postnatal krts inhibits proliferation and forces cells to differentiate. This is consistent with Elf5's known role in epithelial cells to tightly regulate differentiation processes, such as, CD61+ progenitors to establish mammary gland development (Oakes et al., 2008).

While there is no significant impact on proliferation on postnatal krts after loss of Elf5 expression, other studies have shown that downregulation of Elf5 is required for cancer formation (Singh et al., 2020; Qu et al., 2021). Of note, both *Cdk16* and *Ccne1*, which are significantly up-and downregulated after Elf5 expression is modulated (Fig 3.7) are important regulators of cell cycle progression and deregulation can lead to cancer formation (Wang et al., 2023). As Elf5 is known as a crucial regulator of differentiation process in other epithelial tissues (Metzger et al., 2008; Ng et al., 2008; Oakes et al., 2008), its potential role during postnatal krt differentiation was investigated. Elf5 expression increased at both transcript and protein levels during calcium-induced krt differentiation overtime (Fig 3.9).

To determine whether Elf5 is an important regulator of krt differentiation, Elf5 activity was inhibited during calcium-induced differentiation, and it was observed that krts lost their ability to differentiation properly (Figure 3.10). This data suggest that Elf5 is crucial for the tight regulation of krts differentiation processes to maintain healthy skin and misexpression of Elf5 can lead to defects in normal krts processes.

Elf5 is also expressed in EpiSC compartments as well as in differentiated layers of the epidermis (Fig 4.1). *Elf5* expression was significantly (*, *p* value <0.05) elevated in FACs sorted CD34-postive SCs compared to CD34-negative SC populations Using qRT-PCR (Fig 4.2) . The expression of Elf5 exhibited a uniform pattern and location in the skin of both aging and young individuals, spanning across mice and humans, as shown in Figure 3.6. This consistent decrease in Elf5 expression with age, coupled with its occurrence in different SC and progenitor compartments, suggests that Elf5 may be involved in regulating the balance between SC and progenitor cell proliferation and differentiation.

This role is likely significant during both normal homeostasis and aging processes, and possibly extends to age-related disorders. This data suggests that Elf5 is a previously uncharacterised stem/progenitor marker in skin and hair development, potentially involved in controlling cellular processes, including, proliferation and differentiation in krts, required for normal skin and hair development/homeostasis.

RNA sequencing analysis of PMEK and ChIP sequencing data confirmed that among the 25 overlapping genes identified in the target genes of Elf5 PMEKs (Elf5 PMEKs low cal vs control) and ChIP Seq PMEKs HI Cal, the majority are involved in cell signaling, programmed cell death, and processes of differentiation/proliferation, including the cell cycle, p53 signaling pathway, cellular senescence, gap junctions etc, such as *Orc5*, *Sfi1*, *Tuba1b, Creb3l1, Ccn2.* This data suggests that Elf5 plays a vital role in maintaining the balance between proliferation and differentiation of krts during skin development. If this balance is disrupted, it could potentially lead to skin diseases, although this needs further investigation.

To investigate the expression of Elf5 in adult skin homeostasis, RT-qPCR and immunofluorescence analysis of Elf5 expression in adult young and ageing mouse and human tissue weas performed (Fig 3.8). Elf5 is expressed in basal and suprabasal layer in the epidermis and within the HF bulge and hair bulb SC compartments. Elf5 is expressed in the ageing epidermis and HFs of both mice and humans. However, a reduced expression level is noted in ageing skin when compared to young skin in both species (Fig 3.6).

To determine whether Elf5 has any impact on SCs, colony forming assay was performed using FACs-sorted basal SCs and HF bulge SCs. These cells were then gown and transduced with control, shElf5 (knockdown) or Elf5 overexpression lenti-viruses. Interestingly, opposing effects were seen after gain-or-loss of Elf5 activities in basal SCs or HF bulge SCs (Fig 4.9, 4.10). In basal SCs, gain-or-loss of Elf5 expression leads to a reduction in size of colonies (*, $p < 0.05$; ***, $p < 0.001$), while overall colony number did not significantly change (Fig 4.9). In HF bulge SCs, gain-or-loss of Elf5 activities leads to a significant increase in both colony size and number (**, $p < 0.01$; ***, $p < 0.001$, Fig 4.10). This data suggests that Elf5 functions in a spatiotemporal manner in skin and HFs, where it balances the proliferative and differentiative potentials of stem/progenitor cells contributing to both skin and hair development and homeostasis.

An Elf5 work model is proposed as below:

A

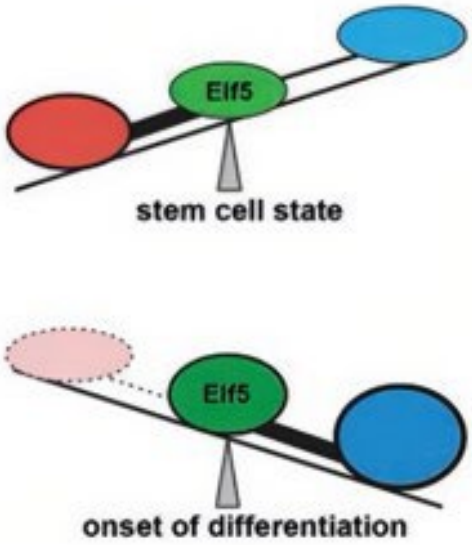
Elf5
stem cell state
Elf5
onset of differentiation

B

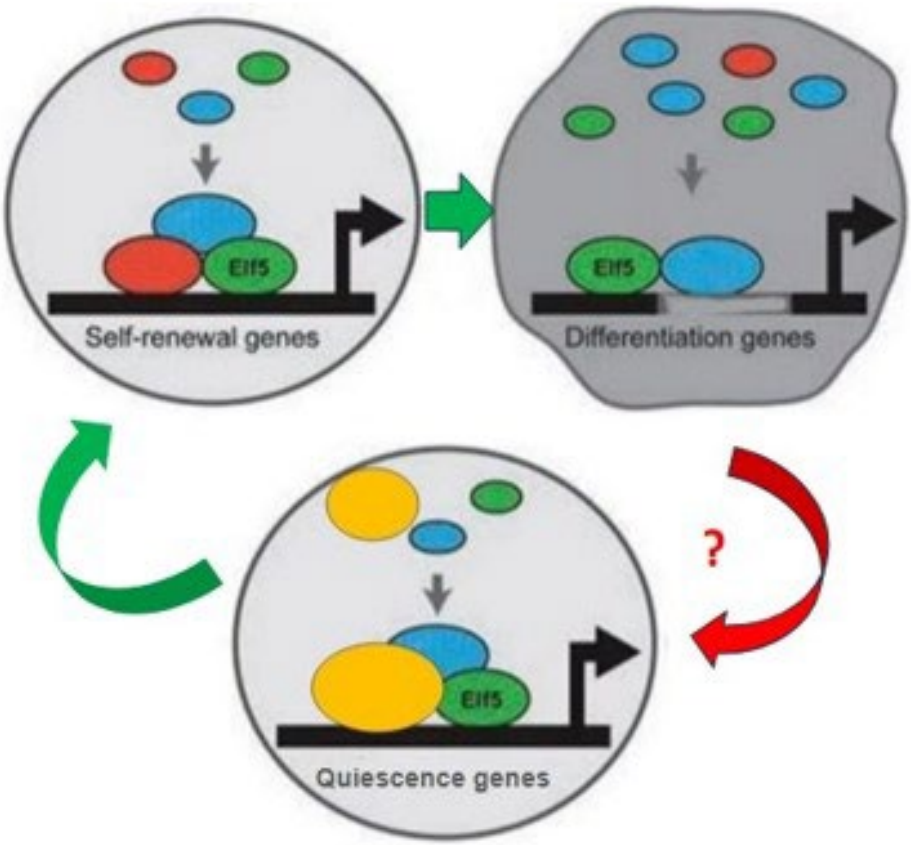
Elf5
Self-renewal genes
Elf5
Differentiation genes
?
Elf5
Quiescence genes

Figure 7.1 Elf5 working models. (A) Simple model of Elf5 -dependent functions in fine-tuning the balance between TSC self-renewal and commitment to differentiate. (B) The Elf5-focused transcription factor hub Model: The transcription factor network centered around Elf5 orchestrates the self-renewal and differentiation of epidermal stem cells by sensitively adjusting the balance in networks of target genes. It is possible that the differentiation can give negative feedback to the activation of quiescent stem cells. Precise levels of Elf5 can be crucial in balancing stem cells self-renewal and the differentiation.

Elf5 appears to have a role that varies with context at the critical point where SC self-renewal interacts with the initiation of differentiation, as shown in the proposed model (Fig 7.1A). This finding indicates that the levels of Elf5 vary depending on time and location during the development of skin epidermis and HFs, as well as during adult homeostasis.

Given that overexpression or inhibition of Elf5 leads to changes in stem cell quiescence, proliferation, and differentiation across various compartments, in addition of the decease in expression level with age, I theorize that this effect stems from Elf5 binding to both double- and single-occupancy sites that contain motifs of other cofactor(s), as shown in the proposed working model (Fig 7.1 B). This binding potentially activates genes promoting self-renewal, differentiation, or stem cell quiescence.

Such as in the case of TSC, Elf5 is known as a critical transcription factor within the trophoblast compartment and plays a key role in strengthening a TSC-specific transcriptional network. Interestingly, Elf5 is also found in differentiating trophoblast cells, even after they have stopped expressing other TSC-associated genes such as Cdx2 and Eomes ((Latos et al., 2015). Regulators of quiescence like RB, cyclin-dependent kinase inhibitors (CKIs), and p53 act as negative controllers of quiescent stem cell activation (Cheung & Rando, 2013).

Research indicates that not only are specific transcription factors (TFs) vital for the self-renewal of TSCs, but the precise quantity of these TFs is also crucial for sustaining the stem cell condition. Studies also reveal that exact concentrations of Elf5 are key in maintaining the

equilibrium between TSC self-renewal and the initiation of differentiation. These studies have proven that both a deficiency and an excess of Elf5 lead to a reduction in the proliferative stem cell pool, observable both *in vitro* and *in vivo*, and result in embryonic fatality around the midpoint of gestation (Latos et al., 2015; Donnison et al. 2005).

Research also demonstrates a similarly delicate equilibrium for Elf5 within TSCs, positioning Elf5 as a pivotal element in the transcriptional networks that regulate both self-renewal and differentiation processes in TSCs (Latos et al., 2015). It is probable that unique transcriptional signatures exist within specific quiescent stem cell populations. Conversely, it might be the case that gene products, whose expression levels vary as stem cells transition from quiescence to activation, are part of signaling pathways shared across different stem cell populations.

Such pathways could unveil mechanisms that are particularly associated with the induction or preservation of the quiescent state (Cheung & Rando, 2013). My findings demonstrate a similarly delicate equilibrium for Elf5 within EpiSCs and/or progenitors during skin and HF development and during homeostasis, positioning Elf5 as a pivotal element in the transcriptional networks that regulate both self-renewal and differentiation processes in EPSCs and/or progenitors.

In practice, the transcription of a single target gene is a dynamic operation involving numerous proteins. This process includes the removal of the gene's negative regulators and the incorporation of positive regulators. These regulators can bind either near the transcription start site or several thousand kilobases away, enabled by chromatin looping. The primary DNA-bound factors involved are regulated in their own activity and subsequently recruit additional proteins, culminating in the initiation of transcription (Levine et al., 2014).

Loss and gain function of Elf5 can result in functional alterations in cells and tissues, contributing to the development of skin disorders and cancers. We must then explore and ascertain the roles of Elf5 in various aspects: (1) the cellular and extracellular factors that influence these alterations, (2) the specific primary regulators responsible for these changes, (3)

the methods for effectively targeting these regulators, and (4) the optimal timing for targeting them.

Recent research has explored the direct manipulation of various transcription factors in cancer treatment using small molecules, immunotherapy, and other methods (Gonda & Ramsay, 2015). For the successful application of transcription targeting in therapy, it is crucial to comprehend not only the initiation but also the timing of transcriptional control over target genes. Gaining insights into these processes can pave the way for developing effective treatments at early stages of skin disorders. Such interventions have the potential to reverse or prevent long-term tissue damage and/or hindered regeneration.

Taken together, this work demonstrate for the first time that: i) Elf5 is dynamically expressed during skin and HF development and cycling: in basal (stem/progenitor cells) and suprabasal (differentiated) layers of the epidermis. While, in the HFs its expression is found in bulge and SH germ SC compartments, as well as, in the highly proliferative and differentiating krts of hair bulb, ii) Elf5 can modulate epidermal and HF-SC colony forming abilities and, iii) Elf5 can modulate and is required for krt proliferation and differentiation. Here, I demonstrate that Elf5 plays an important role in determining cell fate of stem/progenitor cells in skin and HFs. This data identifies a novel stem/progenitor marker and regulator in skin and HFs, with potential future investigations leading to advancements in many areas of research, including SC, regenerative medicine, cancer biology and ageing.

In summary, this study broadens our comprehension of Elf5's role in skin development and the regulation of SCs in the adult epidermis, providing a groundwork for further research into ELF5 and its clinical applications.

7.2 Conclusion

Recent evidence is increasingly showing the pathological roles of abnormally expressed ELF5 in the development, progression, and prognosis of breast cancer, prostate and skin cancer. The current study establishes a connection between skin and ELF5 for the first time.

The potential Elf5 target genes are also shown to be involved in different pathways, which are implicated in cancer, wound healing, and other skin disorders, respectively. Furthermore, Elf5 is implicated in ageing. However, the specific mechanisms through which Elf5 contributes to these remain largely unclear, necessitating further research. The diverse involvement of ELF5 in these conditions suggests its potential as a therapeutic target for both cancer, skin disorders and wound healing as well as ageing. Strategies such as targeting the up or downregulation of ELF5 or its direct target gene mRNA expression through gene intervention methods to conrtrol EpiSCs' priliferation and/or differentiation for SCs therapy are potential approaches.

By understanding the diversity of regulatory pathways with which Elf5 interact, there may be additional therapeutic opportunities based on modulation of Elf5-dependent signaling. Elf5 is expressed in a broad area that includes skin and hair development, adult epidermal krts and hair germ, bulge cells preceding SC activations, proliferation, and differentiation. It is unclear whether the protein acts intrinsically in the SCs and/or their progenitors or acts on SCs and/or progenitors through the niche. My data suggests that Elf5 i) was present and functional at different times of phenotype onset during skin development and skin homeostasis; ii) together with progenitor cells, kept the ability to control the activation, proliferation, and differentiation.

Although a role of Elf5 in the SCs environment through ECM protein downstream targets is an attractive model, we cannot eliminate the possibility that Elf5 also functions within SCs to set the intrinsic rate of SCs/progenitors' proliferation and differentiation. This is suggested by the *in vitro* cell culture assay, that higher Elf5 expressed pure quiescent SCs (HF bulge SCs) could be activated by Elf5 and generate larger krts colonies in the timeframe of my experiments.

The spatial-temporal dynamics of Elf5 expression throughout skin development and the hair growth cycle, in addition the diminution of Elf5 expression in ageing skin of both murine and human specimens, correlate with the apparent effect that Elf5 plays a critical role not only in the proliferation and differentiation of embryonic and postnatal krts but also significantly influences the progenitor cells of basal and HF bulge SCs in the adult epidermis. These findings underscore the multifaceted function of Elf5 in cutaneous biology.

The necessity for further exploration into Elf5's role in controlling the growth of skin epithelial cell cultures is evident. Clinically, the challenge lies in efficiently expanding krts to volumes suitable for constructing artificial skin, a process that, despite its complexity, is essential for the treatment of patients suffering from severe skin disorders such as burn injuries and cell therapy in regenerative medicine (Osorio et al., 2011; Barrandon et al., 2012).

As our comprehension deepens understanding of the mechanisms governing the activation, proliferation, and differentiation of epithelial SCs and progenitors within tissues, and the impact of cellular growth conditions on these processes, we are poised to develop more systematic methodologies for manipulating SCs *in vitro*, specifically for applications in epidermal and HF engineering.

In conclusion, these findings uncover Elf5 as a key regulator of krt proliferation, hair growth, and SC activation. This suggests its vital importance in the development and maintenance of normal skin and HF homeostasis.

7.3 Future perspectives

To gain a more accurate understanding of Elf5's role, RNA sequencing data from FACS-sorted basal SCs and HF bulge SCs was integrated with existing data on overlapping Elf5 target genes in PMEK (Elf5 overexpression low cal vs control overlapped with ChIP Seq PMEKs HI Cal). This identified some important genes involved in skin homeostasis, cancer, ageing and wound healing, as primary target genes for future investigation.

Creb3l1

The cAMP-responsive element-binding protein 3 (CREB3), known for its leucine zipper motif and widespread human expression, is part of a group of DNA-binding proteins. These proteins are involved in several biological processes, such as cellular stress response, endoplasmic reticulum (ER) stress response, energy metabolism, and differentiation. The dysregulation of the CREB3 protein family's expression and regulation is closely associated with the emergence of tumors and various non-tumor diseases.

CREB3L1 is linked to the regulation of the ECM. It is involved in the processes of tumorigenesis, malignancy, drug resistance, and impacts prognosis, functions as a transcription factor that exhibits anti-tumor effects and increases chemosensitivity in breast cancer, prostate cancer, and renal cell carcinoma (Wang et al., 2023). CREB3L1 could promote tumor growth by influencing intercellular communication or altering the composition of ECM.

It regulates various genes, encompassing those associated with differentiation pathways and epithelial-mesenchymal transition (EMT) (Pan et al., 2019; Pan et al., 2022). The continuous expression of the chimeric CREB3L1 transcription may play a role in the overproduction of collagen, which is a notable characteristic of Sclerosing Epithelioid Fibrosarcoma (SEF) (Stockman et al., 2014).

CREB3L1 expression is commonly upregulated in early-stage breast cancer, but it experiences a marked downregulation in advanced and metastatic breast cancers, especially in triple-negative breast cancers (TNBCs), where this pattern is observed in approximately 75% of cases (Plett et al., 2022; Denard et al.,2012; Ward et al., 2016; Mellor et al., 2013; Mellor et al., 2022). The use of inhibitor of the protease to CREB3L1 to hinder the activation of CREB3L1 could be used in future experiments to diminish the expression of genes targeted by CREB3L1, such as COL1A1 and COL1A2, and also reduces tumor cell invasion (Gorski et al., 2011).

Elf5, known to be closely linked with breast cancer, can directly target and downregulate Creb3l1. This relationship suggests a new method for targeting CREB3L1, presenting it as a potential therapeutic strategy in breast cancer treatment.

Sprr1a

The small proline-rich protein (SPRR) 1A gene codes for a structural protein found in the cornified envelope of the epidermis, serving as a barrier against environmental factors. As individuals age, there is a progressive increase in the expression of SPRR1A.

In various pathophysiological conditions, changes in SPRR expression have been consistently reported in multiple keratinization and skin inflammatory disorders. Specifically, in psoriatic epidermis, higher levels of SPRR-1 have been observed compared to normal epidermis. Additionally, there is an upregulation of SPRR1A in cases of atopic dermatitis (Carregaro et al., 2013). Sprr1a also plays a role in axonal regeneration helping to prevent nerve damage (Argueta et al., 2019). A recent study showed that the SPRR1 protein functions as an antimicrobial agent in the skin, helping to protect the host against systemic infections (Zhang et al., 2022).

As Elf5 can upregulate *Sprr1a*, involvement of ELF5 in these conditions suggests its potential as a therapeutic target for both skin disorders and anti-ageing, antimicrobial.

Igfbf4

The insulin-like growth factor (IGF) system is comprehensively characterized, and is crucial for various cellular functions such as cell growth, differentiation, and cellular senescence. This system encompasses IGFs (IGF-I and IGF-II), type I and type II IGF receptors, IGF-binding proteins (IGFBPs), and IGFBP proteases. The IGFs, specifically IGF-I and IGF-II, are key regulators of cellular proliferation, survival, and differentiation.

The bioactivity of IGFs is modulated by a family of IGF-binding proteins (IGFBPs). Within biological fluids, IGFs are typically bound to IGFBPs. These proteins serve not only as carriers for IGFs, extending their lifespan, but also act as regulators of IGF availability and activity. The IGFBP family includes six structurally similar proteins (IGFBP-1 to -6), each with unique cell- and tissue-specific expression patterns.

The six high-affinity insulin-like growth factor binding proteins (IGFBPs) are versatile proteins that influence cell signaling through various pathways. They bind to IGF with high affinity, limiting IGF's interaction with its receptor, which in turn inhibits cell proliferation, differentiation, and survival.

The IGF1 receptor mediates most of the actions of IGF1 and IGF2 through its tyrosine kinase activity, triggers intracellular signaling pathways such as MAP kinase and PI3 kinase/AKT (Adams et al., 2000; Ning et al., 2008; Baxer,2023). While their primary role is to limit the access of IGF-1 and IGF-2 to the IGF1R receptor, IGFBPs can also alter IGF1R signaling. This alteration occurs either through their own post-translational modifications, such as phosphorylation or proteolysis, or through interactions with other regulatory proteins.

IGFBPs impact cell survival, migration, metabolism, and other functions through mechanisms independent of the IGF-IGF1R system. They achieve this by directly or functionally interacting with other cell surface proteins like integrins, transforming growth factor β family receptors, as well as with intracellular ligands involved in various pathways. In the nucleus, IGFBPs regulate the functions of class II nuclear hormone receptors and play roles in cell senescence and DNA damage repair via the nonhomologous end-joining pathway. These functions could potentially affect the effectiveness of certain cancer treatments (Baxter,2023).

IGFBP4 acts as a powerful inhibitor of IGF-I activity. Pregnancy-associated plasma protein-A (PAPP-A) can cleave IGFBP4, thereby releasing active IGF-I. (Wu et al., 2017). While IGFBP-4 is generally considered to mainly inhibit IGF1R signaling, there is evidence of its activity beyond this function. It can regulates cell growth and glucose metabolic process. There have been

reports indicating that IGFBP-4 can function as both a promoter and inhibitor of IGF activity *in vivo* (Ning et al., 2008). For example, in a study involving murine cardiomyocyte differentiation, IGFBP-4 significantly stimulated this process, independent of its effects on IGF signaling. Interestingly, the introduction of IGF-1 lessened this effect.

In the context of cardiogenesis, where canonical Wnt signaling through β-catenin is known to be inhibitory at certain stages, IGFBP-4 was observed to enhance cardiomyocyte differentiation. It achieved this by obstructing Wnt pathway signaling, which is activated by Wnt3A or the receptors LRP6 or Frz8. Notably, IGFBP-4 has the capacity to bind directly to these receptor proteins, demonstrating its influence in cardiomyocyte differentiation beyond its interaction with IGF1R signaling (Zhu et al., 2008; Foley & Mercola, 2005).

Several studies have indicated that the presence of IGFBP-4 in both the dermis and epidermis may contribute to the regulation of IGF-I activity within the skin (Chen et al., 2003; Hwa et al., 1999). Balding scalp follicles were discovered to secrete significantly lower levels of IGFBP-4 alongside with IGF-1 (Panchaprateep & Asawanonda, 2014). A significant decrease in IGFBP-4 and IGF-1 has been detected in balding scalp follicles. Additionally, the decline in serum IGFBP-4 levels with age, coupled with the increase of Col3a1 upon overexpression of Elf5, collectively reinforce the strong link between ELF5 and IGFBP-4. This, in turn, underscores the role of Elf5 in hair growth and aging.

Col1a1,Col3a, Col6a1, Col6a2

The ECM is a dynamic and multifunctional compartment that, by adjusting the production, degradation, and remodelling of its components, supports organ development, functionality, and repair. It plays a pivotal role in SC niches, significantly influencing various aspects of SC behaviour. It directly or indirectly modulates the maintenance, proliferation, self-renewal, and differentiation of SCs, thereby majorly affecting tissue homeostasis and regeneration under both physiological and pathological conditions (Gattazzo et al., 2014).

Numerous studies have demonstrated the significant role of ECM in supporting SC niches across various tissues, including the skin. In the epidermis, the ECM is predominantly characterized by the BM (BM), a specialized ECM structure that delineates the boundary between the epidermal and dermal layers. EpiSCs maintain contact with the BM, but upon losing this contact and migrating to the surface layers, they commence terminal differentiation. Given these dynamics, the ECM is fundamentally crucial in the regulation of EpiSC maintenance, mobilization, and differentiation. Recent research has made significant advancements in understanding the role of ECM in determining the fate of EpiSCs, with a particular focus on the HF SC niche (Chermnykh et al., 2018).

Collagen, widely regarded as the most prevalent protein in ECM, plays a crucial role in sustaining the cellular microenvironment. It offers a range of functionalities, including facilitating cell adhesion, enabling cell migration, and contributing to tissue morphogenesis and repair (Xu et al., 2012; Kadler et al., 2007). It constitutes 25-35% of the total protein content in mammals and is crucial for providing tissue stiffness and integrity (Ricard-Blum et al., 2018; Shoulders et al., 2009).

Among collagen proteins, type I collagen (COL-I) and type III collagen (COL-III) are the most abundant and significant, predominantly found in the dermal layer of the skin (Gelse et al., 2003; Bailey et al., 1998; Ervin et al., 1978). COL-I forms the coarse fibers, acting as a structural scaffold to enhance skin's mechanical strength It's also a key component of reticular fibers in skin's interstitial tissue (Gelse et al., 2003; Wen et al., 2021). On the other hand, COL-III, consisting of fine fibers, often coexists with COL-I to augment skin elasticity (Kim et al.,2016). Recent studies have shown that besides age-related changes impacting skin properties like strength and elasticity, the content and ratio of type I collagen (COL-I) and type III collagen (COL-III) are indicative of the onset and progression of certain diseases, such as in scar tissues (Roman et al., 2020; Chang et al., 2013; Friedman et al., 1993; Brown et al., 2017; Epstein, 1971; Stumpf et al., 2001). Collagen VI is abundantly present in the skin and notably deposited in HFs. Its expression is significantly increased in response to skin wounding (Chen et al., 2015).

My data showed that Elf5 can regulate Cola1a1, Cola3a, Col6a1, and Col6a2 directly or indiretly. Direct targets include Creb3l1, which can directly activate Cola1a1 transcription, whereas its inhibition can be used to diminish expression of COL1A1 and COL1A2, and also reduces tumor cell invasion (Gorski et al., 2011). Elf5's overexpression and downregulation affect Col1a expression (downregulated in both cases). In the group with Elf5 overexpression, Col3a1 is observed to be upregulated. Conversely, in the group where Elf5 is inhibited, Col6a1 and Col6a2, which are elevated compared to those in differentiated krts, and these molecules are involved in hair growth as well as post-wound hair regeneration (Chen et al., 2015), show downregulation.

Col1a, Col3a1, Col6a1, Col6a2, along with Itgb4, are collectively involved in ECM organization and wound healing signaling pathways. Therefore I hypothesise that Elf5 might affect EpiSCs' activities through modulating ECM production, destruction and/or remodulation, thus in turn take a role in hair growth, wound healing, skin ageing and disorders.

In conclusion, by analyzing the RNA and ChIP-seq data, this has led to the identification of potential target genes of Elf5. Among these, genes involved in skin cancer, wound healing, hair growth, and aging have emerged as particularly intriguing targets for future validation experiments and further additional research.

References

Abe, Y., & Tanaka, N. (2017). Roles of the Hedgehog Signaling Pathway in Epidermal and Hair Follicle Development, Homeostasis, and Cancer. *Journal of developmental biology*, 5(4), 12. https://doi.org/10.3390/jdb5040012

Adachi, K., Nikaido, I., Ohta, H., Ohtsuka, S., Ura, H., Kadota, M., ... & Niwa, H. (2013). Context-dependent wiring of Sox2 regulatory networks for self-renewal of embryonic and trophoblast stem cells. *Molecular cell*, 52(3), 380-392.

Adams Grace. (2020). *A beginner's guide to RT-PCR, qPCR and RT-qPCR*. http://portlandpress.com/biochemist/article-pdf/42/3/48/917384/bio20200034.pdf

Adams, T. E., Epa, V. C., Garrett, T. P., & Ward, C. W. (2000). Structure and function of the type 1 insulin-like growth factor receptor. Cellular and molecular life sciences: CMLS, 57(7), 1050–1093. https://doi.org/10.1007/PL00000744

Adan, A., Alizada, G., Kiraz, Y., Baran, Y., & Nalbant, A. (2017). Flow cytometry: basic principles and applications. In *Critical Reviews in Biotechnology* (Vol. 37, Issue 2, pp. 163–176). Taylor and Francis Ltd. https://doi.org/10.3109/07388551.2015.1128876

Ahmed, M. I., Alam, M., Emelianov, V. U., Poterlowicz, K., Patel, A., Sharov, A. A., Mardaryev, A. N., & Botchkareva, N. V. (2014). MicroRNA-214 controls skin and hair follicle development by modulating the activity of the Wnt pathway. *The Journal of cell biology*, 207(4), 549–567. https://doi.org/10.1083/jcb.201404001

Albers, K. M., Greif, F., Setzer, R. W. & Taichman, L. B. (1987). Cell-cycle withdrawal in cultured keratinocytes. Differentiation 34, 236–240. https://doi.org/10.1111/j.1432-0436.1987.tb00071.x

Albers, K. M., Setzer, R. W. & Taichman, L. B. (1986). Heterogeneity in the replicating population of cultured human keratinocytes. Differentiation 31, 134–140. https://doi.org/10.1111/j.1432-0436.1986.tb00394.x

Albert, M. R., Foster, R. A., & Vogel, J. C. (2001). Murine epidermal label-retaining cells isolated by flow cytometry do not express the stem cell markers CD34, Sca-1, or Flk-1. The Journal of investigative dermatology, 117(4), 943–948. https://doi.org/10.1046/j.0022-202x.2001.01517.x

Alcolea, M. P., & Jones, P. H. (2014). Lineage analysis of epidermal stem cells. Cold Spring Harbor Perspectives in Medicine, 4(1). https://doi.org/10.1101/cshperspect.a015206

Alonso, L., & Fuchs, E. (2006). The hair cycle. *Journal of Cell Science*, 119(3), 391–393. https://doi.org/10.1242/jcs02793

Amin, A., Wu, R., Cheung, M. H., Scott, J. F., Wang, Z., Zhou, Z., Liu, C., Zhu, G., Wong, C. K. C., Yu, Z., & Liang, C. (2020). An Essential and Cell-Cycle-Dependent ORC Dimerization Cycle Regulates Eukaryotic Chromosomal DNA Replication. *Cell Reports*, *30*(10), 3323-3338.e6. https://doi.org/10.1016/j.celrep.2020.02.046

Andl, T., Ahn, K., Kairo, A., Chu, E. Y., Wine-Lee, L., Reddy, S. T., Croft, N. J., Cebra-Thomas, J. A., Metzger, D., Chambon, P., Lyons, K. M., Mishina, Y., Seykora, J. T., Crenshaw, E. B., 3rd, & Millar, S. E. (2004).

Epithelial Bmpr1a regulates differentiation and proliferation in postnatal hair follicles and is essential for tooth development. Development (Cambridge, England), 131(10), 2257–2268. https://doi.org/10.1242/dev.01125

Andl, T., Reddy, S.T., Gaddapara, T., and Millar, S.E. (2002). WNT signals are required for the initiation of hair follicle development. *Dev. Cell*, 2, 643–653

Argueta, D. A., Aich, A., Lei, J., Nekhai, S., Ammosova, T., Lin, X., Bagchi, A., & Gupta, K. (2019). Downregulation of Sprr1a Contributes to the Pathobiology of Sickle Cell Disease. *Blood*, *134*(Supplement_1), 75–75. https://doi.org/10.1182/blood-2019-129004

Auden, A., Caddy, J., Wilanowski, T., Ting, S. B., Cunningham, J. M., & Jane, S. M. (2006). Spatial and temporal expression of the Grainyhead-like transcription factor family during murine development. *Gene expression patterns,* 6(8), 964-970.

Bach, L. A. (2018). 40 years of IGF1: IGF-binding proteins. In *Journal of Molecular Endocrinology* (Vol. 61, Issue 1, pp. T11–T28). BioScientifica Ltd. https://doi.org/10.1530/JME-17-0254

Bailey, AJ., Paul, RG. & Knott, L. (1998). Mechanisms of maturation and aging of collagen. *Mech Ageing Dev.* 106:1–56.

Bale, A. E., & Yu, K.-P. (2001). The hedgehog pathway and basal cell carcinomas. In *Human Molecular Genetics,* 10(7).

Barbieri, J.S., Wanat, K., & Seykora, J. (2014). Skin: Basic Structure and Function. 10.1016/B978-0-12-386456-7.03501-2.

Barrandon, Y., & Green, H. (1987). Three clonal types of keratinocytes with different capacities for multiplication. In *Proc. Nati. Acad. Sci. USA* (Vol. 84). https://www.pnas.org

Barrandon, Y., Grasset, N., Zaffalon, A., Gorostidi, F., Claudinot, S., Droz-Georget, S. L., Nanba, D., & Rochat, A. (2012). Capturing epidermal stemness for regenerative medicine. In *Seminars in Cell and Developmental Biology* (Vol. 23, Issue 8, pp. 937–944). Elsevier Ltd. https://doi.org/10.1016/j.semcdb.2012.09.011

Baxter R. C. (2023). Signaling Pathways of the Insulin-like Growth Factor Binding Proteins. *Endocrine reviews*, 44(5), 753–778. https://doi.org/10.1210/endrev/bnad008

Behl, C., & Ziegler, C.A. (2013). Cell Aging: Molecular Mechanisms and Implications for Disease. *SpringerBriefs in Molecular Medicine*.

Benitah, S. A., & Frye, M. (2012). Stem cells in ectodermal development. *Journal of molecular medicine* (Berlin, Germany), 90(7), 783–790. https://doi.org/10.1007/s00109-012-0908-x

Bikle, D. D., Xie, Z., & Tu, C. L. (2012). Calcium regulation of keratinocyte differentiation. In *Expert Review of Endocrinology and Metabolism* (Vol. 7, Issue 4, pp. 461–472). https://doi.org/10.1586/eem.12.34

Blanpain, C., & Fuchs, E. (2006). Epidermal Stem Cells of the Skin. *Annu Rev Cell Dev Biol*, 22: 339–373.

Blanpain, C., & Fuchs, E. (2007). p63: revving up epithelial stem-cell potential. *Nature cell biology*, 9(7), 731–733. https://doi.org/10.1038/ncb0707-731

Blanpain, C., & Fuchs, E. (2009). Epidermal homeostasis: A balancing act of stem cells in the skin. In *Nature Reviews Molecular Cell Biology*, 10(3), 207–217. Nature Publishing Group. https://doi.org/10.1038/nrm2636

Blanpain, C., Lowry, W. E., Geoghegan, A., Polak, L., & Fuchs, E. (2004). Self-renewal, multipotency, and the existence of two cell populations within an epithelial stem cell niche. *Cell*, 118(5), 635–648. https://doi.org/10.1016/j.cell.2004.08.012

Blanpain, C., Lowry, W. E., Geoghegan, A., Polak, L., & Fuchs, E. (2004). Self-renewal, multipotency, and the existence of two cell populations within an epithelial stem cell niche. *Cell*, *118*(5), 635–648. https://doi.org/10.1016/j.cell.2004.08.012

Blanpain. (2008). Medical applications of epidermal stem cells. StemBook. https://doi.org/10.3824/stembook.1.27.1

Boglev, Y., Wilanowski, T., Caddy, J., Parekh, V., Auden, A., Darido, C., ... & Jane, S. M. (2011). The unique and cooperative roles of the Grainy head-like transcription factors in epidermal development reflect unexpected target gene specificity. *Developmental biology*, 349(2), 512-522.

Bose, A., Teh, M. T., Mackenzie, I. C., & Waseem, A. (2013). Keratin K15 as a biomarker of epidermal stem cells. In *International Journal of Molecular Sciences* (Vol. 14, Issue 10, pp. 19385–19398). https://doi.org/10.3390/ijms141019385

Botchkarev, V. A., Botchkareva, N. V., Nakamura, M., Huber, O., Funa, K., Lauster, R., Paus, R., & Gilchrest, B. A. (2001). Noggin is required for induction of the hair follicle growth phase in postnatal skin. *FASEB journal: official publication of the Federation of American Societies for Experimental Biology*, 15(12), 2205–2214. https://doi.org/10.1096/fj.01-0207com

Briquez, P. S., Hubbell, J. A., & Martino, M. M. (2015). Extracellular Matrix-Inspired Growth Factor Delivery Systems for Skin Wound Healing. *Advances in Wound Care*, *4*(8), 479–489. https://doi.org/10.1089/wound.2014.0603

Brix, N., Samaga, D., Belka, C., Zitzelsberger, H., & Lauber, K. (2006). Analysis of clonogenic growth in vitro. *Nature Protocols*, *1*(5), 2315–2319. https://doi.org/10.1038/nprot.2006.339

Brown, SR., Cleveland, EM., Deeken, CR., Huitron, SS., Aluka, KJ. & Davis, KG. (2017). Type I/type III collagen ratio associated with diverticulitis of the colon in young patients. *J Surg Res*. 207:229–34.

Byrne, C., Tainsky, M., & Fuchs, E. (1994). Programming gene expression in developing epidermis. *Development*, 120(9), 2369–2383. https://doi.org/10.1242/dev.120.9.2369

Cai. Z., Chattopadhyay, N., Liu, WJ., Chan, C., Pignol, J-P., et al. (2011). Optimized digital counting colonies of clonogenic assays using ImageJ software and customized macros: comparison with manual counting. *Int J Radiat Biol* 87: 1135–1146. http://doi:10.3109/09553002.2011.622033

Carbonnel, S., Das, D., Varshney, K., Kolodziej, M. C., Villaécija-Aguilar, J. A., and Gutjahr, C. (2020). The Karrikin Signaling Regulator SMAX1 Controls Lotus Japonicus Root and Root Hair Development by

Suppressing Ethylene Biosynthesis. *Proc. Natl. Acad*. Sci. U.S.A. 117 (35), 21757–21765. doi:10.1073/pnas.2006111117

Carlson, B. (2014). Development of the Integumentary System. Reference Module in Biomedical Research. http://dxdoiorg/101016/B978-0-12-801238-305436-2

Carregaro, F., Stefanini, A. C. B., Henrique, T., & Tajara, E. H. (2013). Study of small proline-rich proteins (SPRRs) in health and disease: A review of the literature. In Archives of Dermatological Research (Vol. 305, Issue 10, pp. 857–866). Springer Verlag. https://doi.org/10.1007/s00403-013-1415-9

Carsin, H., Ainaud, P., le Bever, H. et al. (2000). Cultured epithelial autografts in extensive burn coverage of severely traumatized patients: a five-year single-center experience with 30 patients, *Burns*, 26(4), 379–387.

Celso, C. L., Prowse, D. M., & Watt, F. M. (2004). Transient activation of β-catenin signalling in adult mouse epidermis is sufficient to induce new hair follicles, but continuous activation is required to maintain hair follicle tumours. *Development,* 131,1787–1799.

Chakrabarti, R., Wei, Y., Romano, RA., DeCoste, C., Kang, Y., & Sinha, S. (2012). Elf5 regulates mammary gland stem/progenitor cell fate by influencing notch signaling. *Stem Cells*, 30(7), 1496-508. doi: 10.1002/stem.1112. PMID: 22523003; PMCID: PMC5606133.

Chan, C. P., Kok, K. H., & Jin, D. Y. (2011). CREB3 subfamily transcription factors are not created equal: Recent insights from global analyses and animal models. *Cell & bioscience*, 1(1), 6. https://doi.org/10.1186/2045-3701-1-6

Chen X., Liu B., Li Y., Han L., Tang X., Deng W., et al. (2019). Dihydrotestosterone Regulates Hair Growth through the Wnt/β-Catenin Pathway in C57BL/6 Mice and In Vitro Organ Culture. *Front. Pharmacol*. 10, 1528. 10.3389/fphar.2019.01528

Chen, B. K., Leiferman, K. M., Pittelkow, M. R., Overgaard, M. T., Oxvig, C., & Conover, C. A. (2003). Localization and regulation of pregnancy-associated plasma protein A expression in healing human skin. *Journal of Clinical Endocrinology and Metabolism*, 88(9), 4465–4471. https://doi.org/10.1210/jc.2003-030193

Chen, J. (2016). The Cell-Cycle Arrest and Apoptotic Functions of p53 in Tumor Initiation and Progression. Cold Spring Harbor perspectives in *medicine*, 6(3), a026104. https://doi.org/10.1101/cshperspect.a026104

Chen, P., Cescon, M., & Bonaldo, P. (2015). Lack of Collagen VI Promotes Wound-Induced Hair Growth. *Journal of Investigative Dermatology*, *135*(10), 2358–2367. https://doi.org/10.1038/jid.2015.187

Cheng, W., Yan, HR., Fang, GN. & Guo, AZ. (2013). The content and ratio of type I and III collagen in skin differ with age and injury. *Afr Biotechnol*. 10:2524–9.

Chermnykh, E., Kalabusheva, E., & Vorotelyak, E. (2018). Extracellular matrix as a regulator of epidermal stem cell fate. *In International Journal of Molecular Sciences* (Vol. 19, Issue 4). MDPI AG. https://doi.org/10.3390/ijms19041003

Cheung, T. H., & Rando, T. A. (2013). Molecular regulation of stem cell quiescence. In *Nature Reviews Molecular Cell Biology* (Vol. 14, Issue 6, pp. 329–340). https://doi.org/10.1038/nrm3591

Choi B. Y. (2020). Targeting Wnt/β-Catenin Pathway for Developing Therapies for Hair Loss. *International journal of molecular sciences*, 21(14), 4915. https://doi.org/10.3390/ijms21144915

Choi, Y. S., Cheng, J., Segre, J., & Sinha, S. (2008). Generation and analysis of Elf5-LacZ mouse: Unique and dynamic expression of Elf5 (ESE-2) in the inner root sheath of cycling hair follicles. *Histochemistry and Cell Biology*, 129(1), 85–94. https://doi.org/10.1007/s00418-007-0347-x

Choi, YS., Chakrabarti R., Escamilla-Hernandez, R. & Sinha, S. (2009). Elf5 conditional knockout mice reveal its role as a master regulator in mammary alveolar development: failure of Stat5 activation and functional differentiation in the absence of Elf5. *Dev Biol*, 329(2):227-241.

Chugh, R. M., Chaturvedi, M., & Yerneni, L. K. (2015a). An evaluation of the choice of feeder cell growth arrest for the production of cultured epidermis. *Burns*, 41(8), 1788–1795. https://doi.org/10.1016/j.burns.2015.08.011

Chugh, R. M., Chaturvedi, M., & Yerneni, L. K. (2015b). Occurrence and Control of Sporadic Proliferation in Growth Arrested Swiss 3T3 Feeder Cells. *PLoS ONE*, *10*(3). https://doi.org/10.1371/journal.pone.0122056

Chugh, R. M., Chaturvedi, M., & Yerneni, L. K. (2017). An optimization protocol for Swiss 3T3 feeder cell growth-arrest by Mitomycin C dose-to-volume derivation strategy. *Cytotechnology*, *69*(2), 391–404. https://doi.org/10.1007/s10616-017-0064-9

Chugh, R.M., Chaturvedi, M. & Yerneni, L.K. (2016). Exposure cell number during feeder cell growth-arrest by mitomycin C is a critical pharmacological aspect in stem cell culture system. *J Pharmacol Toxicol Methods* 80:68–74.

Chuong, E. B., Rumi, M. K., Soares, M. J., & Baker, J. C. (2013). Endogenous retroviruses function as species-specific enhancer elements in the placenta. *Nature genetics*, 45(3), 325-329.

Clayton, E., Doupé, D. P., Klein, A. M., Winton, D. J., Simons, B. D., & Jones, P. H. (2007). A single type of progenitor cell maintains normal epidermis. *Nature*, *446*(7132), 185–189. https://doi.org/10.1038/nature05574

Collas P. (2010). The current state of chromatin immunoprecipitation. *Molecular biotechnology*, 45(1), 87–100. https://doi.org/10.1007/s12033-009-9239-8

Cotsarelis, G., Sun, TT., & Lavker, RM. (1990) Label retaining cells reside in the bulge area of pilosebaceous unit: implications for follicular stem cells, hair cycle, and skin carcinogenesis. *Cell,* 61,1329–37.

Dahle, J., Kakar, M., Steen, HB. & Kaalhus, O. Automated counting of mammalian cell colonies by means of a flatbed scanner and image processing. *Cytometry A*. 2004;60(2):182–8.

De Luca, M., Pellegrini, G., & Green, H. (2006). Regeneration of squamous epithelia from stem cells of cultured grafts. *Regenerative Medicine*, 1(1), 45–57.

DeCaprio, J. & Kohl, TO. (2020). Chromatin Immunoprecipitation. *Cold Spring Harb Protoc*. 3;2020(8):098665. doi: 10.1101/pdb. prot098665. PMID: 32747583.

del Mar Vivanco, M. (2015). *Methods in Molecular Biology*. Springer Science+Business Media, New York. [eBook] DOI: 10.1007/978-1-4939-2519-3. ISBN: 978-1-4939-2519-3.

Denard, B., Lee, C. & Ye, J. (2012). Doxorubicin blocks proliferation of cancer cells through proteolytic activation of CREB3L1, *eLife* 1, e00090.

Díaz-García, D., Filipová, A., Garza-Veloz, I., & Martinez-Fierro, M. L. (2021). A Beginner's Introduction to Skin Stem Cells and Wound Healing. *International journal of molecular sciences*, 22(20), 11030. https://doi.org/10.3390/ijms222011030

Dlugosz A. (1999). The Hedgehog and the hair follicle: a growing relationship. *The Journal of clinical investigation*, 104(7), 851–853. https://doi.org/10.1172/JCI8416

Donnison, M., Beaton, A., Davey, HW. et al. (2005). Loss of the extraembryonic ectoderm in Elf5 mutants leads to defects in embryonic patterning. *Development,* 132:2299–2308. [PubMed: 15829518]

Donnison, M., Beaton, A., Davey, HW., Broadhurst, R., L'Huillier, P., & Pfeffer, PL. (2005). Loss of the extraembryonic ectoderm in Elf5 mutants leads to defects in embryonic patterning. *Development* 132: 2299–2308.

Dover, R. & Potten, C. S. (1983). Cell cycle kinetics of cultured human epidermal keratinocytes. *J. invest. Derm*. 80, 423–429. https://doi.org/10.1111/1523-1747.ep12555494

Eckert, R. L. (1997). The epidermal keratinocyte as a model for the study of gene regulation and cell differentiation. Physiological Reviews.

El-Deiry, WS., Tokino, T., Velculescu, VE., Levy, DB., Parsons, R., Trent, JM., Lin, D., Mercer, WE., Kinzler, KW., & Vogelstein, B. (1993). WAF1, a potential mediator of p53 tumor suppression. Cell, 75: 817–825.

Epstein, E. (1971). Changes in human dermal collagen types with age. *ClinRes*. 19:359–60.

Ermolaeva, M., Neri, F., Ori, A., & Rudolph, K. L. (2018). Cellular and epigenetic drivers of stem cell ageing. *Nature reviews. Molecular cell biology*, 19(9), 594–610. https://doi.org/10.1038/s41580-018-0020-3

Ervin, H., Epstein, JR. & Munderloh, NH. (1978). Human skin collagen. *J BioChem*. 253:1336–7.

Estrach, S., Ambler, C. A., Lo Celso, C. L., Hozumi, K., & Watt, F. M. (2006). Jagged 1 is a β-catenin target gene required for ectopic hair follicle formation in adult epidermis. *Development*, 133, 4427–4438.

Evano, B. & Tajbakhsh, S. (2018). Skeletal muscle stem cells in comfort and stress. *NPJ Regenerative medicine*, 3, 24. https://doi.org/10.1038/s41536-018-0062-3

Feldman, R.J., Sementchenko, V.I., & Watson, D.K. (2003). The epithelial-specific Ets factors occupy a unique position in defining epithelial proliferation, differentiation and carcinogenesis. *Anticancer Res*, 23, 2125–2131.

Firth, S. M., & Baxter, R. C. (2002). Cellular actions of the insulin-like growth factor binding proteins. In *Endocrine Reviews* (Vol. 23, Issue 6, pp. 824–854). https://doi.org/10.1210/er.2001-0033

Fleming, J. M., Leibowitz, B. J., Kerr, D. E., & Cohick, W. S. (2005). IGF-I differentially regulates IGF-binding protein expression in primary mammary fibroblasts and epithelial cells. *Journal of Endocrinology*, *186*(1), 165–178. https://doi.org/10.1677/joe.1.06164

Flora, P., & Ezhkova, E. (2020). Regulatory mechanisms governing epidermal stem cell function during development and homeostasis. In *Development* (Cambridge), 147(22). Company of Biologists Ltd. https://doi.org/10.1242/dev.194100

Flora, P., & Ezhkova, E. (2020). Regulatory mechanisms governing epidermal stem cell function during development and homeostasis. *Development* (Cambridge, England), 147(22), dev194100. https://doi.org/10.1242/dev.194100

Foley, A.C., & Mercola, M. (2005). Heart induction by Wnt antagonists depends on the homeodomain transcription factor Hex. *Genes & development*, 19 3, 387-96.

Forni, M. F., Trombetta-Lima, M., & Sogayar, M. C. (2012). Stem cells in embryonic skin development. In *Biological Research*, 45(3), 215–222. https://doi.org/10.4067/S0716-97602012000300003

Friedman, DW., Boyd, CD., Mackenzie, JW., Norton, P., Olson, RM. & Deak, SB. (1993). Regulation of collagen gene expression in keloids and hypertrophic scars. *J Surg Res*. 55:214–22.

Fuchs E. (2007). Scratching the surface of skin development. *Nature*, 445(7130), 834-42. Epub 2007/02/23. doi: 10.1038/nature05659. PubMed PMID: 17314969; PubMed Central PMCID: PMCPMC2405926.

Fuchs E. (2008). Skin stem cells: rising to the surface. *J Cell Biol*, 180(2):273-84. Epub 2008/01/23. doi: 10.1083/jcb.200708185. PubMed PMID: 18209104; PubMed Central PMCID: PMCPMC2213592.

Fuchs, E., & Horsley, V. (2008). More than one way to skin. In *Genes and Development*, 22(8), 976–985. https://doi.org/10.1101/gad.1645908

Gallego-Ortega, D., Ledger, A., Roden, D.L., Law, A.M., Magenau, A., Kikhtyak, Z., Cho, C., Allerdice, S.L., Lee, H.J., Valdes-Mora, F. et al. (2015). ELF5 Drives Lung Metastasis in Luminal Breast Cancer through Recruitment of Gr1+ CD11b+ Myeloid-Derived Suppressor Cells. *PLoS Biol*, 13, e1002330.

Gao, J., Guo, Z., Zhang, Y., Liu, Y., Xing, F., Wang, J., Luo, X., Kong, Y., & Zhang, G. (2023). Age-related changes in the ratio of Type I/III collagen and fibril diameter in mouse skin. *Regenerative Biomaterials,* 10. https://doi.org/10.1093/rb/rbac110

Gao, Q., Zhou, G., Lin, S. J., Paus, R., & Yue, Z. (2019). How chemotherapy and radiotherapy damage the tissue: comparative biology lessons from feather and hair models. *Experimental dermatology*, 28(4), 413-418.

Gat, U., DasGupta, R., Degenstein, L., & Fuchs, E. (1998). De novo hair follicle morphogenesis and hair tumors in mice expressing a truncated β-catenin in skin. *Cell*, 95(5), 605-614.

Gattazzo, F., Urciuolo, A. & Bonaldo, P. (2014) Extracellular matrix: a dynamic microenvironment for stem cell niche. *Biochim Biophys Acta* 1840:2506–19.

Gawkrodger, DJ & Ardern-Jones, MR. (2017). Dermatology: an illustrated colour text, 6th Edn. Elsevier, 2017.

Geissmann, Q. (2013). OpenCFU, a New Free and Open-Source Software to Count Cell Colonies and Other Circular Objects. *PLoS ONE*, *8*(2). https://doi.org/10.1371/journal.pone.0054072

Gelse, K., Poschl, E. & Aigner, T. (2003). Collagens-structure, function, and biosynthesis. *Adv Drug Deliv Rev*. 55:1531–46.

Giangreco, A., Qin, M., Pintar, JE., & Watt, FM. (2008). Epidermal stem cells are retained in vivo throughout skin aging. *Aging Cell*. Mar;7(2):250-9. doi: 10.1111/j.1474-9726.2008.00372. x. Epub 2008 Jan 21. PMID: 18221414; PMCID: PMC2339763

Gniadecki, R. (1998). Regulation of Keratinocyte Proliferation. In *Gen. Pharmac* (Vol. 30, Issue 5).

Gonzales, K. A. U., & Fuchs, E. (2017). Skin and Its Regenerative Powers: An Alliance between Stem Cells and Their Niche. In *Developmental Cell* (Vol. 43, Issue 4, pp. 387–401). *Cell Press*. https://doi.org/10.1016/j.devcel.2017.10.001

Gorski, J.P., Huffman, N.T., Chittur, S., Midura, R.J., Black, C., Oxford, J. et al. (2011). Inhibition of proprotein convertase SKI-1 blocks transcription of key extracellular matrix genes regulating osteoblastic mineralization. *J. Biol. Chem*. 286 (3) 1836–1849.

Greco, V., Chen, T., Rendl, M., Schober, M., Pasolli, H. A., Stokes, N., dela Cruz-Racelis, J., & Fuchs, E. (2009). A Two-Step Mechanism for Stem Cell Activation during Hair Regeneration. *Cell Stem Cell*, 4(2), 155–169. https://doi.org/10.1016/j.stem.2008.12.009

Green, H. (2008). The birth of therapy with cultured cells. *BioEssays*, 30(9), 897-903. https://doi.org/10.1002/bies.20797

Greenwood, M., Gillard, B. T., Farrukh, R., Paterson, A., Althammer, F., Grinevich, V., Murphy, D., & Greenwood, M. P. (2022). Transcription factor Creb3l1 maintains proteostasis in neuroendocrine cells. *Molecular Metabolism*, *63*. https://doi.org/10.1016/j.molmet.2022.101542

Grymowicz, M., Rudnicka, E., Podfigurna, A., Napierala, P., Smolarczyk, R., Smolarczyk, K., & Meczekalski, B. (2020). Hormonal Effects on Hair Follicles. *International journal of molecular sciences*, 21(15), 5342. https://doi.org/10.3390/ijms21155342

Gudjonsson, T., & Magnusson, M. K. (2005). Stem cell biology and the cellular pathways of carcinogenesis. In *APMIS* (Vol. 113, Issues 11–12, pp. 922–929). https://doi.org/10.1111/j.1600-0463.2005.apm_371.x

Guzmán, C., Bagga, M., Kaur, A., Westermarck, J., & Abankwa, D. (2014). ColonyArea: An ImageJ plugin to automatically quantify colony formation in clonogenic assays. *PLoS ONE*, *9*(3). https://doi.org/10.1371/journal.pone.0092444

Hahn, H., Wicking, C., Zaphiropoulos, P. G., Gailani, M. R., Shanley, S., Chidambaram, A., ... & Bale, A. E. (1996). Mutations of the human homolog of Drosophila patched in the nevoid basal cell carcinoma syndrome. *Cell*, 85(6), 841-851.

Hall, P. A. & Watt, F. M. (1989). Stem cells: the generation and maintenance of cellular diversity. *Development*, 106,619–633.

Hemberger, M., Udayashankar, R., Tesar, P., Moore, H., & Burton, G. J. (2010). ELF5-enforced transcriptional networks define an epigenetically regulated trophoblast stem cell compartment in the human placenta. *Human Molecular Genetics*, 19(12), 2456–2467. https://doi.org/10.1093/hmg/ddq128

Hennings, H., Cheng, M. D., Steinert, P., Holbrook, K. S. & Yuspa, S. H. (1980). Calcium regulation of growth and differentiation of mouse epidermal cells in culture. *Cell*. 19:245-254.

Hirsch, T., Rothoeft, T., Teig, N., Bauer, J. W., Pellegrini, G., De Rosa, L., Scaglione, D., Reichelt, J., Klausegger, A., Kneisz, D., Romano, O., Secone Seconetti, A., Contin, R., Enzo, E., Jurman, I., Carulli, S., Jacobsen, F., Luecke, T., Lehnhardt, M., Fischer, M., … De Luca, M. (2017). Regeneration of the entire human epidermis using transgenic stem cells. *Nature*, 551(7680), 327–332. https://doi.org/10.1038/nature24487

Holmes, C., & Stanford, W. L. (2007). Concise review: stem cell antigen-1: expression, function, and enigma. *Stem cells* (Dayton, Ohio), 25(6), 1339–1347. https://doi.org/10.1634/stemcells.2006-0644

Honari, G., & Maibach, H. (2014). Skin Structure and Function. Skin Structure and Function. *Applied Dermatotoxicology*, Academic Press,2014, Pages 1-10, ISBN 9780124201309. https://doi.org/10.1016/B978-0-12-420130-9.00001-3.

Horsley, V. (2020). Skin in the Game: Stem Cells in Repair, Cancer, and Homeostasis. In *Cell* (Vol. 181, Issue 3, pp. 492–494). Cell Press. https://doi.org/10.1016/j.cell.2020.03.019

Horsley, V., Aliprantis, A. O., Polak, L., Glimcher, L. H., & Fuchs, E. (2008). NFATc1 Balances Quiescence and Proliferation of Skin Stem Cells. *Cell*, 132(2), 299–310. https://doi.org/10.1016/j.cell.2007.11.047

Hsu, Y. C., Li, L., & Fuchs, E. (2014a). Emerging interactions between skin stem cells and their niches. In *Nature Medicine* (Vol. 20, Issue 8, pp. 847–856). Nature Publishing Group. https://doi.org/10.1038/nm.3643

Hsu, Y. C., Li, L., & Fuchs, E. (2014b). Transit-amplifying cells orchestrate stem cell activity and tissue regeneration. *Cell*, 157(4), 935–949. https://doi.org/10.1016/j.cell.2014.02.057

Hsu, Y. C., Pasolli, H. A., & Fuchs, E. (2011). Dynamics between stem cells, niche, and progeny in the hair follicle. *Cell*, 144(1), 92–105. https://doi.org/10.1016/j.cell.2010.11.049

Huang da, W., Sherman, BT. & Lempicki, RA. (2009). Systematic and integrative analysis of large gene lists using DAVID bioinformatics resources. *Nat Protoc*. 4(1):44–57.

Huelsken, J., Vogel, R., Erdmann, B., Cotsarelis, G., & Birchmeier, W. (2001). β-Catenin controls hair follicle morphogenesis and stem cell differentiation in the skin. *Cell*, 105(4), 533-545.

Huelsken, J., Vogel, R., Erdmann, B., Cotsarelis, G., and Birchmeier, W. (2001). beta-Catenin controls hair follicle morphogenesis and stem cell differentiation in the skin. *Cell,*105, 533–545

Hwa, V., Oh, Y., & Rosenfeld, R. G. (1999). The insulin-like growth factor-binding protein (IGFBP) superfamily. *Endocrine reviews*, 20(6), 761–787. https://doi.org/10.1210/edrv.20.6.0382

Ichinose, J., Sako, Y., Murata, M. & Yanagida, T. (2002). Single molecule observation of amplification of EGF receptor activation in semiintact A431 cells. *Seibutsu Butsuri*. 42. S80. 10.2142/biophys.42. S80_3.

Iglesias-Bartolome, R., & Gutkind, J. S. (2010). Keeping the epidermal stem cell niche in shape. In *Cell Stem Cell* (Vol. 7, Issue 2, pp. 143–145). https://doi.org/10.1016/j.stem.2010.07.008

Ingraham, C. R., Kinoshita, A., Kondo, S., Yang, B., Sajan, S., Trout, K. J., ... & Schutte, B. C. (2006). Abnormal skin, limb and craniofacial morphogenesis in mice deficient for interferon regulatory factor 6 (Irf6). *Nature genetics*, 38(11), 1335-1340.

Ingthorsson, S., Briem, E., Bergthorsson, J. T., & Gudjonsson, T. (2016). Epithelial Plasticity During Human Breast Morphogenesis and Cancer Progression. In *Journal of Mammary Gland Biology and Neoplasia* (Vol. 21, Issues 3–4, pp. 139–148). Springer New York LLC. https://doi.org/10.1007/s10911-016-9366-3

Ito, M., Yang, Z., Andl, T., Cui, C., Kim, N., Millar, S.E., and Cotsarelis, G. (2007). Wnt-dependent de novo hair follicle regeneration in adult mouse skin after wounding. *Nature,* 447, 316–320.

J. Tymms, M., & Kola, I. (1994). Regulation of gene expression by transcription factors Ets-1 and Ets-2. In *Molecular Reproduction and Development* (Vol. 39, Issue 2, pp. 208–214). https://doi.org/10.1002/mrd.1080390214

Jamora, C., DasGupta, R., Kocieniewski, P., & Fuchs, E. (2003). Links between signal transduction, transcription and adhesion in epithelial bud development. *Nature*, 422(6929), 317-322.

Jaubert, J., Cheng, J., & Segre, J. A. (2003). Ectopic expression of kruppel like factor 4 (Klf4) accelerates formation of the epidermal permeability barrier. *Development* (Cambridge, England), 130(12), 2767–2777. https://doi.org/10.1242/dev.00477

Jensen, K. B., Driskell, R. R., & Watt, F. M. (2010). Assaying proliferation and differentiation capacity of stem cells using disaggregated adult mouse epidermis. *Nature Protocols*, 5(5), 898–911. https://doi.org/10.1038/nprot.2010.39

Jensen, U. B., Yan, X., Triel, C., Woo, S. H., Christensen, R., & Owens, D. M. (2008). A distinct population of clonogenic and multipotent murine follicular keratinocytes residing in the upper isthmus. *Journal of Cell Science*, 121(5), 609–617. https://doi.org/10.1242/jcs.025502

Ji, F., & Sadreyev, R. I. (2018). RNA-seq: Basic Bioinformatics Analysis. *Current Protocols in Molecular Biology*, *124*(1). https://doi.org/10.1002/cpmb.68

Ji, S., Zhu, Z., Sun, X., & Fu, X. (2021). Functional hair follicle regeneration: an updated review. In *Signal Transduction and Targeted Therapy* (Vol. 6, Issue 1). Springer Nature. https://doi.org/10.1038/s41392-020-00441-y

Jones, P. H., Harper, S., & Watt, F. M. (1995). Stem Cell Patterning and Fate in Human Epidermis England Department of Nephrology Leicester General Hospital Gwendoline Road Leicester LE5 4PW England. In *Cell* (Vol. 80).

Jones, PH & Watt, FM. (1993). Separation of human epidermal stem cells from transit amplifying cells on the basis of differences in integrin function and expression. *Cell,* 73(4), 713-724. https://doi.org/10.1016/0092-8674(93)90251-K

Kadler, K. E., Baldock, C., Bella, J., & Boot-Handford, R. P. (2007). Collagens at a glance. *Journal of Cell Science*, 120(12), 1955–1958. https://doi.org/10.1242/jcs.03453

Kalyuga, M., Gallego-Ortega, D., Lee, H.J., Roden, D.L., Cowley, M.J., Caldon, C.E., Stone, A., Allerdice, S.L., Valdes-Mora, F., Launchbury, R. et al. (2012). ELF5 suppresses estrogen sensitivity and underpins the acquisition of anti-estrogen resistance in luminal breast cancer. *PLoS Biol*, 10, e1001461.

Kanehisa, M. (2013). Molecular network analysis of diseases and drugs in KEGG. *Methods Mol Biol*. 939:263–75.

Kenny, RA & Ross MM. (2020). Collagens and elastin genetic variations and their potential role in aging related diseases and longevity in humans. *Exp Gerontol* 129:1–12.

Kidder, BL., & Palmer, S. (2010). Examination of transcriptional networks reveals an important role for TCFAP2C, SMARCA4, and EOMES in trophoblast stem cell maintenance. *Genome Res*, 20, 458–472.

Kim, T., Sridharan, .I, Ma, Y., Zhu, B., Chi, N., Kobak, W., Rotmensch, J.,Schieber, JD. & Wang, R. (2016) Identifying distinct nanoscopic features of native collagen fibrils towards early diagnosis of pelvic organ prolapse. *Nanomedicine*. 12:667–75.

Kobielak, K., Pasolli, H., Alonso, L., Polak, L., & Fuchs, E. (2003). Defining BMP functions in the hair follicle by conditional ablation of BMP receptor IA. *The Journal of cell biology*, 163, 609-23. 10.1083/jcb.200309042.

Kobielak, K., Stokes, N., de la Cruz, J., Polak, L., & Fuchs, E. (2007). Loss of a quiescent niche but not follicle stem cells in the absence of bone morphogenetic protein signaling. *Proceedings of the National Academy of Sciences*, 104(24), 10063-10068.

Kolarsick, P., Kolarsick, M.A., & Goodwin, C. (2011). Anatomy and Physiology of the Skin. *Journal of the Dermatology Nurses' Association*, 3, 203-213.

Koster, M. I., & Roop, D. R. (2007). Mechanisms regulating epithelial stratification. In *Annual Review of Cell and Developmental Biology*, 23, 93–113. https://doi.org/10.1146/annurev.cellbio.23.090506.123357

Kratochwil, K., Dull, M., Farinas, I., Galceran, J., & Grosschedl, R. (1996). Lef1 expression is activated by BMP-4 and regulates inductive tissue interactions in tooth and hair development. *Genes & development*, 10(11), 1382-1394.

Kretzschmar, K., & Watt, F. M. (2014). Markers of epidermal stem cell subpopulations in adult mammalian skin. Cold Spring Harbor Perspectives in Medicine, 4(10). https://doi.org/10.1101/cshperspect.a013631

Kretzschmar, K., Cottle, D. L., Schweiger, P. J., & Watt, F. M. (2015). The Androgen Receptor Antagonizes Wnt/β-Catenin Signaling in Epidermal Stem Cells. *Journal of Investigative Dermatology*, 135(11), 2753–2763. https://doi.org/10.1038/jid.2015.242

Krtolica, A. (2005). Stem cell: Balancing aging and cancer. In *International Journal of Biochemistry and Cell Biology* (Vol. 37, Issue 5 SPEC. ISS., pp. 935–941). Elsevier Ltd. https://doi.org/10.1016/j.biocel.2004.10.007

Kuivaniemi, H., & Tromp, G. (2019). Type III collagen (COL3A1): Gene and protein structure, tissue distribution, and associated diseases. In *Gene* (Vol. 707, pp. 151–171). Elsevier B.V. https://doi.org/10.1016/j.gene.2019.05.003

Kurtenbach, S., Reddy, R., & Harbour, J. W. (2019). ChIPprimersDB: A public repository of verified qPCR primers for chromatin immunoprecipitation (ChIP). *Nucleic Acids Research*, *47*(D1), D46–D49. https://doi.org/10.1093/nar/gky813

Lajtha, L. G. (1979). Differentiation Views Stem Cell Concepts. In *Differentiation* (Vol. 14).

Lapinskas, E.J., Svobodova, S., Davis, I.D., Cebon, J., Hertzog, P.J., & Pritchard, M.A. (2011). The Ets transcription factor ELF5 functions as a tumor suppressor in the kidney. *Twin Res. Hum. Genet*, 14, 316–322.

Latos, P. A., Sienerth, A. R., Murray, A., Senner, C. E., Muto, M., Ikawa, M., Oxley, D., Burge, S., Cox, B. J., & Hemberger, M. (2015). Elf5-centered transcription factor hub controls trophoblast stem cell self-renewal and differentiation through stoichiometry sensitive shifts in target gene networks. *Genes and Development*, 29(23), 2435–2448. https://doi.org/10.1101/gad.268821.115

Lee, J., & Tumbar, T. (2012). Hairy tale of signaling in hair follicle development and cycling. In *Seminars in cell & developmental biology*, 23(8), 906-916. Academic Press.

Levy, V., Lindon, C., Harfe, B. D., & Morgan, B. A. (2005). Distinct stem cell populations regenerate the follicle and interfollicular epidermis. In *Developmental Cell* (Vol. 9, Issue 6, pp. 855–861). https://doi.org/10.1016/j.devcel.2005.11.003

Li, K. N., & Tumbar, T. (2021). Hair follicle stem cells as a skin-organizing signaling center during adult homeostasis. *The EMBO Journal*, 40(11). https://doi.org/10.15252/embj.2020107135

Li, K., Guo, Y., Yang, X., Zhang, Z., Zhang, C., & Xu, Y. (. 2017). ELF5-Mediated AR Activation Regulates Prostate Cancer Progression. *Sci. Rep*, 7, 42759.

Li, N., & Clevers, H. (2010). Coexistence of quiescent and active adult stem cells in mammals. In *Science*, 327(5965), 542–545. https://doi.org/10.1126/science.1180794

Li, P., Wang, S., Zhan, L., He, X., Chi, G., Lv, S., Xu, Z., Xia, Y., Teng, S., Li, L., & Li, Y. (2017). Efficient feeder cells preparation system for large-scale preparation and application of induced pluripotent stem cells. *Scientific Reports*, 7(1). https://doi.org/10.1038/s41598-017-10428-5

Lichti, U., Anders, J., & Yuspa, S. H. (2008). Isolation and short-term culture of primary keratinocytes, hair follicle populations and dermal cells from newborn mice and keratinocytes from adult mice for in

vitro analysis and for grafting to immunodeficient mice. Nature Protocols, 3(5), 799–810. https://doi.org/10.1038/nprot.2008.50

Lim, X., & Nusse, R. (2013). Wnt signaling in skin development, homeostasis, and disease. Cold Spring Harbor Perspectives in *Biology*, 5(2). https://doi.org/10.1101/cshperspect.a008029

Lin, KK., Chudova, D., HatWeld, GW., Smyth, P. & Andersen, B. (2004). Identification of hair cycle - associated genes from time-course gene expression profile data by using replicate variance. *Proc Natl Acad Sci USA.* 101:15955–15960.

Lin, X., Zhu, L., & He, J. (2022). Morphogenesis, Growth Cycle and Molecular Regulation of Hair Follicles. In *Frontiers in Cell and Developmental Biology* (Vol. 10). Frontiers Media S.A. https://doi.org/10.3389/fcell.2022.899095

Lin, X., Zhu, L., & He, J. (2022). Morphogenesis, Growth Cycle and Molecular Regulation of Hair Follicles. In *Frontiers in Cell and Developmental Biology* (Vol. 10). Frontiers Media S.A. https://doi.org/10.3389/fcell.2022.899095

Liu, B., Zhu, F., Xia, O., Park, E., & Hu, Y. (2009). A tale of terminal differentiation IKKα, the master keratinocyte regulator. In *Cell Cycle* (Vol. 8, Issue 4, pp. 527–531). Taylor and Francis Inc. https://doi.org/10.4161/cc.8.4.7598

Liu, JC., Zhou, L., Wang, F., Cheng, ZQ. & Rong, C. (2018). Osthole decreases collagen I/III contents and their ratio in TGF-b1-overexpressed mouse cardiac fibroblasts through regulating the TGF-b/smad signaling pathway. *Chin J Net Med*. 16:321–9.

Liu, L., & Rando, T. A. (2011). Manifestations and mechanisms of stem cell aging. *In Journal of Cell Biology*, 193 (2), 257–266. https://doi.org/10.1083/jcb.201010131

Liu, S., Zhang, H., & Duan, E. (2013). Epidermal development in mammals: Key regulators, signals from beneath, and stem cells. *In International Journal of Molecular Sciences* (Vol. 14, Issue 6, pp. 10869–10895). MDPI AG. https://doi.org/10.3390/ijms140610869

Llames, SG., Garcıa., E, Meana, A., Larcher, F. & Del Rio, M. (2015). Feeder layer cell actions and applications. *Tissue Eng* Part B 21:345–353. https://doi:10.1089/ten.teb.2014.0547

Luk, I. Y., Reehorst, C. M., & Mariadason, J. M. (2018). ELF3, ELF5, EHF and SPDEF transcription factors in tissue homeostasis and cancer. In *Molecules* (Vol. 23, Issue 9). MDPI AG. https://doi.org/10.3390/molecules23092191

M'boneko, V., & Merker, H. J. (1988). Development and morphology of the periderm of mouse embryos (days 9–12 of gestation). *Cells Tissues Organs*, 133(4), 325-336.

Maadi, H., Soheilifar, M. H., & Wang, Z. (2022). Analysis of Cell Cycle by Flow Cytometry. In *Methods in Molecular Biology* (Vol. 2579, pp. 183–195). Humana Press Inc. https://doi.org/10.1007/978-1-0716-2736-5_14

Mack, J. A., Anand, S., & Maytin, E. V. (2005). Proliferation and cornification during development of mammalian epidermis. In *Birth Defects Research Part C - Embryo Today: Reviews*, 75(4), 314–329. https://doi.org/10.1002/bdrc.20055

Magerl, M., Tobin, D. J., Müller-Röver, S., Hagen, E., Lindner, G., McKay, I. A., & Paus, R. (2001). Patterns of proliferation and apoptosis during murine hair follicle morphogenesis. *The Journal of investigative dermatology*, 116(6), 947–955. https://doi.org/10.1046/j.0022-202x.2001.01368.x

Marescal, O., & Cheeseman, I. M. (2020). Cellular Mechanisms and Regulation of Quiescence. In *Developmental Cell* (Vol. 55, Issue 3, pp. 259–271). Cell Press. https://doi.org/10.1016/j.devcel.2020.09.029

Martin, M. T., Vulin, A., & Hendry, J. H. (2016). Human epidermal stem cells: Role in adverse skin reactions and carcinogenesis from radiation. *Mutation Research - Reviews in Mutation Research*, 770, 349–368. https://doi.org/10.1016/j.mrrev.2016.08.004

Mathew-Steiner, S. S., Roy, S., & Sen, C. K. (2021). Collagen in wound healing. *In Bioengineering* (Vol. 8, Issue 5). MDPI AG. https://doi.org/10.3390/bioengineering8050063

McLafferty, E., Hendry, C., & Alistair, F. (2012). The integumentary system: anatomy, physiology and function of skin. *Nurs Stand*. 27(3):35-42. Epub 2012/12/20. doi: 10.7748/ns2012.10.27.7.35.c9358. PubMed PMID: 23248884.

McMaughan, D. J., Oloruntoba, O., & Smith, M. L. (2020). Socioeconomic Status and Access to Healthcare: Interrelated Drivers for Healthy Aging. *Frontiers in public health*, 8, 231. https://doi.org/10.3389/fpubh.2020.00231

Meiliana, A., Dewi, N., & Wijaya, A. (2015). Heterogeneous Stem Cells in Skin Homeostatis and Wound Repair. *The Indonesian Biomedical Journal*. 7. 87. 10.18585/inabj. v7i2.74

Mellor, P., Deibert, L., Calvert, B., Bonham, K., Carlsen, S.A., & Anderson, D.H. (2013). CREB3L1 is a metastasis suppressor that represses expression of genes regulating metastasis, invasion, and angiogenesis. *Mol. Cell. Biol*. 33 (24) 4985–4995.

Mellor, P., Kendall, S., Smith, S., Saxena, A. & D.H. Anderson. (2022). Reduced CREB3L1 expression in triple negative and luminal breast cancer cells contributes to enhanced cell migration, anchorage-independent growth, and metastasis. *PLoSOne* 17 (7) e0271090.

Meng, X., Qiu, L., Song, H., & Dang, N. (2018). MAPK pathway involved in epidermal terminal differentiation of normal human epidermal keratinocytes. *Open Medicine* (Poland), 13(1), 189–195. https://doi.org/10.1515/med-2018-0029

Merrill, B. J., Gat, U., DasGupta, R., & Fuchs, E. (2001). Tcf3 and Lef1 regulate lineage differentiation of multipotent stem cells in skin. *Genes & development*, 15(13), 1688-1705.

Metzger, D. E., Stahlman, M. T., & Shannon, J. M. (2008). Misexpression of ELF5 disrupts lung branching and inhibits epithelial differentiation. *Developmental Biology*, *320*(1), 149–160. https://doi.org/10.1016/j.ydbio.2008.04.038

Millar, S. E. (2002). Molecular mechanisms regulating hair follicle development. In *Journal of Investigative Dermatology* (Vol. 118, Issue 2, pp. 216–225). Blackwell Publishing Inc. https://doi.org/10.1046/j.0022-202x.2001.01670.x

Millar, S. E., Willert, K., Salinas, P. C., Roelink, H., Nusse, R., Sussman, D. J., & Barsh, G. S. (1999). WNT signaling in the control of hair growth and structure. *Developmental biology,* 207(1), 133-149.

Mills, AA., Zheng, B., Wang, XJ., Vogel, H., Roop, DR., & Bradley, A. (1999). p63 is a p53 homologue required for limb and epidermal morphogenesis. *Nature*. 398, 708–713.

Miyakoshi N, Qin X, Kasukawa Y, Richman C, Srivastava AK, Baylink DJ & Mohan S 2001 Systemic administration of insulin-like growth factor (IGF)-binding protein-4 (IGFBP-4) increases bone formation parameters in mice by increasing IGF bioavailability via an IGFBP-4 protease-dependent mechanism. *Endocrinology*. 1422641–2648

Mohan, S., & Baylink, D. J. (2002). BEYOND CARRIER PROTEINS IGF-binding proteins are multifunctional and act via IGF-dependent and-independent mechanisms. *In Journal of Endocrinology* (Vol. 175). http://www.endocrinology.org

Morgan, B. A. (2013). The "skinny" on Wnt signaling in stem cells. In *Cell Stem Cell* (Vol. 13, Issue 6, pp. 638–640). *Cell Press*. https://doi.org/10.1016/j.stem.2013.11.012

Moriyama, M., Durham, A. D., Moriyama, H., Hasegawa, K., Nishikawa, S. I., Radtke, F., & Osawa, M. (2008). Multiple roles of Notch signaling in the regulation of epidermal development. *Developmental cell*, 14(4), 594-604.

Morris, R. J. (2000). Keratinocyte stem cells: targets for cutaneous carcinogens. *The Journal of Clinical Investigation*, 106,1.

Morris, R. J. (2000). Keratinocyte stem cells: targets for cutaneous carcinogens. *The Journal of Clinical Investigation*, 106, 1.

Mullen, A. C., Orlando, D. A., Newman, J. J., Lovén, J., Kumar, R. M., Bilodeau, S., ... & Young, R. A. (2011). Master transcription factors determine cell-type-specific responses to TGF-β signaling. *Cell*, 147(3), 565-576.

Mundade, R., Ozer, H. G., Wei, H., Prabhu, L., & Lu, T. (2014). Role of ChIP-seq in the discovery of transcription factor binding sites, differential gene regulation mechanism, epigenetic marks and beyond. In *Cell Cycle* (Vol. 13, Issue 18, pp. 2847–2852). Landes Bioscience. https://doi.org/10.4161/15384101.2014.949201

Nagarajan, P., Romano, R. A., & Sinha, S. (2008). Transcriptional control of the differentiation program of interfollicular epidermal keratinocytes. In *Critical Reviews in Eukaryotic Gene Expression* (Vol. 18, Issue 1, pp. 57–79). Begell House Inc. https://doi.org/10.1615/critreveukargeneexpr.v18.i1.50

Nam, D., & Reineke, E. L. (2017). Timing and Targeting of Treatment in Left Ventricular Hypertrophy. In *Methodist DeBakey cardiovascular journal* (Vol. 13, Issue 1, pp. 9–14). https://doi.org/10.14797/mdcj-13-1-9

Nassar, D., & Blanpain, C. (2012). Epidermal development and homeostasis. *Semin. Cell Dev. Biol*. 23, 883 10.1016/j.semcdb.2012.09.005

Naylor, E. C., Watson, R. E., & Sherratt, M. J. (2011). Molecular aspects of skin ageing. *Maturitas*, 69(3), 249–256. https://doi.org/10.1016/j.maturitas.2011.04.011

Ng, R. K., Dean, W., Dawson, C., Lucifero, D., Madeja, Z., Reik, W., & Hemberger, M. (2008). Epigenetic restriction of embryonic cell lineage fate by methylation of Elf5. *Nature Cell Biology*, 10(11), 1280–1290. https://doi.org/10.1038/ncb1786

Ng, R. K., Dean, W., Dawson, C., Lucifero, D., Madeja, Z., Reik, W., & Hemberger, M. (2008). Epigenetic restriction of embryonic cell lineage fate by methylation of Elf5. *Nature Cell Biology*. *10*(11), 1280–1290. https://doi.org/10.1038/ncb1786

Ng, RK., Dean. W., Dawson, C., Lucifero, D., Madeja, Z., Reik, W & Hemberger, M. (2008). Epigenetic restriction of embryonic cell lineage fate by methylation of Elf5. *Nat Cell Biol*.10:1280–1290. [PubMed: 18836439].

Nguyen, B. C., Lefort, K., Mandinova, A., Antonini, D., Devgan, V., Gatta, G. Della, Koster, M. I., Zhang, Z., Wang, J., Di Vignano, A. T., Kitajewski, J., Chiorino, G., Roop, D. R., Missero, C., & Dotto, G. P. (2006). Cross-regulation between Notch and p63 in keratinocyte commitment to differentiation. *Genes and Development*, 20(8), 1028–1042. https://doi.org/10.1101/gad.1406006

Niemela, M., Kauko, O., Sihto, H., Mpindi, J-P., Nicorici, D. et al. (2012) CIP2A signature reveals the MYC dependency of CIP2A-regulated phenotypes and its clinical association with breast cancer subtypes. *Oncogene*. 31: 4266–4278. https://doi:10.1038/onc.2011.599.

Ning, Y., Schuller, A. G., Conover, C. A., & Pintar, J. E. (2008). Insulin-like growth factor (IGF) binding protein-4 is both a positive and negative regulator of IGF activity in vivo. *Molecular Endocrinology*, *22*(5), 1213-1225.

Nowak, J. A., & Fuchs, E. (2009). Isolation and culture of epithelial stem cells. *Methods in Molecular Biology,* 482, 215–232. https://doi.org/10.1007/978-1-59745-060-7_14

O'Connor, N.E., Mulliken, J.B., Banks-Schlegel, S., Kehinde, O. & Green, H. (1981). Grafting of burns with cultured epithelium prepared from autologous epidermal cells. *Lancet*, 317, 75-78

Oakes, S. R., Naylor, M. J., Asselin-Labat, M. L., Blazek, K. D., Gardiner-Garden, M., Hilton, H. N., Kazlauskas, M., Pritchard, M. A., Chodosh, L. A., Pfeffer, P. L., Lindeman, G. J., Visvader, J. E., & Ormandy, C. J. (2008). The Ets transcription factor Elf5 specifies mammary alveolar cell fate. *Genes & development*, 22(5), 581–586. https://doi.org/10.1101/gad.1614608

Oh, J. W., Kloepper, J., Langan, E. A., Kim, Y., Yeo, J., Kim, M. J., Hsi, T. C., Rose, C., Yoon, G. S., Lee, S. J., Seykora, J., Kim, J. C., Sung, Y. K., Kim, M., Paus, R., & Plikus, M. V. (2016). A Guide to Studying Human Hair Follicle Cycling In Vivo. *The Journal of investigative dermatology*, 136(1), 34–44. https://doi.org/10.1038/JID.2015.354

Oh, J., Lee, Y. D., & Wagers, A. J. (2014). Stem cell aging: Mechanisms, regulators and therapeutic opportunities. In *Nature Medicine* (Vol. 20, Issue 8, pp. 870–880). Nature Publishing Group. https://doi.org/10.1038/nm.3651

Ohyama, M. (2007). Hair follicle bulge: A fascinating reservoir of epithelial stem cells. In *Journal of Dermatological Science*, 46 (2), 81–89. https://doi.org/10.1016/j.jdermsci.2006.12.002

Ojeh, N., Pastar, I., Tomic-Canic, M., & Stojadinovic, O. (2015). Stem cells in skin regeneration, wound healing, and their clinical applications. In *International Journal of Molecular Sciences*, 16(10), 25476–25501. MDPI AG. https://doi.org/10.3390/ijms161025476

Oliver, R. F., & Jahoda, C. A. (1988). Dermal-epidermal interactions. *Clinics in dermatology*, 6(4), 74–82. https://doi.org/10.1016/0738-081x(88)90069-7

Omata, F., McNamara, K.M., Suzuki, K., Abe, E., Hirakawa, H., Ishida, T., Ohuchi, N., & Sasano, H. (2018). Effect of the normal mammary differentiation regulator ELF5 upon clinical outcomes of triple negative breast cancers patients. *Breast Cancer*, 25, 489–496.

Oro, A. E., & Higgins, K. (2003). Hair cycle regulation of Hedgehog signal reception. *Developmental biology*, 255(2), 238-248.

Oshimori, N., & Fuchs, E. (2012). The harmonies played by TGF-β in stem cell biology. *Cell stem cell,* 11(6), 751–764. https://doi.org/10.1016/j.stem.2012.11.001

Osorio, K. M., Lilja, K. C., & Tumbar, T. (2011). Runx1 modulates adult hair follicle stem cell emergence and maintenance from distinct embryonic skin compartments. *Journal of Cell Biology*, *193*(1), 235–250. https://doi.org/10.1083/jcb.201006068

Otsuka, A., Levesque, M. P., Dummer, R., & Kabashima, K. (2015). Hedgehog signaling in basal cell carcinoma. *Journal of dermatological science*, 78(2), 95–100. https://doi.org/10.1016/j.jdermsci.2015.02.007

Otto, T., & Sicinski, P. (2017). Cell cycle proteins as promising targets in cancer therapy. Nature reviews. Cancer, 17(2), 93–115. https://doi.org/10.1038/nrc.2016.138

Owczarczyk-Saczonek, A., Krajewska-Włodarczyk, M., Kruszewska, A., Banasiak, Ł., Placek, W., Maksymowicz, W., & Wojtkiewicz, J. (2018). Therapeutic potential of stem cells in follicle regeneration. In *Stem Cells International* (Vol. 2018). Hindawi Limited. https://doi.org/10.1155/2018/1049641

Paladini, R. D., Saleh, J., Qian, C., Xu, G. X., & Rubin, L. L. (2005). Modulation of hair growth with small molecule agonists of the hedgehog signaling pathway. *The Journal of investigative dermatology*, 125(4), 638–646. https://doi.org/10.1111/j.0022-202X.2005.23867.x

Pan, Z., Li, L., Fang, Q., Qian, Y., Zhang, Y., Zhu, J. et al. (2019). Integrated bioinformatics analysis of master regulators in anaplastic thyroid carcinoma, *BioMed. Res. Int*. 2019 9734576.

Pan, Z., Xu, T., Bao, L., Hu, X., Jin, T., Chen, J., Chen, J., Qian, Y., Lu, X., Li, L., Zheng, G., Zhang, Y., Zou, X., Song, F., Zheng, C., Jiang, L., Wang, J., Tan, Z., Huang, P., & Ge, M. (2022). CREB3L1 promotes tumor growth and metastasis of anaplastic thyroid carcinoma by remodeling the tumor microenvironment. *Molecular cancer*, 21(1), 190. https://doi.org/10.1186/s12943-022-01658-x

Panchaprateep, R., & Asawanonda, P. (2014). Insulin-like growth factor-1: Roles in androgenetic alopecia. *Experimental Dermatology*, 23(3), 216–218. https://doi.org/10.1111/exd.12339

Panich, U., Sittithumcharee, G., Rathviboon, N., & Jirawatnotai, S. (2016). Ultraviolet Radiation-Induced Skin Aging: The Role of DNA Damage and Oxidative Stress in Epidermal Stem Cell Damage Mediated Skin Aging. *Stem cells international*, 2016, 7370642. https://doi.org/10.1155/2016/7370642

Panteleyev, A. A., Jahoda, C. A., & Christiano, A. M. (2001). Hair follicle predetermination. *Journal of cell science*, 114(Pt 19), 3419–3431. https://doi.org/10.1242/jcs.114.19.3419

Park PJ. ChIP-seq: advantages and challenges of a maturing technology. *Nat Rev Genet*. 2009;10(10):669–80.

Pearton, D. J., Smith, C. S., Redgate, E., van Leeuwen, J., Donnison, M., & Pfeffer, P. L. (2014). Elf5 counteracts precocious trophoblast differentiation by maintaining Sox2 and 3 and inhibiting Hand1 expression. *Developmental biology*, 392(2), 344-357.

Perez-Moreno, M., Davis, M. A., Wong, E., Pasolli, H. A., Reynolds, A. B., & Fuchs, E. (2006). p120-catenin mediates inflammatory responses in the skin. *Cell*, 124(3), 631-644.

Pickup, M. E., Hu, A., Patel, H. J., & Ahmed, M. I. (2023). MicroRNA-148a Controls Epidermal and Hair Follicle Stem/Progenitor Cells by Modulating the Activities of ROCK1 and ELF5. *The Journal of investigative dermatology*, 143(3), 480–491.e5. https://doi.org/10.1016/j.jid.2022.06.028

Piggin, C.L., Roden, D.L., Gallego-Ortega, D., Lee, H.J., Oakes, S.R., & Ormandy, C.J. (2016). ELF5 isoform expression is tissue-specific and significantly altered in cancer. *Breast Cancer Res*, 18, 4.

Pimentel, H.J., Bray, N., Puente, S., Melsted, P. & Pachter, L. (2017). Differential analysis of RNA-Seq incorporating quantification uncertainty, *Nature Methods advanced access* http://dx.doi.org/10.1038/nmeth.4324.

Pinto, F., Suzuki, D., & Senoo, M. (2020). The simplest protocol for rapid and long-term culture of primary epidermal keratinocytes from human and mouse. In *Methods in Molecular Biology* (Vol. 2109, pp. 1–22). *Humana Press Inc.* https://doi.org/10.1007/7651_2019_263

Plett, R., Mellor, P., Kendall, S., Hammond, S.A., Boulet, A., Plaza, K. et al. (2022). Homoharringtonine demonstrates a cytotoxic effect against triple-negative breast cancer cell lines and acts synergistically with paclitaxel. *Sci. Rep*. 12 (1) 15663.

Plikus, M. V., Mayer, J. A., de La Cruz, D., Baker, R. E., Maini, P. K., Maxson, R., & Chuong, C. M. (2008). Cyclic dermal BMP signalling regulates stem cell activation during hair regeneration. *Nature*, 451(7176), 340-344.

Potten, CS., Saffhill, R., & Maibach, HI. (1987). Measurement of the transit time for cells through the epidermis and stratum corneum of the mouse and Guineapig. *Cell Tissue Kinet*, 20,461–472.

Pruszak, J., Sonntag, K.-C., Aung, M. H., Sanchez-Pernaute, R., & Isacson, O. (2007). Markers and Methods for Cell Sorting of Human Embryonic Stem Cell-Derived Neural Cell Populations. https://www.abcam.com

Pu, S. Y., Huang, Y. L., Pu, C. M., Kang, Y. N., Hoang, K. D., Chen, K. H., & Chen, C. (2023). Effects of Oral Collagen for Skin Anti-Aging: A Systematic Review and Meta-Analysis. In *Nutrients* (Vol. 15, Issue 9). Multidisciplinary Digital Publishing Institute (MDPI). https://doi.org/10.3390/nu15092080

Qu, X., Li, Q., Tu, S., Yang, X., & Wen, W. (2021). ELF5 inhibits the proliferation and invasion of breast cancer cells by regulating CD24. *Molecular biology reports*, 48(6), 5023–5032. https://doi.org/10.1007/s11033-021-06495-7

Reddy, S. T., Andl, T., Lu, M. M., Morrisey, E. E., & Millar, S. E. (2004). Expression of Frizzled genes in developing and postnatal hair follicles. *Journal of investigative dermatology*, 123(2), 275-282.

Reddy, S., Andl, T., Bagasra, A., Lu, M. M., Epstein, D. J., Morrisey, E. E., & Millar, S. E. (2001). Characterization of Wnt gene expression in developing and postnatal hair follicles and identification of Wnt5a as a target of Sonic hedgehog in hair follicle morphogenesis. *Mechanisms of development*, 107(1-2), 69-82.

Reguart, N., He, B., Taron, M., You, L., Jablons, D.M., & Rosell, R. (2005). The role of Wnt signaling in cancer and stem cells. *Future oncology*, 1 6, 787-97.

Reya, T., Morrison, S., Clarke, M. et al. (2001). Stem cells, cancer, and cancer stem cells. *Nature*, 414, 105–111. https://doi.org/10.1038/35102167

Rheinwald, JG. & Green, H. (1975). Serial cultivation of strains of human epidermal keratinocytes: The formation of keratinizing of colonies from single cells. *Cell*. 6:331-334.

Ricard-Blum, S., Baffet, G. & The´ret, N. (2018). Molecular and tissue alterations of collagens in fibrosis. *Matrix Biol*. 68–69:122–49.

Richardson, R. J., Dixon, J., Malhotra, S., Hardman, M. J., Knowles, L., Boot-Handford, R. P., ... & Dixon, M. J. (2006). Irf6 is a key determinant of the keratinocyte proliferation-differentiation switch. *Nature genetics*, 38(11), 1329-1334.

Rocco, J. W., Leong, C. O., Kuperwasser, N., DeYoung, M. P., & Ellisen, L. W. (2006). p63 mediates survival in squamous cell carcinoma by suppression of p73-dependent apoptosis. *Cancer cell*, 9(1), 45–56. https://doi.org/10.1016/j.ccr.2005.12.013

Sada, A., Jacob, F., Leung, E., Wang, S., White, BS., Shalloway, D., & Tumbar, T. (2016). Defining the cellular lineage hierarchy in the interfollicular epidermis of adult skin. *Nat. Cell Biol*, 18:619–631.

Sakai, Y., & Demay, M. B. (2000). *Evaluation of Keratinocyte Proliferation and Differentiation in Vitamin D Receptor Knockout Mice**. https://academic.oup.com/endo/article/141/6/2043/2988469

Sato, N., Leopold, P. L., & Crystal, R. G. (1999). Induction of the hair growth phase in postnatal mice by localized transient expression of Sonic hedgehog. *The Journal of clinical investigation*, 104(7), 855-864.

Saxena, N., Mok, K. W., & Rendl, M. (2019). An updated classification of hair follicle morphogenesis. In *Experimental Dermatology*, 28(4), 332–344. Blackwell Publishing Ltd. https://doi.org/10.1111/exd.13913

Scheitz, C. J. F., & Tumbar, T. (2013). New insights into the role of Runx1 in epithelial stem cell biology and pathology. *Journal of Cellular Biochemistry*, 114(5), 985–993. https://doi.org/10.1002/jcb.24453

Schmidt-Ullrich, R., & Paus, R. (2005). Molecular principles of hair follicle induction and morphogenesis. In *BioEssays*, 27(3), 247–261. https://doi.org/10.1002/bies.20184

Schneider, M. R., Schmidt-Ullrich, R., & Paus, R. (2009). The Hair Follicle as a Dynamic Miniorgan. In *Current Biology*,19(3). https://doi.org/10.1016/j.cub.2008.12.005

Scholl, F. A., Dumesic, P. A., & Khavari, P. A. (2004). Mek1 alters epidermal growth and differentiation. Cancer research, 64(17), 6035-6040.

Scholl, F. A., Dumesic, P. A., Barragan, D. I., Harada, K., Bissonauth, V., Charron, J., & Khavari, P. A. (2007). Mek1/2 MAPK kinases are essential for Mammalian development, homeostasis, and Raf-induced hyperplasia. *Developmental cell*, 12(4), 615-629.

Schönthal, A.H. (ed.) 2004. *Checkpoint Controls and Cancer*. Totowa, New Jersey: Humana Press Inc. (Methods in Molecular Biology; vol. 280-281).

Schultz, M. B. & Sinclair, D. A. (2016). When stem cells grow old: Phenotypes and mechanisms of stem cell aging. In Development (Cambridge) (Vol. 143, Issue 1, pp. 3–14). Company of Biologists Ltd. https://doi.org/10.1242/dev.130633

Segre, JA., Bauer, C., & Fuchs, E. (1999). Klf4 is a transcription factor required for establishing the barrier function of the skin. *Nat Genet*, 22, 356–360.

Sennett, R., & Rendl, M. (2012). Mesenchymal–epithelial interactions during hair follicle morphogenesis and cycling. In *Seminars in cell & developmental biology*, 23(8), 917-927. Academic Press.

Senoo, M., Pinto, F., Crum, CP., & McKeon, F. (2007). p63 is essential for the proliferative potential of stem cells in stratified epithelia. *Cell*, 129, 523–536.

Sharpless, N., DePinho, R. How stem cells age and why this makes us grow old. *Nat Rev Mol Cell Biol*, 8, 703–713 (2007). https://doi.org/10.1038/nrm2241

Sharrocks, A.D. (2001). The ETS-domain transcription factor family. *Nat. Rev. Mol. Cell. Biol*, 2, 827–837.

Shaul, Y. D., & Seger, R. (2007). The MEK/ERK cascade: from signaling specificity to diverse functions. *Biochimica et Biophysica Acta (BBA)-Molecular Cell Research*, 1773(8), 1213-1226.

Shen, Y., Vignali, P., & Wang, R. (2017). Rapid Profiling Cell Cycle by Flow Cytometry Using Concurrent Staining of DNA and Mitotic Markers. *BIO-PROTOCOL*, *7*(16). https://doi.org/10.21769/bioprotoc.2517

Sherr, C. J. (2000). The Pezcoller lecture: cancer cell cycles revisited. *Cancer research*, *60*(14), 3689-3695.

Shi, C., Zhu, Y., Su, Y., & Cheng, T. (2006). Stem cells and their applications in skin-cell therapy. Trends in biotechnology, 24(1), 48–52. https://doi.org/10.1016/j.tibtech.2005.11.003

Shoulders, MD. & Raines, RT. (2009). Collagen structure and stability. Annu Rev Biochem. 78:929–58.

Silva-Vargas, V., Celso, C. L., Giangreco, A., Ofstad, T., Prowse, D. M., Braun, K. M., & Watt, F. M. (2005). β-catenin and Hedgehog signal strength can specify number and location of hair follicles in adult epidermis without recruitment of bulge stem cells. *Developmental cell*, 9(1), 121-131.

Singh, S., Kumar, S., Srivastava, R. K., Nandi, A., Thacker, G., Murali, H., Kim, S., Baldeon, M., Tobias, J., Blanco, M. A., Saffie, R., Zaidi, M. R., Sinha, S., Busino, L., Fuchs, S. Y., & Chakrabarti, R. (2020). Loss of ELF5-FBXW7 stabilizes IFNGR1 to promote the growth and metastasis of triple-negative breast cancer through interferon-γ signalling. *Nature cell biology*, 22(5), 591–602. https://doi.org/10.1038/s41556-020-0495-y

Soteriou, D., Kostic, L., Sedov, E., Yosefzon, Y., Steller, H., & Fuchs, Y. (2016). Isolating hair follicle stem cells and epidermal keratinocytes from dorsal mouse skin. *Journal of Visualized Experiments*, 2016(110). https://doi.org/10.3791/53931

Sotiropoulou, P. A., & Blanpain, C. (2012). Development and homeostasis of the skin epidermis. *Cold Spring Harbor Perspectives in Biology*, 4(7), 1–9. https://doi.org/10.1101/cshperspect.a008383

St-Jacques, B., Dassule, H. R., Karavanova, I., Botchkarev, V. A., Li, J., Danielian, P. S., ... & McMahon, A. P. (1998). Sonic hedgehog signaling is essential for hair development. *Current Biology*, 8(19), 1058-1069.

Stockman, D.L., Ali, S.M., He, J., Ross, J.S. & Meis, J.M. (2014). Sclerosing epithelioid fibrosarcoma presenting as intraabdominal sarcomatosis with a novel EWSR1 CREB3L1 gene fusion. *Hum. Pathol.* 45 (10) 2173–2178.

Stumpf, M., Cao, W., Klinge, U., Klosterhalfen, B., Kasperk, R. & Schumpelick, V. (2001). Increased distribution of collagen type III and reduced expression of matrix metalloproteinase 1 in patients with diverticular disease. *Int J Colorectal Dis*. 16:271–5.

Suzuki, D., & Senoo, M. (2013). Expansion of epidermal progenitors with high p63 phosphorylation during wound healing of mouse epidermis. *Experimental dermatology*, 22(5), 374–376. https://doi.org/10.1111/exd.12139

Suzuki, K., Yamaguchi, Y., Villacorte, M., Mihara, K., Akiyama, M., Shimizu, H., Taketo, M. M., Nakagata, N., Tsukiyama, T., Yamaguchi, T. P., Birchmeier, W., Kato, S., & Yamada, G. (2009). Embryonic hair follicle fate change by augmented β-catenin through Shh and Bmp signaling. *Development*, 136(3), 367–372. https://doi.org/10.1242/dev.021295

Sylvie, RB. (2011). The collagen family. *CSH Perspect Biol*. 3: a004978.

Tadeu, A. M. B., & Horsley, V. (2014). Epithelial stem cells in adult skin. *Current topics in developmental biology,* 107, 109-131.

Taipale, J., & Beachy, P. A. (2001). The Hedgehog and Wnt signalling pathways in cancer. *Nature*, 411(6835), 349–354. https://doi.org/10.1038/35077219

Takeo, M., Asakawa, K., Toyoshima, K. ei, Ogawa, M., Tong, J. J., Irié, T., Yanagisawa, M., Sato, A., & Tsuji, T. (2021). Expansion and characterization of epithelial stem cells with potential for cyclical hair regeneration. *Scientific Reports*, *11*(1). https://doi.org/10.1038/s41598-020-80624-3

Tarutani, M., Cai, T., Dajee, M., & Khavari, P. A. (2003). Inducible activation of Ras and Raf in adult epidermis. Cancer research, 63(2), 319-323.

Ting, S. B., Caddy, J., Hislop, N., Wilanowski, T., Auden, A., Zhao, L. L., ... & Jane, S. M. (2005). A homolog of Drosophila grainy head is essential for epidermal integrity in mice. *Science*, 308(5720), 411-413.

Trempus, C. S., Morris, R. J., Bortner, C. D., Cotsarelis, G., Faircloth, R. S., Reece, J. M., & Tennant, R. W. (2003). Enrichment for living murine keratinocytes from the hair follicle bulge with the cell surface marker CD34. *Journal of Investigative Dermatology*, *120*(4), 501–511. https://doi.org/10.1046/j.1523-1747.2003.12088.x

Triel, C., Vestergaard, M. E., Bolund, L., Jensen, T. G., & Jensen, U. B. (2004). Side population cells in human and mouse epidermis lack stem cell characteristics. *Experimental Cell Research*, 295(1), 79–90. https://doi.org/10.1016/j.yexcr.2003.11.032

Truong, A. B., & Khavari, P. A. (2007). Control of keratinocyte proliferation and differentiation by p63. In *Cell Cycle*, 6(3), 295–299. Taylor and Francis Inc. https://doi.org/10.4161/cc.6.3.3753

Uyttendaele, H., Panteleyev, A. A., De Berker, D., Tobin, D. T., & Christiano, A. M. (2004). Activation of Notch1 in the hair follicle leads to cell-fate switch and Mohawk alopecia. Differentiation, 72(8), 396-409.

van Genderen, C., Okamura, R. M., Farinas, I., Quo, R. G., Parslow, T. G., Bruhn, L., & Grosschedl, R. (1994). Development of several organs that require inductive epithelial-mesenchymal interactions is impaired in LEF-1-deficient mice. *Genes & development*, 8(22), 2691-2703.

van Velthoven, C. T. J., & Rando, T. A. (2019). Stem Cell Quiescence: Dynamism, Restraint, and Cellular Idling. In *Cell Stem Cell* (Vol. 24, Issue 2, pp. 213–225). Cell Press. https://doi.org/10.1016/j.stem.2019.01.001

Vasioukhin, V., Bauer, C., Degenstein, L., Wise, B., & Fuchs, E. (2001). Hyperproliferation and defects in epithelial polarity upon conditional ablation of α-catenin in skin. *Cell*, 104(4), 605-617.

Vooijs, M., Ong, C. T., Hadland, B., Huppert, S., Liu, Z., Korving, J., ..., & Kopan, R. (2007). Mapping the consequence of Notch1 proteolysis in vivo with NIP-CRE. *Development*, 134, 535–544.

Wang, T., Zhou, Z., Luo, E., Zhong, J., Zhao, D., Dong, H., & Yao, B. (2021). Comprehensive RNA sequencing in primary murine keratinocytes and fibroblasts identifies novel biomarkers and provides potential therapeutic targets for skin-related diseases. *Cellular and Molecular Biology Letters*, 26(1). https://doi.org/10.1186/s11658-021-00285-6

Wang, X., Liu, R., Li, S., Xia, W., Guo, H., Yao, W., Liang, X., Lu, Y., & Zhang, H. (2023). The roles, molecular interactions, and therapeutic value of CDK16 in human cancers. *Biomedicine & pharmacotherapy*, 164, 114929. https://doi.org/10.1016/j.biopha.2023.114929

Wang, X., Liu, Y., He, J., Wang, J., Chen, X., & Yang, R. (2022). Regulation of signaling pathways in hair follicle stem cells. In *Burns and Trauma* (Vol. 10). Oxford University Press. https://doi.org/10.1093/burnst/tkac022

Wang, X., Pasolli ,HA., Williams, T., & Fuchs, E. (2008). AP-2 factors act in concert with Notch to orchestrate terminal differentiation in skin epidermis. *J Cell Biol*, 183, 37 –48.

Ward, A.K., Mellor, P., Smith, S.E., Kendall, S., Just, N.A., Vizeacoumar, F.S. et al. (2016). Epigenetic silencing of CREB3L1 by DNA methylation is associated with high-grade metastatic breast cancers with poor prognosis and is prevalent in triple negative breast cancers. *Breast Cancer Res*.: BCR 18 (112).

Watt, F. M. (1998). Epidermal stem cells: markers, patterning and the control of stem cell fate.

Watt, F. M. (2002). Review Catherin Niemann. *In TRENDS in Cell Biology* (Vol. 12, Issue 4). http://tcb.trends.com0962-8924/02/$-seefrontmatter

Watt, F. M., & Fujiwara, H. (2011). Cell-extracellular matrix interactions in normal and diseased skin. *Cold Spring Harbor perspectives in biology*, 3(4), a005124. https://doi.org/10.1101/cshperspect.a005124

Watt, F. M., & Jensen, K. B. (2009). Epidermal stem cell diversity and quiescence. In *EMBO Molecular Medicine,* 1(5), 260–267. https://doi.org/10.1002/emmm.200900033

Watt, F. M., Celso, C. Lo, & Silva-Vargas, V. (2006). Epidermal stem cells: an update. In *Current Opinion in Genetics and Development* (Vol. 16, Issue 5, pp. 518–524). https://doi.org/10.1016/j.gde.2006.08.006

Watt, F. M., Estrach, S., & Ambler, C. A. (2008). Epidermal Notch signalling: differentiation, cancer and adhesion. *Current opinion in cell biology*, 20(2), 171–179. https://doi.org/10.1016/j.ceb.2008.01.010

Wen, L., Chi, N., Rathnayake, RA. & Wang, R. (2021). Distinctive roles of fibrillar collagen I and collagen III in mediating fibroblast-matrix interaction: a nanoscopic study. *Biochem Biophys Res Commun*. 560:66–71.

Westfall, M. D., Mays, D. J., Sniezek, J. C., & Pietenpol J. A. (2003). The Np63 Phosphoprotein Binds the p21 and 14-3-3 Promoters In Vivo and Has Transcriptional Repressor Activity That Is Reduced by Hay-Wells Syndrome-Derived Mutations. *Mol. Cell. Biol*, 23, 2264–2276. 10.1128/MCB.23.7.2264-2276.2003

WHO, 2023: Ageing and health (who.int)

Wilson, P. A., & Hemmati-Brivanlou, A. (1995). Induction of epidermis and inhibition of neural fate by Bmp-4. *Nature*, 376(6538), 331–333. https://doi.org/10.1038/376331a0

Wilson, S., Rydström, A., Trimborn, T., Willert, K., Nusse, R., Jessell, T. M., & Edlund, T. (2001). The status of Wnt signalling regulates neural and epidermal fates in the chick embryo. *Nature,* 411(6835), 325-330.

Wilson, V. G. (2013). Growth and Differentiation of HaCaT Keratinocytes (pp. 33–41). https://doi.org/10.1007/7651_2013_42

Woo, W. M., Zhen, H. H., & Oro, A. E. (2012). Shh maintains dermal papilla identity and hair morphogenesis via a Noggin-Shh regulatory loop. *Genes & development*, 26(11), 1235–1246. https://doi.org/10.1101/gad.187401.112

Wu, B., Cao, X., Liang, X., Zhang, X., Zhang, W., Sun, G., & Wang, D. (2015). Epigenetic regulation of Elf5 is associated with epithelial-mesenchymal transition in urothelial cancer. *PLoS ONE*, 10, e0117510.

Wu, J., Wang, C., Miao, X., Wu, Y., Yuan, J., Ding, M., Li, J., & Shi, Z. (2017). Age-Related Insulin-Like Growth Factor Binding Protein-4 Overexpression Inhibits Osteogenic Differentiation of Rat Mesenchymal Stem Cells. *Cellular Physiology and Biochemistry*, 42(2), 640–650. https://doi.org/10.1159/000477873

Xu, HF., Bihan, D., Chang, F., Huang, P., Farndale, R. & Leitinger, B. (2012). Discoidin domain receptors promote a1b1- and a2b1-integrin mediated cell adhesion to collagen by enhancing integrin activation. *PLoS One*. 7: e52209.

Yan, H., Qiu, L., Xie, X., Yang, H., Liu, Y., & Lin, X., & Huang, H. (2017). ELF5 in epithelial ovarian carcinoma tissues and biological behavior in ovarian carcinoma cells. *Oncol. Rep*, 37, 1412–1418.

Yang, A., Schweitzer, R., Sun, D., Kaghad, M., Walker, N., Bronson, RT., Tabin, C., Sharpe, A., Caput, D., Crum, C. et al. (1999). p63 is essential for regenerative proliferation in limb, craniofacial and epithelial development. *Nature*, 398, 714–718.

Yang, C. C., Chen, M. H., Lin, S. Y., Andrews, E. H., Cheng, C., Liu, C. C., & Chen, J. J. W. (2017). Inferring condition-specific targets of human TF-TF complexes using ChIP-seq data. *BMC Genomics*, 18(1). https://doi.org/10.1186/s12864-016-3450-3

Yang, H., Adam, R. C., Ge, Y., Hua, Z. L., & Fuchs, E. (2017). Epithelial-Mesenchymal Micro-niches Govern Stem Cell Lineage Choices. *Cell*, 169(3), 483-496.e13. https://doi.org/10.1016/j.cell.2017.03.038

Yang, R., Liu, F., Wang, J., Chen, X., Xie, J., & Xiong, K. (2019). Epidermal stem cells in wound healing and their clinical applications. In *Stem Cell Research and Therapy* (Vol. 10, Issue 1). BioMed Central Ltd. https://doi.org/10.1186/s13287-019-1312-z

Yang, R., Wang, J., Chen, X., Shi, Y., & Xie, J. (2020). Epidermal Stem Cells in Wound Healing and Regeneration. In *Stem Cells International* (Vol. 2020). Hindawi Limited. https://doi.org/10.1155/2020/9148310

Yaniw, D., & Hu, J. (2005). Epithelium-specific ets transcription factor 2 upregulates cytokeratin 18 expression in pulmonary epithelial cells through an interaction with cytokeratin 18 intron 1. In *Cell Research* (Vol. 15, Issue 6). www.cell-research.com

Yao, B., Zhao, J., Li, Y., Li, H., Hu, Z., Pan, P., Zhang, Y., Du, E., Liu, R., & Xu, Y. (2015). Elf5 inhibits TGF-beta-driven epithelial-mesenchymal transition in prostate cancer by repressing SMAD3 activation. *Prostate*, 75,872–882.

Yuspa, SH., Kilkenny, AE., Steinert, PM. & Roop, DR. (1989) Expression of murine epidermal differentiation markers is tightly regulated by restricted extracellular calcium concentrations in vitro. *JCell Biol*. 109:1207–17.

Yuxiong, W., Faping, L., Bin, L., Yanghe, Z., Yao, L., Yunkuo, L., Yishu, W., & Honglan, Z. (2023). Regulatory mechanisms of the cAMP-responsive element binding protein 3 (CREB3) family in cancers. In Biomedicine and Pharmacotherapy (Vol. 166). Elsevier Masson s.r.l. https://doi.org/10.1016/j.biopha.2023.115335

Zhang, C., Hu, Z., Lone, A. G., Artami, M., Edwards, M., Zouboulis, C. C., Stein, M., & Harris-Tryon, T. A. (2022). Small proline-rich proteins (SPRRs) are epidermally produced antimicrobial proteins that defend the cutaneous barrier by direct bacterial membrane disruption. *ELife*, 11. https://doi.org/10.7554/eLife.76729

Zhang, J., Li, C., Rahaman, M. M., Yao, Y., Ma, P., Zhang, J., Zhao, X., Jiang, T., & Grzegorzek, M. (2022). A comprehensive review of image analysis methods for microorganism counting: from classical image processing to deep learning approaches. *Artificial Intelligence Review*, *55*(4), 2875–2944. https://doi.org/10.1007/s10462-021-10082-4

Zhang, L. (2018). Keratins in Skin Epidermal Development and Diseases. In *Keratin. IntechOpen*. https://doi.org/10.5772/intechopen.79050

Zhang, L. (2018). Keratins in Skin Epidermal Development and Diseases. In *Keratin*. IntechOpen. https://doi.org/10.5772/intechopen.79050

Zhang, N., Shi, L., & Wang, Y. (2022). CREB-associated glycosylation and function in human disease. *Advances in Clinical and Experimental Medicine*, 31(11). https://doi.org/10.17219/acem/151026

Zhang, X., Lei, T., Chen, P., Wang, L., Wang, J., Wang, D., ... & Du, H. (2021). Stem cells from human exfoliated deciduous teeth promote hair regeneration in mouse. *Cell Transplantation*, 30, 09636897211042927.

Zhang, Y., Andl, T., Yang, S.H., Teta, M., Liu, F., Seykora, J.T., Tobias, J.W., Piccolo, S., Schmidt-Ullrich, R., Nagy, A., et al. (2008). Activation of b-catenin signaling programs embryonic epidermis to hair follicle fate. *Development*, 135, 2161–2172.

Zhao, B., Li, J., Zhang, X., Dai, Y., Yang, N., Bao, Z., ... & Wu, X. (2022). Exosomal miRNA-181a-5p from the cells of the hair follicle dermal papilla promotes the hair follicle growth and development via the Wnt/β-catenin signaling pathway. *International Journal of Biological Macromolecules*, 207, 110-120.

Zhou, J., Chehab, R., Tkalcevic, J., Naylor, M. J., Harris, J., Wilson, T. J., Tsao, S., Tellis, I., Zavarsek, S., Xu, D., Lapinskas, E. J., Visvader, J., Lindeman, G. J., Thomas, R., Ormandy, C. J., Hertzog, P. J., Kola, I., & Pritchard, M. A. (2005). Elf5 is essential for early embryogenesis and mammary gland development during pregnancy and lactation. *The EMBO journal*, 24(3), 635–644. https://doi.org/10.1038/sj.emboj.7600538

Zhou, P., Byrne, C., Jacobs, J., & Fuchs, E. (1995). Lymphoid enhancer factor 1 directs hair follicle patterning and epithelial cell fate. *Genes & development*, 9(6), 700-713.

Zhou, R., Diehl, D., Hoeflich, A., Lahm, H., & Wolf, E. (2003). REVIEW IGF-binding protein-4: biochemical characteristics and functional consequences. In *Journal of Endocrinology* (Vol. 178). http://www.endocrinology.org

Zhu, W., Shiojima, I., Ito, Y., Li, Z., Ikeda, H., Yoshida, M., … Komuro, I. (2008). IGFBP-4 is an inhibitor of canonical Wnt signalling required for cardiogenesis. *Nature,* 454(7202), 345–349. https://doi.org/10.1038/nature07027

Zhu, X. J., Liu, Y. D., Dai, Z. M., Zhang, X., Yang, X. Q., Li, Y., Qiu, M., Fu, J., Hsu, W., Chen, Y. P., & Zhang, Z. (2014). BMP-FGF Signaling Axis Mediates Wnt-Induced Epidermal Stratification in Developing Mammalian Skin. *PLoS Genetics*, 10(10). https://doi.org/10.1371/journal.pgen.1004687

Zomer, H. D., & Trentin, A. G. (2018). Skin wound healing in humans and mice: Challenges in translational research. *Journal of dermatological science*, 90(1), 3–12. https://doi.org/10.1016/j.jdermsci.2017.12.009

Zouboulis C. C. (2004). The human skin as a hormone target and an endocrine gland. *Hormones* (Athens, Greece), 3(1), 9–26. https://doi.org/10.14310/horm.2002.11109

Zouboulis, C. C., Adjaye, J., Akamatsu, H., Moe-Behrens, G., & Niemann, C. (2008). Human skin stem cells and the ageing process. *In Experimental Gerontology*, (Vol. 43(11), 986–997. https://doi.org/10.1016/j.exger.2008.09.001

Appendix

Appendix table:

Appendix A	Glossary of hair follicle anatomy
Appendix B:	
Appendix 1	Chelated heat-inactivated foetal bovine serum
Appendix 2	Primers table
Appendix 3	Isolation of Primary Mouse Keratinocytes (PMEKs) from new-born mice procedure with images
Appendix 4	The procedure of Stem cell isolation from adult mouse skin for live cell sorting with images
Appendix 5	Recipe of ChIP cell Lysis Buffer
Appendix 6	Recipe of ChIP Buffer
Appendix 7	Recipe of Sodium citrate buffer (10 mM Sodium citrate, 0.05% Tween 20, pH 6.0)

Appendix A

Glossary of hair follicle anatomy: (Schneider et al.,2009).

Arrector pili muscle: Tiny smooth muscle that connects the hair follicle with the dermis. When contracted the arrector pili causes the 'raising 'of the hair.

Bulb: Thickening of the proximal end of the hair follicle. Contains rapidly proliferating, rather undifferentiated matrix cells (transient amplifying cells), melanocytes and outer root sheath cells.

Bulge: Convex protrusion of the outer root sheath in the most distal permanent portion of the hair follicle, just below the sebaceous gland and at the insertion site of the muscle arrector pili. Contains the hair follicle SCs.

Dermal papilla: Mesodermal signaling center of the hair follicle consisting of closely packed specialized mesenchymal fibroblasts. Framed by the enlarged bulb matrix in anagen.

Hair canal: Tubular connection between the epidermal surface and the most distal part of the inner root sheath. Contains the hair shaft.

Hair germ: Also called 'hair placode' depending on the developmental stage. Bud-like thickening in the fetal epidermis consists of elongated keratinocytes, which at the distal end are in touch with numerous aggregated specialized dermal fibroblasts, the dermal condensate.

Hair peg: Column of keratinocytes growing into the dermis during embryonic hair follicle development. The concave proximal end starts to encase the dermal condensate, the future dermal papilla.

Hair shaft: The hair per se, composed of trichocytes, which are terminally differentiated hair follicle keratinocytes. It is composed of the medulla, the central part with loosely connected keratinized cells and large air spaces, and the cortex, which is the bulk of the hair shaft, consisting of keratinized cells, keratin filaments, and melanin granules in pigmented hairs.

Infundibulum: Most proximal part of the hair follicle relative to the epidermis, extending from the sebaceous duct to the epidermal surface. Includes the hair canal and the distal Outer root sheath.

Inner root sheath: A multilayered, rigid tube composed of terminally differentiated hair follicle keratinocytes, surrounded by the outer root sheath.

Isthmus: Middle part of the hair follicle extending from the sebaceous duct to the bulge.

Outer root sheath: The outermost layer of the hair follicle. Merges proximally with the basal layer of the interfollicular epidermis and distally with the hair bulb.

Sebaceous gland: Acinar gland composed of lipid-filled sebocytes, localized close to the insertion of the arrector pili muscle. Secretes sebum to the epidermal surface via a holocrine mechanism. Sebum helps make hair and skin waterproof. Together with the HF and the arrector pili muscle it forms the pilosebaceous unit.

Appendix B

Appendix 1

Chelated heat-inactivated foetal bovine serum

Calcium was eliminated from heat-inactivated foetal bovine serum through a chelation process utilizing BT Chelex 100 resin. Initially, 100 grams of Chelex resin were dissolved in 450 mL of H2O and adjusted to a pH of 7.4 before passing through filter paper with a pore size of 5-13 µm. Subsequently, the resin slurry was introduced into a 500 mL container containing heat-inactivated foetal bovine serum and agitated at room temperature for a duration of 3 hours. The resulting mixture was then filtered through filter paper, with the resin slurry being discarded and subjected to re-filtration. Prior to its application in cell culture, the chelated heat-inactivated foetal bovine serum was filtered through a 0.2 µm filter. The Chelex resin effectively removes calcium from the solution through ion exchange. At a pH of 7.4, the Chelex resin binds to Ca2+ ions via its charged carboxylic acid groups, which are subsequently filtered out of the solution using filter paper.

Appendix 2

Primers

Gene symbol	Gene name	Accession no.	Sense sequence (5'-3')	Anti-sense sequence (5'-3')
Actb	Actin, beta	*NM_007393.5*	CCAACCGTGAAAAGATGACC	CCATCACAATGCCTGTGGTA
Ccnb2	Cyclin B2	*NM_007630.2*	AGCAGCAGTATTACACAGGC	GGAGGCCAGGTCTTTGATGA
Ccnd1	Cyclin D1	*NM_001379248.1*	CCCCAACAACTTCCTCTCCT	CCTTGGGGTCGACGTTCT
Ccnd2	Cyclin D2	*NM_009829.3*	GCCAAGATCACCCACACTGA	ATGCTGCTCTTGACGGAACT
Ccne1	Cyclin E1	*NM_007633.2*	ACTCCCACAACATCCAGACC	CGCTGCTCTGCTTCTTACTG
Cdk1	Cyclin-dependent kinase 1	*NM_007659.4*	GGGCACTCCTAACAACGAAG	CCAGAGATTCGTTTGGCAGG
Cdk16	Cyclin-dependent kinase 16	*NM_011049.5*	GCAATCGGATCTCTGCTGA	CAGGCATAGAAGTGGACCGA
Elf5	E74-like factor 5	*NM_010125.3*	GTGGCATCAAGAGTCAAGACTGTC	CTCAGCTTCTCGTACGTCATCCTG
Ivl	Involucrin	*NM_008412.3*	TGCCTTCTCCCTCCTGTGA	CAGTCTTGAGAGGTCCCTGA
Krt1	Keratin 1	*NM_008473.2*	CATATTAGTAGCAGTCTGA	TGAAGTCCTCTTTCAAAT
Krt10	Keratin 10	*NM_010660.2*	AGTTCCTTGCTCTTCTGATTG	CAAGTCTGACCTGGAAATGC

Appendix 3

Isolation of Primary Mouse Keratinocytes (PMEKs) from new-born mice procedure with images (Based on Lichti et al., 2008): These images with animal work may not be suitable for those of a sensitive disposition.

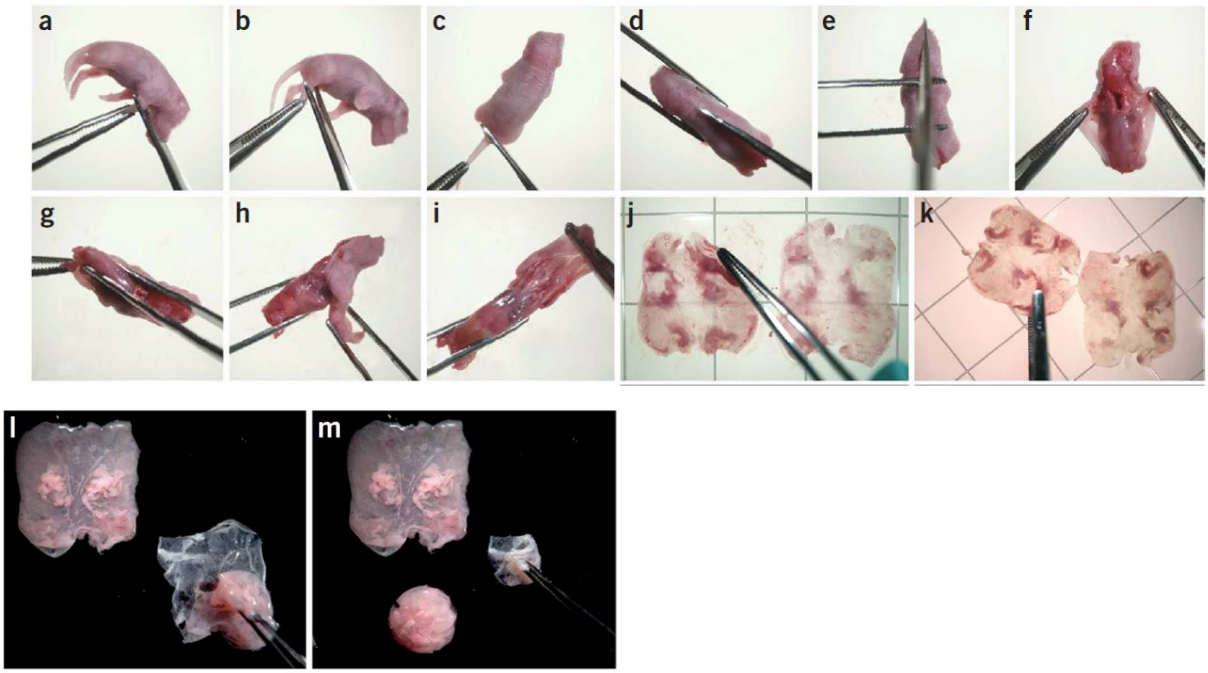

(Based on Lichti et al., 2008)

(a-k) The procedure to remove epidermis from new-born mice:

The head was cut and removed before this procedure. (a-b) Remove lower forelimbs and hindlimbs; (c) push and cut tail close to the body including genitals; (d-e) cut the skin along dorsal midline from the tail end to the neck of the body; (f-i) loose and gather the skin on the ventral side and pull it toward the neck. (j-K) unfold and float skin, dermis side down, in ice cold trypsin (0.25% without EDTA, ThermoFisher, UK) in the 100-mm sterile culture dish. The floating

skins in the dishes were stored at 4°C overnight in a refrigerator. Next day, (i) in a laminar-flow hood spread and put the dermis upside, hold the epidermis with forceps and peel off dermis from epidermis to a tube for later disposal; (m) transfer the paper like epidermis to a 50-ml conical tubes containing PMEK complete media prior to the dissection.

Appendix 4

The procedure of Stem cell isolation from adult mouse skin for live cell sorting

Day 1:

- Pre-skin collection shave the skin as close as possible with an electric shaver.
- Collect dorsal and ventral skin separately.
- Wash skin 3xs in 70% ethanol and 3xs in autoclaved PBS.
- Keep on ice until ready.

- Hair side down
- Scrape blood vessels and fat from dermis off the skin with a scalpel

- Cut skin into 1-2cm pieces.

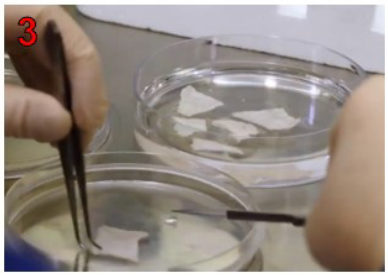

- Float the skin hairy side up in ice cold 0.25% Trypsin-EDTA or 5mg/ml dispase solution.
- Incubate O/N at 4ºC. Can do 37ºC for 2 hours.

Day 2:

- You will need 30ml of NO Ca2+ complete EMEM media (all other supplements required).
- You will need staining buffer: 2ml – 2% BSA/PBS.

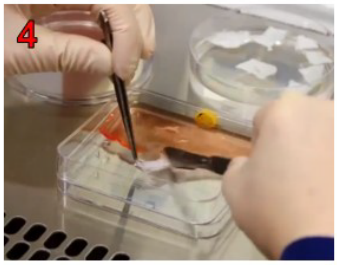

- Use a slanted petri dish with ice cold 0.25% Trypsin-EDTA.
- Scape the epidermis and HFs from the dermis into the trypsin (epidermis will come in chunks; the dermis is durable and will not break easily).

- Collect epidermis and hair in a tube and incubate at 37ºC for 30 minutes.
- When collecting, rinse the collection petri dish to collect all the epidermal cells and HFs.

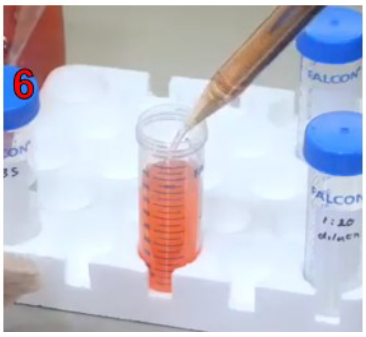

- Add 20ml of NO Ca2+ complete EMEM media.
- Repeatedly pipette up and down with a 10ml pipette to triturate the tissue.
- Note: tissue may be large chunks with hair so may need to snip with large scissors for approx. 5 mins.

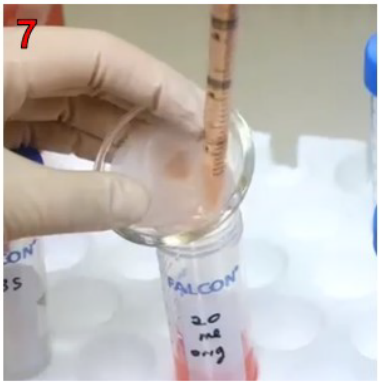

- Filter the cell mixture through a 70um strainer into a new tube.
- Use forceps to push the larger hairs and tissue through the strainer.
- Wash the strainer with an additional 5ml No Ca2+ EMEM media, pipetting slowly, pushing tissue through the strainer with the end of the pipette.
- Repeat filtration with all material through a new 70um strainer.

- Pass the cell mixture through a 40um cell strainer into a new falcon tube.
- This can be repeated through the same strainer to wash through cells and create a single cell suspension.
- Place the tube on ice until ready for the next step.

- Centrifuge the tubes for 10 mins at 250xg to pellet the cells.
- Note: it is normal for the media to be cloudy after spinning due to dead cells and debris.
- Re-suspend the pellet in 1ml NO Ca2+ complete EMEM media and keep on ice.
- Re-filter through 40um filter before going on to staining.

Appendix 5

Recipe of ChIP cell Lysis Buffer:

50mM HEPES-KOH pH 7.5

140mM NaCl

1mM EDTA pH 8.0

0.5M 1% Triton X-100

0.1% Sodium Deoxycholate

0.1% SDS

(To make 1ml 50mM HEPES KOH buffer 7.5:

HEPES molecular weight 238.3 g/mol (sigma, H4034)

1 ml ultrapure water

0.012 g HEPES

KOH (potassium hydroxide) pellets to adjust pH to 7 and make up to 1ml with ultrapure water

Sterilise by filtration with Syringe Filters of 0.2 um pore size (Corning, #431224)

Appendix 6

Recipe of ChIP **Buffer:**

20ul HEPES (1M) (Fisher, BP310-100)

860ul H2O

200ul EDTA (0.5M) (Fisher scientific, 11568896)

50ul of 20% SDS solution to make 1% SDS CHIP buffer (make 0.1% and 0.4 % SDS CHIP buffer using 1% SDS CHIP buffer)

Quarter tablet of ULTRA pure PIC (Merck, 5892970001)

Mix and dissolve, then sterilise by filtration with Syringe Filters of 0.2 um pore size (Corning, #431224)

Appendix 7

Recipe of Sodium citrate buffer (10 mM Sodium citrate, 0.05% Tween 20, pH 6.0):

Tri-sodium citrate (dihydrate) 2.94 g (Merck, 6132-04-3)

Distilled water 1 L

Mix to dissolve. Adjust pH to 6.0 with 1N HCl (Merck, 7647-01-0)

Add 0.5 mL Tween 20 and mix well. Store at room temperature.